

Doctoral Dissertation

**High Cycle Fatigue Modeling of Concrete Pavement
coupled with Soil Foundation**

「地盤との複合を考慮したコンクリート舗装の高サイクル疲労モデル」

By

NGUYEN HUU QUOC HUNG

A dissertation submitted to
Graduate School of Urban Innovation
of
Yokohama National University
in partial fulfillment of the requirements for the award of the degree of

Doctor of Philosophy in Engineering

Academic Supervisor

Professor KOICHI MAEKAWA

Yokohama National University
Yokohama, Japan

September 2020

YOKOHAMA NATIONAL UNIVERSITY
GRADUATE SCHOOL OF URBAN INNOVATION

This dissertation, written by Nguyen Huu Quoc Hung, has been accepted by his supervisor and dissertation committee members. And, it is submitted to the Graduate School of Urban Innovation – Yokohama National University – Japan in partial fulfillment of the requirements for the award of the degree of Doctor of Philosophy in Engineering.

Committee members

Prof. Koichi Maekawa, Chair

Faculty of Urban Innovation – Yokohama National University

Prof. Ryoichi Sato

Hiroshima University

Prof. Kimitoshi Hayano

Faculty of Urban Innovation – Yokohama National University

Prof. Akira Hosoda

Faculty of Urban Innovation – Yokohama National University

Assoc. Prof. Chikako Fujiyama

Faculty of Urban Innovation – Yokohama National University

ABSTRACT

Concrete pavements are mechanically coupled between the concrete slab and the soil foundation to ensure the long-lasting service time and the smooth in the operation as well as to minimize the cost for maintenance. The application of the concrete pavements has been increasing in high/expressways and airfields owing to the benefit in the life-cycle service and the load capacity for traffic vehicles. The principles for the pavement design have been originally developed by Westergaard based on an elastic slab over a dense liquid subgrade. The damage of the pavements is therefore localized at the deterioration of the concrete slab only.

In the life-cycle assessment of the RC slab decks, Maeda and Matsui have conducted experiments to discuss the significant reduction of the fatigue life under the moving loads compared to the fixed-point pulsating loads. Maekawa et al. proposed the high cycle fatigue constitutive models to investigate the service life of RC slab decks subjected to traveling loads by tracing the exact transient process of damages. The nonlinear FE analyses were implemented and the sharp decrease of the fatigue life under the moving loads in RC slab decks has been observed. These models have been extended to the combined effects of ambient environments for the life-cycle assessment of concrete decks.

To evaluate the fatigue life of concrete pavements in the existing design codes, soil is considered as linear, isotropic, homogeneous and elastic foundation and the concrete slab is suffered from the concentrated truck axle loads. This load application is consistent with static vehicles on parking lots but does not reflect real vehicles in motion on roads. The fatigue failures are thus focused on the damage of the concrete slab only. Therefore, two points are raised in this study. One is the type of loading, i.e. fixed or moving. The fixed-point pulsating loads show the localized damage of the concrete slab and soil. Conversely, under the traffic motion, the deterioration of the concrete slab and soil occur concurrently and is distributed along with the moving load directions. The fatigue life is therefore dramatically reduced compared to the fixed-point ones. The other point is the nonlinear high cycle fatigue interaction of soil and concrete. The fatigue characteristics of the concrete slab (shear, tension, and

compression) and the soil foundation (shear and volumetric fatigue) are investigated in this study.

To meet the above challenges, a series of fatigue loading experiments are arranged in this dissertation. The small-scale mock-ups have been conducted in accordance with the specifications of the wheel load testing equipment as well as the size effects of soil and concrete slabs. The models are expected to qualitatively reflect the real scale of the concrete pavement. The nonlinear FEM analysis program is developed by coupling the code of RC bridge decks for prediction the shortened fatigue life of the slabs under the moving loads and the numerical program of the shear band formation of the soil foundation. These separated codes are based upon the combined thermodynamic and structural mechanics which have been experimentally validated. The development and experimental validation of the upgraded and coupled code of the concrete slab and the soil foundation are presented in this dissertation by using small-scale mock-ups of concrete pavements.

The failure mechanism of concrete pavements with a diversity of the soil density under the fixed-point and moving loads is first investigated. The failure mode and the fatigue life for each case have been examined. The fatigue damage of pavements can be the soil, the concrete slab or both of them, opposite to the sole damage of the concrete slab under the concentrated truck axle loads in the existing design codes. The comparison between the full-scale numerical simulation (based on nonlinear mechanics of soil and the concrete slab under moving loads) and the required thickness in some existing design guidelines (based on the principle of an elastic slab over a dense liquid subgrade under the concentrated loads) is conducted to elucidate the restrictions of the current pavement design codes. The newly balanced thickness in the concrete pavement is approached and proposed to bridge the gap between the existing design codes and engineering practices. The thinner thickness of the concrete slab on the non-compacted soil is computationally and experimentally observed. Meanwhile, the thicker one on the compacted soil is required when the nonlinear coupling of the concrete slab and soil is investigated. This will be a key factor to revise the design code of pavement which has been modeled based on in-plane theory on elastic foundation without considering shear localization.

In the structural design of concrete pavements, the effects of the construction-joint to the fatigue life are investigated. The failure support of the dowel bars in the jointed concrete pavements shows the sharp decrease of the fatigue life under the moving load compared to continuously reinforced concrete. It is due to the localized damage of the soil and concrete slabs at the edges. The reinforcement ratio and density of the soil foundation can be sufficient tools to support the jointed concrete pavements if the dense soil and the rational thickness of the concrete slab are examined concurrently.

The mechanism for the damage of the concrete slab when the stagnant water exists in the cracked concrete is also observed by examining the water pressure in concrete. Under the moving loads, cracks can open and close, hence the water pressure may be negative or positive. When the cracks close, the development of high pressure inside cracks occurs. It can cause the large internal force around the crack tips and leads to further crack propagation. In this dissertation, by incorporating the constitutive models of the concrete slab, the soil foundation coupled with multi-scale modeling for pore water inside cracks, the fatigue life of pavement under the water effects may be investigated. The results show the dramatic shortage of fatigue life compared to the fully dry slab. Nonlinear FEM analysis for the water-crack interaction is numerically simulated in the diverse conditions of stagnant water positions in concrete slabs, reinforcement ratios, soil density, and the strength of the slab. The critical positions of the stagnant water are at the near surface of the slab or the fully saturated slab, respectively. When the water exists in the cracked concrete, the reinforcement ratio is computationally simulated to have an inconsiderable impact on the support of the fatigue life of pavements. The dense soil foundation can support the fatigue life if the stagnant water does not stay at the critical positions. Finally, the high strength concrete in pavement construction is recommended due to the decrease of the coarser micropores in concrete structures. It can strengthen the fatigue life under the water effects.

On the deep discussion of the experimental and analytical results, the findings in the dissertation can make a contribution to revising the existing design codes of concrete pavements. The nonlinear mechanics of the soil and the slab under the wheel-type moving load should be approached in pavement studies.

ACKNOWLEDGEMENTS

I would like to express my deepest gratitude and sincere appreciation to my supervisor, Professor Koichi Maekawa, for his superb instruction, continuous encouragement, valuable suggestions, support and guidance throughout this research work. Without his enthusiasm and persistent supervision, this dissertation would have been impossible to be accomplished.

My sincere thanks also go to Professor Akira Hosoda and Associate Professor Chikako Fujiyama for their valuable support and useful advice during my study. My sincere appreciation also goes to Dr. Satoshi Komatsu for his kind support at the beginning of my study. Besides the deepest thank to professors of Concrete Laboratory, I would like also to offer my deep gratitude to Professor Kimitoshi Hayano from Geotechnical Laboratory of Yokohama National University for his advice to conduct experiments in this study. The sincere appreciation is extended to Professor Ryoichi Sato of Hiroshima University for his kind review of this dissertation. I offer my thanks to Ms. Emiko Ishii for her kind supports in administrative concerns.

I wish to show sincere thanks to the supports of Nichireki Institute of Research in Tochigi Prefecture, Japan and highly appreciate Dr. Akiyoshi Hanyu and Mr. Yuki Higuchi for assistance to implement experiments in this study.

I want to thank my colleagues in the Concrete Laboratory of Yokohama National University for friendship, help, kind support, and cheering me up that helped me get much enjoy for my study and life in Japan.

I am grateful to Japanese Ministry of Education, Culture, Sports, Science, and Technology (MEXT) for granting the scholarship. The financial support made me possible to pursue this study.

Finally, I would like to dedicate this research work with my beloved family. They are always a part of support and encouragement to me. Their eternal love is a supreme power for me to finish this work.

LIST OF PUBLICATIONS

During the course of the research work, the following refereed papers have been published or submitted for publication.

International Journals:

1. Nguyen Huu Quoc Hung, Satoshi Komatsu, and Koichi Maekawa, “High-cycle fatigue interaction between soil foundation and concrete slab under moving wheel-type loads,” *Engineering Structures*, Vol. 209, pp. 1-16, 2020.
2. Nguyen Huu Quoc Hung and Koichi Maekawa, “Multi-scale simulation for fatigue life evaluation of concrete pavement subjected to moving load under dry and wet conditions,” *Journal of Advanced Concrete Technology*, Vol. 18, pp. 95-115, 2020.

International Conferences:

3. Nguyen Huu Quoc Hung, Koichi Maekawa, and Satoshi Komatsu, “Three-dimensional high-cycle fatigue simulation of soil-concrete pavement slab interaction under moving loads,” *Proceedings of the 8th International Conference of Asian Concrete Federation*, Fuzhou, China, Vol. 2, pp. 1207–1216, 2018.
4. Nguyen Huu Quoc Hung, Koichi Maekawa, and Satoshi Komatsu, “Numerical simulation of construction-joint effects for fatigue-life assessment of concrete pavement subjected to traveling wheel-type load,” *Proceedings of the Japan Concrete Institute*, Vol. 41, No.1, pp. 1397–1402, 2019.
5. Nguyen Huu Quoc Hung, Koichi Maekawa, and Satoshi Komatsu, “Effects of water-coupled cracks on life-cycle assessment of concrete pavement under moving load,” *Proceedings of Airfield and Highway Pavements*, ASCE, Chicago, Illinois, USA, pp. 111–121, 2019.
6. Nguyen Huu Quoc Hung and Koichi Maekawa, “Effect of soil density on water coupled cracks for life performance of concrete pavement under moving

load,” *Proceedings of the Japan Concrete Institute*, Vol. 42, No.1, pp. 1252-1257, 2020.

7. Nguyen Huu Quoc Hung and Koichi Maekawa, “Numerical simulation on the life-cycle assessment of concrete pavement - diverse soil’s density coupled to moving and fixed-point pulsating loads,” *Proceedings of 12th International Conference on Concrete Pavements*, Minneapolis, Minnesota, USA, 09/2021 (accepted on January 31st, 2020).

TABLE OF CONTENTS

ABSTRACT.....	II
ACKNOWLEDGEMENTS	V
LIST OF PUBLICATIONS	VI
LIST OF FIGURES	XII
CHAPTER 1.....	1
INTRODUCTION.....	1
1.1 Background.....	1
1.2 Objectives / Target and Scope of the Study	5
1.3 Outline of the Dissertation.....	7
References in Chapter 1:	10
CHAPTER 2.....	14
LITERATURE REVIEW	14
2.1 Introduction	14
2.2 Models of Soil Foundations in Concrete Pavements	14
2.3 High Cycle Fatigue Modeling of Soil	18
2.4 High Cycle Fatigue of Concrete Slabs	19
2.5 Existing Design Codes for Concrete Pavements.....	20
2.5.1 AASHTO Guide for the Design of Pavement Structures	20
2.5.2 Thickness Design for Concrete Highway and Street Pavements	21
2.5.3 Mechanistic-Empirical Pavement Design Guide.....	22
2.5.4 Guide for Design of Jointed Concrete Pavements for Streets and Local Roads	23
2.6 Conclusions for Chapter 2.....	23
References in Chapter 2:	25
CHAPTER 3.....	33
EXPERIMENTAL AND ANALYTICAL STUDY FOR HIGH-CYCLE FATIGUE INTERACTION BETWEEN SOIL FOUNDATIONS AND CONCRETE SLABS UNDER MOVING WHEEL-TYPE LOADS.....	33
3.1. Introduction	33
3.2 Experimental Program.....	34

3.2.1 Experimental Cases and Test Specimens	34
3.2.2 Testing Devices for the Experiments.....	37
3.2.3 Materials	38
3.2.4 Testing Implementation.....	38
3.3 Nonlinear FEM Analysis Program.....	39
3.3.1 Multi-Directional Fixed Crack Modeling for High-Cycle Fatigue	40
3.3.2 Multi-Yield Surface Plasticity for High-Cycle Fatigue of Soil.....	46
3.4 Experimental and Analytical Results and Discussion.....	51
3.4.1. Experimental Verification and Validation.....	51
3.4.2. Failure Mode and Fatigue Life: Thickness of Slab=50mm.....	53
3.4.3. Failure Mode and Fatigue Life: Thickness of Slab=20mm.....	56
3.5 Conclusions for Chapter 3	60
References in Chapter 3:	62
CHAPTER 4.....	65
FAILURE MECHANISM OF CONCRETE PAVEMENTS -DIVERSE SOIL'S	
DENSITY COUPLED MOVING AND FIXED-POINT PULSATING LOADS.	65
4.1 Introduction	65
4.2 Research Significance of the Failure Mechanism of Concrete Pavements.....	67
4.3 Methodology	68
4.4 Numerical Modeling for the Concrete Pavement under the Fixed-Point and Moving Loads	70
4.5 Results and Discussion.....	72
4.6 Conclusions for Chapter 4.....	85
References in Chapter 4:	87
CHAPTER 5.....	89
NONLINEAR FEM ANALYSIS FOR THE NEW APPROACH TO PREDICT	
AND ASSESS THE BALANCED THICKNESS OF CONCRETE PAVEMENT	
SLABS RESPONSE TO MOVING LOADS.....	89
5.1 Introduction	89
5.2 Fundamentals of the Current Design Codes.....	90
5.3 Research Methodology – a New Approach for the Slab's Thickness of the Concrete Pavement.....	91
5.4 Nonlinear Full-Scale Simulation for Soil-Concrete Slab Interaction.....	93
5.5 Parametric Sensitivity of Coupled System – Design Concept	97

5.6 New Concept for Balanced Slab Thickness	101
5.6.1 Nonlinear FEM Analysis and Guideline ACI 325.....	101
5.6.2 Nonlinear FEM Analysis and Guideline PCA.....	106
5.7 Conclusions for Chapter 5.....	109
References in Chapter 5:	111
CHAPTER 6.....	112
NUMERICAL SIMULATION OF CONSTRUCTION-JOINT EFFECTS FOR	
FATIGUE-LIFE ASSESSMENT OF CONCRETE PAVEMENTS SUBJECTED	
TO TRAVELING WHEEL-TYPE LOAD	112
6.1 Introduction	112
6.2 Nonlinear FEM Modeling of Construction-Joint Effects.....	115
6.3 Computation for the Fatigue Life of Jointed and Continuously Reinforced	
Concrete with Reinforcement Ratio 1.0%.....	116
6.4 Computation for the Fatigue Life of Jointed and Continuously Reinforced	
Concrete with Reinforcement Ratio 0.1%.....	120
6.5 Conclusions for Chapter 6.....	123
References in Chapter 6:	124
CHAPTER 7.....	126
WATER COUPLED CRACKS ON LIFE-CYCLE ASSESSMENT OF	
CONCRETE PAVEMENTS UNDER MOVING LOADS	126
7.1 Introduction	126
7.2 Fundamentals for the Water-Crack Interaction in Concrete Pavements	128
7.3 Nonlinear FEM Analysis for the Water-Crack Interaction	131
7.3.1 Effects of the Stagnant Water Position in the Concrete Slab.....	133
7.3.2 Effects of Reinforcement Ratios.....	138
7.3.3 Effects of Soil's Density	147
7.3.4 Effects of Strength of Concrete.....	150
7.4 Pore Pressure and Principal Strain of Crack inside Concrete Slab	160
7.5 Computed Fatigue Life for the Fully Dry and Saturated Wet Slab.....	161
7.6 Conclusions for Chapter 7	162
References in Chapter 7:	164
CHAPTER 8.....	166
CONCLUSIONS AND RECOMMENDATIONS.....	166
8.1 General Conclusions	166

8.2 Experimental and Analytical Study for High Cycle Fatigue of Concrete Pavements.....	166
8.3 Failure Mechanism of Concrete Pavements – Diverse Soil’s Density Coupled Moving and Fixed-Point Pulsating Loads.....	167
8.4 Nonlinear FEM Analysis for the Approach to Predict the Balanced Thickness of Concrete Pavements	168
8.5 Effects of Construction Joints in Life Cycle Assessment of Concrete Pavements	169
8.6 Water Coupled Cracks on Life-Cycle Assessment of Concrete Pavements	170
8.7 Recommendations for the Further Study	171

LIST OF FIGURES

Fig. 1-1 Model scheme of concrete pavement by coupling concrete slabs and soil foundations [8].	2
Fig. 1-2 Some typical damages of concrete pavement slabs [34].	4
Fig. 1-3 Rainwater in the cracks of the slab [35].	5
Fig. 1-4 Damage of the sealant and dowel bar of jointed concrete pavements [34].	5
Fig. 1-5 Outline of the dissertation.	9
Fig. 2-1 Filonenko-Borodich for pavements [17].	15
Fig. 2-2 Hetenyi foundation [18].	15
Fig. 2-3 Pasternak foundation [19].	16
Fig. 2-4 Kerr foundation [20].	16
Fig. 2-5 A beam – column – analogy modeling [21].	17
Fig. 2-6 Loading type in the study of concrete pavement in ASSHTO 1993 [1], [75].	21
Fig. 2-7 Axle load position in PCA design guideline [2].	22
Fig. 3-1 Two modelings for concrete pavement experiments.	35
Fig. 3-2 Sand formwork for experiment.	36
Fig. 3-3 Sand preparation for experiment.	36
Fig. 3-4 Facilities for small-scale experiments of concrete pavements.	37
Fig. 3-5 Deflection gauge.	38
Fig. 3-6 Summary of testing implementation for thickness slab 50mm.	39
Fig. 3-7 Summary of testing implementation for thickness slab 20mm.	39
Fig. 3-8 Scheme of constitutive laws for the concrete slab [11], [13], [14].	41
Fig. 3-9 Outline of the multi-directional fixed crack model in concrete structures [14].	41
Fig. 3-10 Constitutive laws of concrete structures for high-cycle fatigue [9], [14], [15].	42
Fig. 3-11 Constitutive model of soil foundations for high cycle fatigue.	47
Fig. 3-12 Outline of soil foundations.	49
Fig. 3-13 The softening branch of two different FEM meshes in views of shear band and load-deformation [12].	50

Fig. 3-14 Summary for high cycle fatigue of the concrete and soil interaction.....	51
Fig. 3-15 Finite element discretization for slab-soil interaction.	53
Fig. 3-16 Displacement and deformational mode under the moving load 1,029N and RD 75%.....	54
Fig. 3-17 Displacement and deformational mode under the moving load 513N and RD 50%.	55
Fig. 3-18 Displacement and deformational mode under the moving load of 1,029N and RD 50%.	56
Fig. 3-19 The experimental and numerical result with moving load 513N + 98N and RD 50%.	57
Fig. 3-20 The experimental and numerical result with moving load 1,029N + 98N and RD 50%.	58
Fig. 3-21 The failure mode of concrete slab 20mm with the static load 1,029N and RD 75%.	58
Fig. 3-22 The load capacity-displacement relationship of concrete slab 20mm with RD 75% and RD 50%.	59
Fig. 4-1 The experiments of the concrete pavement under (a) the fixed-point load [6] and (b) the moving load.	66
Fig. 4-2 Model scheme of concrete pavement by coupling concrete slabs and soil foundations.....	67
Fig. 4-3 Overview of prediction for S-N diagram and failure mode under the fixed-point and moving loads of concrete pavements [16].	70
Fig. 4-4 The full-scale numerical modeling for concrete pavements under the fixed-point and moving loads.	71
Fig. 4-5 S-N diagram and fatigue life of the concrete pavement under RD 50% of the soil foundation.	74
Fig. 4-6 Fatigue life of the concrete pavement under RD 60% of the soil foundation.	75
Fig. 4-7 Fatigue life of the concrete pavement under RD 65% of the soil foundation.	76
Fig. 4-8 Fatigue life of the concrete pavement under RD 70% of the soil foundation.	77
Fig. 4-9 S-N diagram and fatigue life of the concrete pavement under RD 75% of the soil foundation.	79

Fig. 4-10 Fatigue life of the concrete pavement under RD 80% of the soil foundation.	80
Fig. 4-11 Fatigue life of the concrete pavement under RD 85% of the soil foundation.	81
Fig. 4-12 Fatigue life of the concrete pavement under RD 90% of the soil foundation.	82
Fig. 4-13 S-N diagram and the fatigue life of the concrete pavement under RD 95% of the soil foundation.	83
Fig. 4-14 Typical failure mode of the concrete pavement under the fixed-point load (156kN).	85
Fig. 4-15 Typical failure mode of the concrete pavement under the moving load (156kN).	85
Fig. 5-1 Overview for prediction and assessment of the thickness in the pavement.	93
Fig. 5-2 The full-scale numerical modeling for concrete pavement under moving load.	94
Fig. 5-3 The fatigue life and failure mode of the full-scale simulation of concrete pavement with RD 50%.	95
Fig. 5-4 The fatigue life and failure mode of the full-scale simulation of concrete pavement with RD 75%.	96
Fig. 5-5 The failure mode of a variety of soil relative density and concrete slab thickness.	101
Fig. 5-6 Balanced thickness of concrete slab to maximize the fatigue life of pavement system and the specified recommended thickness by ACI 325 [13].	104
Fig. 5-7 Failure mode of numerical simulation (a) RD 50%, (b) RD 75%, and (c) RD 95%.	105
Fig. 5-8 Balanced thickness of concrete slab to maximize the fatigue life of pavement system and the specified recommended thickness by PCA [13].	108
Fig. 6-1 The jointed concrete slab in the concrete pavement.	112
Fig. 6-2 Three levels for the joint sealant damage: a) low, b) medium, and c) high severity [1].	113
Fig. 6-3 Construction joint used in this study.	115
Fig. 6-4 Simulation model for investigation of construction-joint effects to fatigue life	116

Fig. 6-5 The comparison of fatigue life between continuous and jointed concrete pavement (RR 1.0%).....	117
Fig. 6-6 The comparison of failure mode between continuous and jointed concrete pavement (RR 1.0%).....	119
Fig. 6-7 The comparison of fatigue life between continuous and jointed concrete pavement (RR 0.1%).....	121
Fig. 6-8 The comparison of failure mode between continuous and jointed concrete pavement (RR 0.1%).....	122
Fig. 7-1 Multi-scale simulation scheme of water-crack interaction in pavement.....	127
Fig. 7-2 Modeling of stagnant water inside cracked concrete.	130
Fig. 7-3 Summary of the coupled code for concrete, soil and pore water inside cracks.	131
Fig. 7-4 Simulation model for water coupled cracks in concrete pavement.....	132
Fig. 7-5 The stagnant water position in the slab of FEM analysis.....	133
Fig. 7-6 Fatigue life and failure mode with water at top layer of 5 and 10 cm.	135
Fig. 7-7 Fatigue life and failure mode subjected to water at the bottom layer.	136
Fig. 7-8 Horizontal cracking at top surface of concrete bridge deck under moving loads [16].	137
Fig. 7-9 Fatigue life and failure mode under water effect at each layer.	138
Fig. 7-10 Fatigue life and failure mode of concrete pavement under water effects with RR 0.1%.....	140
Fig. 7-11 Fatigue life and failure mode of concrete pavement under water effects with RR 0.3%.....	141
Fig. 7-12 Fatigue life and failure mode of concrete pavement under water effects with RR 0.4%.....	143
Fig. 7-13 Fatigue life and failure mode of concrete pavement under water effects with RR 0.5%.....	144
Fig. 7-14 Fatigue life and failure mode of concrete pavement under water effects with RR 0.6%.....	144
Fig. 7-15 Fatigue life and failure mode of concrete pavement under water effects with RR 0.8%.....	146
Fig. 7-16 Fatigue life and failure mode of concrete pavement under water effects with RR 1.0%.....	146

Fig. 7-17 Fatigue life and failure mode of concrete pavement under water effects with RR 0.1% and RD 75%.	148
Fig. 7-18 Fatigue life and failure mode of concrete pavement under water effects with RR 1.0% and RD 75%.	149
Fig. 7-19 Fatigue life and failure mode of concrete pavement under water effects with W/C 30%.....	152
Fig. 7-20 Fatigue life and failure mode of concrete pavement under water effects with W/C 35%.....	153
Fig. 7-21 Fatigue life and failure mode of concrete pavement under water effects with W/C 40%.....	154
Fig. 7-22 Fatigue life and failure mode of concrete pavement under water effects with W/C 45%.....	155
Fig. 7-23 Fatigue life and failure mode of concrete pavement under water effects with W/C 50%.....	156
Fig. 7-24 Fatigue life and failure mode of concrete pavement under water effects with W/C 55%.....	157
Fig. 7-25 Fatigue life and failure mode of concrete pavement under water effects with W/C 60%.....	158
Fig. 7-26 Fatigue life and failure mode of concrete pavement under water effects with W/C 65%.....	159
Fig. 7-27 Summary for the fatigue life of pavement under water effects.....	160
Fig. 7-28 Pore water pressure and principal strain of concrete slab at the top surface with RD 50% and RR 0.3%.	161
Fig. 7-29 Computed S-N diagram for concrete pavement with fully dry and wet slab under moving loads.....	162

CHAPTER 1

INTRODUCTION

1.1 Background

Concrete pavements can be mechanically represented by the coupled soil foundations and concrete slabs in order to realize both long-life and smooth trafficability. They have been increasingly utilized in highways and airfields around the world due to the primacy of life-cycle service and the load capacity of traffic vehicles. The design of concrete pavements aims to provide safe and durable road surfaces. The damage of the concrete pavement slab is therefore necessarily minimized under operation.

The study of pavements was initiated based on the linear beam/slab theorem with homogeneous elastic foundation [1]–[3] and has been applied to the practice by Westergaard [4]–[7]. This dissertation aims to assess the service life of concrete pavements under various ranges of traffic loads based upon the previous work [8].

The fatigue life of reinforcement concrete (RC) slabs on bridges has been experimentally discussed by Maeda and Matsui [9], [10] under the wheel-type moving loads as well as the fixed-point pulsation. The experimental results showed a dramatic reduction of fatigue life under moving loads compared to fixed-point ones. By tracing the exact transient process of damages, Maekawa et al. proposed the high-cycle fatigue constitutive models to investigate the service life of RC bridge decks subjected to traveling loads [11], [12]. In order to clearly elucidate behaviors of RC bridge slabs, three-dimensional analyses under high-cycle moving loads were implemented and compared to experiments so as to depict the sharp decrease of the fatigue life in the case of moving loads [11]–[13]. These models have been extended to the combined effects of ambient environments for the life-cycle assessment of concrete decks [14], [15].

For evaluating the fatigue life of concrete pavements, two points are raised in this study. One is the type of loading, i.e., fixed or moving. The fixed point loading is consistent with static vehicles on parking lots, but it does not reflect real vehicles in motion on roads. It can be seen from Fig. 1-1, the damage of the concrete slab and soil

under the fixed-point pulsating load is absolutely localized at the positions applied the loads. In case of the moving load, the damage is distributed along the moving load directions and the fatigue damage under the moving load is clearly more critical compared to the fixed-point load. As a result, it is essential to define the characteristics of both concrete (shear, tension, and compression) and soil (shear and volumetric issues) [8]. The other point is the nonlinear fatigue interaction of soil and concrete. In fact, soil and concrete have their own fatigue lives but do differently. Currently, concrete slabs and supporting soil have been individually investigated. Thus, the mechanism of the systematized soil-concrete under high-cycle fatigue loads shall be understood in more detail [8], [16].

To meet this challenge, a series of fatigue loading experiments are arranged in this dissertation. As can be seen in Fig. 1-1 for the field of pavement engineering, the numerical investigation was systematically conducted and it is concluded that the fatigue life of concrete pavements is much shortened by the wheel-type moving loads compared to the ones under the fixed point case [16].

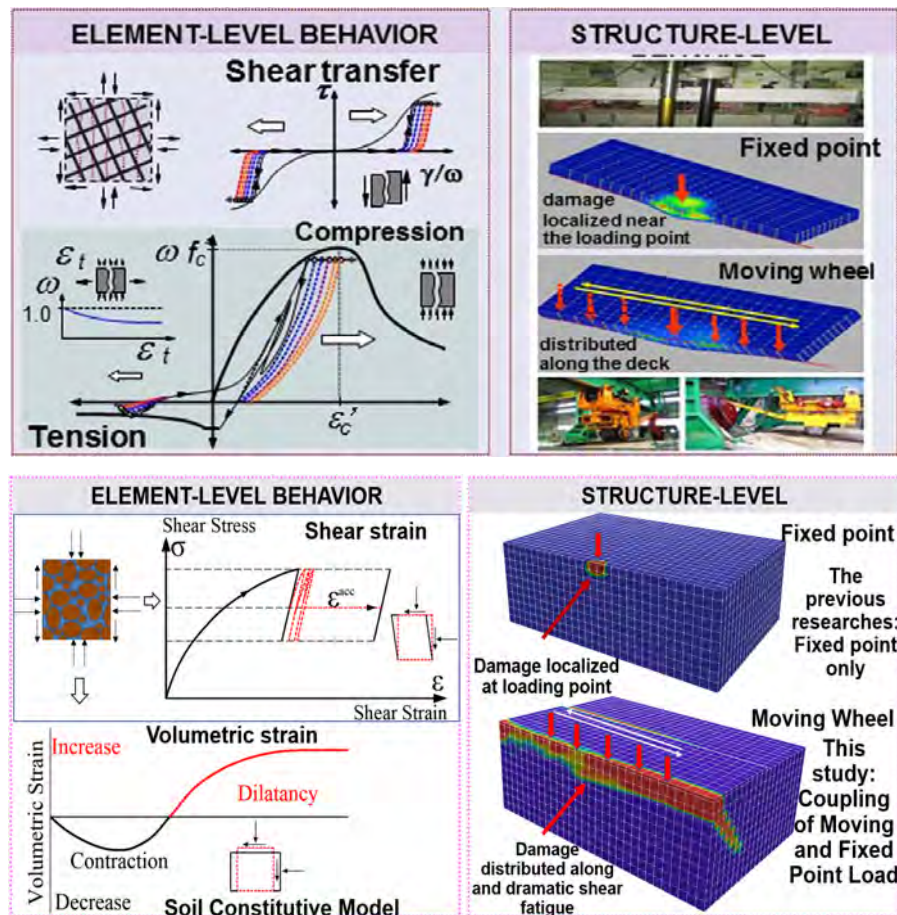


Fig. 1-1 Model scheme of concrete pavement by coupling concrete slabs and soil foundations [8].

As an analogy, let us consider concrete slabs on soil foundations. A large number of cycles is higher than 10^3 with a small relative amplitude $\varepsilon^{\text{ampl}} < 10^{-3}$ to be called as a high-cyclic or poly-cyclic loading [17]–[21]. It is a key determinant for many fields in practice where the effects of supporting foundations play an important role in serviceability as railways or high/freeways. Soil foundations and concrete pavements have been idealized as beams or plates on homogeneous plates/foundations [22]–[26] or half-space/plane layers [27]–[31], and considered as a linear continuum of one-dimensional stress states. Most of the practical works have dealt with simple models and being calibrated in the field experiments [32]. Nonlinear mechanics of soil foundation consists of elastic and plastic behavior, and it can only be dealt with utilizing constitutive models for soil. The failure mode of soil foundations in constitutive models of concrete pavements may be simultaneously attained through the elastic behavior at the low stress level and the plasticity at the high stress level near the failure. There remain some gaps between the practice and the reality of nonlinear concrete and soil foundation [33].

By utilizing the principle of slabs supported on the linear, homogeneous, elastic foundation and the concentrated truck axle loads, the philosophy to approach and predict the balanced thickness of concrete pavement slabs is therefore inappropriate in the current studies and design codes. The service life of concrete pavements is thus significantly reduced. The typical deterioration of concrete pavement slabs is shown in Fig. 1-2. To avoid these issues, two mentioned points should be considered and tackled as discussed above. The FEM analysis based on the nonlinearly coupled code of the concrete slab and soil in this dissertation aims to determine the balanced thickness for concrete pavements under the moving loads with the diversity of soil's density.



a) D-cracking



b) ASR cracking



c) Transverse cracking



d) Multiple transverse cracking



e) Longitudinal cracking



f) Broken concrete slab

Fig. 1-2 Some typical damages of concrete pavement slabs [34].

Moreover, when the cracks in concrete slabs occur, rainwater from the top surface of concrete slabs can come, easily ingress and be stagnant in the cracks as well. The stagnant water inside concrete can migrate under the deformation of the solid-concrete skeleton and cause the increase of pore pressure. The damage of the concrete slab is therefore accelerated. The cracks in the concrete slabs can open and close under the traffic wheel loads. The water pressure may be negative or positive. When the cracks close, the development of high pressure inside cracks occurs. It can cause a large internal force around the crack tips and leads to further crack propagation. The study of water coupled cracks in concrete pavements is therefore critical to define how the fatigue life and failure mode of concrete pavements change compared to the fully dry concrete slab. Figure 1-3 depicts the severe damage of the concrete slab when the stagnant water exists in the cracks.

In the field of structural design for concrete pavements, the broken dowel bars of jointed concrete pavements can be easily occurred when the joint sealant is damaged as shown in Fig. 1-4. The failure for the support of the dowel bar in the load transfer under the wheel loading is therefore reduced or equal to zero if the severe

damage takes place. The fatigue life of concrete pavements under the loss of dowel bar support is therefore essential to be investigated and compared to the continuously reinforced concrete.



Water is
stagnant inside
concrete cracks.

Fig. 1-3 Rainwater in the cracks of the slab [35].



Fig. 1-4 Damage of the sealant and dowel bar of jointed concrete pavements [34].

Finally, the strength and reinforcement ratio of concrete pavement slabs may affect the service time of concrete pavements. They can be sensitivity parameters in the studies of pavements, chiefly attributed to the cases of water coupled cracks.

1.2 Objectives / Target and Scope of the Study

As mentioned in the above background, this study aims to deeply understand the nonlinear coupling of the concrete slab and the soil foundation to determine the fatigue life and failure mode of concrete pavements under moving loads. In order to achieve this main purpose, this research includes four following objectives:

1. To investigate the nonlinear behaviors of concrete pavement slabs coupled to soil foundations subjected to the fixed-point pulsating and moving loads through experiments and nonlinear analysis.

2. To investigate the nonlinear behaviors of concrete pavements under the effects of the ambient environment, chiefly attributed to water coupled cracks.
3. To evaluate the structural design in concrete pavements through jointed and continuously reinforced concrete.
4. To propose the balanced thickness of concrete pavement slabs approached the new philosophy in nonlinear FEM analysis.

Two experimental programs were implemented in this study in accordance with these objectives:

The first experimental program studied the nonlinear behavior of the soil foundation in concrete pavements under the high-cycle fatigue wheel loading. A total of 3 specimens were conducted in this experiment. The mechanism for the shear band of the soil foundation was observed and discussed in the multi-yield surface plasticity modeling in the coupled code.

The second experimental program was to investigate the behavior of the concrete slab under the high-cycle fatigue wheel loading. A total of 3 specimens were carried on in this experiment. The mechanism for the loading types in concrete slabs, i.e fixed point and loading loads, has been observed and discussed in the multi-directional fixed crack modeling in the coupled code.

By coupling the nonlinear constitutive models for concrete slabs and soil foundations, the FEM code analysis has been verified and validated to assess the life cycle of concrete pavements.

The findings in this study are to provide a deep understanding of nonlinear behaviors of concrete slabs coupled to soil foundations, which have been considered the various affecting parameters as the strength/reinforcement ratios of concrete slabs or the diversity of soil's density. The effects of stagnant water in cracks are also discussed on the emphasis of the skeleton-pore phases of concrete. The target for this study is to revise the current design code in pavements which are based on the in-plane theory of slabs supported on the distributed elastic springs. The optimized thickness of concrete pavements slabs has been proposed based upon the nonlinearly integrated soil-slab composite.

1.3 Outline of the Dissertation

The flow of this dissertation is depicted in the form of the flowchart as shown in Fig. 1-5. The dissertation consists of eight chapters. The contents of each chapter are briefly explained as follows.

Chapter 1 introduces the background and research motivation in this study. The objectives and research methodology are also shortly described.

Chapter 2 reviews the basic knowledge of failure mechanism for concrete pavements. The principles for soil foundations, loading types and testing/equations for the fixed-point load experiments are introduced. The study for the fatigue life of the RC slab decks is demonstrated based upon high cycle fatigue for concrete. The limitations of the existing design codes for concrete pavements have been also discussed. The ambient-environmental effects in RC slab decks are reviewed on the emphasis of the reduction of life-cycle assessment.

Chapter 3 is related to the experimental and analytical programs for high cycle fatigue of concrete pavements. In this chapter, the contents are mainly divided into two sections. The first section is to explain the experimental program in detail, including experimental cases, material properties, and test specimens and devices as well as the procedure for experiments. The second section illustrates the nonlinear FEM coupled code for soil and concrete slabs. The results of the experiments are compared to the FEM analysis for the verification and validation of the coupled program.

Chapter 4 explains the mechanism of the nonlinear FEM analysis in two cases of the fixed-point and moving loads to clarify how the fatigue life and failure mode of concrete pavements change. The affecting factors of the nonlinearity of soil's density are investigated in the loose, medium dense, dense and very dense compaction. The computed S-N diagrams are also illustrated to show the reduction in life of the cases of moving wheel passages compared to the fixed-point pulsating loads.

Chapter 5 illustrates the comparison between the full-scale FEM analysis based upon the nonlinear mechanics of soil and concrete slabs under moving loads and the balanced thickness of slabs in the existing design guidelines based on the principle of

an elastic slab over a dense liquid subgrade under concentrated loads. By utilizing the nonlinear couple of soil and concrete slabs combined with the real working conditions of the traffic motion, the new philosophy in the slab thickness of pavements is approached to bridge the gap between the current design codes and engineering practices.

Chapter 6 presents the nonlinear FEM analysis of the three-dimensional high cycle fatigue for concrete pavements to investigate the influences of the existing construction joints at the transverse direction in case of the failure or no existing of the dowel bars. The comparison with the continuously reinforced concrete is also conducted. The failure mode and fatigue life of the jointed concrete slabs are reasonably observed through the FEM analysis. The sensitivity parameters are examined through a mass of slab's thickness, soil's density, and reinforcement ratios.

Chapter 7 gives information of the FEM analysis to investigate the effects of the stagnant water inside cracks of the concrete slab. The mechanism for the damage of the concrete slab when the water exists is introduced. Firstly, the critical positions of the stagnant water in the concrete slab are examined. Secondly, the effects of reinforcement ratios and soil's density are investigated, respectively. The strength of concrete is also discussed to emphasize the importance of using the high strength concrete in the pavement construction. The development of the pore water pressure and principal strain of crack inside concrete is evaluated to explain how the damage of concrete is accumulated.

Chapter 8 concludes the findings in this study. The recommendations for further studies are also given in this chapter for revising the existing guidelines in the concrete pavement design.

Chapter 1 Introduction

Background, research objectives, and outline of dissertation

Chapter 2 Literature Review

Knowledge of failure mechanism for concrete pavements, the principles of soil foundations, loading types, the fatigue life of RC slab decks, the limitations of the existing codes, the ambient-environmental effects in RC slab decks

Chapter 3 Experimental and Analytical Study for High Cycle Fatigue Interaction between Soil Foundations and Concrete Slabs under Moving Wheel-Type Loads

Explanation of experimental programs for high cycle fatigue concrete pavements
Explanation of FEM analysis for high cycle fatigue concrete pavements

Chapter 4 Failure Mechanism of Concrete Pavement – Diverse Soil's Density Coupled Moving and Fixed-Point Pulsating Loads

Nonlinear FEM analysis in fixed point and moving loads, the affecting factors of soil's density, S-N diagram for fixed point and moving loads

Chapter 5 Nonlinear FEM Analysis for the New Approach to Predict and Assess the Balanced Thickness of Concrete Pavement Slabs Response to Moving Loads

The slab thickness in existing design codes, the new proposal for the balanced thickness based on full-scale nonlinear FEM analysis

Chapter 6 Numerical Simulation of Construction-Joint Effects for Fatigue-Life Assessment of Concrete Pavements Subjected to Traveling Wheel-Type Load

Life cycle assessment of the jointed and continuously reinforced concrete

Chapter 7 Water Coupled Cracks on Life-Cycle Assessment of Concrete Pavements under Moving Loads

The mechanism for the damage of concrete slabs when the stagnant water exists, effects of the positions of stagnant water, reinforcement ratio, soil's density and strength of concrete

Chapter 8 Conclusions and Recommendations

Conclusions of the study and recommendations for further study

Fig. 1-5 Outline of the dissertation.

References in Chapter 1:

- [1] V. A. Patil, V. A. Sawant, and K. Deb, “3D Finite-element dynamic analysis of rigid pavement using infinite elements,” *Int. J. Geomech.*, vol. 13, pp. 533–544, 2013.
- [2] Y. H. Huang, *Pavement Analysis and Design*. Pearson, 2003.
- [3] C.-P. Wu and P.-A. Shen, “Dynamic Analysis of Concrete Pavements Subjected to Moving Loads,” *J. Transp. Eng.*, vol. 122 (5), pp. 367–373, 2002.
- [4] H. M. Westergaard, “Analysis of stress in concrete pavements due to variations of temperature,” in *Proceedings of 6th Annual Meeting of the Highway Research Board*, 1926, pp. 201–215.
- [5] H. M. Westergaard, “Theory of concrete pavement design,” *Proc. Highw. Res. Board*, vol. 7, no. Part 1, pp. 175–181, 1927.
- [6] H. M. Westergaard, “New Formula for Stresses in Concrete Pavement of Airfields,” *Am. Soc. Civ. Eng. ASCE*, vol. 113, pp. 425–444, 1947.
- [7] H. M. Westergaard, “Analytical Tools for Judging Results of Structural Tests of Concrete Pavements,” *Public Roads*, vol. 14 (10), pp. 185–188, 1933.
- [8] H. Q. H. Nguyen, K. Maekawa, and S. Komatsu, “Three-dimensional high-cycle fatigue simulation of soil-concrete pavement slab interaction under moving loads,” *Proc. 8th Int. Conf. Asian Concr. Fed.*, vol. 2, pp. 1207–1216, 2018.
- [9] S. Matsui, “Fatigue strength of RC-slabs of highway bridge by wheel running machine and influence of water on fatigue,” *Proc. JCI*, no. 9(2), pp. 627–632, 1987.
- [10] Y. Maeda and S. Matsui, “Fatigue of reinforced concrete slabs under trucking wheel load,” *Proc. JCI*, no. 6, pp. 221–224, 1984.
- [11] K. Maekawa, E. Gebreyouhannes, T. Mishima, and X. An, “Three-dimensional fatigue simulation of RC slabs under traveling wheel-type loads,” *J. Adv.*

Concr. Technol., 2006.

- [12] K. Maekawa, K. Toongoenthong, E. Gebreyouhannes, and T. Kishi, “Direct path-integral scheme for fatigue simulation of reinforced concrete in shear,” *J. Adv. Concr. Technol.*, vol. 4, no. 1, pp. 159–177, 2006.
- [13] K. Maekawa, T. Ishida, and T. Kishi, *Multi-scale modeling of structural concrete*. London: Taylor and Francis, 2008.
- [14] Y. Hiratsuka and K. Maekawa, “Multi-scale and multi-chemo-physics analysis applied to fatigue life assessment of strengthened bridge decks,” *XIII Int. Conf. Comput. Plast. - Appl.*, 2015.
- [15] K. Maekawa, Y. Hiratsuka, T. Ishida, and Y. Tanaka, “Numerical modeling and data assimilation for life-cycle assessment of concrete bridge structures,” *Conf. Strateg. Sustain. Concr. Struct. Brazil*, no. December, 2015.
- [16] H. Q. H. Nguyen, K. Maekawa, and S. Komatsu, “High-cycle fatigue interaction between soil foundation and concrete slab under moving wheel-type loads,” *Eng. Struct.*, 2019.
- [17] T. Wichtmann, A. Niemunis, and T. Triantafyllidis, “On the influence of the polarization and the shape of the strain loop on strain accumulation in sand under high-cyclic loading,” *Soil Dyn. Earthq. Eng.*, vol. 27, no. 1, pp. 14–28, 2007.
- [18] T. Wichtmann, A. Niemunis, and T. Triantafyllidis, “Improved simplified calibration procedure for a high-cycle accumulation model,” *Soil Dyn. Earthq. Eng.*, vol. 70, pp. 118–132, 2015.
- [19] T. Wichtmann, “Soil behaviour under cyclic loading - experimental observations, constitutive description and applications,” *Publ. Inst. Soil Mech. Rock Mech. Karlsruhe Inst. Technol.*, no. 181, 2016.
- [20] T. Wichtmann, H. a. Rondón, A. Niemunis, T. Triantafyllidis, and A. Lizcano, “Prediction of permanent deformations in pavements using a high-cycle accumulation model,” *J. Geotech. Geoenvironmental Eng.*, vol. 136, no. 5, pp.

728–740, 2010.

- [21] T. Wichtmann, A. Niemunis, and T. Triantafyllidis, “Validation and calibration of a high-cycle accumulation model based on cyclic triaxial tests on eight sands,” *Soils Found. - Japanese Geotech. Soc.*, vol. 49, no. 5, pp. 711–728, 2009.
- [22] M.-H. Huang and D. . Thambiratnam, “Deflection response of plate on Winkler foundation to moving accelerated loads,” *Eng. Struct.*, vol. 23, no. 9, pp. 1134–1141, Sep. 2001.
- [23] M.-H. Huang and D. P. Thambiratnam, “Dynamic Response of Plates on Elastic Foundation to Moving Loads,” *J. Eng. Mech.*, vol. 128, no. 9, pp. 1016–1022, Sep. 2002.
- [24] L. Sun, “Analytical dynamic displacement response of rigid pavements to moving concentrated and line loads,” *Int. J. Solids Struct.*, vol. 43, no. 14–15, pp. 4370–4383, Jul. 2006.
- [25] A. V. Kononov and R. A. M. Wolfert, “Load motion along a beam on a viscoelastic half-space,” *Eur. J. Mech. - A/Solids*, vol. 19, no. 2, pp. 361–371, Mar. 2000.
- [26] M. J. M. M. Steenbergen and A. V. Metrikine, “The effect of the interface conditions on the dynamic response of a beam on a half-space to a moving load,” *Eur. J. Mech. - A/Solids*, vol. 26, no. 1, pp. 33–54, Jan. 2007.
- [27] K. M. Rasmussen, S. R. K. Nielsen, and P. H. Kirkegaard, “Boundary element method solution in the time domain for a moving time-dependent force,” *Comput. Struct.*, vol. 79, no. 7, pp. 691–701, Mar. 2001.
- [28] V. V. Krylov, “Generation of ground elastic waves by road vehicles,” *J. Comput. Acoust.*, vol. 09, no. 03, pp. 919–933, Sep. 2001.
- [29] H.-H. Hung and Y.-B. Yang, “Elastic waves in visco-elastic half-space generated by various vehicle loads,” *Soil Dyn. Earthq. Eng.*, vol. 21, no. 1, pp. 1–17, Jan. 2001.

- [30] S.-H. Ju, “Finite element investigation of traffic induced vibrations,” *J. Sound Vib.*, vol. 321, no. 3–5, pp. 837–853, Apr. 2009.
- [31] Y. M. Cao, H. Xia, and G. Lombaert, “Solution of moving-load-induced soil vibrations based on the Betti-Rayleigh Dynamic Reciprocal Theorem,” *Soil Dyn. Earthq. Eng.*, 2010.
- [32] N. D. Beskou and D. D. Theodorakopoulos, “Dynamic effects of moving loads on road pavements: A review,” *Soil Dynamics and Earthquake Engineering*. 2011.
- [33] P. V. Lade, “Overview of constitutive models for soils,” in *ASCE Geotechnical Special Publication No. 128, Soil Constitutive Models: Evaluation, Selection, and Calibration*, 2005.
- [34] M. Ayers *et al.*, “Guide for concrete pavement distress assessments and solutions: identification, causes, prevention, and repair,” *Iwota State Univ. Natl. Concr. Pavement Technol. Cent.*, 2018.
- [35] Website, “<https://www.airalliance.it/overlay-on-concrete-pavements-is-this-a-time-effective-solution/?lang=en>.”

CHAPTER 2

LITERATURE REVIEW

2.1 Introduction

In this chapter, the review for the mechanism of the soil-slab composite system is described. The soil modelings are reviewed based on the current studies as a beam, a plate, or the top of a layered soil medium. The behavior of the soil foundations in concrete pavements is considered as a coupled system of elastic springs or a homogeneous or layered half-space with the concrete slabs. Then, the high cycle fatigue modeling for soil is discussed through some of the constitutive models. Due to the fundamentals for the high cycle fatigue of the concrete slabs based upon the investigation of RC slab decks, the high cycle fatigue life of RC slab decks is reviewed through the fixed-point and moving loads. The principles of pavement design of several design codes, including *AASHTO Guide for the Design of Pavement Structures* [1], *Thickness Design for Concrete Highway and Street Pavements* [2], *Mechanistic-empirical Pavement Design Guide* [3], *Guide for Design of Jointed Concrete Pavements for Streets and Local Roads* [4] are presented and compared. Moreover, the effects of the ambient environment on the fatigue life of RC slab decks are also reviewed.

2.2 Models of Soil Foundations in Concrete Pavements

The models for soil foundations in concrete pavements are usually assumed to be an elastic beam or a plate resting on the soil medium which may be modeled as Winkler springs or homogeneous or layered elastic or half-space medium. The foundation of concrete pavements is therefore mostly tackled under the linear elastic materials [5]. The fundamental for the pavement design is originally developed by Westergaard [6]–[10] based on the Winkler foundation or Springs Foundation in 1867 [11]. The Winkler foundation had a simple advantage for the structural analysis in engineering practices but it is maybe limited the correct in the calculation [12]. In the Winkler foundation, the subgrade is depicted by springs in which the vertical stress is directly applied to each one and there is no transmission to any adjacent spring. The

Winkler foundation can be called as one parameter model [13]. The external loads (p) is applied to any point as [14]

$$P = kw \quad (1)$$

Where, k is the modulus of subgrade reaction and w is a displacement of foundation.

The general principle for the pavement design based on the Westergaard's theory has been reviewed in some of the design book of road pavements [5] by Yoder and Witczak [15] or Huang [16].

Based on the one-parameter model of the Winkler foundation, the Filonenko-Borodich model was proposed in 1940 by applying the stretched membrane with tension T on the top of the springs as shown in Fig. 2-1. According to Ling and Zhu [17], some partial interaction between springs can be obtained by this method. In case of the Winkler foundation, k as modulus of subgrade reaction is kept as constant. Two parameters in the Filonenko-Borodich model are demonstrated as k and T (tension in the membrane per unit length).

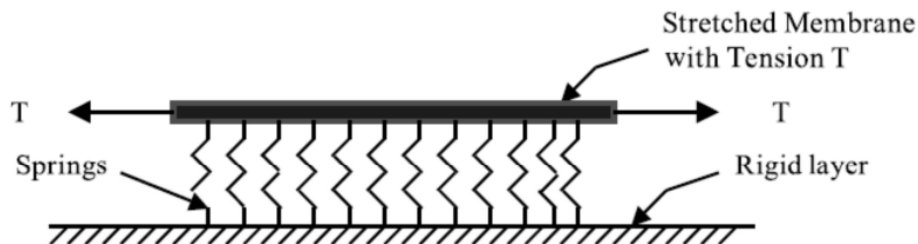


Fig. 2-1 Filonenko-Borodich for pavements [17].

The modification for the Winkler foundation can be conducted by adding some beam or plate to interact among spring elements [14]. Hetenyi has proposed the method to connect the independent spring elements by adding the beam or plate with the flexural rigidity D on the top of the springs [14][18].

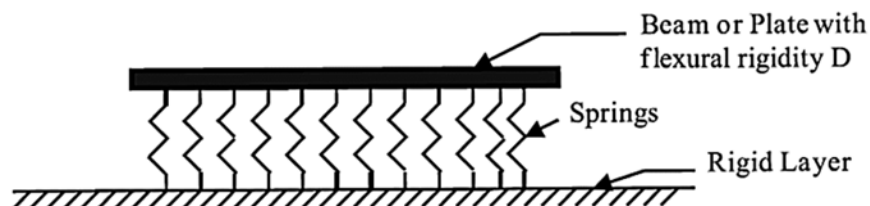


Fig. 2-2 Hetenyi foundation [18].

Pasternak (1954) demonstrated the shear interaction between the spring elements in the Winkler foundation by adding the shear layer with shear modulus G on the top of spring elements. The vertical elements were only deformed by transverse shear [14], [19].

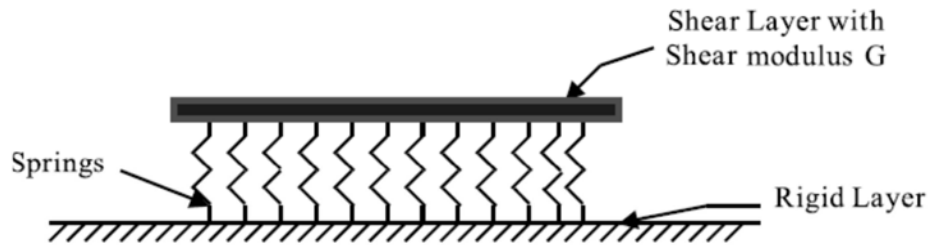


Fig. 2-3 Pasternak foundation [19].

Kerr (1965) has developed the new foundation based on Pasternak one by adding one more layer above the shear layer as shown in Fig. 2-4. This method can determine the stiffness matrix by introducing a special 8 noded, and 24 degree of freedom element [14][11][20].

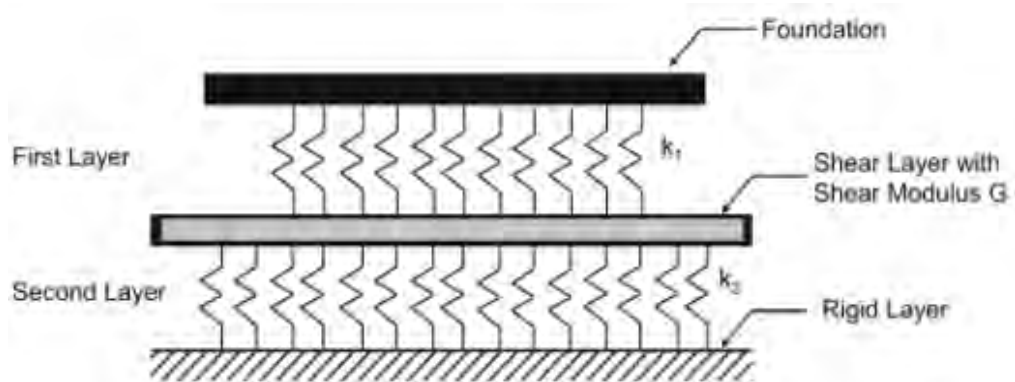


Fig. 2-4 Kerr foundation [20].

The Filoneko-Borodich, Hetenyi, and Pasternak foundation are generally developed based on the theory of the Winkler foundation [11], the continuum foundation is approached by Reissner in 1958 to avoid the horizontal displacement at the upper and lower surfaces of the foundation [14]. Based on the continuum foundation by Reissner and Pasternak foundation, Horvath (1993) has developed a beam-column-analogy foundation model as shown in Fig. 2-5. A mathematical model for a combined soil subgrade and structural element in contact with the subgrade is presented. It allows for more accurate modeling of soil-structure interaction in computation [21].

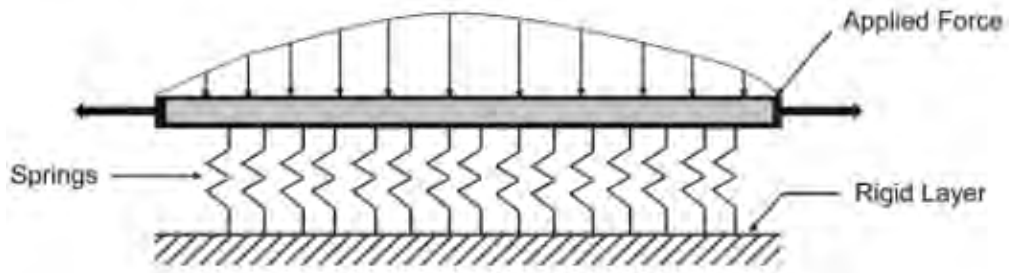


Fig. 2-5 A beam – column – analogy modeling [21].

It can be seen that the original principles for pavement designs have been developed based on the linear homogeneous elastic foundations. A practical viewpoint for the inelastic material behavior should be approached appropriately.

In the consideration of the modeling for the road, beams and plates on elastic damped or foundation of the Winkler type are firstly introduced by Keney [22], Hardy [23], Kim and Roeset [24], Huang and Thambiratnam [25], [26], Sun [27]. The dynamic pavement response presented in these studies aims to investigate the behavior of the thin slab on the elastic Winkler foundation.

In the consideration of the modeling for the road as beams and plates on homogeneous or layered half-plane or half-space, Lombaert et al. have dealt with the numerical modeling of the free field traffic-induced vibration during the passage of a vehicle on an even road. This method is calculated utilizing the boundary element method for the soil and analytical beam model the road [28]. Steenbergen and Metrikine have discussed the classical model of a beam on elastic half-space as a benchmark model. The interface between the beam and the half-space responds to the track and surrounding soil [29]. Pan and Atluri studied a finite elastic plate on an elastic half-space in both cases of an elastic foundation alone as well as a finite-sized elastic plate resting on an elastic foundation [30]. Francois et al. have dealt with the dynamic response of building due to traffic-induced wave fields. The structures supported by a slab foundation, a strip foundation, and a box foundation are calculated [31].

In the event of homogeneous or layered half-plane or half-space assuming the pavement on the top soil or the top layer, F. de Barros and J. Luco have investigated the response of a layered viscoelastic half-space to moving point load by a buried or

surface point load moving with constant speed parallel to the surface of the half-space [32]. Krylov presented the ground elastic waves caused by road vehicles. Two mechanisms approached in his study as the vehicle traveling on rough or bumpy road surfaces and acceleration and braking of road vehicles [33]. Hao and Ang presented ground vibrations induced by moving forces and propagating along the surface of an elastic homogeneous half-space [34]. Hung and Yang investigated the response of a viscoelastic half-space subjected to moving loads with static and dynamic components [35].

According to Beskou et al. [5], the modelings of the material behavior of pavement and soil are currently investigated as 1) the linear elastic material behavior for the beam or plate (for slab) and the foundation springs or half-space/plane (for soil foundation), 2) linear elastic material behavior for the slab and inelastic for half-space soil medium, 3) linear elastic behavior of the soil or some soil layers, 4) linear material for the homogeneous or layered half-plane/space. The pavement is dealt with linear elastic behavior only and rarely assumed as inelastic material behavior.

2.3 High Cycle Fatigue Modeling of Soil

Niemunis et al. have proposed the high-cycle accumulation model to predict permanent deformations or excess pore water pressures in non-cohesive soils owing to high cycles (over 10^3) and small strain amplitude ($\epsilon < 10^{-3}$) [36]. Based on this study, Wichtmann et al. have developed a set of material constants for a high-cycle accumulation model for non-cohesive soil [37]. After that, the influence of the polarization and the shape of the strain loop on strain accumulation in the sand under high-cyclic loading are proposed based on the results of cyclic triaxial tests. The direction of accumulation is affected by the polarization and the shape of the cycles [38]. The prediction and summary of the constitutive laws of soil behavior are presented by Wichtmann in [39]. The high cycle accumulation model is simplified in the calibration procedure for the well-graded sand [40]. Pasten et al. applied and combined with other models in the study of repetitive loading which can induce volumetric and shear strain accumulation in soils [41]. The comparison between the experiments and FEM analysis is still the remaining limitation in this study. The effects of the soil's density have been not yet considered in these models.

Under the traffic motion, the behavior of soil can be reflected by the volumetric and shear strain [41]. Soil is observed with elasticity at low stress levels near the isotropic stress and plasticity at higher stress levels near to failure. The behavior of soil is therefore considered by the constitutive models [42]. Based on this fundamental, the constitutive models applied under the high cycle fatigue moving loads should be composed of the nonlinear behavior of the volumetric and shear strain.

The development of a constitutive model of soil is always considered as the central topic in soil mechanics [43]. The idea for this model was originally achieved with the application of plasticity theory to soil presented by the Cam Clay model [43]. A similar idea was obtained by Towhata and Ishihara in the multi-spring model [44] or multi-yield surface plasticity. This model consists of a number of inelastic springs and each of them represents a shear mechanism in its corresponding direction [43]. Soil is assumed as a congregation of finite numbers of inelastic constituents. Nonlinear mechanics of soil in multi-yield surface plasticity consists of volumetric and shear fatigue. Many loading situations caused by earthquakes, vehicular traffic, and sea waves have been applied by utilizing the multi-yield surface plasticity modeling [45], [46]. It is therefore possible to apply this model for soil-structure interaction. Soltani and Maekawa integrated into the numerical analysis with concrete structures [47]. The formulation of an elastoplastic constitutive model for the deformation of sand can be obtained in [44], [47]–[50].

2.4 High Cycle Fatigue of Concrete Slabs

The experiments for the fatigue life of RC slab decks under the moving and fixed-point pulsating loads were firstly conducted by Maeda and Matsui [51], [52]. The results show the dramatic reduction of life under the moving loads compared to the fixed-point ones. Perdikaris et al. also considered the small-scale tests for reinforced concrete bridge decks under a fixed point and moving constant wheel-load. The moving wheel load results in far more damage than the fixed pulsating load, and the cracking pattern due to the former loading is segmental and more extensive [53]. Okada et al. investigated the fatigue failure mechanism of reinforced concrete bridge deck slabs to discuss the deflection characteristic and reserve fatigue strength of cracked slabs subjected to actual traffic loads [54]. Joh and Yoon have proposed the fatigue strength formulas in prestressed concrete slabs using the moving wheel load to

replace the formulas based on the fixed pulsating load [55]. Maekawa et al. have proposed constitutive models for concrete to show the shortened life of RC slab decks in three-dimensional fatigue simulation and check the sensitivity of this model. The concrete constitutive model has been developed as a method to investigate the fatigue mechanism by tracing the exact transient process of gradual damage under repeated loading by utilizing the direct path-integral scheme [56]–[58]. These models have been extended to the combined effects of ambient environments for the life-cycle assessment of concrete decks. By using the theory of Biot [59], [60] (multi-phase model of liquid-solid composite), the deformation and stagnant water inside concrete cracks have been coupled in crack-water interaction modeling. When the water is stagnant in cracked concrete, it can cause high pressure. It is the main reason to reduce the fatigue life of crack concrete compared to the case of the dry slab [61]–[67].

In the assessment of the fatigue life of the concrete pavement slab, there were several studies to predict the life cycle of the concrete pavement slab based on the application of fixed-point loading. It is, in practical engineering, not suitable to the real working conditions under the traffic moving [68]–[70]. Smith et al. reviewed the fatigue model for concrete pavements [71]. The results showed that all of the experimental tests have been conducted in the fixed-point loading only. Roesler et al. have carried on the large-scale airfield concrete slab fatigue tests under the fixed-point pulsating load. An S-N curve was obtained in this experiment [72], [73].

2.5 Existing Design Codes for Concrete Pavements

2.5.1 AASHTO Guide for the Design of Pavement Structures

AASHTO Guide for Design was developed based on the knowledge of engineering practices and required/assumed a lot of parameters. It is an empirical approach in the pavement design [74]–[77]. The parameters require for pavement thickness design in AASHTO Guide for Design as performance criteria, design variables, material properties for structural design, and pavement structural characteristics [1], [75]. In case of the performance criteria, initial and terminal serviceability index and serviceability loss are considered. These factors reflect the condition of pavement operation ranging from 5 (perfect condition) to 0 (impossible

to travel) [75]. The design variables present the analysis period (recommended within 50 years) and the design traffic (estimate the number of equivalent single axle loads (ESALs)). The damage of ESALs is the localized damage under a point loading as shown in Fig. 2-6. It is a key factor to revise the failure mode of concrete pavements in ASSHTO Guide for Design.

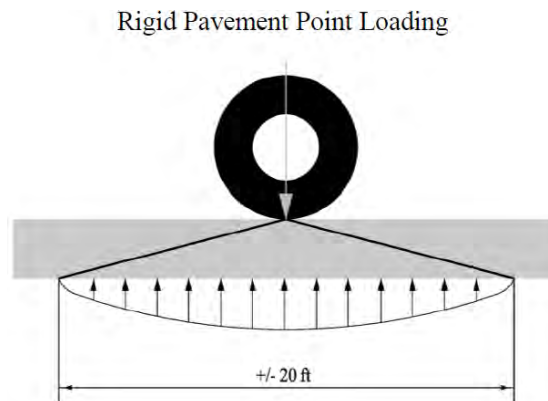


Fig. 2-6 Loading type in the study of concrete pavement in ASSHTO 1993 [1], [75].

The design variables also show the reliability of the life of the pavement. This value is 80%, 88%, or 95% for the local, collector, or arterial street, respectively. The influence of soil's density is demonstrated in material properties for structural design. In concrete pavement design, the strength of the soil is characterized by the modulus of subgrade reaction (commonly referred to "k"). The required "k" value is changed depending on the types of the subbases [1]. Finally, the pavement structural characteristics consist of the coefficient of drainage (from excellent to very poor drainage conditions), load transfer coefficients for jointed and jointed reinforced pavements, and the loss of support.

In the flowchart of the analysis process for the thickness pavement in ASSHTO 1993, the calculated ESAL value is firstly and importantly considered. As a preceding section, this value is calculated based on a point loading, and the pavement damage is solely localized under the loading.

2.5.2 Thickness Design for Concrete Highway and Street Pavements

Guideline for Thickness Design for Concrete Highway and Street Pavements was proposed by Portland Cement Association. The theoretical fundamentals of the pavement slab were based on Westergaard's theory and developed finite-element

computer analysis [2], [9], [78]. The design factors consist of the flexural strength of the concrete (modulus of rupture), the strength of the subgrade, or subgrade and subbase combination (k), the weights, frequencies, and types of truck axle loads, the design period (20 years).

Starting from the flexural strength of concrete, they are commonly made at 7, 14, 28, and 90 days. The 7-and 14-day test results are compared with specification requirements for job control and determining when pavements can be opened for traffic. The 28-day test results are commonly used for the thickness design of highways and streets. The 90-day test results are utilized for airfield designs. The subgrade-subbase strength in PCA guideline is characterized by the words as low, medium, high, and very high which are equivalent to the loose, medium dense, dense, and very dense compaction when we use the term of soil's density. The truck axle loads are described based on the categories of the stress and the average daily truck traffic. It is similar to AASHTO 1993, the truck axle loads are developed at a point loading which depicts the single or tandem axle load as shown in Fig. 2-7.

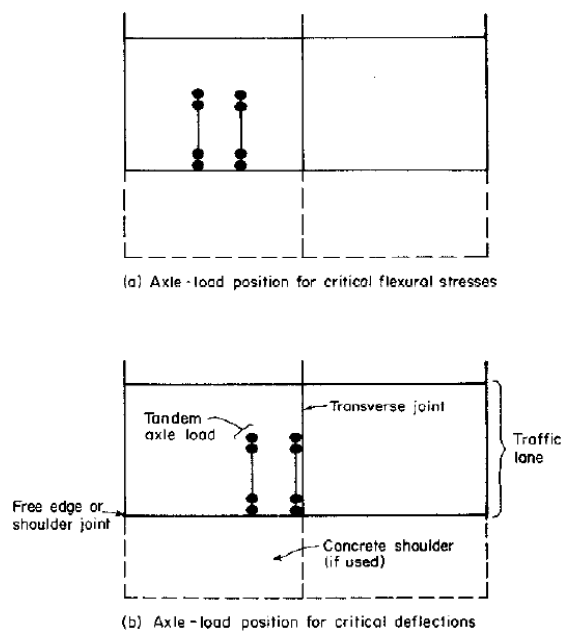


Fig. 2-7 Axle load position in PCA design guideline [2].

2.5.3 Mechanistic-Empirical Pavement Design Guide

The Mechanistic-Empirical Pavement Design Guide (MEPDG) is a new design program. It is costly and requires a great deal of data [75]. The design approach in MEPDG consists of three stages. The first stage is to develop input parameters. The

second stage is the structural or performance analysis. The third stage is the evaluation of the engineering and life cost analysis [3], [77], [79], [80]. The input parameters can be environmental effects, traffic characterization, material characterization, subgrade/foundation design, pavement structures, design reliability, etc. It is noted that instead of using equivalent single axle load (ESAL) as in AASHTO Guide for Design 1993, MEPDG requires the full axle-load spectrum traffic inputs [3], [77]. The loading type is therefore more accurate compared to AASHTO 1993 [77]. However, loading points are the typical loads in MEPDG as AASHTO 1993 or PCA. The MEPDG method does not generate a pavement thickness, it is a set-up to analyze the failure potential for a given thickness design. It is therefore complicated and not generally used by local agencies. It is due to if the program does not match the project, it should not be used [75].

2.5.4 Guide for Design of Jointed Concrete Pavements for Streets and Local Roads

The guide for Design of Jointed Concrete Pavements for Streets and Local Roads (ACI 325) is proposed for the low-volume concrete pavements based on the principles developed by Portland Cement Association and others for analyzing an elastic slab over a dense liquid subgrade. It can be applied for the jointed reinforced/plain concrete [4]. It is similar to the AASHTO 1993 and PCA, the subgrade conditions in ACI 325 are determined by the modulus of subgrade reaction k , and California Bearing ratio (CBR). This value is divided into the poor, poor to fair, fair to good, and good to excellent conditions of the soil foundation. The pavement thickness is determined based on the modulus of rupture (MOR) which depends on the concrete strength at 28 days and the traffic loads. The truck traffic loading in ACI 325 is determined by vehicle classification data and 80kN equivalent single-axle load (ESAL) factors as shown in AASHTO design procedure [4]. It means the loading type in ACI 325 is a point load and the damage is localized at a loading point only.

2.6 Conclusions for Chapter 2

In this chapter, the fundamentals for concrete pavement design have been reviewed approached to the principles for the elastic, homogeneous, linear foundations. There are rarely studies in the inelastic foundation of the soil pavements.

The principles in existing design codes are originally developed based on Westergaards and elastic dense springs. The loading types are the concentrated point of the truck axles. It can not reflect the real working conditions of traffic motions. Moreover, the assessment of high cycle fatigue life has not yet coupled to demonstrate the soil-slab composite interaction. The high cycle fatigue of soil or concrete slabs is represented separately in a few studies. In the end, when the stagnant water exists in the cracked concrete, it can cause the high pore pressure and accelerate the damage of the slabs. The life cycle of the pavement is thus dramatically reduced. This ambient-environmental effects in pavements have not been discussed in previous studies.

References in Chapter 2:

- [1] AASHTO, *AASHTO Guide for Design of Pavement Structures*. 1993.
- [2] P. C. Association, *Thickness design for concrete highway and street pavements*. 1984.
- [3] AASHTO, *Mechanistic Empirical Pavement Design Guide: A Manual Practice*. 2008.
- [4] ACI 325, *Guide for design of jointed concrete pavements for streets and local roads*. ACI Committe 325, 2002.
- [5] N. D. Beskou and D. D. Theodorakopoulos, “Dynamic effects of moving loads on road pavements: A review,” *Soil Dynamics and Earthquake Engineering*. 2011.
- [6] H. M. Westergaard, “Analysis of stress in concrete pavements due to variations of temperature,” in *Proceedings of 6th Annual Meeting of the Highway Research Board*, 1926, pp. 201–215.
- [7] H. M. Westergaard, “New Formula for Stresses in Concrete Pavement of Airfields,” *Am. Soc. Civ. Eng. ASCE*, vol. 113, pp. 425–444, 1947.
- [8] H. M. Westergaard, “Analytical Tools for Judging Results of Structural Tests of Concrete Pavements,” *Public Roads*, vol. 14 (10), pp. 185–188, 1933.
- [9] H. M. Westergaard, “Theory of concrete pavement design,” *Proc. Highw. Res. Board*, vol. 7, no. Part 1, pp. 175–181, 1927.
- [10] H. M. Westergaard, “Analysis of stresses in concrete roads,” in *Proceedings of the Highway Research Board*, 1926, vol. 5, pp. 90–112.
- [11] A. D. Kerr, “Elastic and viscoelastic foundation models,” *J. Appl. Mech. Trans. ASME*, 1964.
- [12] J. S. Horvath, “New subgrade model applied to mat foundations,” *J. Geotech. Eng.*, 1983.

- [13] R. O. Davis and A. P. S. Selvadurai, *Elasticity and geomechanics*. 1996.
- [14] H. Bing Sii, “Three-dimensional finite element analysis of concrete pavement on weak foundation,” Griffith University, 2014.
- [15] E. J. Yoder and M. W. Witczak, *Principles of Pavement Design*. 1975.
- [16] Y. H. Huang, *Pavement Analysis and Design*. Pearson, 2003.
- [17] R. Y. Liang and J. X. Zhu, “Dynamic analysis of infinite beam on modified vlasov subgrade,” *J. Transp. Eng.*, 1995.
- [18] M. Hetényi, “A general solution for the bending of beams on an elastic foundation of arbitrary continuity,” *J. Appl. Phys.*, 1950.
- [19] P. L. Pasternak, “On a New Method of Analysis of an Elastic Foundation by Means of Two Foundation Constants,” *Gos. Izd. Lit. po Stroit. I Arkhitecture*, Jul. 1954.
- [20] A. D. Kerr, “A study of a new foundation model,” *Acta Mech.*, 1965.
- [21] J. S. Horvath, “Beam-column-analogy model for soil-structure interaction analysis,” *J. Geotech. Geoenvironmental Eng.*, 1993.
- [22] J. T. Kenney, “Steady-state vibrations of beam on elastic foundation for moving load,” *J. Appl. Mech. ASME*, 1954.
- [23] M. S. A. Hardy, “The generation of waves in infinite structures by moving harmonic loads,” *J. Sound Vib.*, 1995.
- [24] S. M. Kirn and J. M. Roesset, “Moving loads on a plate on elastic foundation,” *J. Eng. Mech.*, 1998.
- [25] M.-H. Huang and D. P. Thambiratnam, “Dynamic Response of Plates on Elastic Foundation to Moving Loads,” *J. Eng. Mech.*, vol. 128, no. 9, pp. 1016–1022, Sep. 2002.
- [26] M.-H. Huang and D. . Thambiratnam, “Deflection response of plate on Winkler foundation to moving accelerated loads,” *Eng. Struct.*, vol. 23, no. 9, pp. 1134–

1141, Sep. 2001.

- [27] L. Sun, “Analytical dynamic displacement response of rigid pavements to moving concentrated and line loads,” *Int. J. Solids Struct.*, vol. 43, no. 14–15, pp. 4370–4383, Jul. 2006.
- [28] G. Lombaert, G. Degrande, and D. Clouteau, “Numerical modelling of free field traffic-induced vibrations,” *Soil Dyn. Earthq. Eng.*, 2000.
- [29] M. J. M. M. Steenbergen and A. V. Metrikine, “The effect of the interface conditions on the dynamic response of a beam on a half-space to a moving load,” *Eur. J. Mech. - A/Solids*, vol. 26, no. 1, pp. 33–54, Jan. 2007.
- [30] G. Pan and S. N. Atluri, “Dynamic response of finite sized elastic runways subjected to moving loads: A coupled BEM/FEM approach,” *Int. J. Numer. Methods Eng.*, 1995.
- [31] S. François, L. Pyl, H. R. Masoumi, and G. Degrande, “The influence of dynamic soil-structure interaction on traffic induced vibrations in buildings,” *Soil Dyn. Earthq. Eng.*, 2007.
- [32] F. C. P. de Barros and J. E. Luco, “Response of a layered viscoelastic half-space to a moving point load,” *Wave Motion*, 1994.
- [33] V. V. Krylov, “Generation of ground elastic waves by road vehicles,” *J. Comput. Acoust.*, vol. 09, no. 03, pp. 919–933, Sep. 2001.
- [34] H. Hao and T. C. Ang, “Analytical modeling of traffic-induced ground vibrations,” *J. Eng. Mech.*, 1998.
- [35] H.-H. Hung and Y.-B. Yang, “Elastic waves in visco-elastic half-space generated by various vehicle loads,” *Soil Dyn. Earthq. Eng.*, vol. 21, no. 1, pp. 1–17, Jan. 2001.
- [36] A. Niemunis, T. Wichtmann, and T. Triantafyllidis, “A high-cycle accumulation model for sand,” *Comput. Geotech.*, 2005.
- [37] T. Wichtmann, A. Niemunis, and T. Triantafyllidis, “On the determination of a

- set of material constants for a high-cycle accumulation model for non-cohesive soils,” *Int. J. Numer. Anal. Methods Geomech.*, 2010.
- [38] T. Wichtmann, A. Niemunis, and T. Triantafyllidis, “On the influence of the polarization and the shape of the strain loop on strain accumulation in sand under high-cyclic loading,” *Soil Dyn. Earthq. Eng.*, vol. 27, no. 1, pp. 14–28, 2007.
- [39] T. Wichtmann, “Soil behaviour under cyclic loading - experimental observations, constitutive description and applications,” *Publ. Inst. Soil Mech. Rock Mech. Karlsruhe Inst. Technol.*, no. 181, 2016.
- [40] T. Wichtmann, A. Niemunis, and T. Triantafyllidis, “Improved simplified calibration procedure for a high-cycle accumulation model,” *Soil Dyn. Earthq. Eng.*, vol. 70, pp. 118–132, 2015.
- [41] C. Pasten, H. Shin, and J. Carlos Santamarina, “Long-term foundation response to repetitive loading,” *J. Geotech. Geoenvironmental Eng.*, 2014.
- [42] P. V. Lade, “Overview of constitutive models for soils,” in *ASCE Geotechnical Special Publication No. 128, Soil Constitutive Models: Evaluation, Selection, and Calibration*, 2005.
- [43] S. Nishimura and I. Towhata, “A three-dimensional stress-strain model of sand undergoing cyclic rotation of principal stress axes,” *Soils Found.*, 2004.
- [44] I. Towhata and K. Ishihara, “Modeling soil deformation undergoing cyclic rotation of principal stress axes,” *Proc. 5th Int. Conf. Numer. Method Geomech.*, pp. 523–530, 1985.
- [45] M. Gutierrez, K. Ishihara, and I. Towhata, “Model for the deformation of sand during rotation of principal stress directions,” *Soils Found. - Japanese Geotech. Soc.*, vol. 33(3), pp. 105–117, 2011.
- [46] K. Ishihara, “Soil response in cyclic loading induced by earthquakes, traffic and waves,” in *7th Asian Reg. Conf. on Soil Mechanics and Foundations Engineerings*, 1983, pp. 42–66.

- [47] M. Soltani and K. Maekawa, “Numerical simulation of progressive shear localization and scale effect in cohesionless soil media,” *Int. J. Non. Linear Mech.*, vol. 69, pp. 1–13, 2015.
- [48] I. Towhata, *Geotechnical earthquake engineering*. Germany: Springer, 2008.
- [49] I. Towhata and K. Ishihara, “Modelling soil behavior under principal stress axes rotation,” 1985.
- [50] I. Towhata and K. Ishihara, “Undrained strength of sand undergoing cyclic rotation of principal stress axis,” *Soils Found. - Japanese Geotech. Soc.*, vol. 25(2), pp. 135–147, 1985.
- [51] S. Matsui, “Fatigue strength of RC-slabs of highway bridge by wheel running machine and influence of water on fatigue,” *Proc. JCI*, no. 9(2), pp. 627–632, 1987.
- [52] Y. Maeda and S. Matsui, “Fatigue of reinforced concrete slabs under trucking wheel load,” *Proc. JCI*, no. 6, pp. 221–224, 1984.
- [53] P. C. Perdikaris and S. Beim, “RC bridge decks under pulsating and moving load,” *J. Struct. Eng. (United States)*, 1988.
- [54] K. Okada, H. Okamura, and K. Sonoda, “Fatigue failure mechanism of reinforced concrete bridge deck slabs,” *Transp. Res. Rec.*, 1978.
- [55] C. Joh and H. Yoon, “Fatigue strength evaluation of presressed concrete slabs using moving wheel load,” in *Real Structures: Bridges and Tall Buildings - Proceedings of the 10th East Asia-Pacific Conference on Structural Engineering and Construction, EASEC 2010*, 2006.
- [56] K. Maekawa, N. Fukuura, and M. Soltani, “Path-dependent high cycle fatigue modeling of joint interfaces in structural concrete,” *J. Adv. Concr. Technol.*, vol. 6, no. 1, pp. 227–242, 2008.
- [57] K. Maekawa, E. Gebreyouhannes, T. Mishima, and X. An, “Three-dimensional fatigue simulation of RC slabs under traveling wheel-type loads,” *J. Adv. Concr. Technol.*, vol. 4, no. 3, pp. 445–457, 2006.

- [58] K. Maekawa, K. Toongoenthong, E. Gebreyouhannes, and T. Kishi, “Direct path-integral scheme for fatigue simulation of reinforced concrete in shear,” *J. Adv. Concr. Technol.*, vol. 4, no. 1, pp. 159–177, 2006.
- [59] M. A. Biot, “General theory of three-dimensional consolidation,” *J. Appl. Phys.*, pp. 155–164, 1941.
- [60] M. A. Biot, “Theory of elasticity and consolidation for a porous anisotropic solid,” *J. Appl. Phys.*, vol. 26(2), pp. 182–185, 1955.
- [61] K. Maekawa and C. Fujiyama, “Crack water interaction and fatigue life assessment of RC bridge decks,” *Poromechanics V ASCE 2013*, pp. 2280–2289, 2013.
- [62] K. Maekawa, T. Ishida, N. Chijiwa, and C. Fujiyama, “Multiscale coupled-hygro-mechanistic approach to the life-cycle performance assessment of structural concrete,” *J. Mater. Civ. Eng.*, vol. 27, no. 2, pp. A4014003-1–9, 2015.
- [63] K. Maekawa and C. Fujiyama, “Rate-dependent model of structural concrete incorporating kinematics of ambient water subjected to high-cycle loads,” *Eng. Comput. (Swansea, Wales)*, vol. 30(6), pp. 825–841, 2013.
- [64] A. Shinmura and V. E. Saouma, “Fluid fracture interaction in pressurized reinforced concrete vessels,” *Mater. Struct. Constr.*, vol. 30, pp. 72–80, 1997.
- [65] C. Fujiyama, “Fatigue life simulation of RC members subjected to coupled moving wheel-type load and moisture,” in *7th fib PhD Symposium in Stuttgart, Germany*, 2008.
- [66] H. J. Gilkey, “The effect of varied curing conditions upon the compressive strength of mortar and concrete,” in *Proceedings of ACI*, 1926, pp. 395–436.
- [67] H. Matsushita, H. and Onoue, “Moisture content dependency of the strength of cement based materials from the viewpoint of surface energy,” *Annu. Rep. Cem. Technol.*, vol. 35, pp. 130–133, 2006.
- [68] H. Q. H. Nguyen, K. Maekawa, and S. Komatsu, “Three-dimensional high-

- cycle fatigue simulation of soil-concrete pavement slab interaction under moving loads,” *Proc. 8th Int. Conf. Asian Concr. Fed.*, vol. 2, pp. 1207–1216, 2018.
- [69] H. Q. H. Nguyen, K. Maekawa, and S. Komatsu, “Numerical simulation of construction-joint effects for fatigue-life assessment of concrete pavement subjected to traveling wheel-type load,” *Proc. Japan Concr. Inst.*, vol. 41, pp. 1397–1402, 2019.
- [70] H. Q. H. Nguyen, K. Maekawa, and S. Komatsu, “Effects of water-coupled cracks on life-cycle assessment of concrete pavement under moving load,” *Proc. Airf. Highw. Pavements*, pp. 110–121, 2019.
- [71] K. D. Smith and J. R. Roesler, “Review of fatigue models for concrete airfield pavement design,” in *Airfield Pavement Conference Proceedings*, 2003.
- [72] J. R. Roesler, J. E. Hiller, and P. C. Littleton, “Large-scale airfield concrete slab fatigue tests,” in *Proceedings - 8th International Conference on Concrete Pavements: Innovations for Concrete Pavement: Technology Transfer for the Next Generation*, 2005.
- [73] J. R. Roesler, “Fatigue resistance of concrete pavements,” in *6th International DUT-Workshop on Fundamental Modelling of Design and Performance of Concrete Pavements*, 2006.
- [74] T. Jenjiwattanakul and K. Sano, “Pavement thickness design thresholds of having doveled joints and concrete shoulders,” in *Proceedings of the Eastern Asia Society for Transportation Studies*, 2011, p. Vol 8.
- [75] IOWA, *Design Manual - Chapter 5 - Roadway design*. 2019.
- [76] N. J. Delatte, *Concrete pavement design, construction, and performance, second edition*. 2014.
- [77] Q. Li, D. X. Xiao, K. C. P. Wang, K. D. Hall, and Y. Qiu, “Mechanistic-empirical pavement design guide (MEPDG): A bird’s-eye view,” *J. Mod. Transp.*, 2011.

- [78] P. G. and G. K. Ray, “Influence charts for concrete pavements,” *Am. Soc. Civ. Eng. Trans.*, vol. 116, no. 2425, 1951.
- [79] N. Delatte, “Mechanistic-Empirical Pavement Design Guide,” in *Concrete Pavement Design, Construction, and Performance, Second Edition*, 2014.
- [80] J. Melorose, R. Perroy, and S. Careas, “Guide for Mechanistic-Empirical Design,” *Statew. Agric. L. Use Baselin*, 2015.

CHAPTER 3

EXPERIMENTAL AND ANALYTICAL STUDY FOR HIGH-CYCLE FATIGUE INTERACTION BETWEEN SOIL FOUNDATIONS AND CONCRETE SLABS UNDER MOVING WHEEL-TYPE LOADS

3.1. Introduction

This chapter depicts the outline and summary of the experiments and analyses of the high cycle fatigue for concrete pavements. The main objective of this chapter is to demonstrate the validation and verification of the coupled code program utilized in the numerical analyses of the soil and concrete slab interaction. The test program consists of six specimens that were implemented under the high cycle fatigue moving loads. The required parameters are carefully decided based on the understanding and knowledge at the sites and the previous works. The results of these experiments will be compared to the analytical simulation to verify the coupled code. The content of this chapter describes the outline for experiments, details of the testing specimens, the explanation for the test procedure and results of each experiment, the verification of the nonlinearly coupled code, and the FEM analytical results.

Nonlinear behaviors of soil under high-cyclic loading have been scrutinized by Wichtmann et al. [1]–[5]. By referring to this experiment, the small-scale mock-ups for concrete pavement were conducted by using wheel-track loading facilities [6]. The main objective of this experiment is to clarify the failure mode of combined concrete and soils. Here, failure modes are divided into the part of the soil and the one for concrete slab, respectively. It is clearly seen that the thickness of slabs is a key factor because the fatigue life is comparatively less dependent on the strength of concrete within the range of normal use. In the coupling case of the thick concrete slab with normally compacted soil, the failure of the coupled system was thought to be localized first in the soil foundation with the shear band prior to the failure of concrete

pavement. In contrast, if the thin concrete slab interacts with soil, it is thought that concrete slabs are easily deteriorated prior to the failure of soil.

To obtain the above target, modeling of the high-cycle fatigue interaction between the concrete slab and soil is presented and validated with small-scale mock-ups of pavement. By investigating the sensitivity of influencing factors, a number of key specimens are selected (six ones). After that, the integrated nonlinear analysis was performed for validation. Finally, numerical analyses were carried on.

3.2 Experimental Program

3.2.1 Experimental Cases and Test Specimens

Two types of concrete slabs on soil were made as shown in Fig. 3-1. In consideration of the size of testing beds and the size-effect of structures, the concrete slab was decided to be 300x150mm in plane and 50mm and 20mm in thickness, respectively.

The selection of the specimen dimensions was decided in accordance with the specifications of the wheel load testing equipment as well as the size effects of soil and concrete slabs. The size effect of the nominal shear strength of concrete slab is inconsiderable and normally less than 10% for the case of 5 times size difference. This nominal bearing strength of soil foundation is commonly less than 20% with the shear band of soil for about 5 time scale difference. The selected scale factor of specimens in this study is 1:5 due to the satisfaction of the size effects of the soil and the slab thickness in practices. The slab thickness of 50mm and 20mm was selected based on the model's scale factor for the purpose of observing the shear band of the soil foundation and the damage of the concrete slab, respectively. Moreover, the maximum coarse aggregate is normally used with a diameter of 20mm in practices. The models are expected to qualitatively reflect the real scale of the concrete pavement, and the objective of this chapter to validate the analysis method will be achieved by accepting the possible deviation of 20% of the capacity.

The track length of the running-wheel was 150mm and applied at the center along the longitudinal direction of slabs. The speed of the moving wheel was kept constant at 21 round trips per minute until 75,220 cycles of the capacity of testing

facilities. The speed and the track length of the wheel were followed to the specifications of the wheel load testing equipment. It is equivalent to 20km/h of the real scale tests. The first cycle started when the moving wheel load was applied at the slab center and continuously run until back to the original position. Such a loading was applied so as to minimize the instability when the moving load came nearby the edge of slabs.

Sandy soil from Ohigawa river was set up inside a formwork having transparent plastic walls so that we may observe the shear failure bands as shown in Fig. 3-2. There were two steel bars to prevent the bending of the plastic side walls caused by soil consolidation driven by the moving loads. The dimension of the soil box was similar to two cases of experiments as 300x360mm in plane and 200mm in depth. As these experiments were conducted under 1-g gravity, strictly speaking, the confinement stress to the soil mockup of small scale does not coincide with the reality of the larger sizes unless the centrifuge test is conducted. On the other hand, the major stress field is produced by the bearing action though the concrete slab on the shallow soil close to the surface, where the gravity action is comparatively less than that of the deep location of the foundation. Then, the size effect related to the gravity and associated confinement is thought to be less than the cases of massive soil structures. Details of experimental models can be referred in Fig. 3-1.

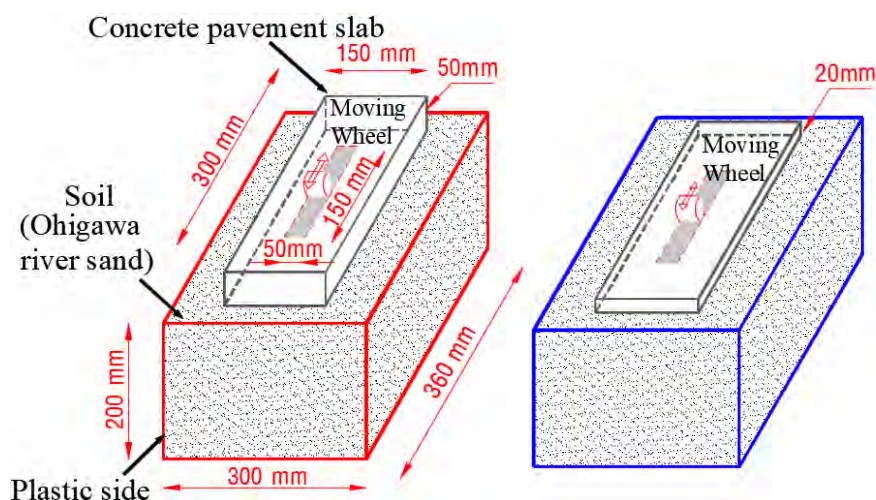


Fig. 3-1 Two modelings for concrete pavement experiments.



Fig. 3-2 Sand formwork for experiment.

These experiments have been carried out under similar conditions at the site. The property of concrete slabs was specified as the normal use (water to cement ratio by weight: $W/C=55\%$) and the relative density (RD) of soil was selected for the loose foundation (RD 50%) and the dense one (RD 75%) as a primary factor. The selection of $W/C=55\%$ is based on the recommendation of the durability and economical consideration for the paving mixtures of the normal concrete in ACI 325. The compaction of the supporting soil was implemented by dividing four layers in 200mm. Each layer was 50mm in depth and the weight of sand to obtain RD 50% or RD 75% could be defined. The compaction was conducted so that the surface of each layer reached the target white line as illustrated in Fig. 3-3. We have totally six experiments (three for 50mm thickness of the concrete slab and three for 20mm).

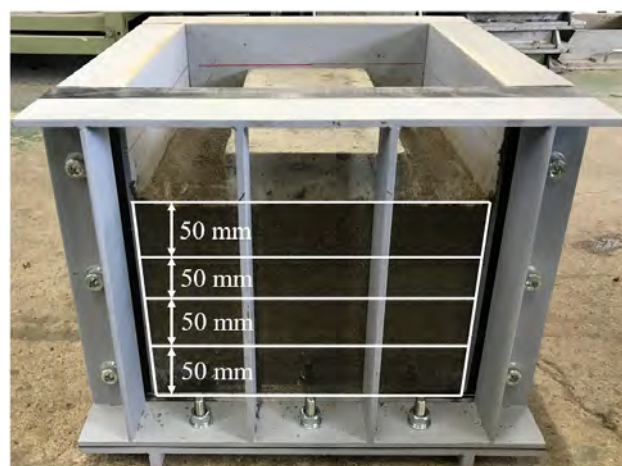


Fig. 3-3 Sand preparation for experiment.

3.2.2 Testing Devices for the Experiments

We can set up three specimens at one time and apply the moving loads simultaneously by the track loading facility as shown in Fig. 3-4. The center of the moving wheel coincides with the centroid of the soil-concrete system. After the loading, the failure mode of the coupled model was examined. The wheel-track moving load of three positions was first applied contemporaneously. After the failure of the weakest specimens, we continued the loading to the other remaining ones until the final failure.

The total displacements of concrete slabs and soils were measured to judge fatigue life. The maximum total displacement of facilities measured on the top of the machine (see Fig. 3-5) is 40mm based on the specifications of the wheel load testing equipment through the displacement transducers located at the top of the machine. As the soil and concrete slab have interacted under the moving wheel load, the total displacements are measured. When the large displacement took place over the limit, the machine stopped automatically and the moving wheel returned to its original position, and the test restarted after re-mounting displacement transducers. Data acquisition was automatic to include the number of cycles, duration for loading (days), displacement of specimens at position No.1-No.3 (mm), and the temperature of air or water ($^{\circ}\text{C}$), respectively.



Fig. 3-4 Facilities for small-scale experiments of concrete pavements.



Fig. 3-5 Deflection gauge.

3.2.3 Materials

The mix proportion of concrete used for the slabs is summarized in Table 3-1. The maximum size of coarse and fine aggregates was 20mm and 5mm, respectively. Concrete compressive strength was 33 N/mm². This is an average value from the compression tests of three samples after curing. The air content was 2.8% by volume. The slump value was 13cm as normal use in practice. Dry sandy soil was used in the pavement experiments from Ohigawa river. The relative density (RD) was adjusted to 50% and 75%, and the specific weight was 2.62, and the void ratio was 0.652.

Table 3-1 Mix proportion of concrete

W/C (%)	water (kg/m ³)	cement (kg/m ³)	gravel (max. size =20mm) (kg/m ³)	sand (kg/m ³)	superplasticizer (kg/m ³)
55.0	164	300	1005	801	1.5

3.2.4 Testing Implementation

Figure 3-6 summarizes the testing process at three positions in case of the slab thickness of 50mm. To investigate the impact of load levels on fatigue life, two levels of magnitude were applied as 1,029N and 513N, respectively. At the first position, the wheel-type load was 1,029N and RD of the supporting soil was 75%. This load level was similar to the third position but its relative density was 50%. At the second

position, the load was reduced to 513N (almost half) and it was also investigated as the weakest case of soil foundation of RD=50%. The wheel track length was immutable at three positions (15cm). As previously mentioned, the total number of cycles was 75,220 and it took more two days for machine operation.

For comparison in terms of the thickness of slabs, the moving-wheel experiment of the thickness of 20mm was also carried out as shown in Fig. 3-7. As the objective of this experiment is to examine the failure mode, the load magnitude of 98N was added at position 2 and position 3 after completing 75,220 cycles. By presiding over six experiments as above, all cases of soil-concrete slab interaction under moving load were completed. The failure mode of the concrete slab, the soil foundation as well as the sensitivity of load levels and the strength of concrete were clarified as the following chapters.

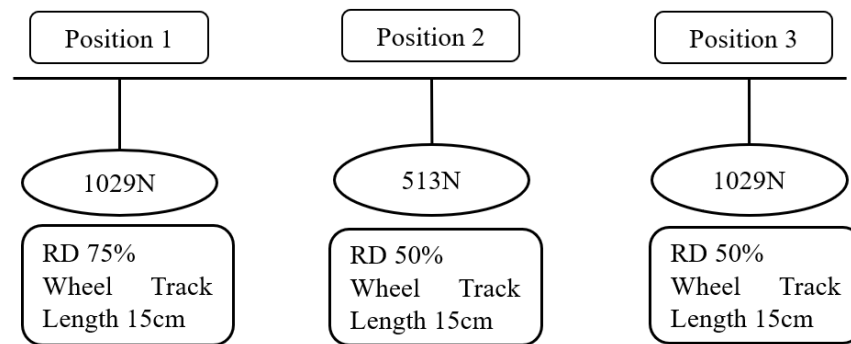


Fig. 3-6 Summary of testing implementation for thickness slab 50mm.

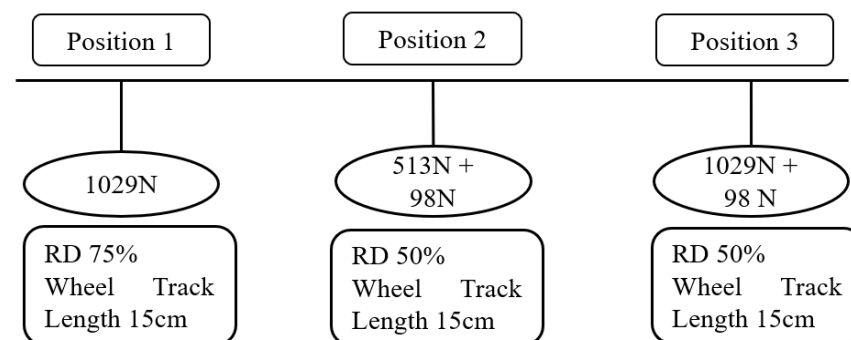


Fig. 3-7 Summary of testing implementation for thickness slab 20mm.

3.3 Nonlinear FEM Analysis Program

For investigating the failure mechanism of the coupled soil and structural concrete, we utilize the nonlinear analysis which has been applied for RC bridge

decks [7]. This model was capable of predicting the shortened fatigue life of the slabs under moving loads than the fixed-point pulsation. The code used in this study is based upon the combined thermodynamic and structural mechanics model [7]–[10] which has been experimentally validated [8]. This code has been mainly utilized for performance assessment of existing structures under the ambient environments and remaining fatigue life [10]. The coupled numerical code has been examined from micro-scales to mesoscales, chiefly in high-cyclic fatigue behaviors of RC slab decks under the moving loads [11] and the shear band formation of the soil foundation [12]. In this chapter, development and experimental validation for the upgraded code are presented by using small-scale mock-ups of concrete pavements.

3.3.1 Multi-Directional Fixed Crack Modeling for High-Cycle Fatigue

The multi-directional fixed crack modeling is summarized in Fig. 3-8. The direct integral of path-dependent constitutive models is applied to simulate the dynamic responses of concrete structures. Maekawa et al. have added the cyclic degradation factor as incremental plasticity and damaging to express high-cycle fatigue damages [13]. One-dimensional stress-strain relations of concrete in compression, tension, and shear are combined to build the 3D space-averaged constitutive model. Each constituent modeling is time-strain path-dependent. Tension and shear models have to be aggrandized to make allowance for the cumulative fatigue damage.

Let us start from the process of assigning orthogonal coordinates to the cracked concrete domain. When the first crack appears in a finite element, the crack coordinate (x-axis) is set up normal to crack plane. If the second, third or fourth crack occur, they will be tackled the same method as the first one. In the case of the RC element with four-way cracks, there are four different regions to be defined with respect to the direction of the first crack. It depends on the position of the crack in each region, the quasi-orthogonal or non-orthogonal direction of crack can be determined [14]. A pair of quasi-orthogonal cracks with the first coordinate will form the non-orthogonal crack plane associated with the other pair with the second coordinate [14]. There are two types of coordinate originated on crack which are called active and dormant. The largest width of cracks among existing cracks is assigned to be an active crack and the other is dormant one which does not bear chief

nonlinearity. If a non-orthogonal relation is formed by two cracks, the shear strain is only caused by the active crack. The outline of the multi-directional fixed crack model and the above explanation are summarized in Fig. 3-9 [14].

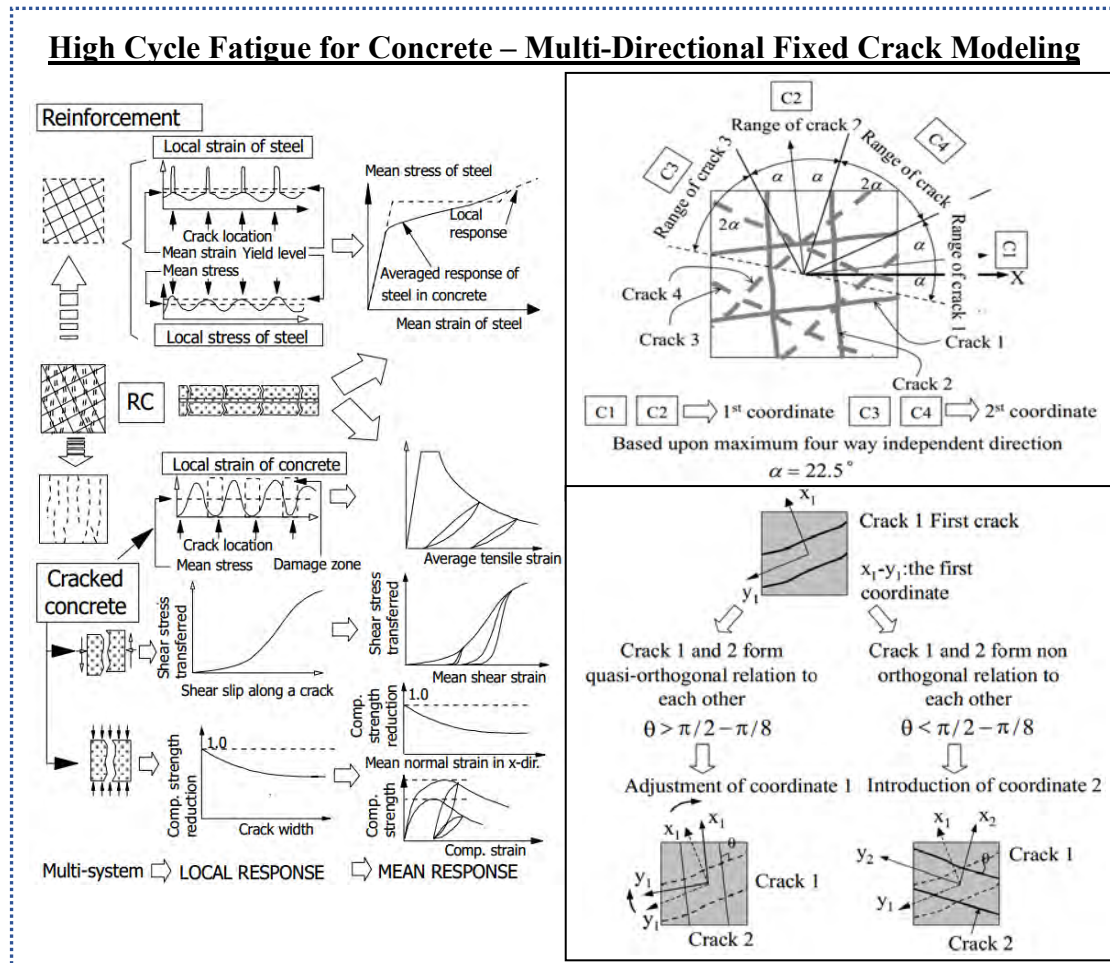


Fig. 3-8 Scheme of constitutive laws for the concrete slab [11], [13], [14].

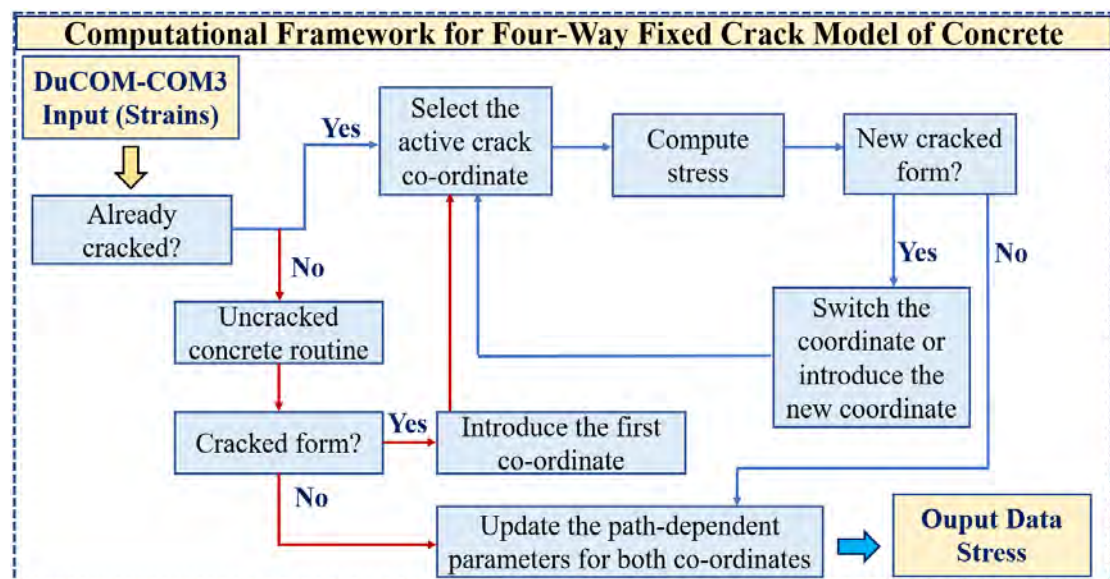


Fig. 3-9 Outline of the multi-directional fixed crack model in concrete structures [14].

To consider the time-dependent high cycle damaging, the fracture parameter K_C is defined in the compression model. This value shows the capacity to store the elastic strain energy, and the elastic strain path controls the damage evolution. Damage under high cyclic compression is expressed by the fracture degradation rate (λ) [15], [16]. For tension, the tensile fracture parameter K_T is a scalar to stand for path-dependent instantaneous fracture, time-dependent creep and accumulation of fatigue damage [13]. Parameter X is assumed as fatigue damage of shear transfer based upon the contact density model and formulated by Gebreyouhannes [15]–[17]. Factors related to fatigue of the concrete model are lined up in Fig. 3-10 and summarized in the following section.

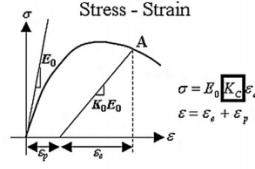
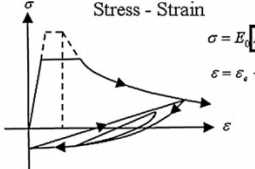
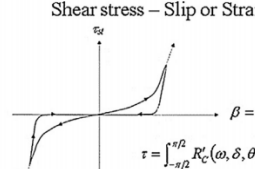
	Compression	Tension	Shear
Core Constitutive Laws	 <p>Stress - Strain</p> <p>Maekawa et al. 2003</p>	 <p>Stress - Strain</p> <p>Maekawa et al. 2003</p>	 <p>Shear stress – Slip or Strain</p> <p>Maekawa et al. 2003</p>
Enhanced model for high cycle fatigue	<p>Fracture parameter K_C considers time dependent plasticity & fracturing and cyclic fatigue damage</p> $dK_C = \left(\frac{\partial K_C}{\partial t} \right) dt + \left(\frac{\partial K_C}{\partial \varepsilon_e} \right) d\varepsilon_e$ <p>Time dependency Cyclic fatigue</p> $\left(\frac{\partial K_C}{\partial \varepsilon_e} \right) = \lambda \sim \text{when } F_k > 0$ $\left(\frac{\partial K_C}{\partial \varepsilon_e} \right) = - \left(\frac{\partial F_k}{\partial \varepsilon_e} \right) \left(\frac{\partial F_k}{\partial K} \right) + \lambda \sim \text{when } F_k = 0$ $\lambda = K^3 \cdot (1 - K^4) \cdot g \cdot R$ <p>El-Kashif and Maekawa 2004</p>	<p>Fracture parameter K_T considers time dependent fracturing and cyclic fatigue damage</p> $dK_T = F dt + G d\varepsilon_e + H d\varepsilon_e$ <p>Time dependent fracturing Cyclic fatigue damage</p> <p>Maekawa et al. 2003, Hisasue 2005</p>	<p>Accumulated path function X reduce shear associated with cyclic fatigue damage</p> $\tau = X \tau_0(\delta, \omega)$ <p>function Original model</p> $X = 1 - \frac{1}{10} \log_{10} \left\{ 1 + \int d(\delta/\omega) \right\} \geq 0.1$ <p>Contact density model by Li & Maekawa 1989 Modification of accumulated path function by Gebreyouhannes et al. 2006</p>
Physical meaning	Decrease of stiffness and plasticity accumulation by continuous fracturing concrete	Decrease of tension stiffness by bond fatigue	Decrease of shear transfer normal to crack by continuous deterioration of rough crack surface

Fig. 3-10 Constitutive laws of concrete structures for high-cycle fatigue [9], [14], [15].

a. High cycle fatigue of concrete in compression

The compression model of concrete is based on the scheme of elasto-plastic and fracture [13]. We have total compression strain ε defined as the sum of plastic ε_p and elastic strains ε_e as,

$$\varepsilon = \varepsilon_e + \varepsilon_p \quad (1)$$

Thus, we have the compressive stress σ associated with the elastic strain and fracture parameter K_C as,

$$\sigma = E_0 \varepsilon_e K_C \quad (2)$$

where E_0 is initial stiffness of concrete.

Two parameters (ε_p and K_C) express the rates of plasticity and damage as,

$$d\varepsilon_p = \left(\frac{\partial \varepsilon_p}{\partial t} \right) dt + \left(\frac{\partial \varepsilon_p}{\partial \varepsilon_e} \right) d\varepsilon_e \quad (3)$$

$$dK_C = \left(\frac{\partial K_C}{\partial t} \right) dt + \left(\frac{\partial K_C}{\partial \varepsilon_e} \right) d\varepsilon_e \quad (4)$$

The derivatives of elastic strain increment show the instantaneous nonlinearity as,

$$\left(\frac{\partial \varepsilon_p}{\partial \varepsilon_e} \right) = 0 \text{ when } F_p > 0, \text{ and } \left(\frac{\partial \varepsilon_p}{\partial \varepsilon_e} \right) = -(\partial F_p / \partial \varepsilon_e) / (\partial F_p / \partial \varepsilon_p) \text{ when } F_p = 0 \quad (5)$$

$$\left(\frac{\partial K_C}{\partial \varepsilon_e} \right) = \lambda \text{ when } F_k < 0, \text{ and } \left(\frac{\partial K_C}{\partial \varepsilon_e} \right) = -(\partial F_k / \partial \varepsilon_e) / (\partial F_k / \partial K) + \lambda \text{ when } F_k = 0 \quad (6)$$

Then, we have the rate of fatigue accumulated damage (λ), which was validated the plastic potential (F_p) and damage one (F_k) by the experiments as,

$$F_p = \varepsilon_p - 0.038 \left(\exp \left(\frac{\varepsilon_e}{0.55} \right) - 1 \right) \quad (7)$$

$$F_k = K - \exp[-0.73\beta(1 - \exp(-1.25\beta))] \quad (8)$$

$$\beta = -\frac{1}{0.35} \left(\ln \left(1 - \frac{7\varepsilon_e}{20} \right) \right) \quad (9)$$

$$\lambda = K^3 \cdot (1 - K)^4 \cdot g \cdot R \quad (10)$$

$$R = 9\gamma^8, \gamma = -\frac{\varepsilon - \varepsilon_{e,tp}}{\varepsilon_{e,max}} \quad (11)$$

$$g = \frac{0.6}{1 + 10^{(30K-22)}} \text{ when } d\varepsilon_e < 0, \text{ otherwise } g = 0 \quad (12)$$

where K is remaining effective volume, R is the effect of strain amplitude in high nonlinearity, γ indicates the normalized amplitude corresponding to updated stress variation, $\varepsilon_{e,tp}$ denotes the turning point of compressive elastic strain, and $\varepsilon_{e,max}$ is maximum elastic strain.

In order to apply for high-cycle fatigue, the parameter g [13] was added. Then, the rate functions of plasticity and damage are given as,

$$\frac{\partial \varepsilon_p}{\partial t} = \phi \left(\frac{\partial \varepsilon_p}{\partial t} \right)_b, \left(\frac{\partial \varepsilon_p}{\partial t} \right)_b = 0.034 \left(\exp \left(\frac{\varepsilon_e}{4} \right) - 1 \right) \quad (13)$$

$$\phi = \exp \left(-6 \left(\frac{F_p^{0.6}}{\varepsilon_e^{1.2}} \right) \right), \frac{\partial K}{\partial t} = \left(\frac{\partial K}{\partial t} \right)_b \exp \left(\xi \left(\frac{K}{K - F_k} - 1 \right) \right) \quad (14)$$

$$\xi = 45 \left(\psi^{-0.5(1 - \exp(-5\varepsilon_e))} \right) \quad (15)$$

$$\left(\frac{\partial K}{\partial t} \right)_b = \left(\frac{\partial K}{\partial t} \right)_n (K - F_k), \left(\frac{\partial K}{\partial t} \right)_n = -0.05 (0.95 - K + F_k)^2 \quad (16)$$

$K - F_k < 0.95$, otherwise = 0

where ϕ indicates the reduction factor in terms of the plastic evolution, and ξ is the integral acceleration.

b. High cycle fatigue of concrete in tension

Tensile fatigue damage of concrete is integrated with crack propagation [18]–[20]. Similar to the compression model, the tension nonlinearity is expressed by ε and σ . Tensile strain σ is associated with elastic strain ε_e and fracture parameter K_T as [13],

$$\sigma = E_0 K_T \cdot \varepsilon_e \quad (17)$$

Thus, we have the total differentiation as,

$$dK_T = Fdt + Gd\varepsilon + Hd\varepsilon \quad (18)$$

where, H is instantaneous evolution of tension fracture defined as,

$$H = -(1 + \alpha) \left(\frac{f_t}{E_0} \right) \varepsilon_{cr}^\alpha \cdot \varepsilon_{max}^{-(\alpha+2)}, \text{ when } d\varepsilon > 0 \text{ and } \varepsilon = \varepsilon_{max} \quad (19)$$

$$H = 0, \text{ when } d\varepsilon \leq 0 \text{ or } \varepsilon < \varepsilon_{max}$$

where ε_{cr} is the crack strain equal to $2f_t/E_0$, and ε_{max} is the maximum tensile strain in the past strain history measured from the compressive plastic strain.

In the event of RC, α is 0.4. For plain concrete, it depends on the fracture energy in tension and the size of finite elements [21]. Here, the rate of damaging is formulated in terms of S as,

$$S = \frac{E_0 K_T \varepsilon}{f_t} \quad (20)$$

where, f_t is the uniaxial tensile strength, and we have the rate of time-dependent fracture denoted by F as,

$$F = -10^{-5} \cdot S^3 \cdot (K_T - 0.5)^2 \text{ when } \varepsilon_{max} < \varepsilon_{cr}, \text{ and } F = -10^{-6} \cdot S^6 \text{ when } \varepsilon_{max} \geq \varepsilon_{cr} \quad (21)$$

The cyclic fatigue damage in tension after cracking is expressed by G as,

$$Gd\varepsilon = K_T \left(\frac{\sigma_{tp}}{\sigma_{env}} \right)^{20} \cdot d\tilde{\varepsilon}, \sigma_{env} = f_t \left(\frac{\varepsilon_{cr}}{\varepsilon_{tp}} \right)^\alpha \quad (22)$$

This formula is applied to the non-cracked state with $\sigma_{tp}/\sigma_{env}=1.0$.

c. High cycle fatigue shear transfer

The rate of the stiffness decrease was proposed from the original contact density modeling as [13],

$$\tau = X \cdot \tau_{or}(\delta, \omega) \quad (23)$$

$$X = 1 - \frac{1}{10} \log_{10} \left[1 + \int |d(\delta / \omega)| \right] \geq 0.1 \quad (24)$$

where, τ_{or} is the transferred shear stress, (δ, ω) are the shear slip and the width, and X is the fatigue evolution factor to show the stiffness reduction of accumulated intrinsic shear deformation [13].

3.3.2 Multi-Yield Surface Plasticity for High-Cycle Fatigue of Soil

The multi-spring model used in this study was proposed by Towhata and Ishihara [22]–[25] and integrated into the numerical analysis with concrete structures by Soltani and Maekawa [12]. Soil is assumed as a congregation of finite numbers of inelastic constituents. Nonlinear mechanics of soil consists of volumetric and shear fatigue. The volumetric strain is decomposed into shear dilatancy and consolidation. The shear dilatancy is further divided into negative dilation (unrecoverable strain) and positive one (recoverable strain). Both behaviors (shear and volumetric fatigue) have been verified and coupled with structural concrete in the programed code utilized in this study. Core points of the multi-yield surface plasticity model are summarized in Fig. 3-11 and the formulation is lined up as below.

First, let us divide the referential shear-stress strain relation into finite assembly of piecewise linear with tangential stiffness D_i as,

$$D_i = \frac{\tau_i - \tau_{i-1}}{\gamma_i - \gamma_{i-1}}, \quad i = 1 \square n \quad (25)$$

where τ_i is shear stress and γ_i is shear strain. The multi-yield surface modeling shows that the tangential stiffness is consistent with the component stiffness (G_0^m) and the component yield strength (F_{ref}^m) as,

$$\begin{aligned} G_0^m &= D_m - D_{m+1}, \quad m = 1 \square n-1 \\ F_{ref}^m &= G_0^m \cdot \gamma_m, \quad G_0^n = D_n, \quad m = n \end{aligned} \quad (26)$$

We have the linear relation of the deviatoric shear stress and the mean stress as,

$$F^m = \chi F_{ref}^m, \chi = \frac{A + BI_1}{S_u(p_0)}, I_1 = 3|p_0| \quad (27)$$

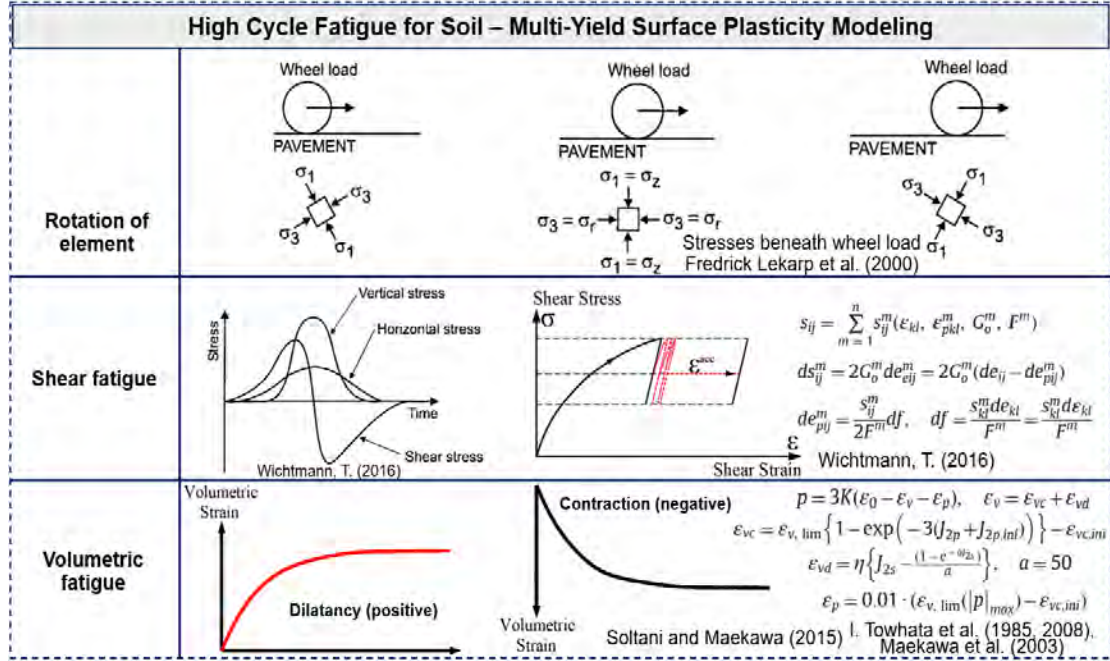


Fig. 3-11 Constitutive model of soil foundations for high cycle fatigue.

where $S_u(p_0)$ is the deviatoric strength corresponding to a referential confinement (p_0), and χ is the confinement index. A and B are constants of the largest yield surface with the friction angle ϕ and the cohesion c as,

$$A = \frac{6\sqrt{3}c \cos \phi}{\sqrt{2\sqrt{3}\pi(9 - \sin^2 \phi)}}, B = \frac{6\sqrt{3}c \sin \phi}{\sqrt{2\sqrt{3}\pi(9 - \sin^2 \phi)}} \quad (28)$$

As previously stated, the dilatancy volumetric strain ($\epsilon_v = \epsilon_{vd} + \epsilon_{vc}$) includes the recoverable strain (ϵ_{vd}) and the non-recoverable one (ϵ_{vc}). These values are calculated with experimental data as,

$$\epsilon_{vd} = \eta \left(J_{2s} - \frac{1 - e^{-aJ_{2s}}}{a} \right), \quad a = 50$$

$$J_{2s} = \sqrt{\frac{1}{2} e_{ij} e_{ij}}, \quad \eta = 0.5 \left(\frac{\epsilon_{vc} + \epsilon_{v, \lim}}{\epsilon_{v, \lim}} \right) \quad (29)$$

where e is void ratio. e_{ij} is deviatoric tensor of total strain. J_{2s} is total shear strain intensity. Then, we have,

$$\begin{aligned}\varepsilon_{vc} &= \varepsilon_{v,\lim} \left(1 - \exp \left(-3 \left(J_{2p} + J_{2p,ini} \right) \right) \right) - \varepsilon_{vc,ini} \\ J_{2p} &= \int dJ_{2p}, \int dJ_{2p} = \frac{1}{2} \beta \frac{S_{kl}}{J_2} d\varepsilon_{kl} \\ \beta &= \sqrt{\frac{J_2}{|p|}}, J_2 = \sqrt{\frac{1}{2} S_{ij} S_{ij}}\end{aligned}\tag{30}$$

where J_{2p} is the accumulated shear strain invariant and ‘ini’ is implied as the initial state of soil, and $\varepsilon_{v,\lim}$ is the intrinsic volumetric strain as,

$$\begin{aligned}\varepsilon_{v,\lim} &= -0.1 \left(\log_{10} |p|^{0.6} + 1 \right) < 0 \\ \varepsilon_{vc,ini} &= \varepsilon_{v,\lim} \left(1 - \exp \left(-3 J_{2p,ini} \right) \right)\end{aligned}\tag{31}$$

where, p is the volumetric nonlinear of soil skeleton as,

$$p = 3K \left(\varepsilon_0 - \varepsilon_v - \varepsilon_p \right)\tag{32}$$

where, ε_0 is the total volumetric strain and equal to $(\varepsilon_{11} + \varepsilon_{22} + \varepsilon_{33})/3$, and K is defined as the volumetric bulk stiffness of soil particles and formulated as,

$$K = \frac{2(1+\nu)}{3(1-2\nu)} G_0 \chi^{0.5}\tag{33}$$

where ν is elastic Poisson’s ratio. The volumetric inelasticity from the consolidation is calculated as,

$$\varepsilon_p = 0.01 \left(\varepsilon_{v,\lim} \left(|p|_{\max} \right) - \varepsilon_{vc,ini} \right)\tag{34}$$

where, p_{\max} is the maximum mean stress. The total shear stress of soil particles is the sum of

$$s_{ij} = \sum_{m=1}^n s_{ij}^m(\varepsilon_{kl}, \varepsilon_{pkl}^m, G_0^m, F^m)$$

$$ds_{ij} = 2G_0^m de_{ij}^m = 2G_0^m (de_{ij} - de_{p_{ij}}^m)$$

$$de_{p_{ij}}^m = \frac{s_{ij}^m}{2F^m} df, \quad df = \frac{s_{kl}^m de_{kl}}{F^m} = \frac{s_{kl}^m d\varepsilon_{kl}}{F^m} \quad (35)$$

where, ε_{kl} and ε_{pkl} are total and plastic strain tensors of (k, l) component and $e_{p_{ij}}^m$ and e_{ij}^m are deviatoric tensors of plastic and elastic strains of the m th component, respectively. The total stress on soil particles are summarized as,

$$\sigma_{ij} = s_{ij} + p\delta_{ij} \quad (36)$$

where δ_{ij} is Kronecker's delta and $p = (\sigma_{11} + \sigma_{22} + \sigma_{33})/3$.

A flowchart for this calculation in the coupled program is shown in Fig. 3-12. Based on the above presented formula, the total stress σ_{ij} can be determined.

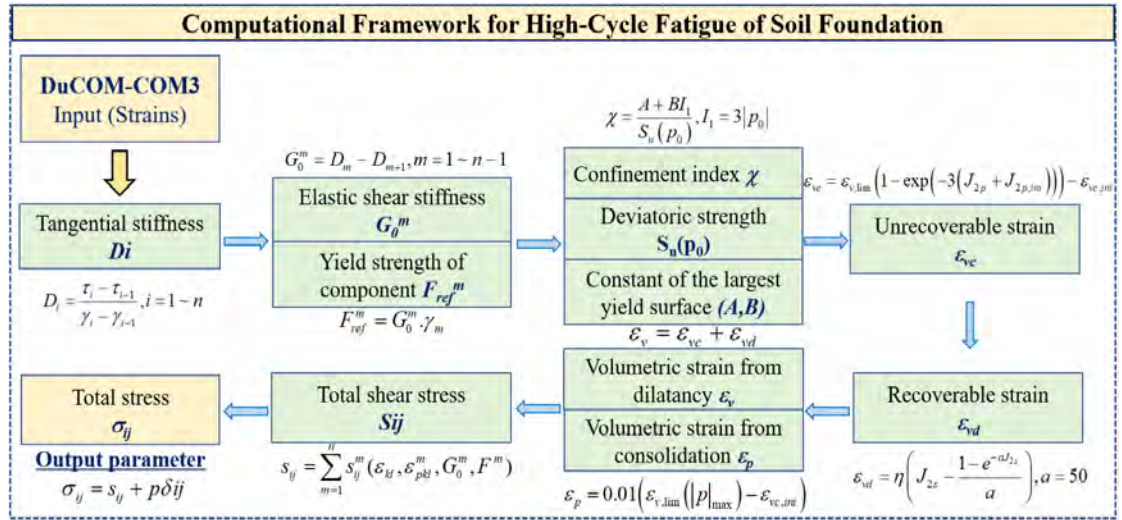


Fig. 3-12 Outline of soil foundations.

The deformation of a granular mass is normally homogeneous up to the peak stress. After the peak, the large shear strains start to localize in the shear band. In case of the small size particle sand, the shear band is localized in a narrower zone. The shear band thickness is a function of mean particle diameter and less dependent to the particle shape [12]. In the FEM, the strain is not local pointwise but defined as the

space-averaged one over the element with finite sizes. When the shear band is formed in a finite element, the strain used in the constitutive models is to be averaged one over the volume of finite element with localized (constant characteristic size) and non-localized volumes (relating to element size) [12]. The conversion from the local to the space averaged shear can be implemented with the same principle of RC crack band localization in tension [12]. In the event of large elements, the post peak softening becomes sharper in views of space-averaged strain and stresses. Fig. 3-13 shows the example of the softening branch of a biaxial compression case of two type meshes, including mesh 1 (number of element: 1600) and mesh 2 (number of element: 400) [12].

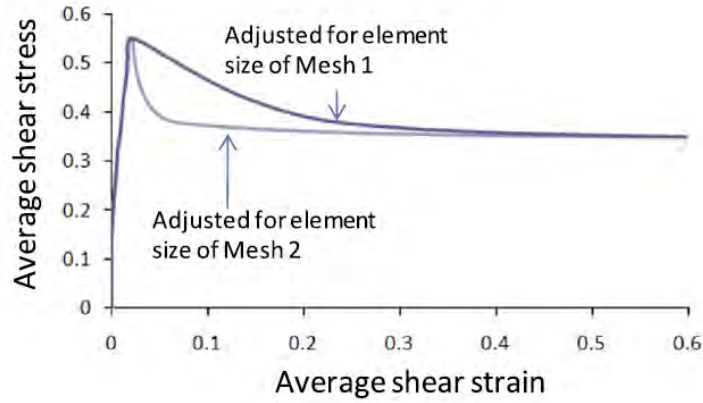


Fig. 3-13 The softening branch of two different FEM meshes in views of shear band and load-deformation [12].

After the peak, the shear deformation develops in the localized shear band whilst the remainder of the medium performs the stress release elastically. The total displacement of the soil medium can be calculated by the summation of the deformation inside and outside the shear band which can be numerically depicted in views of average strain $\bar{\gamma}_{se}$ for a particular shear stress as follows [12]:

$$\bar{\gamma}_{se} = \gamma_u + (\gamma_s - \gamma_u) \frac{L_{sb}}{L_e} \quad (37)$$

Where γ_s and γ_u are the shear strain on the softening and unloading branches along a shear band. L_{sb} is the size of the shear band and L_e is the length of the element. The space-averaged shear stress-strain relation with the softening branch is discretized by equation (25) and (26).

The summary of the constitutive laws of the high cycle fatigue interaction between concrete and the soil foundation is illustrated in Fig. 3-14. By using a nonlinear couple of the multi-directional fixed crack modeling for concrete and the multi-yield surface plasticity modeling for soil, the nonlinear behavior of the pavement may be predicted and investigated.

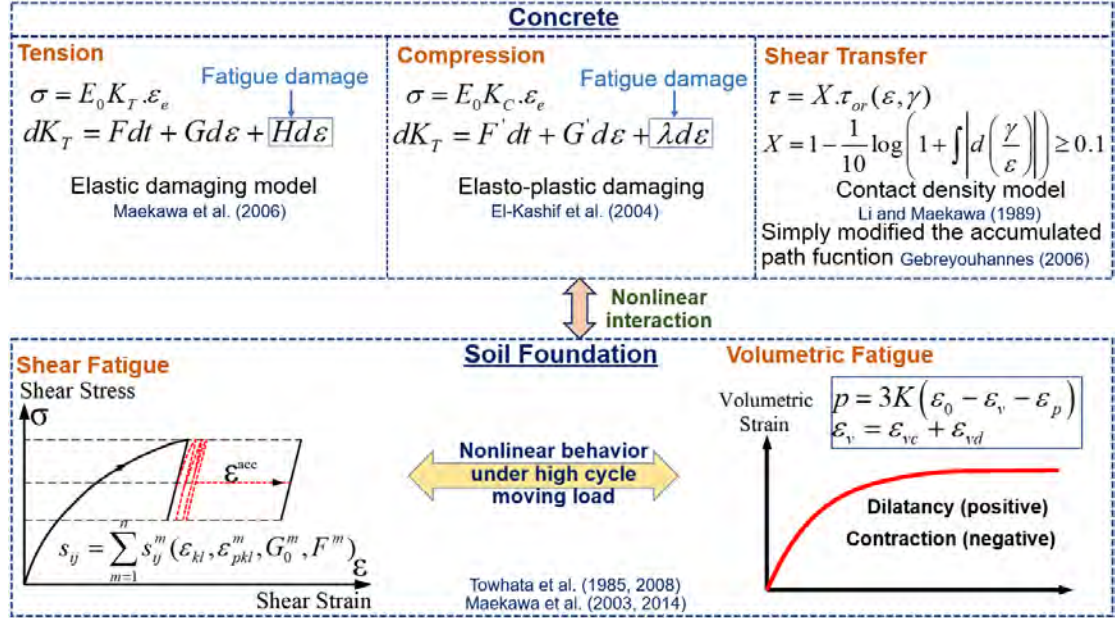


Fig. 3-14 Summary for high cycle fatigue of the concrete and soil interaction.

3.4 Experimental and Analytical Results and Discussion

3.4.1. Experimental Verification and Validation

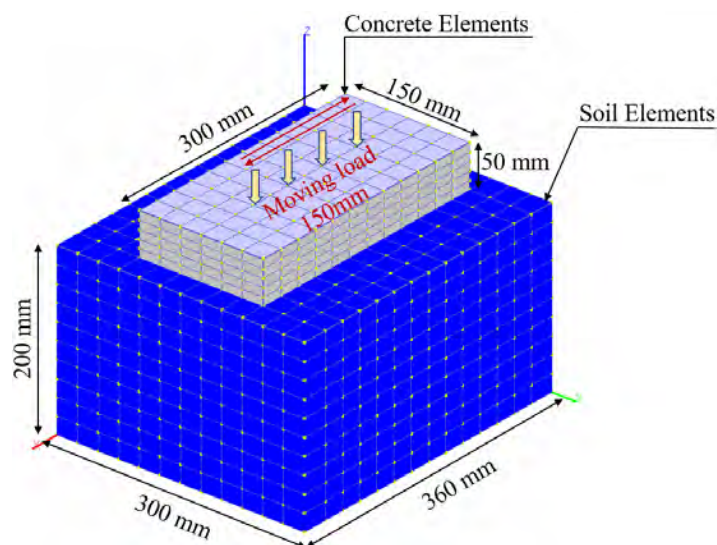
Three-dimensional fatigue failure analysis was conducted in considering shapes, dimensions, loading and ambient conditions as well as boundary conditions as shown in Fig. 3-15. The soil foundation was first built in the multi-scale computational scheme. After that, finite elements of concrete slabs were numerically added at the top layer of the soil. Due to the thinner depth of concrete slabs compared to soil foundations, we have finer discretization of elements. The slabs of 20mm and 50mm in numerical modeling are divided into 2 and 5 layers, respectively. The mesh size of concrete elements are 25 x 25mm in plane and 10mm in depth. Soil elements consist of two different area sizes. The FE elements of the soil area of 300mm x 300mm in plane under the concrete slab are divided into 25mm x 25mm and 10mm in depth. The remaining soil area is 25mm width x 30mm length and 10mm in depth as

well. The enhanced strain formulation for interpolation of deformational field in finite element is applied in order to reduce the shear and volumetric locking and to realize the smooth development of shear localization over elements. Finally, the moving load was applied at the top surface of the slab. Moving forces are applied simultaneously on 3 adjacent nodal points on the central strip of finite concrete elements, and the center of the resultant forces are gradually moved by shifting three nodes on the loading FE strip. This results in a computed width of the wheel track of 50mm. The lateral nodal displacement was confined the same as the case of the soil box.

In order to accelerate the computation of high-cycle loads, the direct strain-path integral method was applied [11] for integrating the constitutive modeling with respect to time. We need about 30 time-steps to conduct a one-way pass of the wheel loading. By discretizing the log-scale time domain, we may have the compressed computation time with just 1,500 time-steps for 75,220 cycles of experiments. A multi-frontal direct linear sparse matrix solution was also used. It takes a half-day of simulation for experiments which took two days to accomplish 75,220 cycles in the testing laboratory.

Details of moving forces in numerical simulation

STEP 1'							
	1	1	1	0	0	0	0
1'+1	0	1	1	1	0	0	0
1'+2	0	0	1	1	1	0	0
⋮							
⋮							



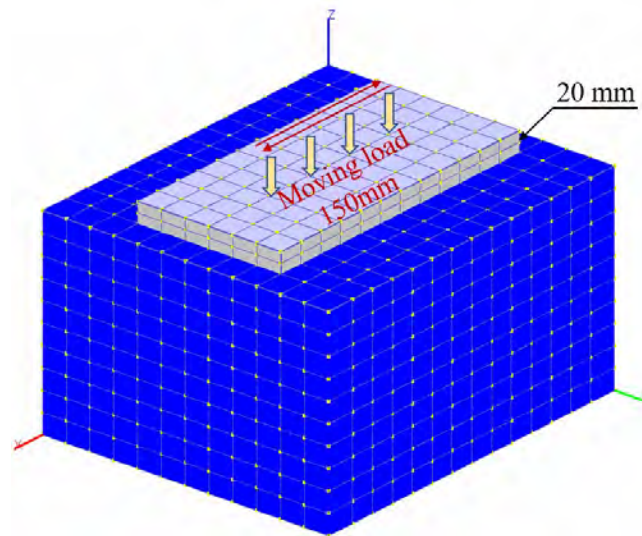


Fig. 3-15 Finite element discretization for slab-soil interaction.

3.4.2. Failure Mode and Fatigue Life: Thickness of Slab=50mm

There are three testing implementations of concrete slab 50mm, including load 1,029N and RD 75%, load 513N and 1,029N with RD 50%, respectively. Firstly, the load level of 1,029N and RD 75% is focused (see in Fig. 3-16). After 75,220 cycles of passage, the maximum total displacement of the combined soil-concrete slab was 7.54 mm. As can be seen in Fig. 3-16, the computed displacement and failure mode are roughly consistent with the experiment. The failure mode of the coupled system exhibits the larger soil's shear deformation which grows underneath the slab. There was no deterioration of the slab irrespective of the high load level. It is convinced that the failure mode of the model is also governed by the soil foundation and significantly distributed under the concrete slab.

At the beginning of loading about a hundred cycles, the displacement of soil-concrete was small. After over several hundred cycles, the displacement gradually increased and the localized deformation of soil started to propagate. The area surrounded by two white curved lines in Fig. 3-16 indicates the highly deformed zone of soil at the final stage of the experiment and the simulation. The localized shear band of soil foundation was hard to be seen by naked eyes in the experiment. Under the moving load, the dense soil foundation became more compacted, and the principal strain of soil increased. The highly localized strain under the slab is thought to

develop in the experiment as well since the similar vertical displacement was reproduced as shown in Fig. 3-16.

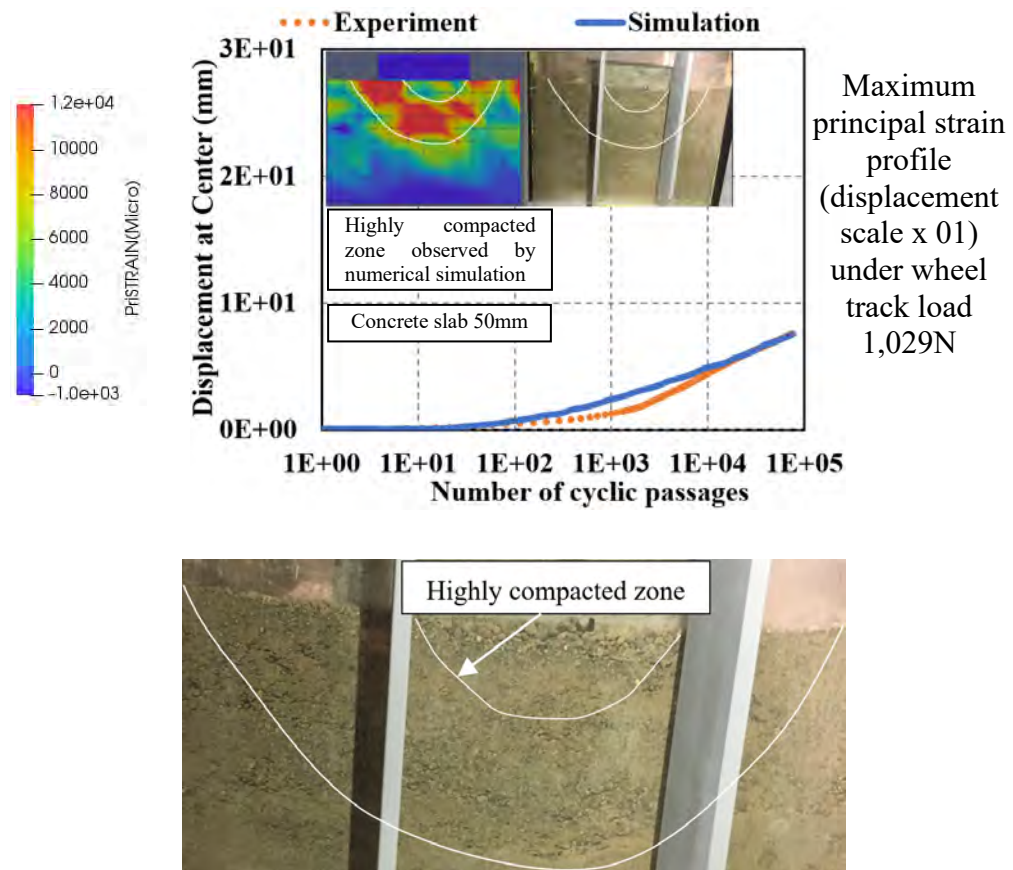


Fig. 3-16 Displacement and deformational mode under the moving load 1,029N and RD 75%.

To investigate the effects of load levels and the compacted weak soil, the moving load 513N and 1,029N with RD 50% were examined, respectively. Figure 3-17 shows the experimental and analytical results of nearly a half of the wheel load of 513N and RD 50%. The maximum total displacement after 75,220 cycles was 13.62 mm. The displacement is nearly congruous with the case of load 1,029N and RD 75% at the first hundred cycles. The displacement evolved gradually in this stage, and there was no occurrence of shear failure of soil. A dramatic jump proceeded after several hundred cycles and the displacement sharply rose. At the final stage of loading, the partial shear band of soil was observed as shown in Fig. 3-17. Soil under the slab was extra compacted. The computed failure mode also shows the increase in the principal strain under the slab. There is no cracking in concrete. The computed displacement is

fairly close to the experiment. The highly compacted zone within the white boundary in Fig. 3-17 is less different from the case of RD 75% and the load of 1,029N.

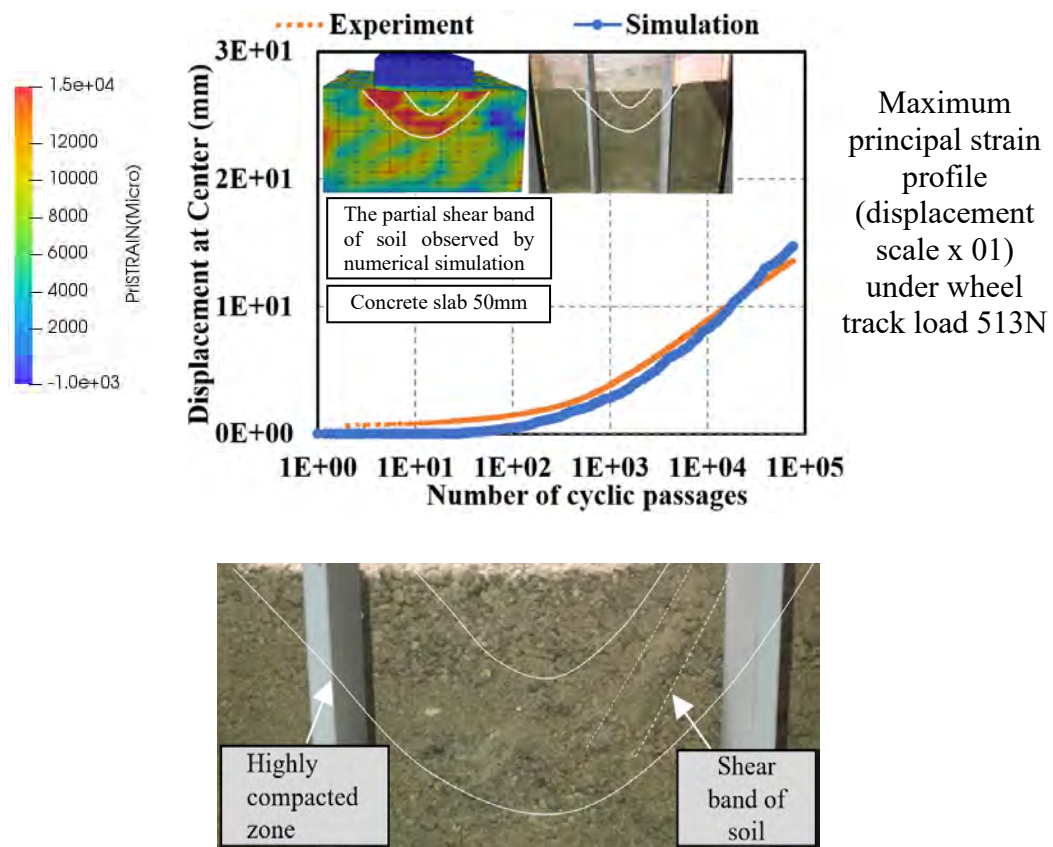


Fig. 3-17 Displacement and deformational mode under the moving load 513N and RD 50%.

Figure 3-18 demonstrates the total displacement in the event of RD 50% and the moving wheel load of 1,029N. The maximum total displacement after 75,220 cycles in this experiment was 20.08 mm and it was the highest one compared to other cases. It was the critical condition for the concrete pavement due to the high load level and the loose soil. The shear failure of soil appeared in the early stage of loading and the displacement rose rapidly at some first cycles. The localized shear band of soil under the slab can be clearly seen in both experiment and analysis. The total displacement can be equally simulated, and Figure 3-18 also indicates the soil's shear band. In the case of load 513N (the same RD 50%), it shows the huge effect of the load level through the dramatically increased displacement. In the event of a similar moving load of 1,029N, we may understand how greatly the soil compaction affects the total displacement. Soil consolidation and the magnitude of the moving loads have a close correlation as a key factor for assessing fatigue life. It is clearly shown with three

cases of 50mm slab that failure of the slab-soil system is primarily governed by the shear of soil foundation. These shear-failure grades depend on the load levels and relative density of soil.

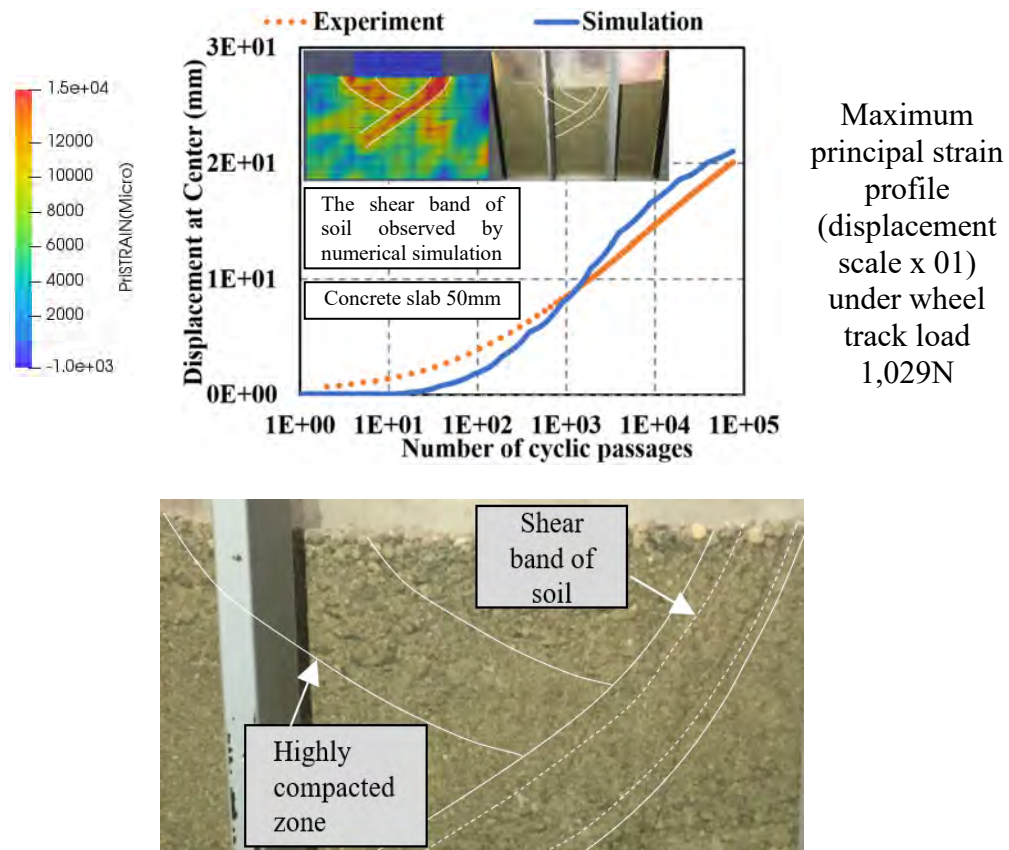


Fig. 3-18 Displacement and deformational mode under the moving load of 1,029N and RD 50%.

3.4.3. Failure Mode and Fatigue Life: Thickness of Slab=20mm

As previously stated, the failure of the concrete slab did not take place in the case of thickness slabs of 50mm. In order to introduce the cracking damage, thin slabs of 20mm were challenged, and three experiments of the small-scale specimens were similarly loaded by 1,029N with RD 50% and 75%, and the load of 513N with RD 50%, respectively.

For the loose soil of RD 50% under the moving load of 513N and 1,029N, the displacement developed similarly to the cases of 50mm slabs as 75,220 cycles. Here, no cracking nor deterioration took place up to the end of the loading program. Then, one more load level (98N) was applied as 513N + 98N and 1,029N + 98N. Figure 3-

19 indicates the simulation and experiment in the case of a moving load of 513N + 98N with RD 50%. There was no damage to the concrete slab irrespective of the increased wheel load. The displacement and the failure mode are close to the simulation as well. As the flexural tension at the bottom surface of the slab was not large, the slab was not cracked. The maximum displacement of the soil- slab was 11.77 mm, and this value was smaller than the one of the slab 50mm at the same RD and the load level. It can be said that the smaller slab can survive even though its flexural capacity is smaller, provided that the slab is supported on the softer foundation which absorbs larger deformation and the plastic energy.

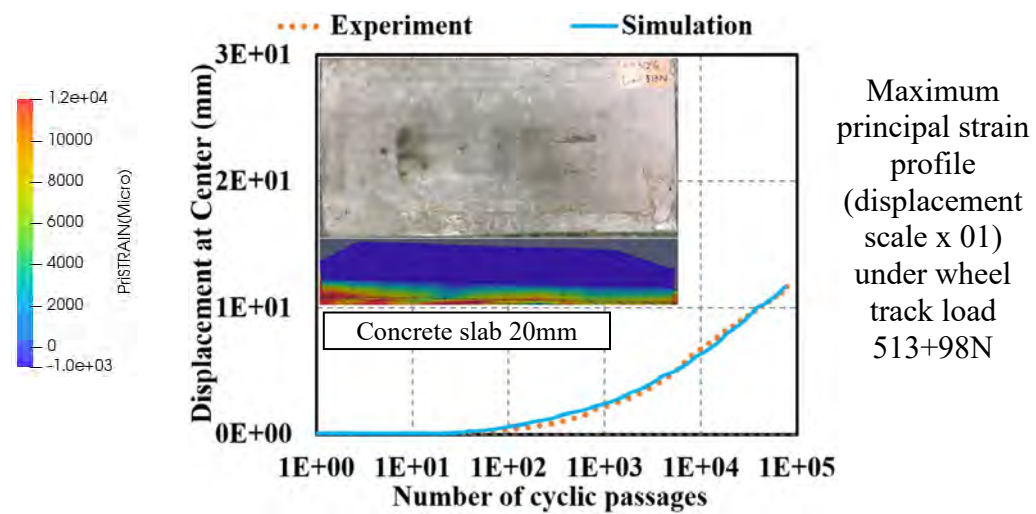


Fig. 3-19 The experimental and numerical result with moving load 513N + 98N and RD 50%.

Figure 3-20 shows the experimental and analytical results of RD 50% with load 1,029N. The flexural tension at the bottom side was severe owing to the smaller thickness of the slab. As a result, the cracking damage occurred at some cycles after increasing more load of 98N. The simulated displacement and the failure mode of concrete seem to be similar to reality. The maximum displacement measured in this experiment was 16.37 mm and 20.08mm of the slab of 50mm thickness. In spite of the thinner concrete slab, the total displacement was smaller. It can be conceivable that the interaction of soil and concrete is more nonlinear in the case of loose soil foundation. The strength of the concrete slab coupled with the compaction of soil plays a key role in the support of the service life for concrete pavements.

In the case of RD 75% and the moving load of 1,029N, the concrete slab was immediately damaged with cracking just after the static load applied at the slab center (see Fig. 3-21). In fact, this was different from the expected result, because well-compacted soil foundation has practically allowed thinner slab according to the current design principle based upon the in-plane theory of slabs supported on the distributed elastic springs. Thus, this result is said as a highlight of this series of experiments.

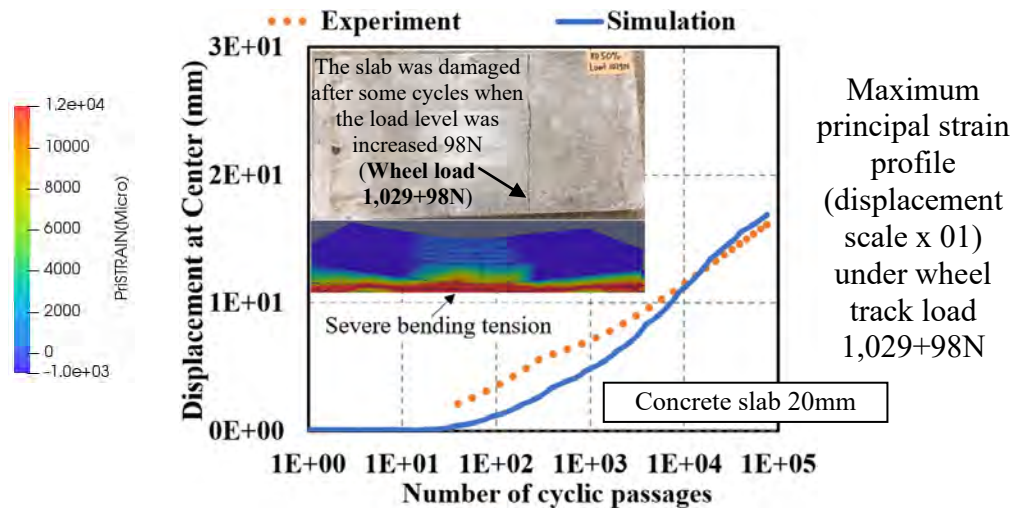


Fig. 3-20 The experimental and numerical result with moving load 1,029N + 98N and RD 50%.

To clarify this nonlinearity, numerical simulation was conducted. The computed load-displacement relation is shown in Fig. 3-22 of the thin slab with RD 50% and 75%, respectively. The computed capacity in the case of RD 75% is about 830 N, and it is interestingly smaller than the case of RD 50%. This simulation is consistent with the experimental nonlinearity.



Fig. 3-21 The failure mode of concrete slab 20mm with the static load 1,029N and RD 75%.

If the stiffness of the foundation is so small, the reacting soil pressure applied to the slab is more uniformly distributed, and if the soil does not fail, the bending moment develops as the maximum. Thus, the greater stiffness of soil foundation would arise the concentrated reacting soil pressure beneath the loading point. As a result, the flexural moment of the slab tends to be reduced and less risk of cracking is thought in accordance with the linear elastic hypothesis. However, the higher concentrated stress leads to the reduced stiffness owing to its nonlinearity, and the moment to the slab is not proportionally reduced. Thus, the experimental results implicitly show the presence of nonlinearity of soil. It can be concluded that the crack risk of the concrete pavement has to do with the soil nonlinearity.

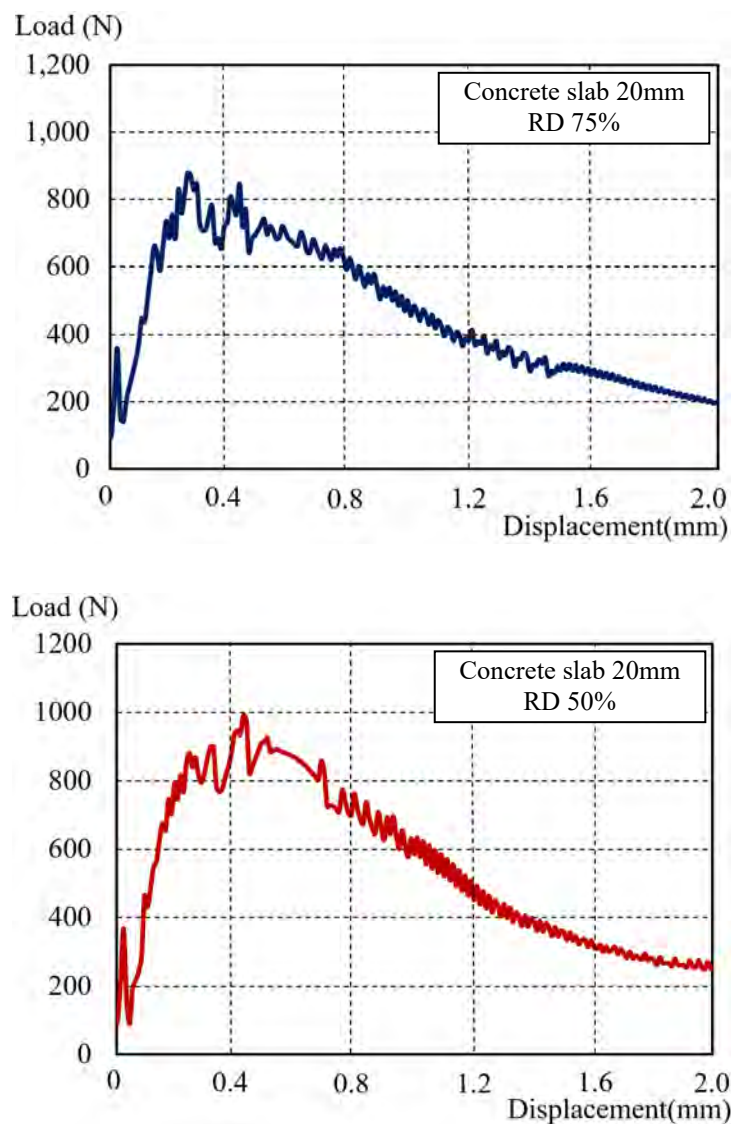


Fig. 3-22 The load capacity-displacement relationship of concrete slab 20mm with RD 75% and RD 50%.

The simulation and results of the load-displacement relationship are consistent with the experimental nonlinearity and it is qualitatively expected to reflect the nonlinear soil-concrete composite in reality. The failure mechanism of the soil-concrete slab interaction is investigated under a mass of the soil density in the next chapter.

3.5 Conclusions for Chapter 3

In this chapter, small-scale experiments of the soil foundation and concrete slab interaction subjected to moving loads are presented. Based on these experiments, a coupled code for the study of concrete pavement under moving loads has been verified by utilizing constitutive models for high-cycle fatigue of concrete structures and soil foundations. The coupled program shows the description of behaviors and failure modes of the concrete slab (tension, compression, and shear) and nonlinear mechanics of soil (shear and volumetric fatigue). The three-dimensional finite element analysis was applied in the small-scale mock-ups. The summary of the experimental results are obtained as follows:

- (1) The fatigue life of concrete pavements is strongly governed by both the slab thickness and the relative density of soil. The exaggerated slab can cause the reduction of fatigue life on the soft soil foundations. The thin slab laid on the dense soil foundation may be the main reason to dramatically reduce the service life owing to the critical flexural tension focused at the bottom side of slabs.
- (2) Due to the nonlinearity of soil, the balanced thickness of the slab in the loose foundation is smaller than the medium dense one. The sharp reduction of the life cycle and the severe damage of the slab may occur if the slab thickness is not selected rationally.
- (3) Depending on the thickness and soil's density, the fatigue failure of the concrete pavement addresses the deterioration of the slab, the shear band of soil and/or both of them. The optimized failure mode is the integrated soil-slab composite.

The thinner thickness of the concrete slab on the non-compacted soil is computationally and experimentally observed. Conversely, the thicker one on the compacted soil is required when the nonlinear coupling of the concrete slab and soil is

investigated. The fatigue damage of nonlinear modeling can occur in the soil, the concrete slab or both of them, opposite to the sole damage of the concrete slab under the concentrated truck axle load in the existing design code of pavement. The balanced thickness of the concrete slab in this study is therefore considered based on the density of the soil foundation subjected to the moving wheel-type load. This will be a key factor to revise the design code of pavement which has been modeled based on in-plane theory on elastic foundation without considering shear localization.

References in Chapter 3:

- [1] T. Wichtmann, A. Niemunis, and T. Triantafyllidis, “On the influence of the polarization and the shape of the strain loop on strain accumulation in sand under high-cyclic loading,” *Soil Dyn. Earthq. Eng.*, vol. 27, no. 1, pp. 14–28, 2007.
- [2] T. Wichtmann, A. Niemunis, and T. Triantafyllidis, “Improved simplified calibration procedure for a high-cycle accumulation model,” *Soil Dyn. Earthq. Eng.*, vol. 70, pp. 118–132, 2015.
- [3] T. Wichtmann, “Soil behaviour under cyclic loading - experimental observations, constitutive description and applications,” *Publ. Inst. Soil Mech. Rock Mech. Karlsruhe Inst. Technol.*, no. 181, 2016.
- [4] T. Wichtmann, H. a. Rondón, A. Niemunis, T. Triantafyllidis, and A. Lizcano, “Prediction of permanent deformations in pavements sing a high-cycle accumulation model,” *J. Geotech. Geoenvironmental Eng.*, vol. 136, no. 5, pp. 728–740, 2010.
- [5] T. Wichtmann, A. Niemunis, and T. Triantafyllidis, “Validation and calibration of a high-cycle accumulation model based on cyclic triaxial tests on eight sands,” *Soils Found. - Japanese Geotech. Soc.*, vol. 49, no. 5, pp. 711–728, 2009.
- [6] H. Q. H. Nguyen, K. Maekawa, and S. Komatsu, “High-cycle fatigue interaction between soil foundation and concrete slab under moving wheel-type loads,” *Eng. Struct.*, 2019.
- [7] K. Maekawa, T. Ishida, and T. Kishi, *Multi-scale modeling of structural concrete*. London: Taylor and Francis, 2008.
- [8] K. Maekawa, R. Chaube, and T. Kishi, *Modeling of concrete performance- hydration, microstructure formation and mass transport*. London: E&FN Spon, 1999.

- [9] K. Maekawa and C. Fujiyama, “Crack water interaction and fatigue life assessment of RC bridge decks,” *Poromechanics V ASCE 2013*, pp. 2280–2289, 2013.
- [10] K. Maekawa, T. Ishida, N. Chijiwa, and C. Fujiyama, “Multiscale coupled-hygro-mechanistic approach to the life-cycle performance assessment of structural concrete,” *J. Mater. Civ. Eng.*, vol. 27, no. 2, pp. A4014003-1–9, 2015.
- [11] K. Maekawa, E. Gebreyouhannes, T. Mishima, and X. An, “Three-dimensional fatigue simulation of RC slabs under traveling wheel-type loads,” *J. Adv. Concr. Technol.*, vol. 4, no. 3, pp. 445–457, 2006.
- [12] M. Soltani and K. Maekawa, “Numerical simulation of progressive shear localization and scale effect in cohesionless soil media,” *Int. J. Non. Linear Mech.*, vol. 69, pp. 1–13, 2015.
- [13] K. Maekawa, K. Toongoenthong, E. Gebreyouhannes, and T. Kishi, “Direct path-integral scheme for fatigue simulation of reinforced concrete in shear,” *J. Adv. Concr. Technol.*, vol. 4, no. 1, pp. 159–177, 2006.
- [14] K. Maekawa, H. Okamura, and A. Pimanmas, *Nonlinear mechanics of reinforced concrete*. London: Spon Press, 2003.
- [15] Y. Takahashi, Y. Tanaka, and K. Maekawa, “Computational life assessment of ASR-damaged RC decks by site-inspection data assimilation,” *J. Adv. Concr. Technol.*, vol. 16, pp. 46–60, 2018.
- [16] K. Maekawa and K. F. El-Kashif, “Cyclic cumulative damaging of reinforced concrete in post-peak regions,” *J. Adv. Concr. Technol.*, vol. 2, no. 2, pp. 257–271, 2004.
- [17] E. Gebreyouhannes, “Shear transfer of cracked concrete under fatigue loading,” *Proc. 6th Int. PhD Symp. Civ. Eng. Zurich*, 2006.

- [18] H. A. W. Cornelissen and H. W. Reinhardt, “Uniaxial tensile fatigue failure of concrete under constant-amplitude and program loading,” *Mag. Concr. Res.*, vol. 36 (129), pp. 216–226, 1984.
- [19] H. W. Reinhardt, H. A. W. Cornelissen, and D. A. Hordijk, “Tensile Tests and Failure Analysis of Concrete,” *J. Struct. Eng.*, vol. 112, no. 11, pp. 2462–2477, Nov. 1986.
- [20] K. V Subramaniam, J. S. Popovics, and S. P. Shah, “Fatigue Fracture of Concrete Subjected to Biaxial Stresses in the Tensile C-T Region,” *J. Eng. Mech.*, vol. 128, no. 6, pp. 668–676, Jun. 2002.
- [21] Z. P. Bažant and B. H. Oh, “Crack band theory for fracture of concrete,” *Matériaux Constr.*, vol. 16, no. 3, pp. 155–177, May 1983.
- [22] I. Towhata, *Geotechnical earthquake engineering*. Germany: Springer, 2008.
- [23] I. Towhata and K. Ishihara, “Modeling soil deformation undergoing cyclic rotation of principal stress axes,” *Proc. 5th Int. Conf. Numer. Method Geomech.*, pp. 523–530, 1985.
- [24] I. Towhata and K. Ishihara, “Undrained strength of sand undergoing cyclic rotation of principal stress axis,” *Soils Found. - Japanese Geotech. Soc.*, vol. 25(2), pp. 135–147, 1985.
- [25] M. Gutierrez, K. Ishihara, and I. Towhata, “Model for the deformation of sand during rotation of principal stress directions,” *Soils Found. - Japanese Geotech. Soc.*, vol. 33(3), pp. 105–117, 2011.

CHAPTER 4

FAILURE MECHANISM OF CONCRETE PAVEMENTS - DIVERSE SOIL'S DENSITY COUPLED MOVING AND FIXED- POINT PULSATING LOADS

4.1 Introduction

The effects of the loading type play an important role in the study of the concrete pavement to investigate the fatigue life and failure mode. As previously stated, the study of pavements was originally initiated based on the linear thin plate on the homogeneous elastic foundation [1]–[3] and applied to the practice by Westergaard [4], [5]. The behavior of the concrete slab is obtained from the concentrated point load. These principles have been applied in the current design code for the concrete pavement.

The concrete pavement is the composite system of the soil-concrete slab interaction. It can be referred from the failure damage of the concrete slab decks. The significant reduction of fatigue life under the moving load may occur due to the severe and distributed damage. In case of the soil-concrete slab interaction, this damage may take place in both of the slab and soil. The assessment of the life cycle of the concrete pavement has been conducted in several studies based on the fixed-point load at some locations in the concrete slab as shown in Fig. 4-1a [6]. It is, however, consistent with the static vehicles in the parking lots and not suitable to the real working conditions under the traffic motion of vehicles. The damage of the experimental modeling was therefore localized at the loading point only. Another thing is the complete seal of the soil containment box. The fatigue failure of soil was therefore not examined. Figure 4-1 demonstrates the difference between the experiment in the fixed-point and moving wheel load.

In the assessment of the fatigue life of the concrete pavement, two factors have been considered in this chapter. One is the effects of the loading type, i.e. fixed or

moving. Another is the effect of the nonlinear soil's density. The mechanism for the deterioration of concrete pavements is investigated based on the small-scale mock-up to validate and verify the coupled code as discussed in the previous chapter. In this chapter, the nonlinear three-dimensional numerical analyses are presented in two cases of the fixed-point and moving loads to show how the fatigue life and failure mode of concrete pavements change. The impacts of the nonlinearity of soil's density are examined in the loose, medium dense, dense and very dense compaction, respectively. The fatigue failure damage of the concrete pavement is thus predicted.

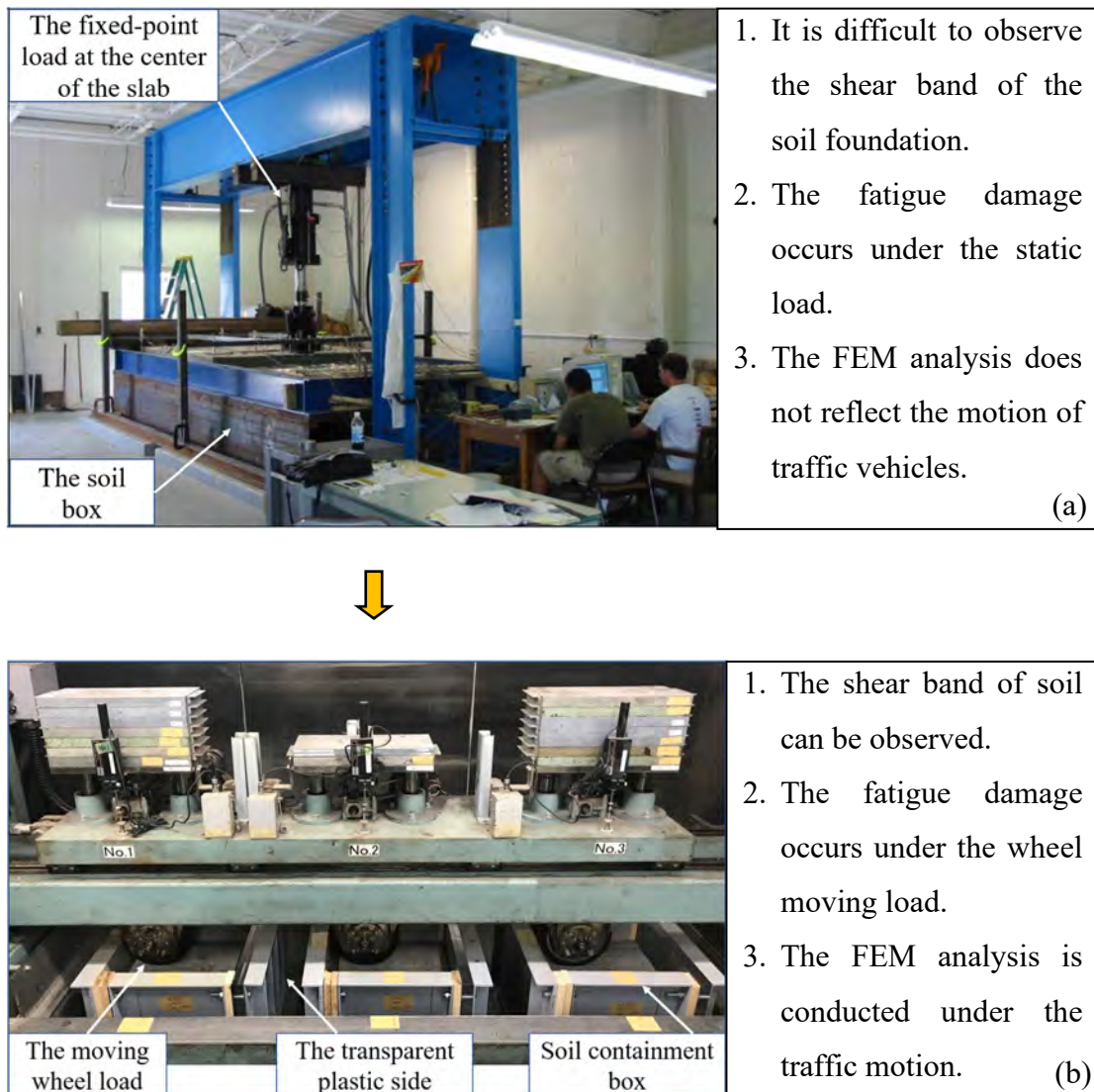


Fig. 4-1 The experiments of the concrete pavement under (a) the fixed-point load [6] and (b) the moving load.

FEM nonlinear analysis shows that the soil's density has a great influence on the fatigue life due to nonlinear behaviors. The results are emphasized on the

significant decrease of fatigue life under the moving loads compared to the fixed-point pulsating ones. This reduction in life is discussed in the views of the computed S-N diagrams to show the distributed damage of concrete slabs and soil over a large number of moving wheel passages, opposite to the localized deterioration of the fixed-point pulsating loads. The specific fatigue failures of the concrete pavement can happen to either soil or concrete slabs as well as both of them depending on the load levels and the soil’s compactness.

4.2 Research Significance of the Failure Mechanism of Concrete Pavements

As can be seen in Fig. 4-2, under the motion of traffic vehicles, the damage of the concrete slab is significantly distributed in space, and the shear failure of the soil foundation is dramatic along the wheel paths. It attributes to that cracks at the surface may develop and existing ones can easily propagate. They become a driving factor to accumulate the fatigue damage of concrete and the soil foundation, concurrently. Conversely, the deterioration of the concrete slab and soil is localized at the loading point in case of the fixed-point pulsating loads. Hence, the failure mode and fatigue life of concrete pavements under the moving loads are absolutely different from the fixed-point ones.

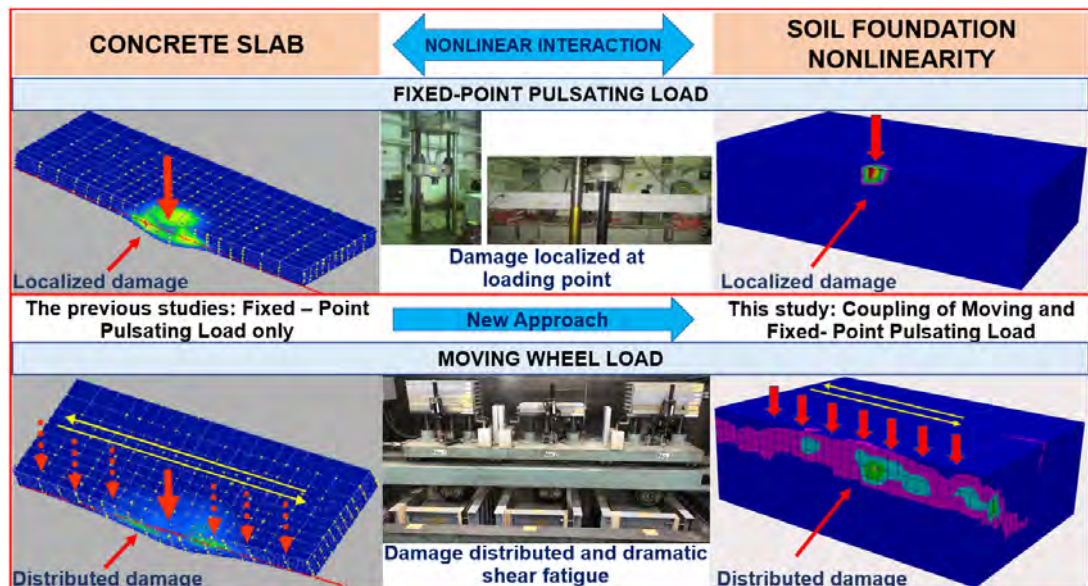


Fig. 4-2 Model scheme of concrete pavement by coupling concrete slabs and soil foundations.

The guidelines for the thickness design of concrete pavements focus on the *Guide for the Design of Pavement Structures* proposed by American Association of State Highway and Transportation Officials [7], *Thickness Design for Concrete Highway and Street Pavements* by Portland Cement Association [8], *Mechanistic-Empirical Pavement Design Guide* [9], and *Guide for Design of Jointed Concrete Pavements for Streets and Local Roads* reported by American Concrete Institute [10]. The design parameters in these guidelines are based upon the principles of the linear, isotropic, homogeneous and elastic soil foundation as well as the concentrated truck axle loads. The concepts may not depict the real working conditions of concrete pavements under the motion of traffic wheels and nonlinearity of the soil foundation. The shear and volumetric failure of soil occur subjected to the wheel-type loading, and they are the key factors to reduce the fatigue life of the pavement.

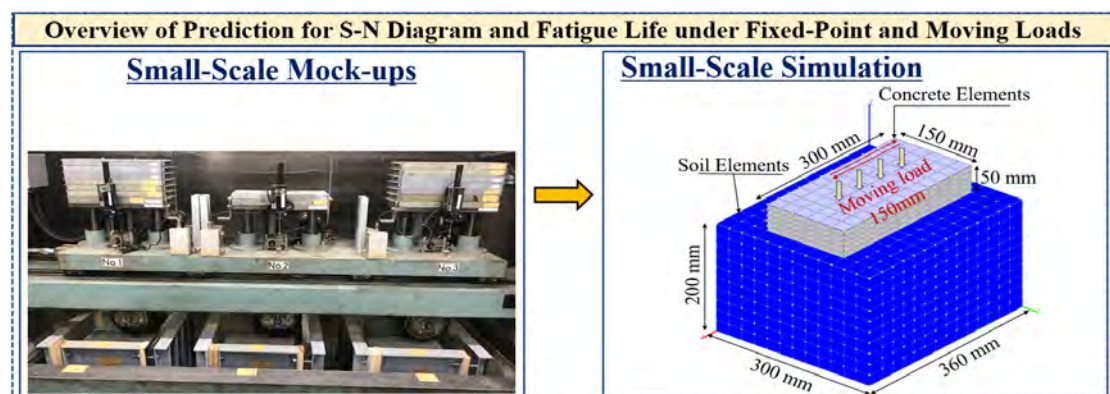
4.3 Methodology

As a preceding section, in consideration of the failure mechanism of the coupled soil and concrete, the nonlinear analysis of RC bridge decks is applied. This model was capable of prediction for the failure mode and fatigue life of the slabs under both moving and fixed-point loads [11]. The coupled code utilized in this study is based on the combination of the thermodynamic and structural mechanics model which has been verified in each scale of experimental evidence [11]–[13]. The coupled numerical code has been investigated from micro to mesoscales, mainly in the evaluation of fatigue life of RC slab decks under the moving load [14] and the shear band of the soil foundation [15].

The summary for the research methodology in a nonlinear couple of the concrete slab and the soil foundation within this chapter is epitomized in Fig. 4-3. The small-scale mock-up was conducted to verify the upgraded code of concrete structures and soil. By combining the constitutive laws of concrete (multi-directional fixed crack modeling) associated with the cumulative high cycle damage and the constitutive modeling for the soil foundation (multi-yield surface plasticity modeling), the nonlinearly coupled code can be applied to predict the behavior of concrete pavements. The full-scale numerical simulations are implemented to show how fatigue life and its mode of pavement change under the fixed point and the wheel path load. Finally, the fatigue life and failure mode of the concrete pavement under the

fixed-point and moving loads as well as S-N diagrams are built based on the diversity of the load magnitudes and the soil's density.

The fatigue failure of concrete pavements is determined based on the limit state either the concrete slab or shear failure of soil, or both of them simultaneously. The behavior of a member in shear is characterized by the propagation of a diagonal shear crack through a major part of the member, not just on a section as in flexural case. When such crack propagation takes place, the shear crack will encounter the pre-existing cracks planes. This multi-crack situation is called as crack-to-crack interaction. Under moving loads, multi-directional flexural cracks occur over the whole domain of the RC slab. Diagonal shear cracks in the longitudinal direction are prevented by crack-to-crack interaction [14][19]. The load-carrying mechanism in the concrete slab may evolve due to crack-to-crack interaction and this results on a reduced area of diagonal shear fracture planes. The limit state of the concrete slab in which the load cycle at failure is estimated by observing the mode of out-of-plane deformation and displacement at the center of the slab. Another point is the soil foundation which is characterized by the shear and volumetric fatigue under the repetitive loading. The fatigue failure limit is analyzed by the shear band and the large displacement of soil. It is noted that the limit state for the fatigue failure of nonlinear FEM analysis is not necessarily the same in practice. In case of FEM analyses, it may be the shear band of soil, the out-of-plane deformation and the large displacement of soil and concrete slab. Meanwhile, in practice, after over the limit state of FEM analyses whether the pavement structure can continue to be used or not depending on the requirements under unusual operation, i.e. the large shear band of soil can cause the unbalance of vehicles. The maximum failure state of pavement system may be obtained when diagonal shear fracture planes of concrete slabs and the shear band of soil occur concurrently.



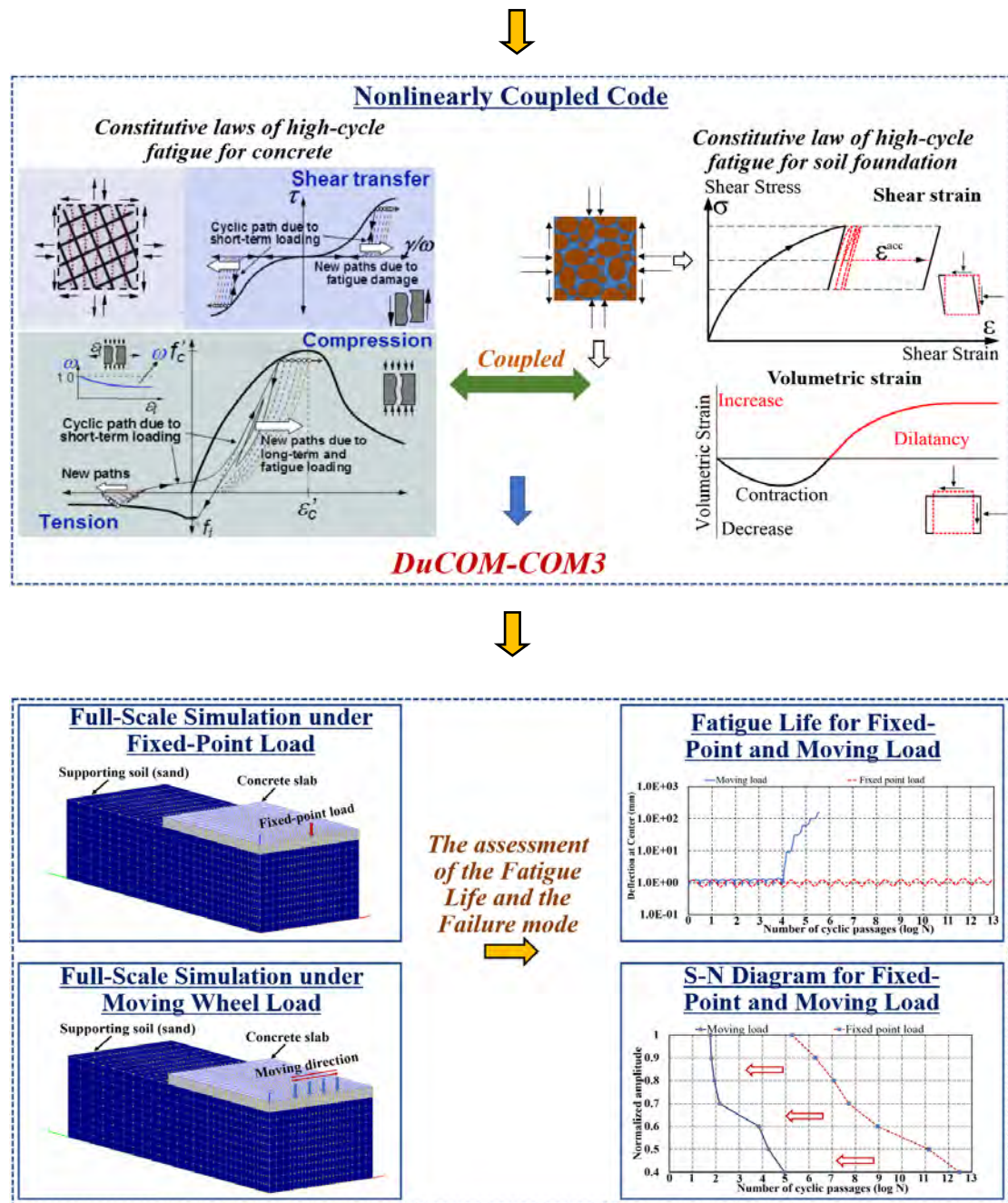


Fig. 4-3 Overview of prediction for S-N diagram and failure mode under the fixed-point and moving loads of concrete pavements [16].

4.4 Numerical Modeling for the Concrete Pavement under the Fixed-Point and Moving Loads

The full-scale three-dimensional FE simulation up to the end of fatigue life on concrete pavements are presented as shown in Fig. 4-4. The half-domain of the concrete pavement with X-coordinate (the moving or fixed-point load direction) is

applied as the symmetric axis. The concrete slab is 3,000 x 4,000mm in plane and the thickness is 250mm.

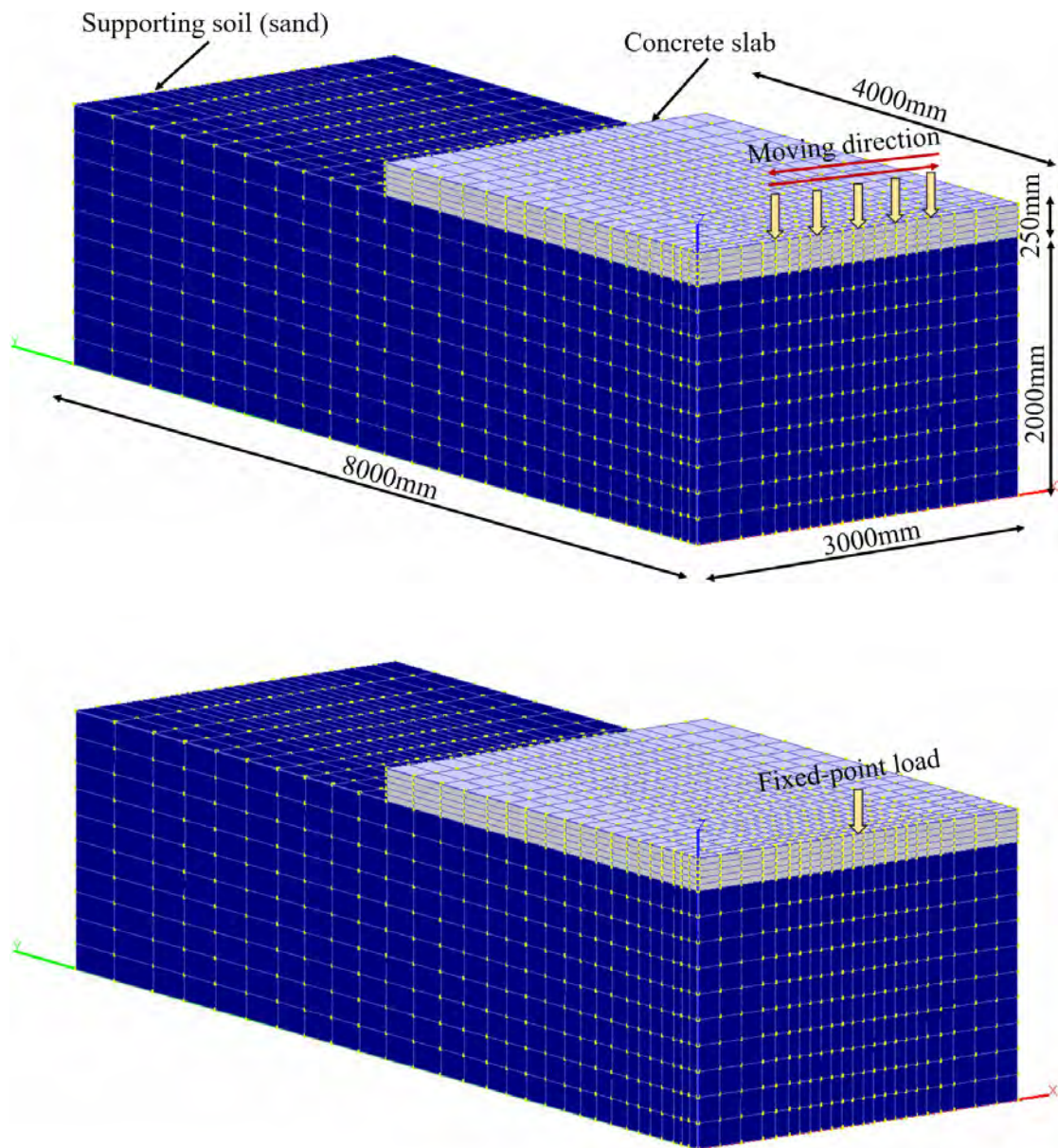


Fig. 4-4 The full-scale numerical modeling for concrete pavements under the fixed-point and moving loads.

A light reinforcement ratio (RR 0.1%) is used in this simulation to illustrate the weak slab in practices. Two types of load, cyclic fixed point and moving loading, are applied in the model to show the comparison of the failure mode and the fatigue life. In the case of comparing the S-N diagram between the fixed point load and the moving one, three typical cases to present the three kinds of the soil foundation are decided as RD 50% (the loose soil), RD 75% (the compacted one), and RD 95% (the

very compacted one), respectively. The S-N diagram shows the gradual reduction of the load level (normalized amplitude of load) and the number of cycles. The gradual reduction of load amplitudes (392kN, 353kN, 313kN, 274kN, 235kN, 196kN, and 156kN) is executed to demonstrate the dramatic decrease of fatigue life in case of the moving load. The moving or fixed-point load is produced by linearly applying nodal forces in each load step at the symmetric axis. Water-to-cement ratio of concrete is 55% as the normal use in practice. The selection of W/C=55% is based on the recommendation of the durability and economical consideration for the paving mixtures of the normal concrete in ACI 325.

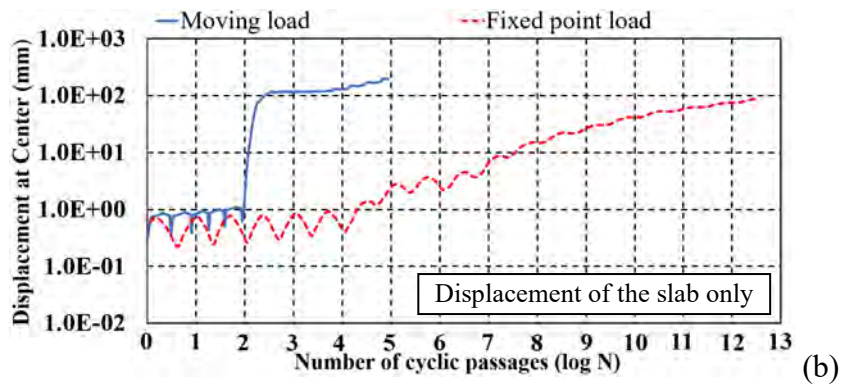
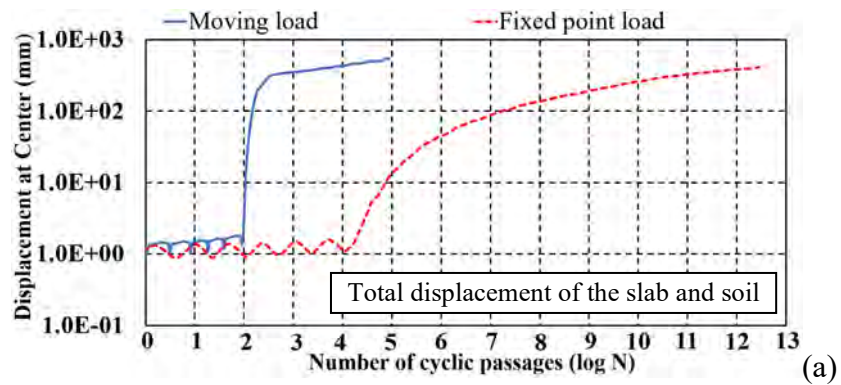
The plane dimension of soil is 3,000mm x 8,000mm and 2,000mm in depth. The soil foundation is assumed as sand with the relative density 50%, 60%, 65%, 70%, 75%, 80%, 85%, 90%, and 95% as the non-compacted, (medium) compacted, very compacted one, respectively. The displacement normal to the side boundaries is restrained as plain strain. The magnified direct path integral is applied by using the binary increasing magnification with each passage along the slab axis [14]. The multi-frontal direct linear sparse matrix solution in the FE solution was also applied to accelerate the time calculation. The drying shrinkage has been automatically reproduced through the moisture loss under the ambient relative humidity of 60% and temperature 20°C [17].

4.5 Results and Discussion

Figure 4-5 shows the S-N diagram and one typical case (load level 156kN) for the fatigue life of the concrete pavement under the moving and fixed-point load with soil's density 50%. As can be seen in Fig. 4-5a, the total displacement of concrete and soil under the traffic motion suddenly and dramatically increase at the very early stage. The fatigue life is significantly shortened compared to the fixed-point load. It can be explained due to the severe shear band failure of the non-compacted soil foundation. The displacement of soil is excessively higher than the concrete slab. In case of the fixed-point load, the total displacement of the concrete slab and soil gradually increases at the belatedly cycle. Hence, the fatigue life sharply rises compared to the moving load. It is similar to the case of moving load, the total displacement in the fixed-point one is strongly governed by the soil's displacement. We can say the damage of the soft supporting soil is more critical than the concrete

slab in both cases. A nonlinear couple of the concrete slab and the soil foundation under the high cycle fatigue are different from the moving and fixed-point load.

As previously stated, a range of diverse magnitudes has been applied to investigate the S-N diagram as shown in Fig. 4-5d. The fatigue life of concrete pavements under the moving load is dramatically decreased by computations compared to the fixed-point load. The disparateness of the fatigue life has rapidly risen when the load levels reduced. Due to the nonlinear mechanics of soil and the effect of the load amplitude, the shear failure of the soil and the damage of the slab occur at the different cycles in both fixed and moving loads. When the very high load amplitude has been applied, the deterioration of the concrete slab easily occurred after loading. Conversely, under the low load levels, the shear band of soil is predominant compared to the damage of the concrete slab [16]. The shear band thickness is a function of mean particle diameter and less dependent on the particle shape [15]. Under the moving load, the shear and volumetric fatigue of soil occur concurrently. Its relation is defined based on the multi-yield surface plasticity modeling and coupled in the nonlinear interaction with the concrete slab as depicted in section 3.3.2.



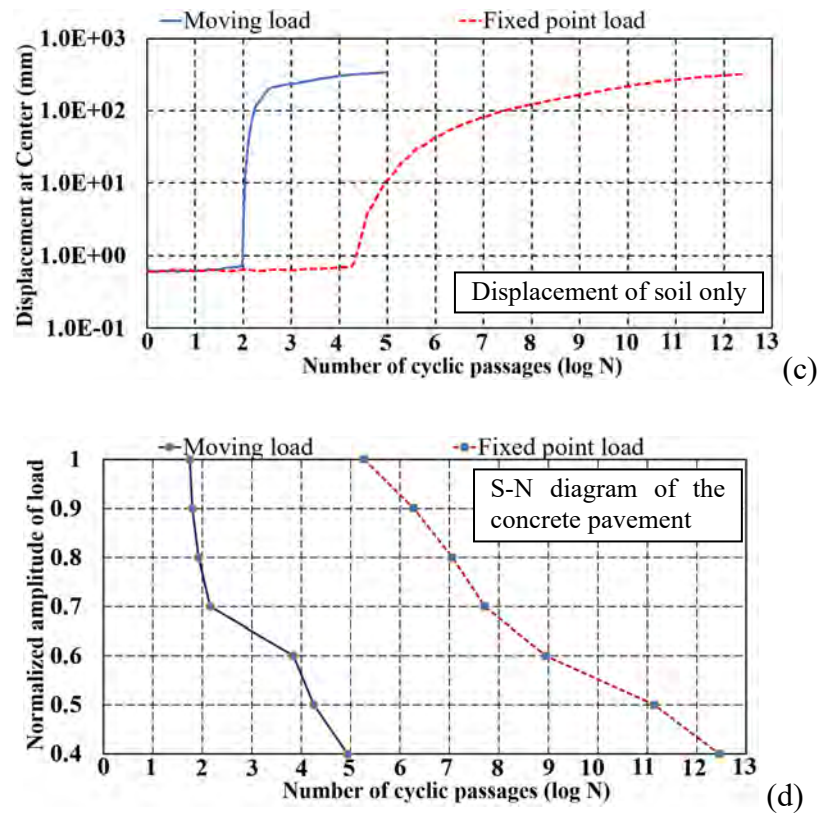


Fig. 4-5 S-N diagram and fatigue life of the concrete pavement under RD 50% of the soil foundation.

Fig. 4-6 shows the fatigue life of the concrete pavement (load level 156 kN) under RD 60% (it is equivalent to the poor to fair or medium dense of the soil foundation). It can be seen that under the fixed-point load, the shear band of soil started at the later stage compared to soil of RD 50%. This behavior is similarly observed in the case of the moving load. The displacement of the soil foundation is superior to the concrete slab in both cases. It can be assumed that under the medium dense foundation (RD 60%), the total displacement of the concrete pavement is strongly governed by the displacement of the soil foundation. FEM analysis of the fixed-point and moving load in the concrete pavement shows better results in both of the concrete slab and soil compared to the case of soil's density 50% due to the more compacted soil applied in this numerical modeling. However, under the moving load, the severe shear band of soil and the deterioration of the slab take place at the earlier compared to the fixed-point load obviously. The fatigue life of the pavement under the moving load is thus dramatically decreased compared to the fixed-point one. As can be seen from Fig. 4-5 and Fig. 4-6, we may say that the fatigue failure in the

concrete pavement under the loose or medium dense (RD 50% or 60%) has presided in the shear band of the soil foundation.

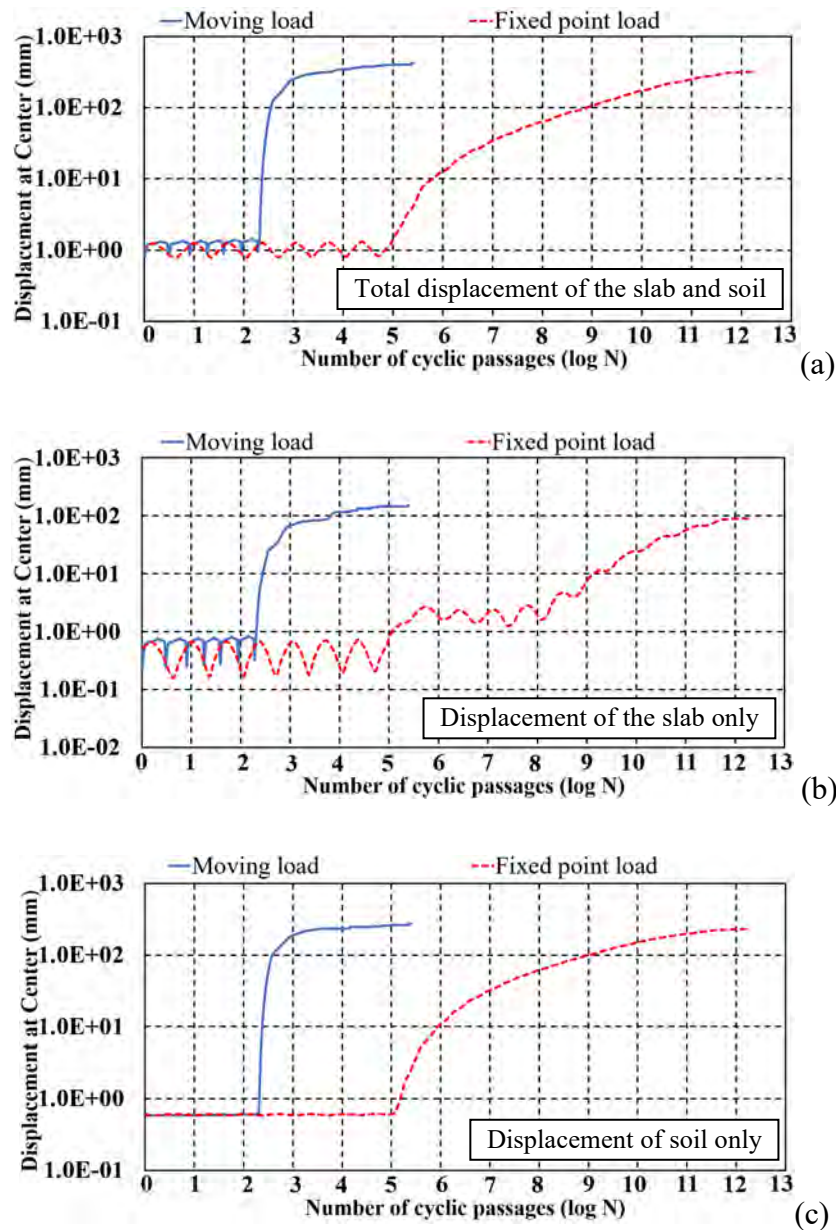


Fig. 4-6 Fatigue life of the concrete pavement under RD 60% of the soil foundation.

Fig. 4-7 depicts the fatigue life of the concrete pavement under RD 65%. This is the case of the dense soil foundation. Owing to the denser supporting soil, the shear failure of soil under the fixed -point load occurs at the later period compared to the cases of RD 50% and 60%. The damage of the concrete slab is therefore less critical. It is differently observed in the case of the moving load. When the soil becomes more compacted, the fatigue failure of the concrete pavement occurs both of the concrete slabs and soil. It is due to that the displacement of the concrete slab and soil is nearly

similar at the final fatigue cycle. It is predicted that the fatigue failure of the concrete pavement under the moving wheel load is the coupling damage of the slab and the soil foundation. In the event of the fixed-point load, the damage of the soil is stronger than the slab. It is impossible to apply the fixed-point load to predict the real working condition of the pavement in the case of RD 65%.

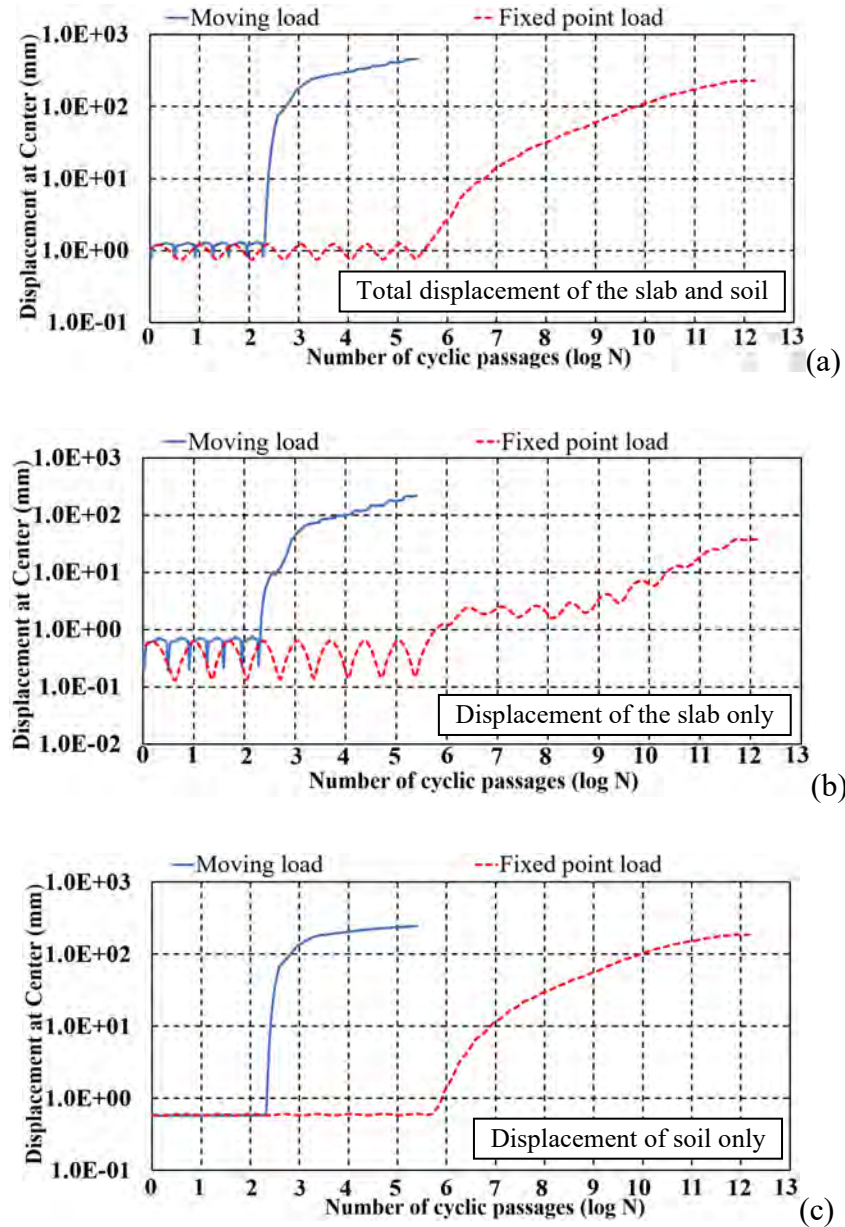


Fig. 4-7 Fatigue life of the concrete pavement under RD 65% of the soil foundation.

Figure 4-8 shows the fatigue life of the concrete pavement under RD 70% of the soil foundation. Comparing to the case of RD 65%, the shear band of soil occurs at the later stage under the moving load. The displacement of the slab and soil is nearly similar at the final cycle. The fatigue failure may be also the coupling damage of the

concrete slab and the soil foundation under the moving load. In case of the fixed-point load, the fatigue failure of soil does not take place. The displacement of the concrete slab shows the small value compared to the case of the moving load. Similarly to the case of RD 65%, when the soil becomes more compacted (RD 70%), it is insurmountable to predict the failure mode and the fatigue life of the pavement by applying the fixed-point load.

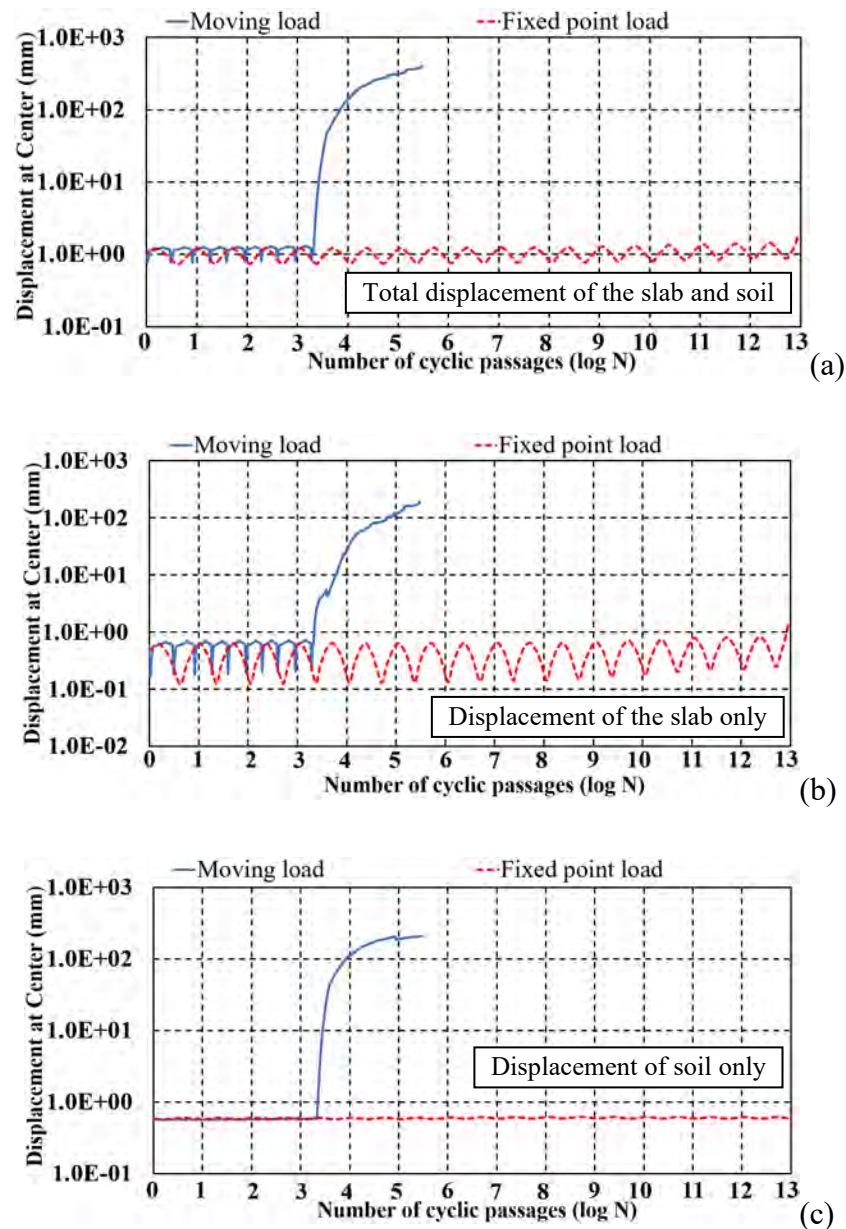
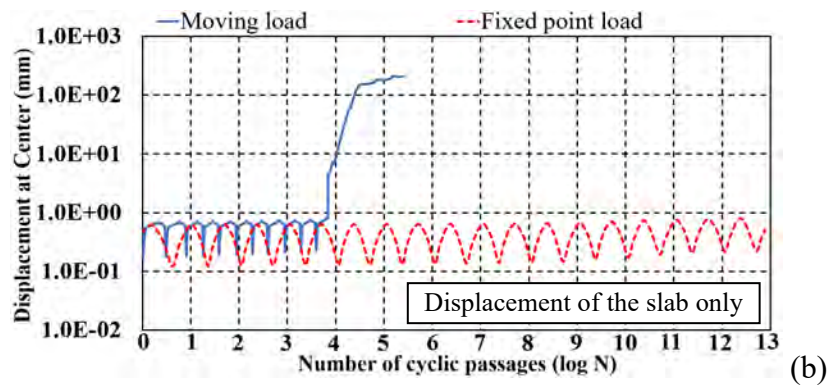
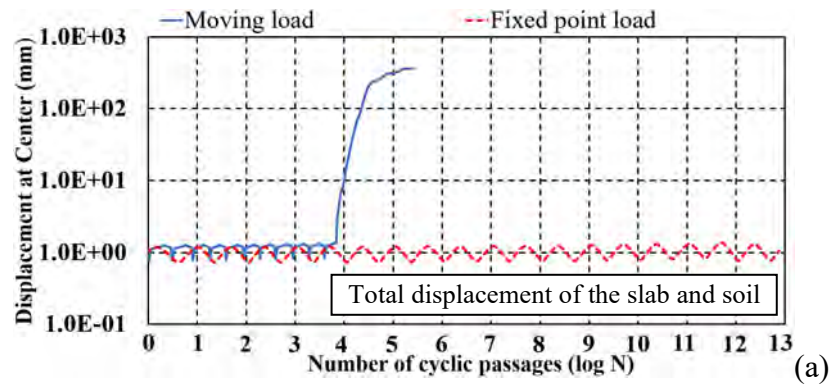


Fig. 4-8 Fatigue life of the concrete pavement under RD 70% of the soil foundation.

Figure 4-9 shows the S-N diagram and the fatigue life of concrete pavement under the fixed-point and the moving loads with soil’s relative density 75% (compacted one). Due to the denser soil, the shear band of soil under the moving load

took place at the later period compared to previous cases. The total fatigue life is thus increased. There is less different from the displacement of the slab and soil. The total displacement is a couple of the separate displacement of the concrete slab and soil. It is an interesting point that the shear failure of soil is not observed in case of the fixed-point load as the case of RD 70%. The total displacement of concrete slab and soil is primarily governed by the displacement of the slab only under the fixed-point load. It can be concluded that when the more compacted soil is applied (RD 75%), the fixed-point load can not reflect the real working condition of vehicle motions. The fatigue failure in FEM analysis under the moving load is the coupling damage of the slab and the soil foundation.

It is similar to the case of RD 50%, a mass of load levels is applied to investigate the S-N diagram. The computed S-N diagram curve for the moving load case shows a remarkable reduction in life. This result illustrates the same trend of the case of RD 50% [16].



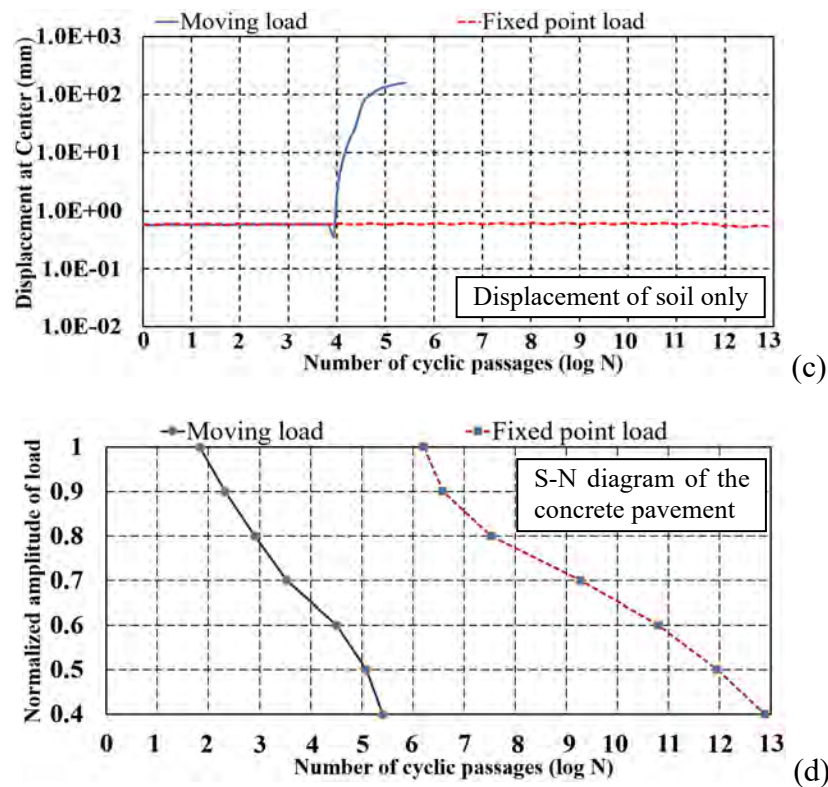
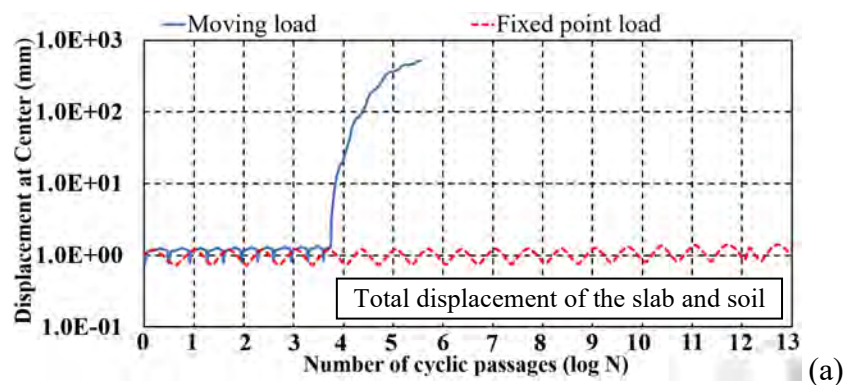


Fig. 4-9 S-N diagram and fatigue life of the concrete pavement under RD 75% of the soil foundation.

Figure 4-10 shows the fatigue life of pavements under the RD 80%. This soil's density is a value between the compacted and very compacted one. As can be seen in Fig. 4-10, the displacement of soil is dramatically decreased compared to the displacement of the slab under the moving load. The shear band of soil occurs at the late cycle after loading. However, this shear band is significantly reduced to the previous cases. The fatigue failure is thus governed by the damage of the concrete slab more than the failure of soil.



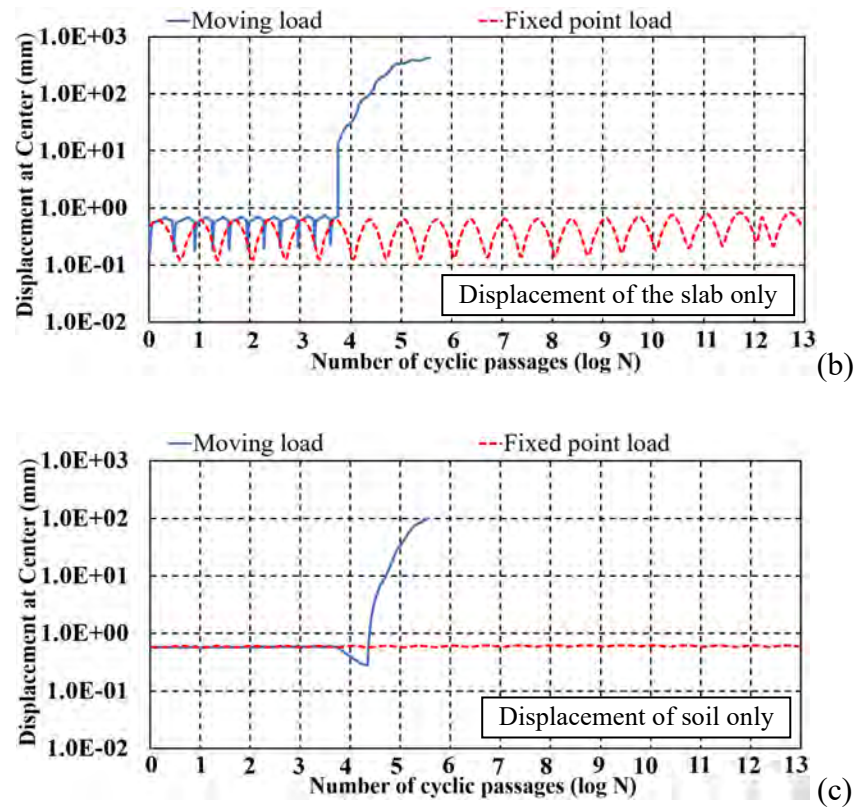
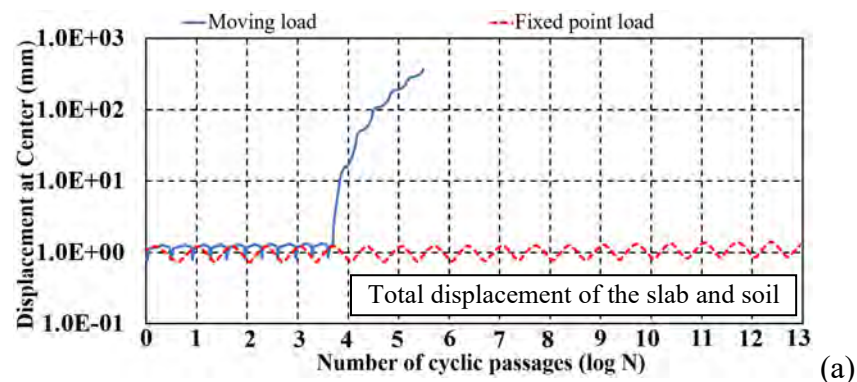


Fig. 4-10 Fatigue life of the concrete pavement under RD 80% of the soil foundation.

Figure 4-11 shows the fatigue life of the concrete pavement under the very dense soil foundation (RD 85%). It can be seen that the shear band of soil is critically reduced compared to the case of RD 80%. The total displacement is governed by the displacement of the slab only. It means that the fatigue failure is demonstrated by the deterioration of the slab. In the event of the fixed-point load, It is similar to the case of the compacted soil. There is no damage in both of the slab or soil.



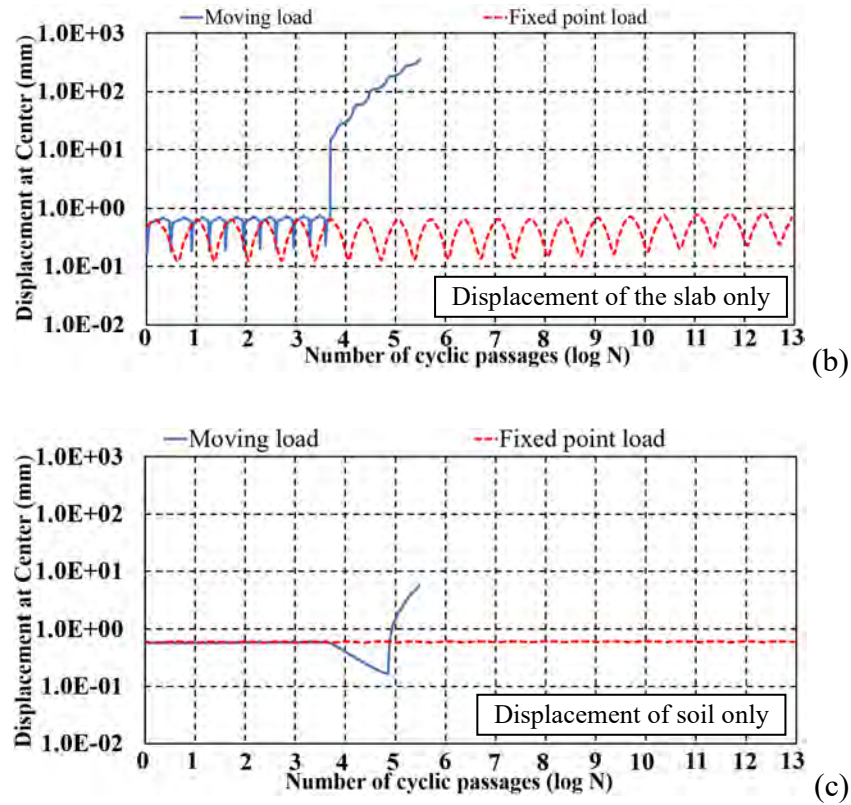
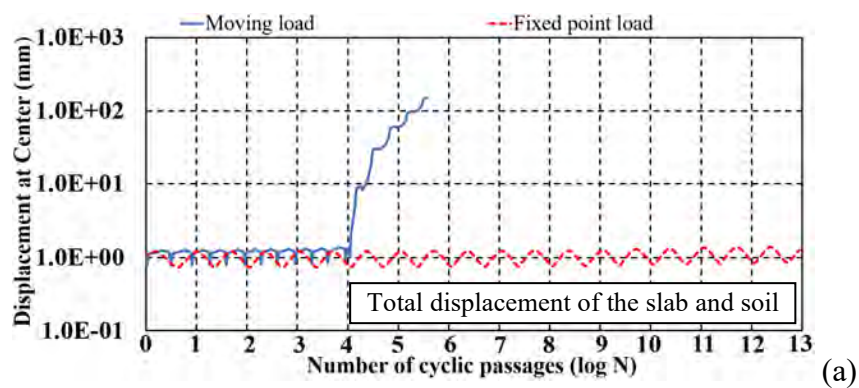


Fig. 4-11 Fatigue life of the concrete pavement under RD 85% of the soil foundation.

Figure 4-12 depicts the case of pavement under RD 90%. It is similar to the case of RD 85%. The shear failure of soil is small compared to the damage of the slab. The total displacement is thus governed by the displacement of the concrete slab only. The fatigue failure under the moving load is therefore the deterioration of the slab. There is no shear band of soil and the damage of the slab under the fixed-point load.



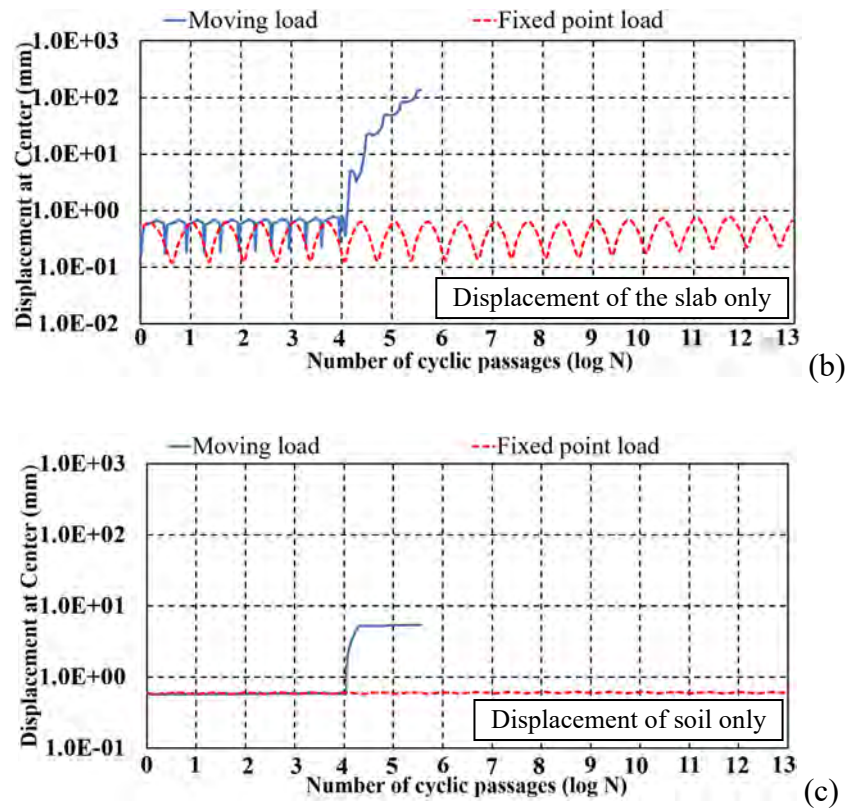


Fig. 4-12 Fatigue life of the concrete pavement under RD 90% of the soil foundation.

Figure 4-13 illustrates the S-N curve and the fatigue life of pavements under the highly compacted foundation (RD 95%). Owing to the density of soil, the shear failure of soil will not occur in both the fixed-point and the moving loads. The behavior of the foundation under the fixed point or moving load is similar as shown in Fig. 4-13c. The total displacement of the slab and soil in both cases is governed solely by the displacement of the concrete slab. However, this value in the moving load is more critical than the fixed-point one. The fatigue life is thus sharply decreased. It is predictable that the failure mode for the damage of pavements focuses on the deterioration of the slab alone. The computed S-N curve depicts the reduction of fatigue life in the event of moving loads. Frankly speaking, the behavior of pavement under the high or low amplitude is similar to the case of RD 50% and RD 75%. The high load levels can cause a faster deterioration of the concrete slab in both cases compared to the low ones [16].

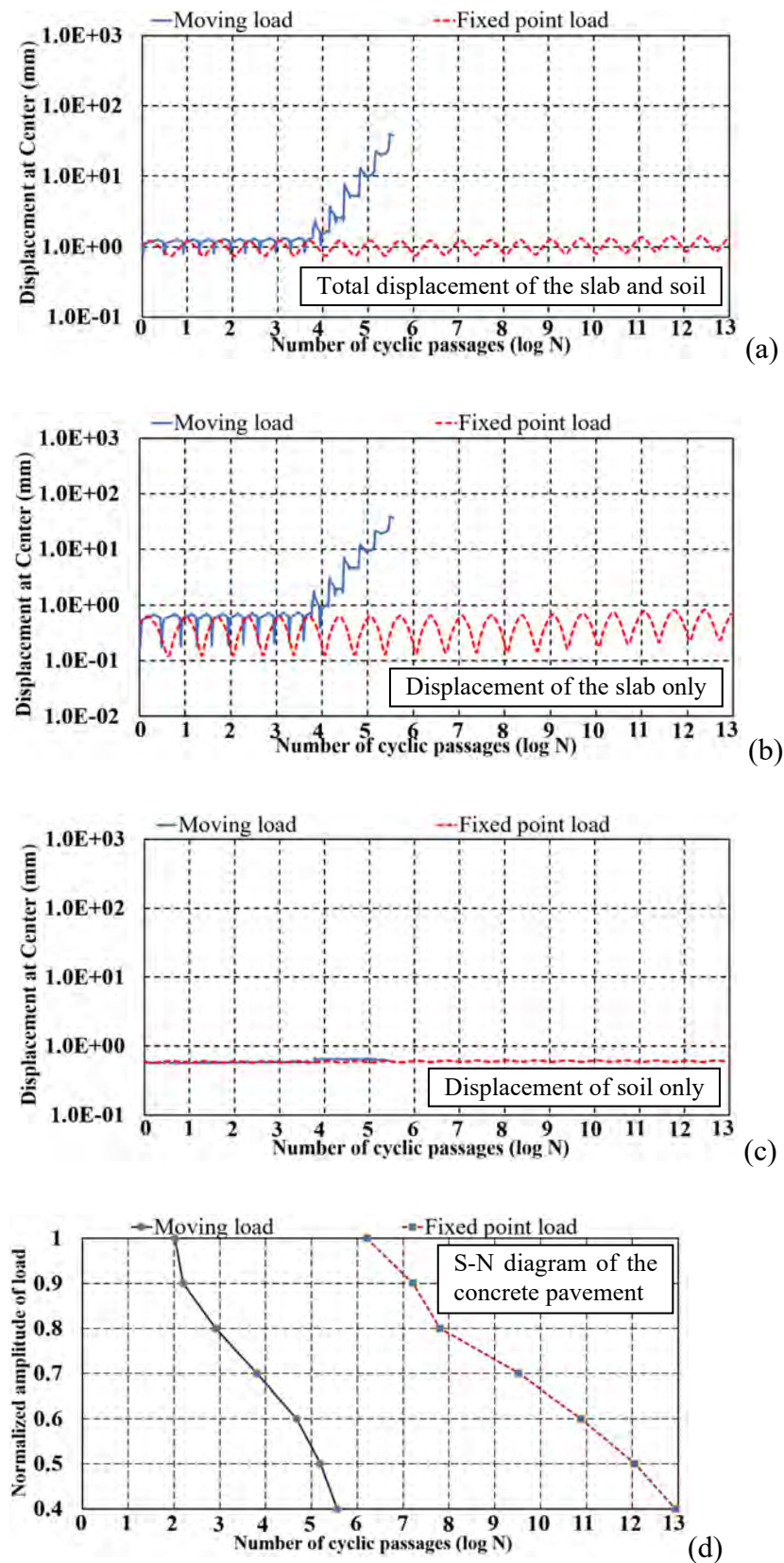
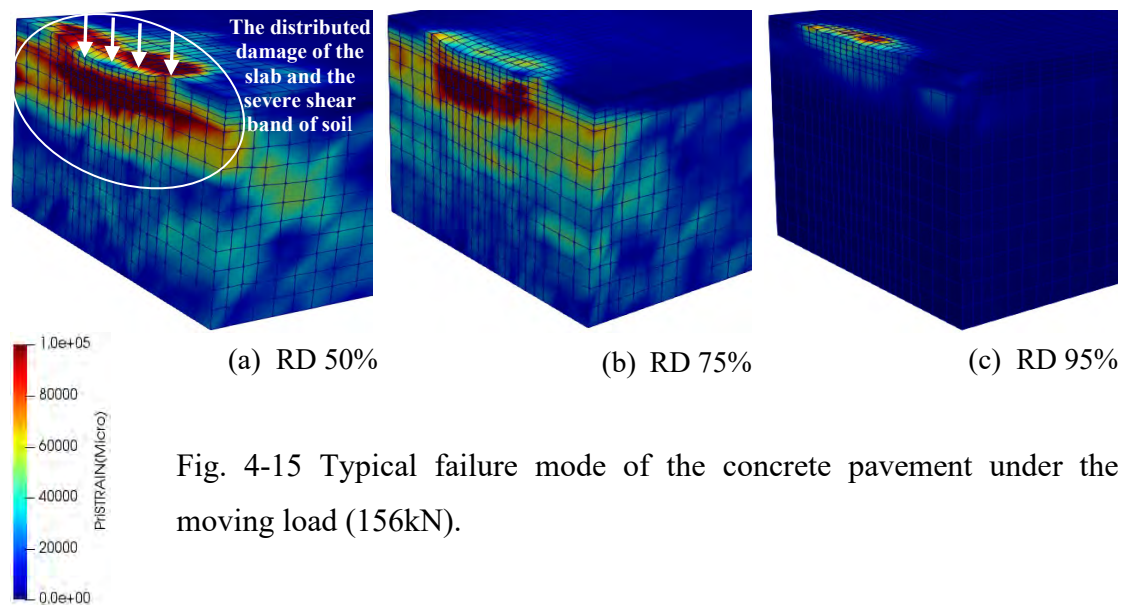
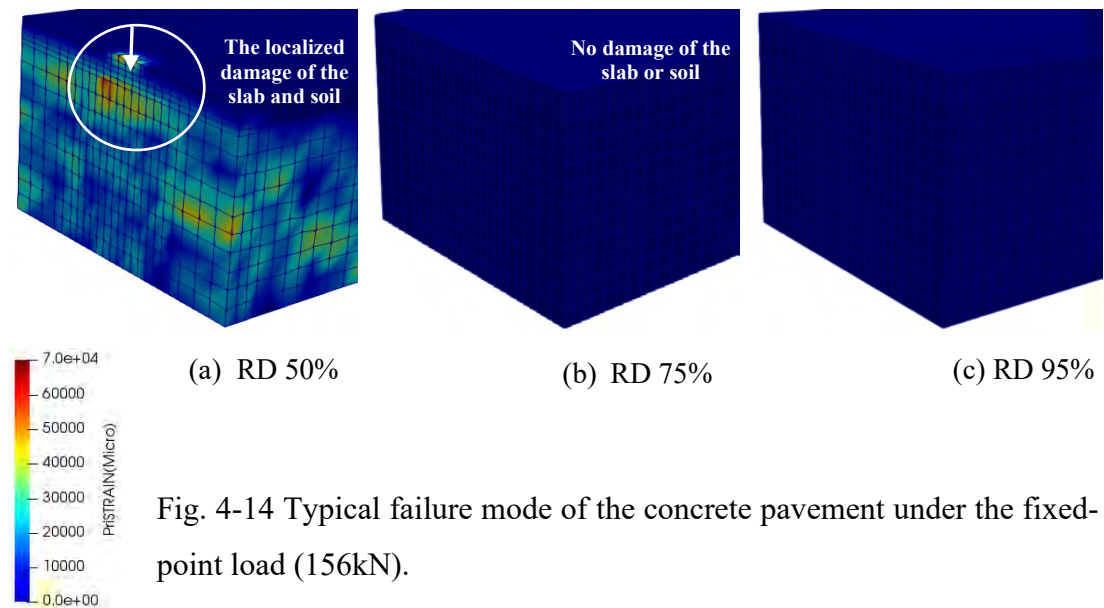


Fig. 4-13 S-N diagram and the fatigue life of the concrete pavement under RD 95% of the soil foundation.

Figure 4-14 and 4-15 show the failure mode of concrete pavements under RD 50%, 75%, and 95%, respectively. It can be seen that under the fixed-point load, the damage of the concrete slab is localized at the loading point only in case of the non-compacted soil (RD 50%). There is no deterioration of the concrete slab or soil in other cases. Conversely, under the moving loads, the damage of the concrete slab is distributed along the wheel-path. Depending on the soil conditions, this damage is much or less. In the event of RD 50%, the severe shear band of soil occurs, the deterioration of concrete slab is thus the most critical case. The failure mode is primarily governed by the shear failure of soil foundation as discussed in Fig. 4-5. When the compacted soil is applied, the damage of the slab and soil occur concurrently. Compared to the RD 50%, the shear band of soil and the deterioration of the slab in RD 75% are less critical. Therefore, the failure mode is the couple of the damage of the concrete slab and soil as previously stated in Fig. 4-9. Finally, the failure mode of the fixed-point and moving load of RD 95% reflects the behavior of the displacement depicted in Fig. 4-13. Under the fixed-point load, it is similar to RD 75%, there is no damage of the concrete slab and soil. In the case of the moving load, the failure mode is strongly governed by the distributed damage of the concrete slab. There is no shear band failure of soil observed in both fixed-point and moving load. It means that when the very compacted soil is applied, the failure of pavement focuses on the damage of the concrete slab only.

The mechanism of the fixed-point load may concentrate on the localized damage of the concrete slab and soil under the soft foundation. When the soil is greatly compacted, this damage may not occur. Under the traveling-wheel type load, the distributed deterioration of concrete slabs may develop due to the crack-to-crack interaction, and it results in the reduced area of diagonal shear fracture planes in concrete slabs [14], [18]. The severe shear band of soil under the high cycle moving loads can be caused by the accumulative failure of the shear and volumetric fatigue.

The fatigue analysis with the high-cycle loading at failure is observed by investigating the mode of out-of-plane deformation of the concrete slab and the shear band of soil foundation as well as the displacement at the center of the slab and/or the foundation.



4.6 Conclusions for Chapter 4

The comparison of the fixed-point pulsating and moving load in the couple with the diverse soil foundation is computationally estimated in the views of the fatigue life of the concrete pavement. The three-dimensional finite element analysis indicates the dramatic reduction of fatigue under the moving loads, and the following conclusions have been obtained.

1. The failure mode of concrete pavements under the fixed-point and moving load is greatly different. One is the localized damage of the concrete slab and soil.

Other is the distributed deterioration of the slab and the severe shear band of soil. The fatigue life of the moving load case is therefore significantly reduced.

2. Three-dimensional high-cycle fatigue simulation of soil-concrete slab interaction shows three types of failure mode depending on the soil's density and load amplitudes as the damage of the soil foundation (the non-compacted one), the coupling damage of the concrete slab and soil (the compacted one), and the damage of the slab only (the very compacted one), respectively.

The study of the concrete slab coupled the soil foundation has been investigated. The traveling-wheel type loads and nonlinear mechanics of soil coupled with the concrete slab should be considered to predict the fatigue life of the concrete pavement.

References in Chapter 4:

- [1] V. A. Patil, V. A. Sawant, and K. Deb, “3D Finite-element dynamic analysis of rigid pavement using infinite elements,” *Int. J. Geomech.*, vol. 13, pp. 533–544, 2013.
- [2] Y. H. Huang, *Pavement Analysis and Design*. Pearson, 2003.
- [3] C.-P. Wu and P.-A. Shen, “Dynamic Analysis of Concrete Pavements Subjected to Moving Loads,” *J. Transp. Eng.*, vol. 122 (5), pp. 367–373, 2002.
- [4] H. M. Westergaard, “Analysis of stress in concrete pavements due to variations of temperature,” in *Proceedings of 6th Annual Meeting of the Highway Research Board*, 1926, pp. 201–215.
- [5] H. M. Westergaard, “Theory of concrete pavement design,” *Proc. Highw. Res. Board*, vol. 7, no. Part 1, pp. 175–181, 1927.
- [6] J. R. Roesler, J. E. Hiller, and P. C. Littleton, “Large-scale airfield concrete slab fatigue tests,” in *Proceedings - 8th International Conference on Concrete Pavements: Innovations for Concrete Pavement: Technology Transfer for the Next Generation*, 2005.
- [7] AASHTO, *AASHTO Guide for Design of Pavement Structures*. 1993.
- [8] P. C. Association, *Thickness design for concrete highway and street pavements*. 1984.
- [9] AASHTO, *Mechanistic Empirical Pavement Design Guide: A Manual Practice*. 2008.
- [10] ACI 325, *Guide for design of jointed concrete pavements for streets and local roads*. ACI Committee 325, 2002.
- [11] K. Maekawa, T. Ishida, and T. Kishi, *Multi-scale modeling of structural concrete*. London: Taylor and Francis, 2008.
- [12] K. Maekawa and C. Fujiyama, “Crack water interaction and fatigue life assessment of RC bridge decks,” *Poromechanics V ASCE 2013*, pp. 2280–2289,

2013.

- [13] K. Maekawa, R. Chaube, and T. Kishi, *Modeling of concrete performance-hydration, microstructure formation and mass transport*. London: E&FN Spon, 1999.
- [14] K. Maekawa, E. Gebreyouhannes, T. Mishima, and X. An, “Three-dimensional fatigue simulation of RC slabs under traveling wheel-type loads,” *J. Adv. Concr. Technol.*, vol. 4, no. 3, pp. 445–457, 2006.
- [15] M. Soltani and K. Maekawa, “Numerical simulation of progressive shear localization and scale effect in cohesionless soil media,” *Int. J. Non. Linear. Mech.*, vol. 69, pp. 1–13, 2015.
- [16] H. Q. H. Nguyen and K. Maekawa, “Numerical simulation on the life-cycle assessment of concrete pavement - diverse soil’s density coupled to moving and fixed-point pulsating loads,” in *12th International Conference on Concrete Pavements, Minneapolis, Minnesota, USA, 2020*.
- [17] H. Q. H. Nguyen, K. Maekawa, and S. Komatsu, “Three-dimensional high-cycle fatigue simulation of soil-concrete pavement slab interaction under moving loads,” *Proc. 8th Int. Conf. Asian Concr. Fed.*, vol. 2, pp. 1207–1216, 2018.
- [18] Y. Maeda and S. Matsui, “Fatigue of reinforced concrete slabs under trucking wheel load,” *Proc. JCI*, no. 6, pp. 221–224, 1984.
- [19] K. Maekawa, A. Pimanmas and H. Okamura, “Nonlinear Mechanics of Reinforced Concrete” *Taylor and Francis*, 2003.

CHAPTER 5

NONLINEAR FEM ANALYSIS FOR THE NEW APPROACH TO PREDICT AND ASSESS THE BALANCED THICKNESS OF CONCRETE PAVEMENT SLABS RESPONSE TO MOVING LOADS

5.1 Introduction

The thickness of the concrete slab in pavement design and construction is discussed as a key factor which directly affects the fatigue life as well as the cost for construction and maintenance. It is therefore necessary to decide the balanced thickness of the slab rationally. As discussed in Chapter 3, there were six mock-ups presented to verify and validate the failure mode of the coupling of the concrete slab and the soil foundation. The key note for the series of these experiments was the high load level 1,029N with the relative density of RD 50% and RD 75%, respectively. At the same load amplitude and thickness, soil's density 75% showed the immediate damage of the concrete slab just after the static load applied at the slab center. Meanwhile, soil's density 50% depicts the better coupling with the concrete slab and the total displacement is therefore smaller than the case of the thicker slab. This result may be opposite to the current design principle based on the in-plane theory of slabs supported on the distributed elastic springs. The fatigue life of the concrete pavement is primarily governed by both the slab thickness and soil's density. The thick slab can cause the decrease of the fatigue life on the soft foundation and the thin one supported by the dense soil foundation can significantly reduce the fatigue life of the concrete pavement due to the severe flexural tension at the bottom side of slabs. Owing to the nonlinearity of the soil foundation, the required thickness of the loose foundation is smaller than the dense one. The thickness of the concrete slab is thus a key factor to revise the design code of the pavement which has been studied based on the in-plane theory on elastic foundation.

This chapter presents the comparison between the full-scale numerical simulation (based on nonlinear mechanics of soil and the concrete slab under moving loads) and the required pavement thickness in some existing design guidelines (based

on the principle of an elastic slab over a dense liquid subgrade under concentrated loads). The newly balanced thickness in the concrete pavement is proposed for the purpose of bridging the gap in the current design codes and engineering practices.

5.2 Fundamentals of the Current Design Codes

The guidelines for the design thickness of concrete pavements have been focused on the *Guide for the Design of Pavement Structures* proposed by American Association of State Highway and Transportation Officials [1], *Thickness Design for Concrete Highway and Street Pavements* by Portland Cement Association (PCA) [2], a newer design program named as the *Mechanistic-Empirical Pavement Design Guide* (MEPDG) [3]–[6], and *Guide for Design of Jointed Concrete Pavements for Streets and Local Roads* reported by American Concrete Institute [7].

AASHTO Design Guide provides the fundamentals for pavement design practices and requires a number of design parameters. It is therefore called as the empirical approach [4], [5], [8]. The basis for the PCA design method is developed based on the theory of the pavement by Westergaard, G and Ray [9], [10] and finite element analysis [2]. The criteria for the design procedures in PCA is based on a comprehensive analysis of pavement's resistance to fatigue and displacements by using the program of finite element computer [2]. The design factors are thus simpler than the AASHTO design method, focused on the flexural strength of the concrete which can be automatically computed in the program, the soil's density and the weight as well as types of truck axle loads (the critical case should be recommended). The PCA method is called as the mechanistic approach [2], [4], [8].

MEPDG method is a software to analyze the failure potential for a given thickness design. It requires huge data and is not convenient to be used by local agencies. Each of paving association provides their different softwares and specific inputs are required [5]. The MEPDG does not depict the particular pavement thickness. Finally, Guideline ACI 325 provides the slab thickness to achieve an acceptable pavement system for streets and local roads. The concepts for ACI 325 is based on the principles developed by PCA and others (AASHTO and ASTM) to analyze the concrete slab supported by the elastic slab over a dense liquid subgrade. we can say that the mechanistic method for the pavement thickness is approached via PCA and ACI 325.

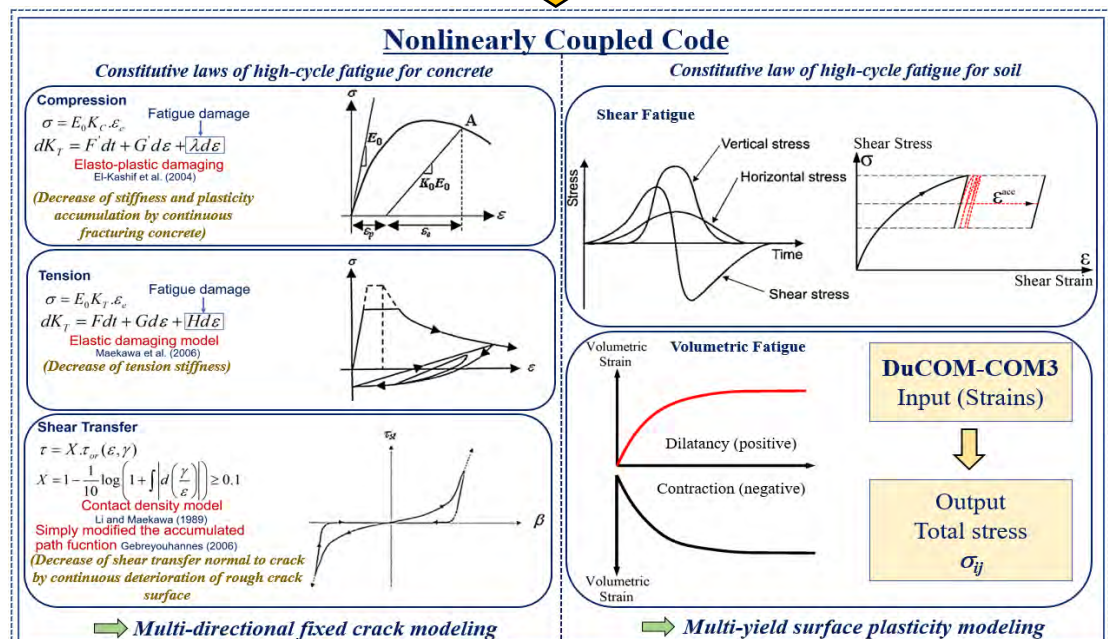
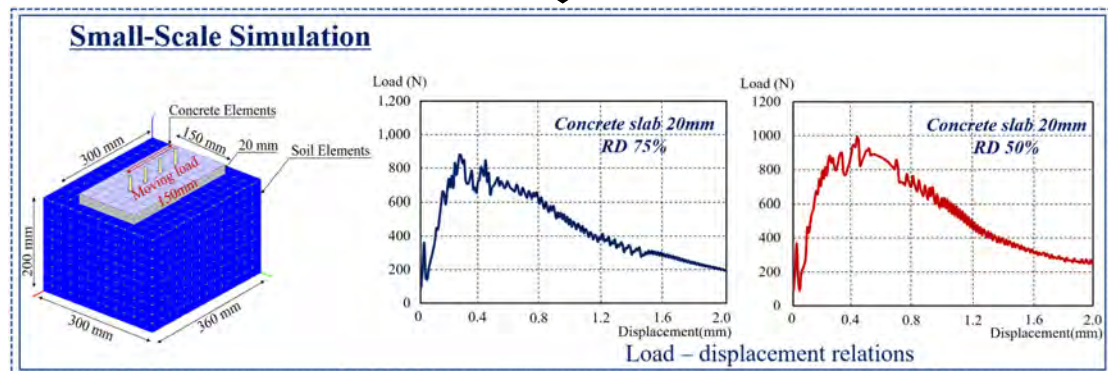
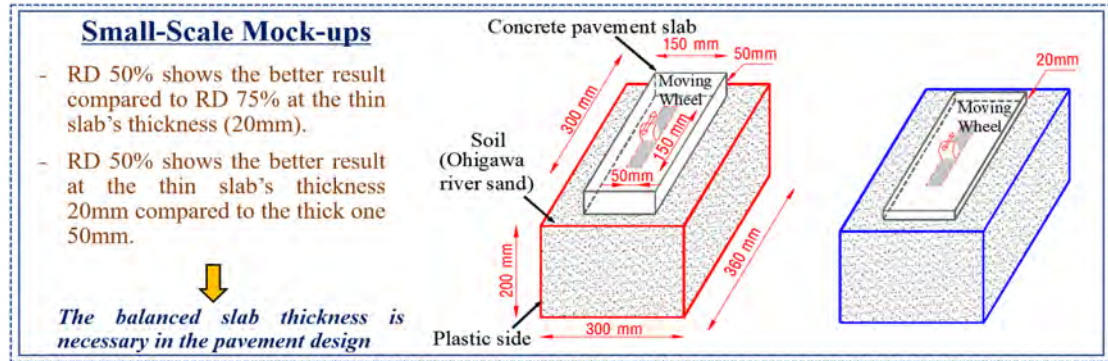
In the case of four current guidelines for the design of pavement structures, soil is considered as the linear, isotropic, homogeneous and elastic foundation. The failure modes are therefore focused on the damage of the concrete slab. In reality, under the high-cycle fatigue of moving traffics, the shear and volumetric failure of the soil foundation appear and they are also the key factor to reduce the fatigue life of the pavement. The nonlinearity of coupling between the concrete slab and soil has been considered in the previous chapter, and the coupled code for high cycle fatigue has been verified and validated as well. In this chapter, PCA and ACI 325 approached by the mechanistic method are selected to compare with the nonlinearly numerical simulation to recommend the rational thickness in the pavement design. The critical cases of thickness design have been proposed in this comparison (the high and low average daily traffic in both directions with all vehicles, the maximum axle load, the normal strength of concrete, and the pavement thickness without curb and gutters or shoulders (unsupported edges)). The support of the soil foundation is considered in four cases of the poor condition (loose), poor to fair condition (medium dense), fair to good condition (dense) and good to excellent condition (very dense).

5.3 Research Methodology – a New Approach for the Slab's Thickness of the Concrete Pavement

The summary of the research methodology of the new proposal for the slab's thickness of the concrete pavement is shown in Fig. 5-1. Starting from the key point of the small-scale mock-ups presented in chapter 3, the experiment and FEM analysis in RD 50% depict the better result compared to RD 75%. The thinner slab also illustrated the better couple with the soil foundation compared to the thick one. These results make a contribution to developing the new proposal for the balanced slab thickness in the concrete pavement. The FEM analytical results match the experimental observation in the load-displacement relationship.

The nonlinearly coupled code has been verified based on the small-scale experiments as discussed in chapter 3. The nonlinear behavior of soil and concrete slab interaction under high cycle moving load has been investigated. Firstly, the full-scale FEM analyses for soil's density RD 50% and 75% have been examined. The sensitivity parameter in this modeling is the diversity of the slab's thickness. The proposed and simulated thickness is based on the recommendation from the current design codes [1]–[3], [7]. The balanced slab thickness in case of RD 50% and 75%

were decided based on the longest fatigue life within each case. This value is rational to the experimental result. After that, the full-scale FEM analyses for all cases of soil's density have been simulated. The applications of the moving load and boundary conditions are kept constant in all cases. The comparison between the existing design codes and analytical results was conducted to finally propose the newly balanced thickness in the concrete pavement. It is promising that this is a new investigation of the slab's thickness approached to the nonlinear interaction with the soil foundation.



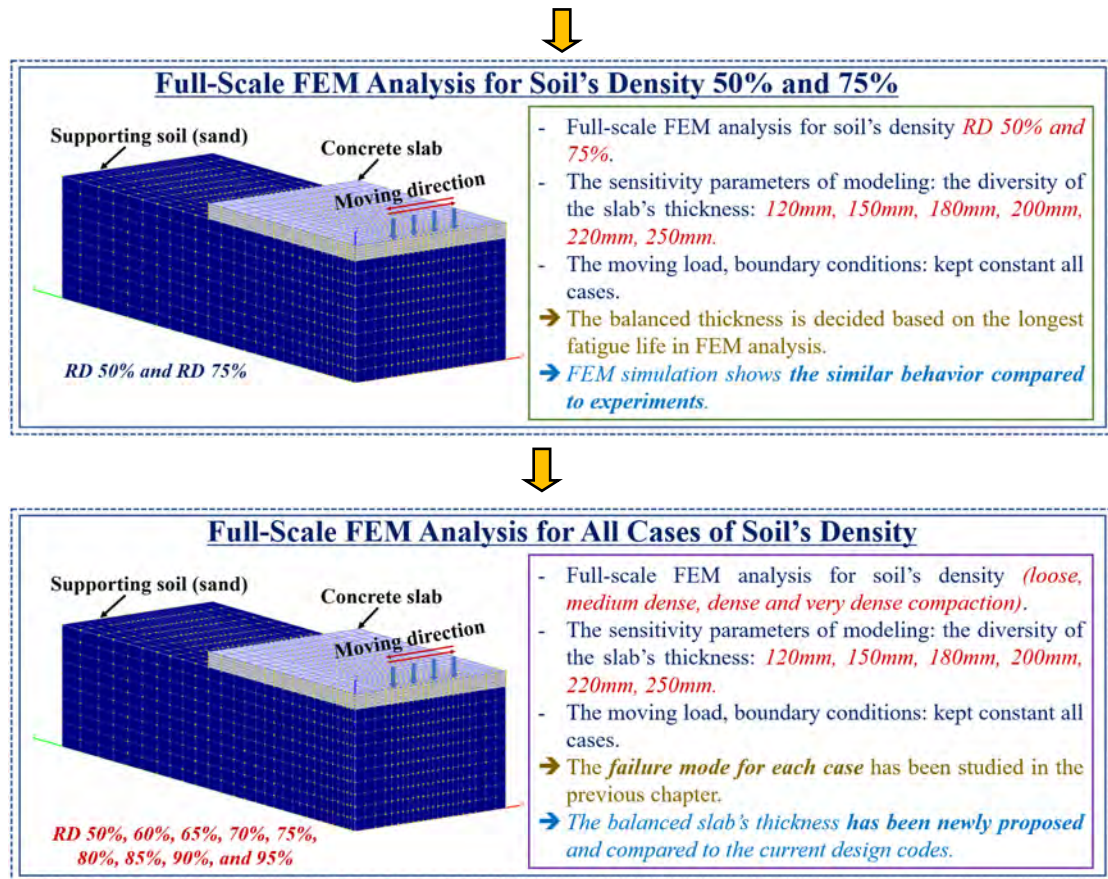


Fig. 5-1 Overview for prediction and assessment of the thickness in the pavement.

5.4 Nonlinear Full-Scale Simulation for Soil-Concrete Slab Interaction

To discuss the real concrete pavements, let us investigate a full-scale numerical model (a half domain: X-axis symmetry) as shown in Fig. 5-2. The concrete slab is 3,000mm x 4,000mm in plane and the thickness is changed as 120mm, 150mm, 180mm, 200mm, 220mm, and 250mm. A light reinforcement ratio (RR 0.1%) is applied in this simulation similar to the plain concrete used in the experiments and the weakest/most critical case in the concrete pavement. Foundation is sandy soil with RD 50% as the non-compacted and RD 75% as the compacted one. The displacement normal to the side boundaries is restrained as plain strain. Water-to-cement ratio (W/C) of concrete is 55% as the normal one in practice. The moving load of heavy traffics is selected to be 156 kN (specified design load). The drying shrinkage has been automatically reproduced through the moisture loss under the ambient relative humidity of 60% and temperature 20°C [11].

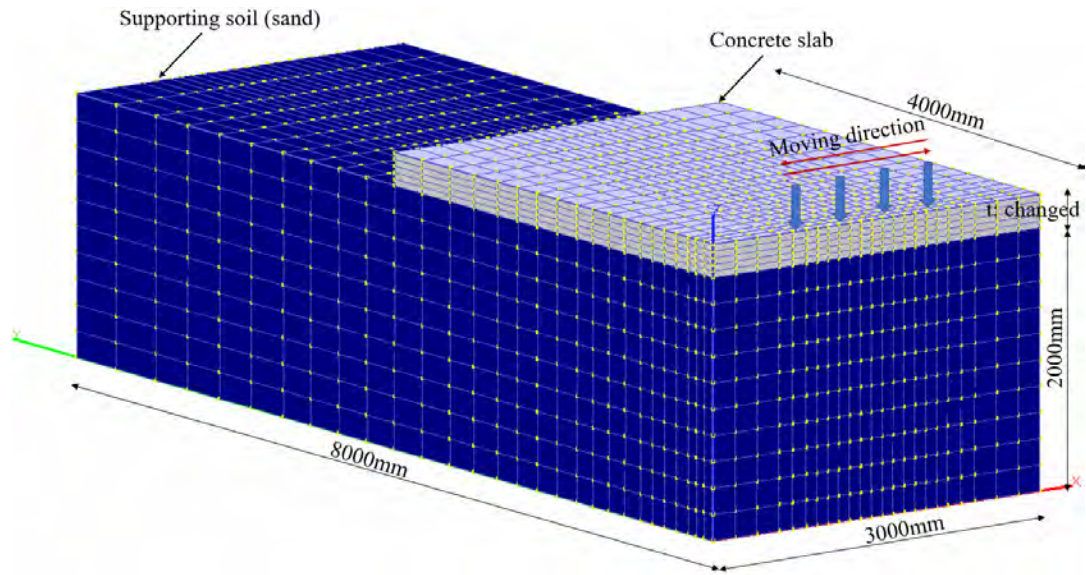


Fig. 5-2 The full-scale numerical modeling for concrete pavement under moving load.

Figure 5-3 indicates the fatigue life and the failure mode of the integrated slab-soil with different thickness in the case of RD 50%. The maximum principal strain profile shows the displacement of the concrete slab and soil behavior under the moving load direction at the fatigue failure of concrete pavements. It shows the deterioration of either concrete slab or soil foundation concurrently. In the case of the thin slab (120mm), the most critical shear failure of soil is seen with the localized band. In addition, the concrete slab is also damaged over the wide area. As the impetuous displacement of the slab is seen (120mm), the service life is only limited at about one hundred cycles. The slab of 150mm behaves similarly to the case of 120mm, and the shear failure of soil also takes place. The life cycle of this model is lower than 10^3 cycles which are higher than the concrete slab of 120mm. Accordingly, the damage of the concrete slab becomes more severe and the failure mode is critical in both slab and soil.

Based on this fundamental, the thickness of the concrete slab is increased as 180mm, 200mm, 220mm, and 250mm, respectively. It can be clearly seen from the failure mode in Fig. 5-3 that the increased thickness of the slab offers the considerable bearing support to the soft foundation. The thickness of the slab is obviously a key determinant to give strength to the fatigue life of concrete pavements. The damage of soil foundation is just severe under the moving load positions irrespective of the soft soil. The fatigue life is also considerably increased.

As can be seen in Fig. 5-3, the shear failure of the soil foundation is inversely proportional to the thickness of the slab. We have the longest fatigue life for the

thickness of 200mm. In the case of 220mm, and 250mm, damages are addressed mostly to the slab, but in contrast, the cases of thin slabs having the thickness less than 200mm exhibit the opposite. Consequently, the total service life is markedly increased at 200mm. In other words, the design of slab thickness should be made in consideration of the soil nonlinearity, especially for medium compacted soft foundation.

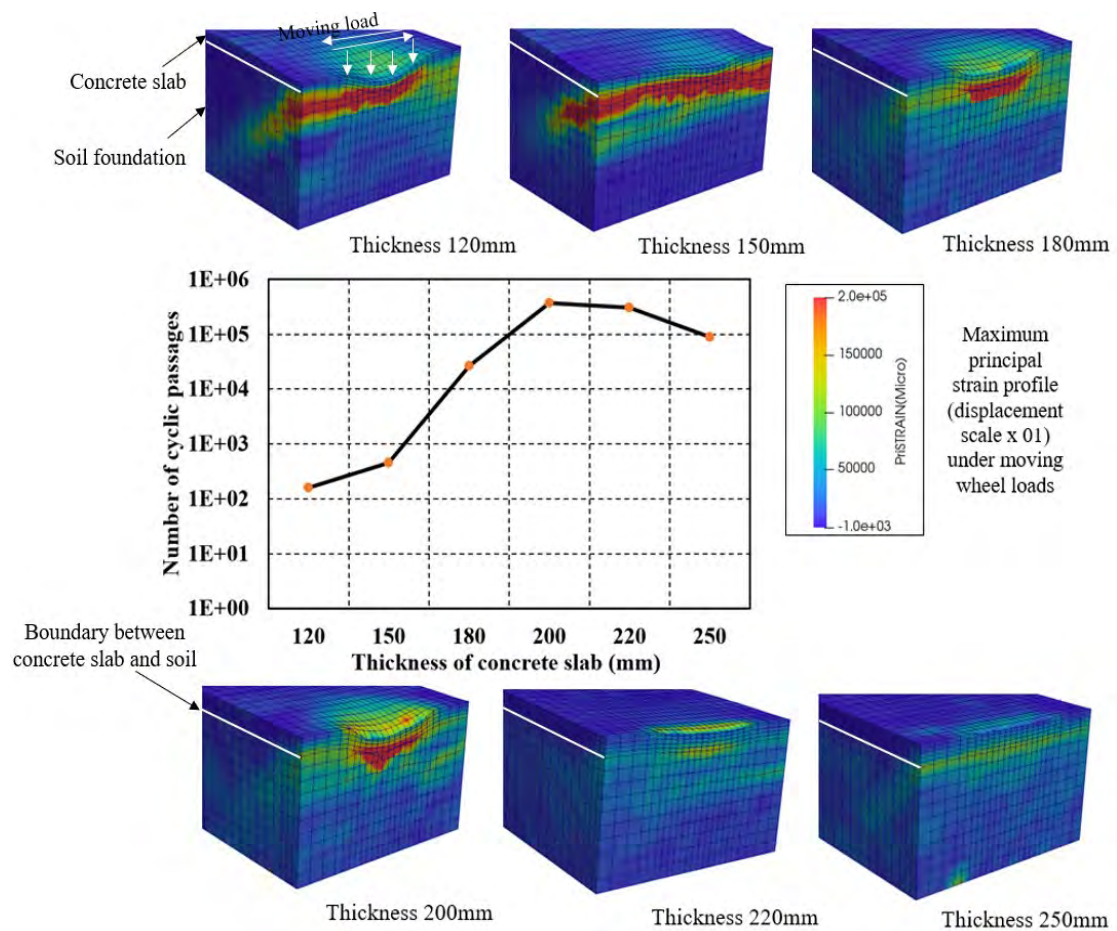


Fig. 5-3 The fatigue life and failure mode of the full-scale simulation of concrete pavement with RD 50%.

The computed simulation reflects the similar behavior of soil nonlinearity in the small-scale mock-ups of the slab of 20mm and 50mm in the event of RD 50%. As discussed in Chapter 3, the maximum displacement of the slab of 20mm shows the smaller value compared to thickness of 50mm at the same load. It can be said that the interaction of concrete slab and soil becomes superior to the case of a slab of 50mm. Due to the extravagant thickness (220mm or 250mm), the concentrated reacting soil pressure is higher than the slab of 200mm underneath the loading point. The concentrated stress causes the reduction of soil stiffness by virtue of nonlinearity. It

can be similarly explained as in Chapter 3 that if the stiffness of the foundation is small (loose soil RD =50%), the reacting soil pressure applied to the slab is more uniformly distributed, and if the soil does not fail, the bending moment develops as the maximum. Thus, the greater stiffness of soil foundation would arise the concentrated reacting soil pressure beneath the loading point. As a result, the flexural moment of the slab tends to be reduced and less risk of cracking is thought in accordance with the linear elastic hypothesis. However, the higher stress leads to the reduced stiffness owing to its nonlinearity. The maximum moment of the slab does not proportionally decrease and get larger than the one of the 200mm case. As a result, the fatigue life of 220mm or 250mm is dramatically decreased.

Figure 5-4 shows the fatigue life and the failure mode of the integrated slab and soil with different thickness in the case of RD 75%.

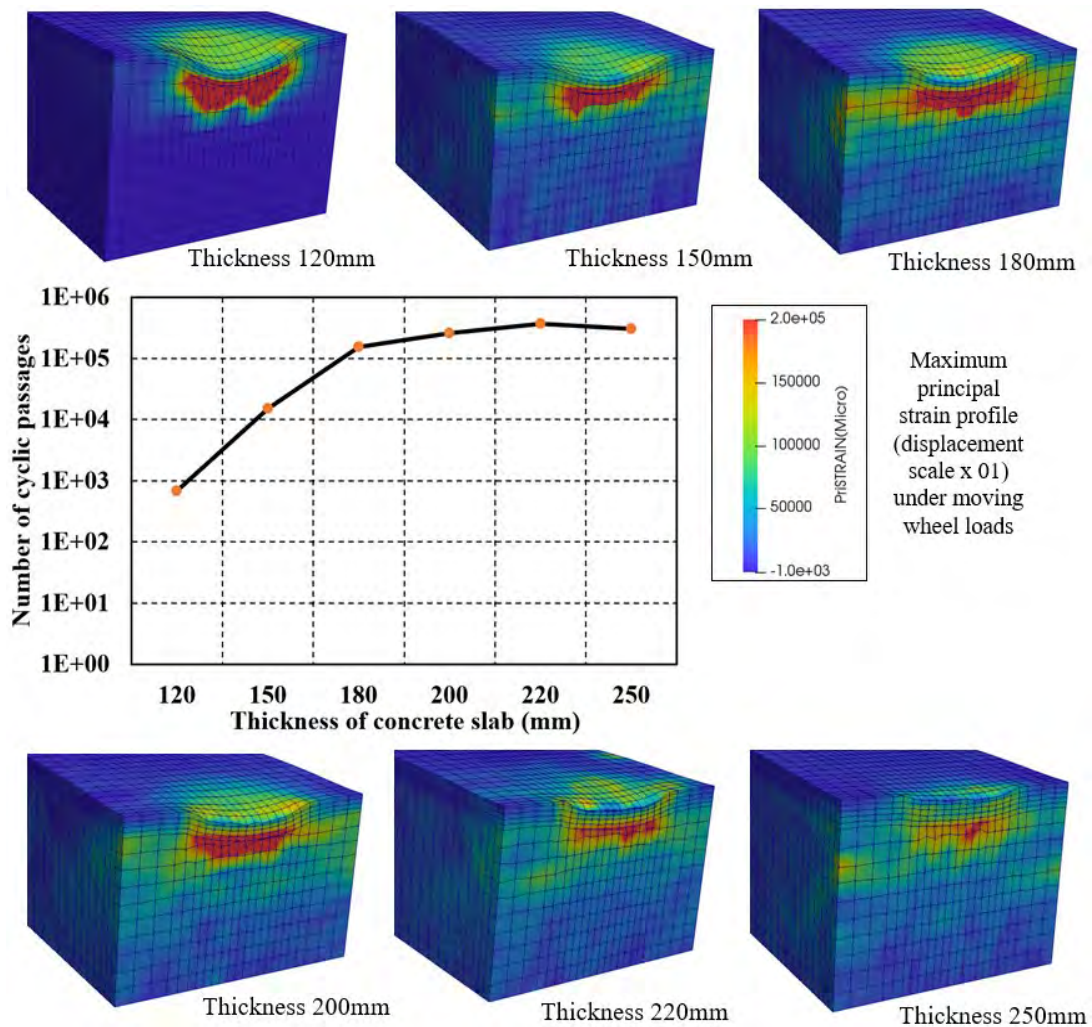


Fig. 5-4 The fatigue life and failure mode of the full-scale simulation of concrete pavement with RD 75%.

It can be seen from Fig. 5-4 that under the dense soil foundation, the fatigue failure is strongly governed by the damage of the concrete slab. In the case of a thin slab (120mm), the most critical displacement of the concrete slab can be seen. The failure mode is focused on the severe deformation of the concrete slab. When the concrete slab thickness increases, the coupling damage of the concrete slab and soil occurs as shown in the thickness of 150mm, 180mm, 200mm, 220mm, and 250mm. In the case of RD 75%, we have the longest fatigue life for the slab of 220mm. The largest thickness (250mm) shows the same behavior with the case of RD 50%. Irrespective of the thicker slab (250mm), the fatigue life is interestingly shorter than the slab of 220mm. It can be explained by the nonlinearity of soil foundation as discussed above.

The balanced thicknesses for concrete slabs for the case of RD 50% and RD 75% are 200mm and 220mm, respectively. In accordance with the linear elastic theorem for pavement design, the slab thickness is proportionally reduced with the increased density of soil, inevitably. This hypothesis may be effective for densely compacted soil foundation. However, due to the nonlinearity of soil, the loose or medium dense foundation can not be predicted by using the elastic theory. The balanced thickness of the slab is the key point for future discussion.

5.5 Parametric Sensitivity of Couped System – Design Concept

As the preceding section, the thickness of the concrete slab is considered as a key factor to affect the total fatigue life of the concrete pavement and foundation system. The supernumerary thickness of the slab is a burden to couple concrete slabs and soils. It may cause the early damage of the concrete slab and the decrease of the fatigue life. The slight slab is a result of the critical deterioration on both concrete slabs and soil foundations. In view of the nonlinear mechanics of the soil foundation coupled with the concrete slab, all specific cases of the soil's density have never been investigated yet, chiefly in the case of loose and medium dense ones. Then, the failure mode for the thick (250mm), medium (200mm), and thin (120mm) thickness of concrete slabs as well as the loose, medium dense, dense, and very dense soil is examined in Fig. 5-5 by using the numerical simulation to inspect how the fatigue failure occurs in concrete pavement. The light reinforcement ratio of 0.1% is selected as the weakest case of the slab. The failure mode in Fig. 5-5 is shown at the final

cycle of numerical simulation. The fatigue failure depended on the damage of the concrete slab, the shear failure of soil or combined both of them.

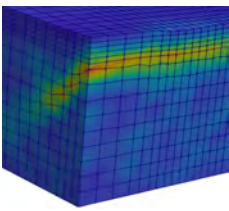
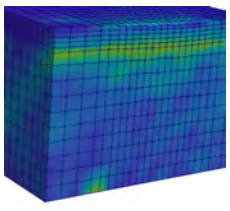
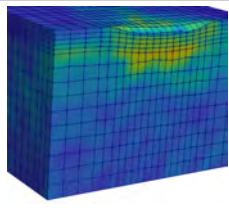
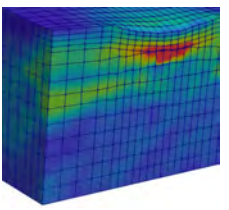
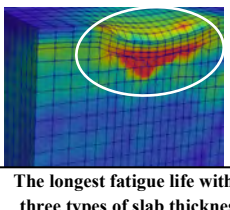
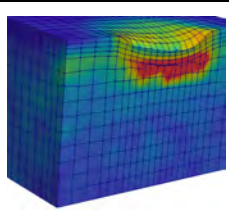
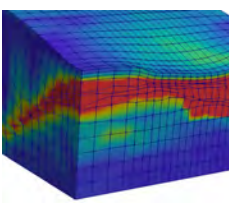
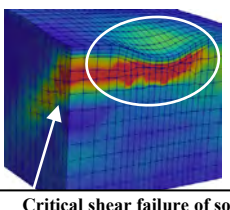
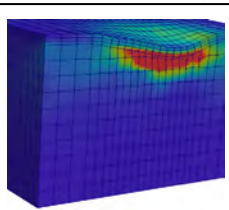
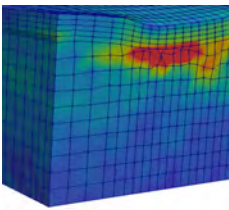
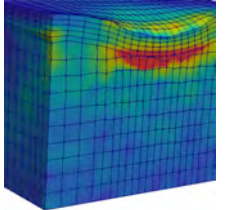
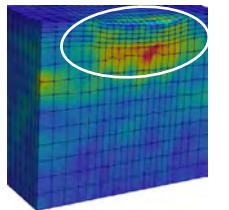
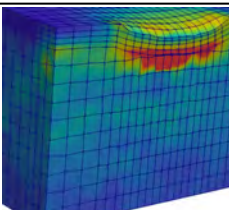
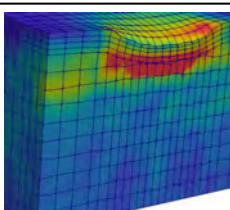
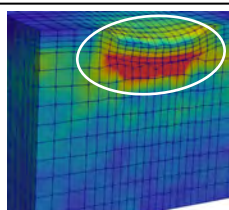
Let us start from the loose soil foundation as RD 40% and RD 50%. The large thickness (250mm) of concrete slabs shows the localized shear band of soil in RD 40%, and the damage focuses on the concrete slab in RD 50%. The medium thickness (200mm) demonstrates the coupling damage of the concrete slab and foundation with the shear failure in both RD 40% and 50%. Due to the loose soil, the damage of the foundation is more critical than the concrete slab. The fatigue life has the significant increase compared to the large thickness as discussed in Section 6.3. The thin slabs (120mm) depict the severe damage of the concrete slab and soil. The displacements of the concrete slab and the shear band of the soil foundation rapidly rise at the early stage of the cycle. Then, the fatigue life is dramatically decreased.

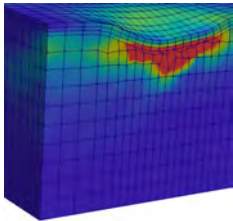
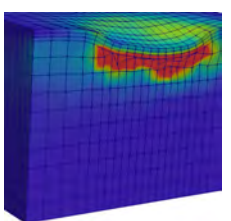
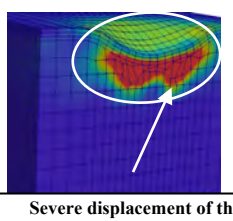
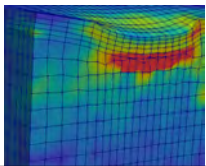
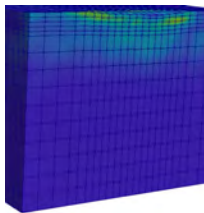
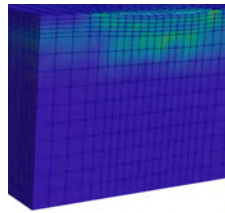
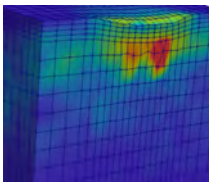
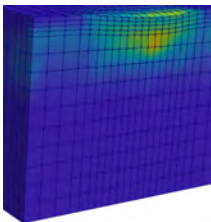
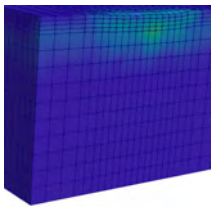
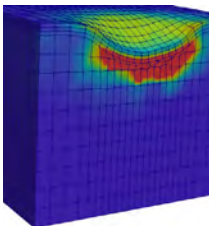
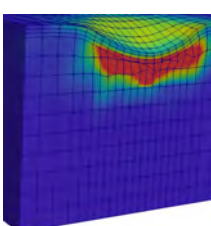
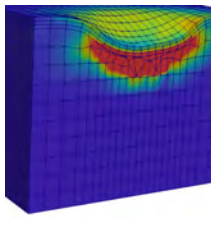
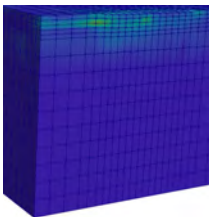
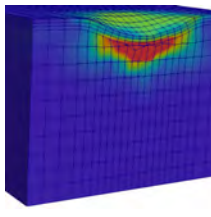
The medium dense soil foundations give information of the similarity to the fatigue failure of the large and medium thickness in case of RD 60% and 65%. The failure mode is the coupling damage of the slab and soil. Owing to the looser soil, the soil failure in the case of RD 60% is more severe than the concrete slab. The thin thickness shows the critical deformation of the concrete slab.

When the dense soil foundations (RD 70%, 75%, and 80%) are applied, the coupling damage of the slab and soil in the event of the large and medium thickness can be observed in computation. The failure mode for the thin one is nearly close to the case of the medium dense soil. The critical deformation of concrete slab causes the decrease of the total fatigue life.

The fatigue failure of the very dense soil foundation (RD 85%, 90%, 95%) is governed by the little damage of the concrete slab. The thin ones show the most critical deformation. As discussed above, the concentrated reacting soil pressure under the load is arisen with the increase of soil's stiffness. Due to the nonlinearity of the soil foundation, the higher concentrated, the stress resorts to the decrease of stiffness, and the moment of the concrete slab can not be proportionally reduced. The concrete slab is thus endured the severe deformation under the dense soil if the much thinner slab is applied. In the case of RD 95%, soil is excessive hard like the rock, there is naturally no damage of concrete slabs as well as the shear band of soil. The thickness of the slab can be dramatically reduced. The option of concrete slab thickness is obviously an ultimate requirement in the design concept of concrete pavements. The coupling of the soil foundation and the concrete slab is necessary to investigate with

each soil's relative density. Due to the full-scale modeling examined in this study, it can be used as a fundamental concept for the revision of the concrete pavement design.

RD (%)	40	50	60
Large thickness 250mm RR 0.1%	The severe shear band of soil 	The shear band of soil 	The damage of concrete slabs and soil (soil is more critical) 
Medium thickness 200mm RR 0.1%	The damage of concrete slab and shear failure of soil (Soil is more critical than concrete) 	 The longest fatigue life within three types of slab thickness	The damage of concrete slabs and soil (soil is more critical) 
Thin thickness 120mm RR 0.1%	The severe damage of both concrete slabs and soil foundations 	 Critical shear failure of soil	The damage of concrete slabs and soil (the slab is more critical) 
RD (%)	65	70	75
Large thickness 250mm RR 0.1%	The coupling damage of concrete slabs and soil		
			
Medium thickness 200mm RR 0.1%	The coupling damage of concrete slabs and soil		
			

Thin thickness 120mm RR 0.1%	Failure mode is focused on the severe deformation of concrete slabs			
			 Severe displacement of the concrete slab	
	RD (%)	80	85	90
Large thickness 250mm RR 0.1%	The coupling damage of concrete slabs and soil  The slab is more critical than soil	A little damage on the slab. No shear band of the soil foundation  		
	The coupling damage of concrete slabs and soil  The slab is more critical than soil	A little damage on the slab. No shear band of the soil foundation  		
	Medium thickness 200mm RR 0.1%	The severe deterioration of the concrete slab		
Thin thickness 120mm RR 0.1%				
	RD (%)	95		
	Large thickness 250mm RR 0.1%	A very little damage on slab. No shear band of soil 	Thin thickness 120mm RR 0.1%	The severe deterioration of the concrete slab 

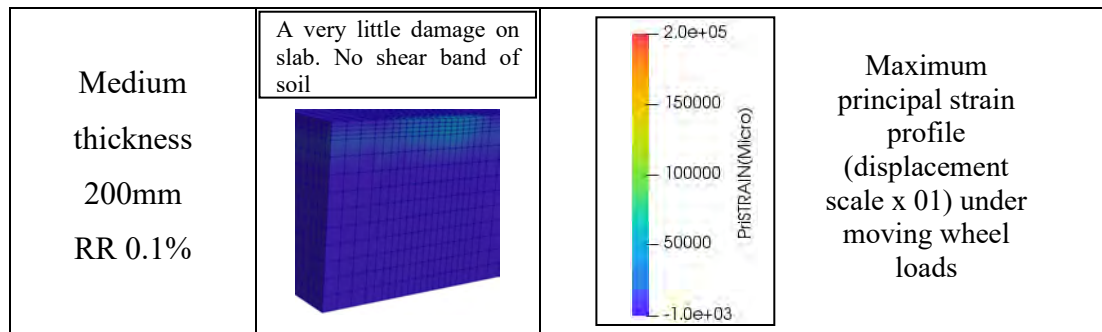


Fig. 5-5 The failure mode of a variety of soil relative density and concrete slab thickness.

5.6 New Concept for Balanced Slab Thickness

The new concept for the balanced slab thickness of concrete pavements was developed based on the numerical coupled code of soil and concrete slab interaction as discussed above. The nonlinear FEM modeling is similar to the case of section 5.4. A mass of the diversity of soil's density from loose, medium dense, dense and very dense compaction is simulated to investigate the failure mode concrete pavements as previously stated. The thickness is numerically examined in the thin, medium and thick slab.

As the preceding section, the newly proposed thickness of concrete pavement slabs is compared to the current design codes as PCA and Guideline ACI 325 due to the similar approach in the mechanistic method.

5.6.1 Nonlinear FEM Analysis and Guideline ACI 325

ACI 325. 12R-02 (Guideline for Design of Jointed Concrete Pavements for Street and Local Roads) reported at ACI committee 325 provides a balanced thickness for the design of concrete pavements based on the principles developed by the Portland Cement Association and other in order to analyse an elastic slab over a dense liquid subgrade. Recommendations in the guideline are applied for streets and local roads under the low volumes of traffic. The properties of the supporting soil are determined by the modulus of subgrade reaction (k). The value of k is defined as the ratio of the load per unit area of horizontal surface of a mass of soil to the corresponding settlement of the surface [7].

In the theory for the basis of the design of ACI 325, the thickness design method can be used for plain or reinforced pavements because the presence or lack of the distributed reinforcement has no significant effect on loaded slab behavior as it

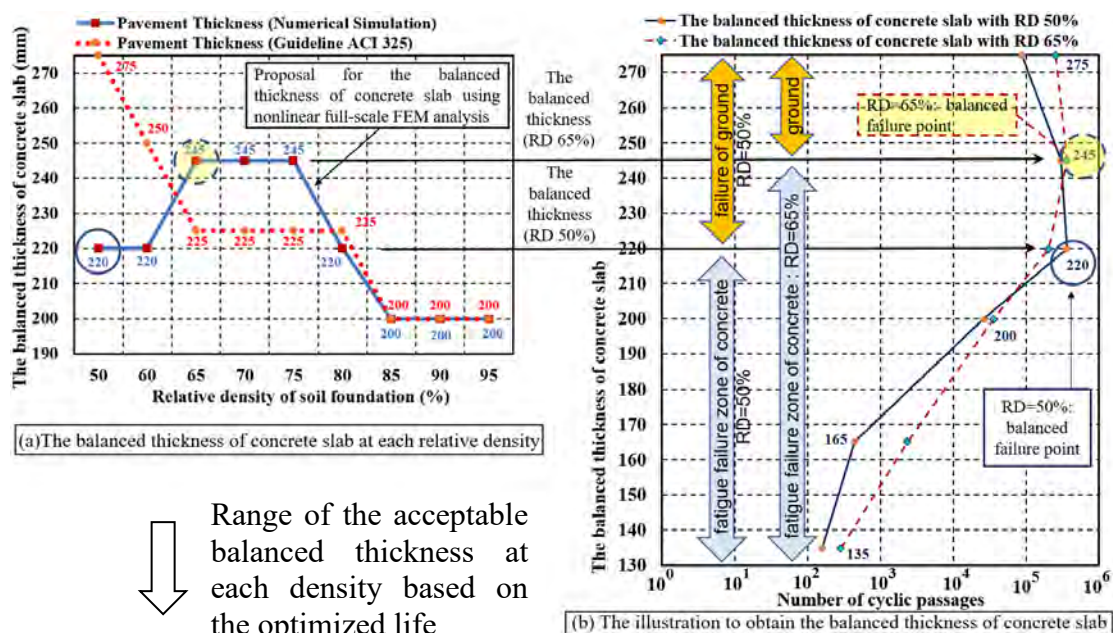
pertains to thickness design [7]. Based on this recommendation, the nonlinear FEM modeling is developed with a very light reinforcement ratio (RR 0.1%) for the purpose of investigating the weakest/most critical case of the concrete slab.

It is noted that the design for the pavement is aimed to serve the long-term operation of the traffic vehicles. The multiplying factor (or the safety factor) should be considered to apply an arbitrary level of reliability with regard to overloads, low concrete strength or thin pavement sections. The required safety factor is 1.1 in ACI 325. There are seven street classifications outlined in ACI 325, and the recommendation for the pavement thickness in business street with ADTT 800 is selected due to its carriage for both expressways and arterials. It may be that the business street in ACI 325 shows the more critical thickness compared to other cases (it depicts the requirement of the thicker thickness). As instructed in ACI 325, concrete flexural strength (MOR) in the range of 3.8 to 4.8 MPa at 28 day-strength is the most economical. Owing to the normal concrete used in simulation and practices (water-to-cement ratio W/C 55%), MOR 4.1 MPa is selected.

Based upon modulus of subgrade reaction (k) for the soil foundation, the equivalent soil's density in FEM analysis is determined from RD 50% to RD 95%. The soil foundation is considered in the range of the loose (RD 50%), medium dense (RD 60%), dense (RD 65% to RD 80%), and very dense (RD 85% to RD 95%) compaction. The rational thickness of each density is picked up from a mass of simulated thickness based on the current design code as 120mm, 150mm, 180mm, 200mm, 220mm, and 250mm. It is noted that the pavement thickness in numerical simulation is not included the safety factor. The required thickness in the numerical simulation will be multiplied 1.1 in the case of the comparison with Guideline ACI 325.

Figure 5-6 shows the comparison between the low volume of traffic (ACI 325) and FEM numerical simulation. The selection for the balanced thickness of the slab in nonlinear FEM analysis is determined at the optimum performance for the fatigue failure of the concrete slab and soil. Firstly, the optimized fatigue life of concrete pavements has been considered. Depending on the relative density of soil, the failure point can take place earlier either soil or the concrete slab, or both of them simultaneously. The best selection of optimized fatigue life in the concrete pavement can be obtained in FEM analysis at each slab's thickness in terms of the failure mode of the slab and/or the soil foundation. The methodology to approach the balanced

thickness of concrete slab in nonlinear FEM analysis at each relative density of soil is typically illustrated in Fig. 5-6b for RD=50% and 65%, respectively. Another soil density is similarly considered to attain the balanced thickness of concrete slab. It can be seen that the reduction for the required thickness in the ACI guideline is linear with the increase of soil's density. It is due to the principle for this recommendation based on Westergaard's theory where the soil foundation is considered as an elastic slab supported by the dense liquid springs. The other is the loading application. The loading in the ACI guideline is the concentrated axle truck. The damage will be localized at the loading point under the concentrated load. The shear band and volumetric failure may not occur in the soil foundation. As discussed above, under the high cycle motion of traffics, the shear and volumetric fatigue of soil appear concurrently and become one of the key factors to reduce the service time of the pavement. The results of numerical simulation show three types of fatigue failure modes at each soil's density. When the soil is loose and medium dense (RD 50% and RD 60%, respectively), the shear band of soil is clearly more critical than the damage of the concrete slab as shown in Fig. 5-7a. The fatigue failure is therefore focused on the shear band of the soil foundation. The support of the concrete slab is inconsiderable, and the large thickness of concrete slab is not necessary due to the more burden for soil foundation [12]. In the consideration of nonlinear mechanics of the loose and medium dense soil and the concrete slab, the pavement thickness is dramatically reduced compared to the guideline ACI 325.



Range of the acceptable balanced thickness at each density based on the optimized life

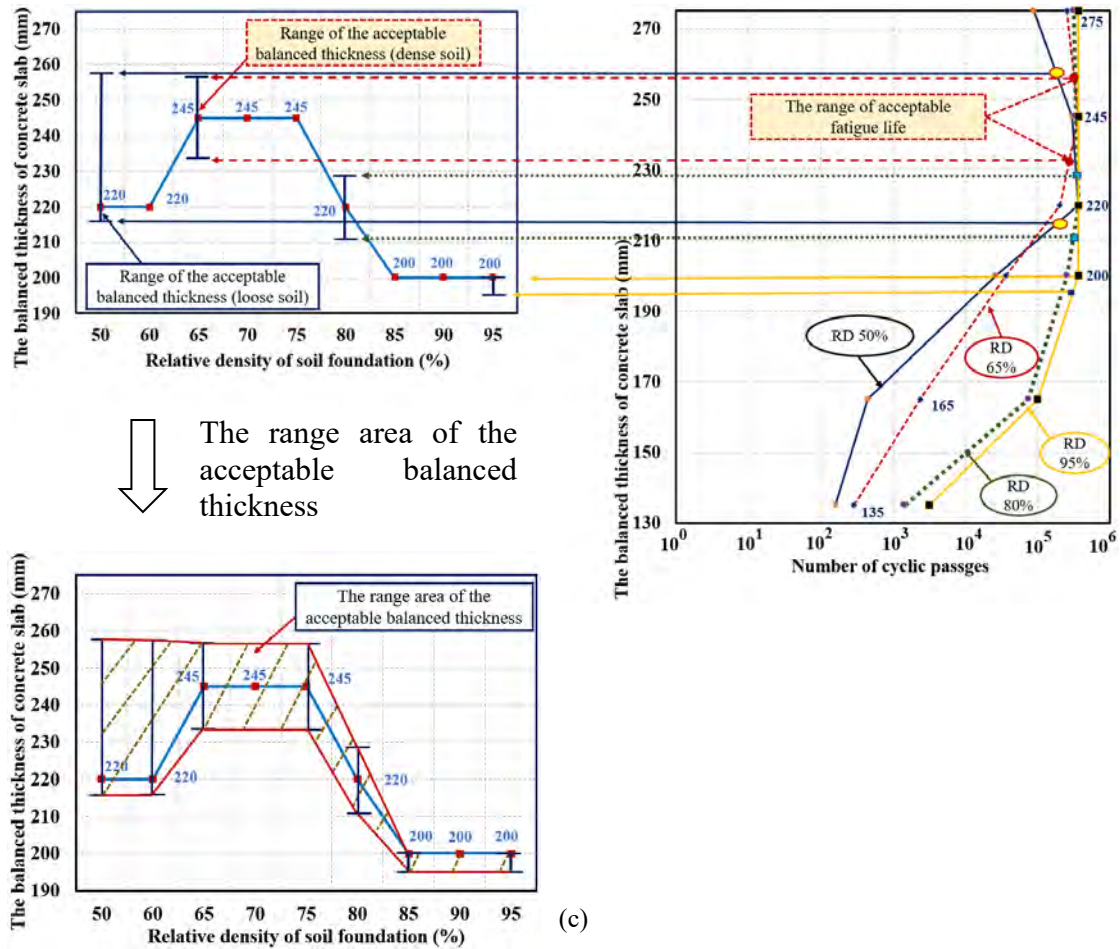


Fig. 5-6 Balanced thickness of concrete slab to maximize the fatigue life of pavement system and the specified recommended thickness by ACI 325 [13].

In the event of the dense soil foundation (RD 65% to RD 80%), the numerical simulation proposes the larger thickness compared to ACI 325. It is due to the fatigue failure focused on the coupling damage of the concrete slab and soil. Soil is more supported by the concrete slab if the pavement thickness is increased. These analytical results have been similarly observed in the experiments as shown in chapter 3. The experiments shows the better results of the thinner slab in the soft foundation (RD 50%). In contrast, the thicker slab is required in the case of RD 75%. The pavement thickness is required to increase at least 20mm in the case of RD 65% to RD 75%. At the soil's density of 80%, the required thickness is reduced 5mm compared to ACI 325. This is the case between the dense and very dense compaction of soil. The fatigue damage focuses on the slab more than the soil foundation (This assumption has been investigated in Fig. 4-10 in Chapter 4. The shear band of soil occurs under the moving load but less critical the deterioration of the slab). The typical failure mode is shown in Fig 5-7b. The numerical simulations demonstrate the nonlinear

relationship between the required thickness and soil's density. This is the key point to revise the current principle of the pavement design code.

When the soil foundation is very hard and compacted (RD 85% to RD 95%), the shear band of soil will not occur as shown in Fig. 5-7c. The fatigue failure in the numerical simulation is strongly governed by the damage of the concrete slab. It is thus similar to the fatigue failure in ACI 325. As a result, the balanced thickness in numerical simulation is similar to the ACI 325.

The nonlinearity of coupling the concrete slab and soil in numerical simulation can be utilized to predict the required pavement thickness in three types of fatigue failure as the shear band of soil, the coupling damage of the concrete slab and soil, and the concrete slab only. The current design code may be revised in terms of the reduction of the pavement thickness if the soft soil foundation is applied. On the contrary, when the concrete slab is supported by the dense soil, the increase of slab thickness should be considered.

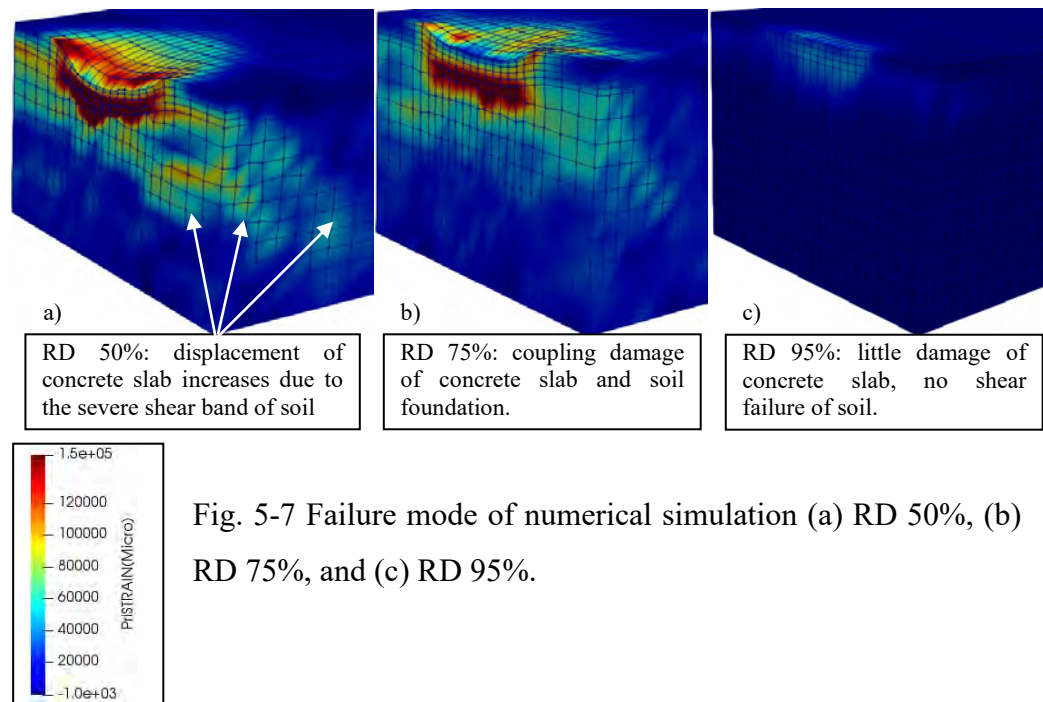


Fig. 5-7 Failure mode of numerical simulation (a) RD 50%, (b) RD 75%, and (c) RD 95%.

Figure 5-6 demonstrates the necessity in the utilization of the nonlinear behavior of the soil foundation in the concrete pavement. In case the nonlinear couple of soil and concrete slab in pavements is conducted, the balanced thickness is determined by the failure mode of the concrete slab/soil or both of them depending on the soil's property. The balanced thickness of the concrete slab has been selected based on the optimized fatigue life at each density of soil. From the practical viewpoint, this

balanced thickness can be adjusted which is so-called the range of the acceptable balanced thickness. The determination of the range area of the acceptable balanced thickness is based on the deviation of the acceptable fatigue life of the concrete pavement which is adjacent to the optimized balanced thickness of the slab as shown in Fig. 5-6c. This methodology is due to that the concrete slab may depict a similar mechanism in case of the tolerance of 5% of optimized fatigue life at the very high cycle. Four range areas of the acceptable balanced thickness consist of the loose/medium soil (RD=50% and 60%), the dense one (RD=65% to 75%, and RD=80%), and the very dense compaction of soil (RD=85% to 95%).

In the event of the very dense compaction (RD=85% to 95%), the balanced thickness is overlapped to the thickness proposal of ACI 325. The balanced thickness of optimized fatigue life is therefore recommended. However, in consideration of the practical views, it may have the deviation of the balanced thickness under construction. The allowable tolerance for this balanced thickness can be identically obtained in other cases as discussed above.

5.6.2 Nonlinear FEM Analysis and Guideline PCA

Thickness Design for Concrete Highway and Street Pavement proposed by Portland Cement Association suggested the balanced thickness for which can apply to the plain, reinforced, and continuously reinforced pavements. The theoretical studies of pavement slab behavior are based on Westergaard, Pickett and Ray, and recently developed finite-element computer analyses. The concentrated loading application is placed at slab interior, edge, joint, and corner. It is similar to Guideline ACI 325, the failure mode of pavements is therefore localized at the loading point only.

The pavement thickness for the high volumes of traffic is proposed in PCA with four strengths as low, medium, high and very high foundation, respectively. Due to the frequency of heavy trucks, the safety factor 1.2 is recommended. It is similar to ACI 325, MOR 600 psi is used for normal concrete in pavement construction, and modulus of subgrade reaction (k) demonstrates the property of supporting soil. The axle-load category 3 in PCA shows the heavy average daily (truck) traffic in both directions (ADT/ADTT), and it is also the most popular case in pavement design. The maximum ADTT in this category at each soil's density based on the fatigue analysis controls has been selected to compare with the proposed pavement thickness in numerical simulation. In chapter 3 of PCA: Design Procedure, the value of the

subgrade or subgrade and subbase combination is demonstrated as the "k" value. To simplify this value, the table 10 of chapter 4 in PCA: Simplified Design Procedure lists approximate k values for different soil types and called as subgrade and subbase support. The values in this table are divided into the low, medium, high, and very high which are equivalent to the loose, medium dense, dense, and very dense soil in FEM analysis, respectively. The equivalent value between the subgrade and subbase support of PCA and relative density (RD) of FEM analyses can be obtained.

The numerical modeling is similar to comparing to ACI 325. The light reinforcement ratio (RR 0.1%) is applied to illustrate the weak/plain concrete slab. Numerical simulation in comparing to PCA is also conducted a mass of soil's density as the loose (RD 50%), medium dense (RD 60%), dense (RD 65% to 80%), and very dense (RD 85% to 95%) compaction. The simulated thickness is multiplied with safety factor 1.2. The proposed thickness of the slab is therefore thicker than the case of comparing to ACI 325.

As can be seen in Fig. 5-8, the trend for the reduction of the slab's thickness is linear and similar to the ACI 325. At the loose and medium dense compaction of soil (RD 50% and 60%), The slab's thickness is only thicker than 5mm compared to ACI 325. However, when the soil is more compacted, the thickness is increased 20mm or 30mm with the dense and very dense soil foundation, respectively. The reduction of the slab's thickness in PCA is also linear to the increase of soil's density.

In the event of the newly proposed FEM analysis, the slab's thickness increases 20mm compared to the case of ACI 325. It is due to the safety factor 1.2 compared to 1.1. We can see the same trend in the proposal of the slab's thickness in both cases as shown in Fig. 5-7 and Fig. 5-8. When the soil is loose or dense, the thickness of the slab is dramatically decreased compared to PCA or Guideline ACI 325. In case of the dense soil foundation, the slab's thickness in the new proposal should be increased 20mm in both cases. This is an interesting point in this study. There are different load and frequent levels in both guidelines, but the same value (20mm) to increase the required thickness in case of the dense foundation. When the soil is very compacted (RD 85% to 95%), the proposal for the slab's thickness is reduced 10mm compared to the PCA.

The explanation for the differences in the recommended thickness of FEM analysis with PCA may be similar to the case of ACI 325. Due to the Westergaard theory applied in PCA (the fixed-point load and linear, homogeneous foundation), the

damage of pavements focuses on the deterioration of the concrete slab. The shear band of the soil foundation will not occur even if loose soil is used. Meanwhile, FEM analyses show the results of the nonlinear soil-concrete slab composite under the moving loads. The fatigue failure can occur in the slab, soil, or both concurrently as depicted in chapter 4. The thick thickness is not demonstrated as the best selection since the greater burden is reproduced in the part of the foundation. The small gap (10mm) between PCA and FEM analysis in the very compacted soil is due to the same failure mode which is concentrated on the damage of the slab only as shown in Fig. 5-7. The FEM results in comparison with PCA also show the similarity with the experimental observations as presented in chapter 3.

The nonlinear FEM modeling shows the good conditions in comparison with two mechanistic guidelines for concrete pavement design. The safety factor is decided based on the load levels and the category of the pavement. Once again, we can say that the nonlinearity of coupling concrete slab and soil in numerical simulation can be utilized to predict the required pavement thickness in three types of fatigue failure as the shear band of soil, the coupling damage of concrete slab and soil, and concrete slab only. The current design code may be revised in terms of the reduction of the pavement thickness if the soft soil foundation is applied. On the contrary, when the concrete slab is supported by the dense soil, the increase of slab thickness should be considered.

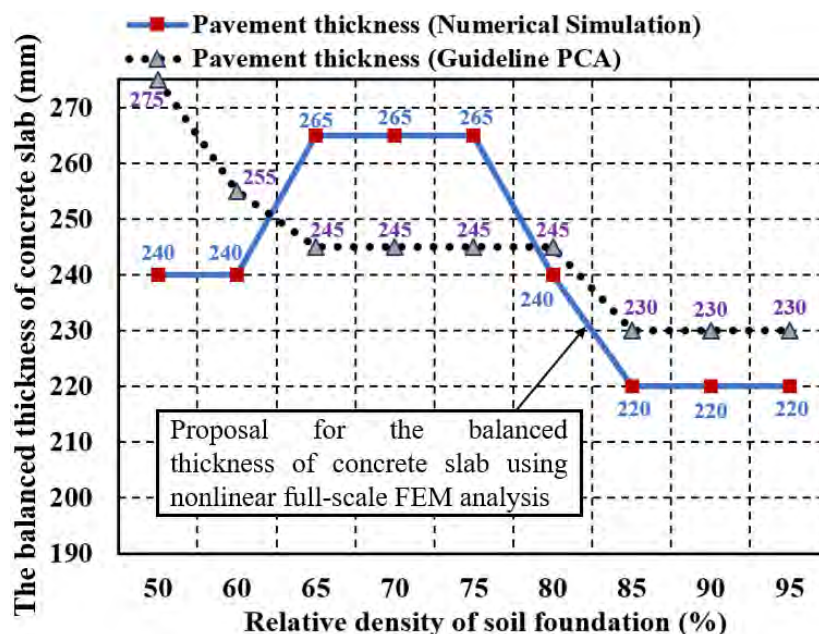


Fig. 5-8 Balanced thickness of concrete slab to maximize the fatigue life of pavement system and the specified recommended thickness by PCA [13].

5.7 Conclusions for Chapter 5

The nonlinear FEM analysis for the new approach to predict and assess the idealized thickness of the concrete pavement slab under moving loads has been implemented with a mass of soil's density. Then, we earn the followings.

1. The required pavement thickness on the loose soil foundation is found to be thinner than the medium/dense one. This is opposite to the on-going design concept based upon the linearity of soil foundation. A key factor can be presented in discussing the rationale of design principle of concrete pavement. In other words, the thickness of the pavement on the medium compacted soil shall be increased than the current design requirement.
2. The design principle for the concrete pavement should be based on the nonlinear mechanics of soil and concrete slab interaction under the moving wheel-type loads. This couple can be dealt with using the constitutive models for the concrete slab and the soil foundation in FEM analysis.
3. Depending on the soil's density, the failure mode can be occurred in the concrete slab, the soil foundation or both of them (the couple damage of the slab and soil). The balanced thickness of the slab is therefore different.
4. The current design code shows the damage at the concrete slab only due to the linear, elastic and homogeneous foundation. It is thus matched to the fatigue failure of FEM analysis in the very compacted soil. Other soil's density depicts as a predominant factor in the pavement design.
5. The balanced thickness of the concrete pavement slab is computationally confirmed to be a primary factor to the total fatigue life. The supernumerary slab's thickness is not demonstrated as the best selection since the greater burden is reproduced in the part of the foundation as shown in case of the loose/medium soil foundation. Meanwhile, the thicker slab is required in the event of the dense soil thanks to its support when coupling with the concrete slab. The fatigue damage is therefore combined the deterioration of the slab the shear band of soil.

The numerical code has been used in the coupling of finite element analysis for the concrete pavement under moving loads. The foreseen optimized thickness of slabs in association with the soil compaction is the target for validation of the computational scheme proposed in this study. The balanced thickness of the slab has been proposed based on the nonlinear principle. It is an important issue to make a contribution to

revising the current design code for the concrete pavement. The balanced thickness of the concrete slab on the nonlinear soil in this study is proposed based on the results of small-scale mock-ups and the full-scale FEM analysis. This study can be fundamental for future discussion when the analytical results are compared to real-size experiments. This is a strategic point to revise the existing design codes of concrete pavements.

References in Chapter 5:

- [1] AASHTO, *AASHTO Guide for Design of Pavement Structures*. 1993.
- [2] P. C. Association, *Thickness design for concrete highway and street pavements*. 1984.
- [3] AASHTO, *Mechanistic Empirical Pavement Design Guide: A Manual Practice*. 2008.
- [4] T. Jenjiwattanakul and K. Sano, “Pavement thickness design thresholds of having doweled joints and concrete shoulders,” in *Proceedings of the Eastern Asia Society for Transportation Studies*, 2011, p. Vol 8.
- [5] IOWA, *Design Manual - Chapter 5 - Roadway design*. 2019.
- [6] A. T. Papagiannakis and E. A. Masad, *Pavement Design and Materials*. 2012.
- [7] ACI 325, *Guide for design of jointed concrete pavements for streets and local roads*. ACI Committe 325, 2002.
- [8] N. J. Delatte, *Concrete pavement design, construction, and performance, second edition*. 2014.
- [9] H. M. Westergaard, “Theory of concrete pavement design,” *Proc. Highw. Res. Board*, vol. 7, no. Part 1, pp. 175–181, 1927.
- [10] P. G. and G. K. Ray, “Influence charts for concrete pavements,” *Am. Soc. Civ. Eng. Trans.*, vol. 116, no. 2425, 1951.
- [11] H. Q. H. Nguyen, K. Maekawa, and S. Komatsu, “Three-dimensional high-cycle fatigue simulation of soil-concrete pavement slab interaction under moving loads,” *Proc. 8th Int. Conf. Asian Concr. Fed.*, vol. 2, pp. 1207–1216, 2018.
- [12] H. Q. H. Nguyen, K. Maekawa, and S. Komatsu, “High-cycle fatigue interaction between soil foundation and concrete slab under moving wheel-type loads,” *Eng. Struct.*, 2019. doi.org/10.1016/j.engstruct.2019.109931.
- [13] H. Q. H. Nguyen, K. Maekawa, “Multi-scale simulation for fatigue life evaluation of concrete pavement subjected to moving load under dry and wet conditions,” *J. Adv. Concr. Technol.*, vol. 18, pp. 95-115, 2020.

CHAPTER 6

NUMERICAL SIMULATION OF CONSTRUCTION-JOINT EFFECTS FOR FATIGUE-LIFE ASSESSMENT OF CONCRETE PAVEMENTS SUBJECTED TO TRAVELING WHEEL-TYPE LOAD

6.1 Introduction

There are two typical types of the concrete pavement as jointed (either plain or reinforced) and continuously reinforced concrete. The systems of jointed concrete can be the longitudinal or transverse direction as shown in Fig. 6-1.

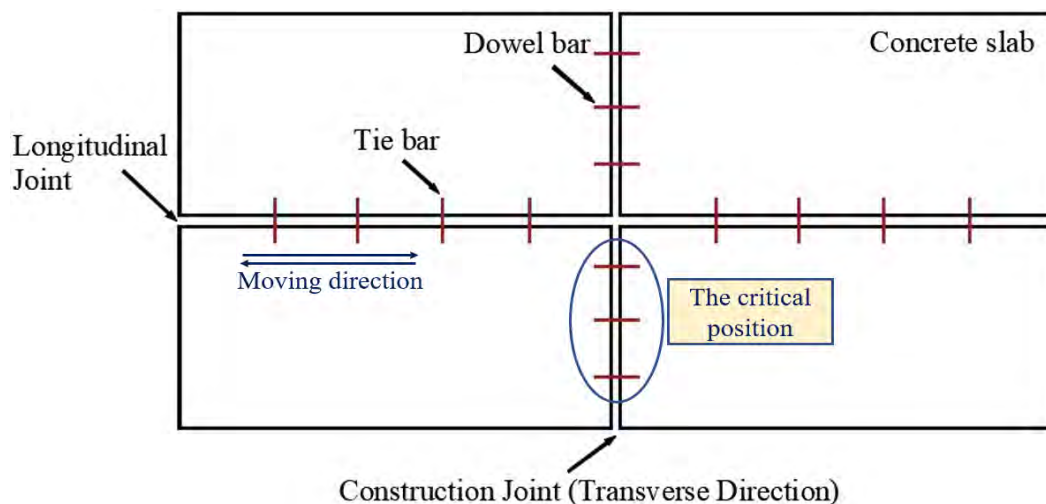


Fig. 6-1 The jointed concrete slab in the concrete pavement.

At the joint position between two concrete slabs, it will be sealed to protect the dowel bar and the substructure under the concrete slab. Under the operation of the pavement, the joint sealant damage can occur and it may be a serious issue affecting the service life of the concrete pavement. The damage of the joint sealant can be divided into three categories as the low, medium and high severity [1]. Figure 6-2a depicts the joint sealant damage in the case of low severity. It can be seen that the joint sealer is generally in the good condition and the connection between two edges of slabs is still acceptable. The joint sealer has debonded but still in the status of contacting two edges of the slabs. The infiltration of water may be difficult to

approach the dowel bar or the subgrade of the pavement. Figure 6-2b shows the damage of the joint sealant under the medium severity. The joint sealer is still in place but water is possible through under the pavement. In the event of the severe damage of the joint sealer as illustrated in Fig 6-2c, the joint sealer is absolutely separated between two concrete slabs and it is required to fix immediately.

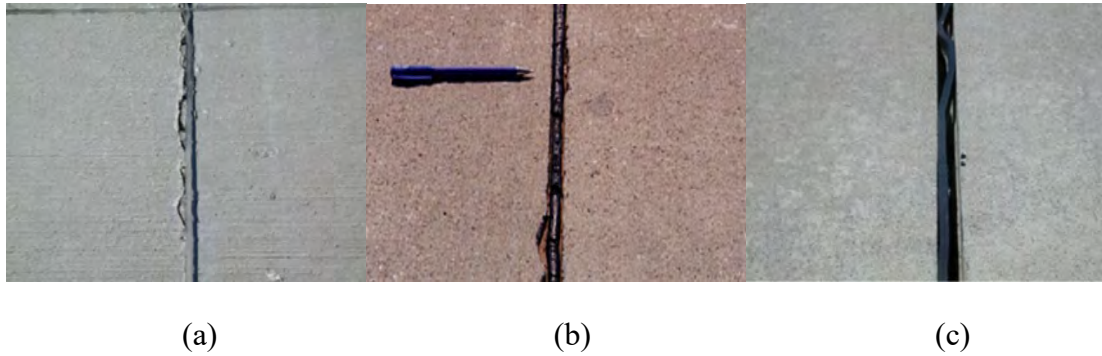


Fig. 6-2 Three levels for the joint sealant damage: a) low, b) medium, and c) high severity [1].

It is found that the critical stresses occurred more severely at transverse joints compared to longitudinal ones [2]. Results of a survey in Japan show that the initiation of longitudinal cracks of concrete pavement under wheel paths started at transverse joints [3]. The transverse joints are therefore more critical than the longitudinal ones under the traffic moving load. In addition, three major types of joints can be defined as contraction, expansion and construction joints. Construction and expansion joints are both used between pavement and adjacent roads, meanwhile, the contraction joints are used as a weakened plane while curing process [2].

The dowel bars in between two concrete slabs at the joint position can be installed to support the load transfer under traffic moving loads [4]. As previously stated, when the joint sealant at the transverse joint is damaged, the effects of the ambient environment can result in the reduction of the life service of dowel bars at this position. The severe damage of dowel bars may take place. In the case of no existence or the failure for supporting the load transfer of dowel bars, each concrete slab apparently endures the fully applied load and it is the most critical case which affects the fatigue life of the concrete pavement. There are less previous researches in view of comparing the fatigue life of jointed concrete slabs without dowel bars and continuously reinforced concrete.

In this chapter, the nonlinear FEM analysis of the three-dimensional high-cycle

fatigue for soil and the concrete slab by coupling the constitutive models of both cases is implemented to investigate the decrease of the fatigue life in the case of existing construction joints (transverse direction) without dowel bars (or failure for supporting of dowel bars) compared to continuously reinforced concrete. As referring from Sii [2], the joints firstly leave a gap between the adjacent concrete slabs (normally 10mm) and then making a cut after a larger area of concrete is set. In the first case, dowel bars may be installed during the concrete pouring but not cutting. Upon cutting the concrete slab, the initial width of joint is expanded more 10mm (the construction joints now become 20mm). The example for the cutting of the slab to remove the dowel bars can be applied when the failure of dowel bars occurs under the operation. Hence, the FEM modeling for the existing construction joints without/failure dowel bars is analyzed under the joint width of 20mm. This may be the most critical case of the construction joints under vehicle movement. The typical construction joint is 20mm in width [2] and applied in this study as shown in Fig. 6-3.

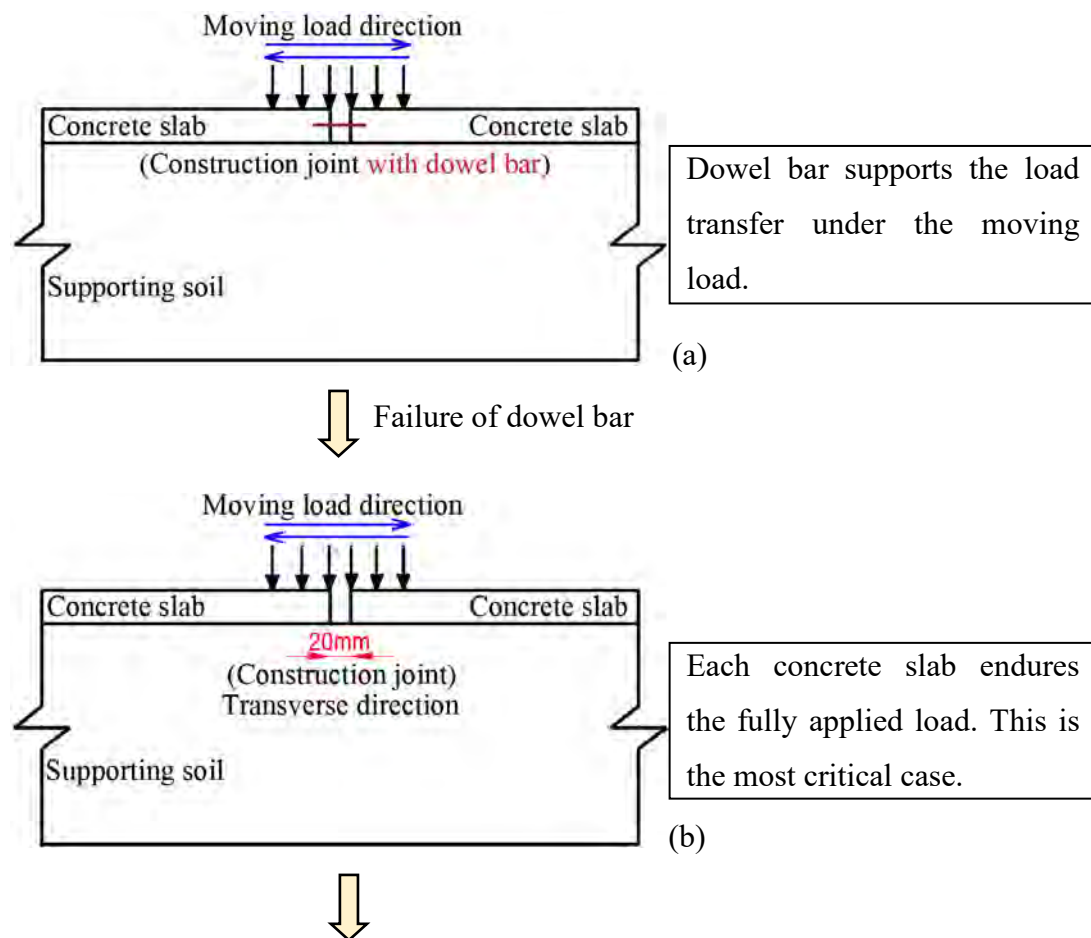




Fig. 6-3 Construction joint used in this study.

6.2 Nonlinear FEM Modeling of Construction-Joint Effects

This section shows the three-dimensional fatigue simulation to compare the fatigue life of concrete pavement under the moving load in case of no existence or failure for supporting of dowel bars at the transverse joint and continuously reinforced concrete. The sensitivity of the model is also investigated the mechanism focused on the thickness and reinforcement ratios of the concrete slab as well as the relative density of soil.

Model used for simulation of construction joint effects in the concrete pavement is presented in Fig. 6-4. The half-domain of the concrete pavement is applied by using the X-coordinate as the symmetric axis. The plane dimension of the concrete slab is 8000mm (length) + 20mm (construction joint) + 8000mm (length), and 3000mm (width). The thickness is changed as 120mm, 150mm, 180mm, 200mm and 250mm. The reinforcement ratio (RR) is 1.0% and 0.1%. The nonlinear mechanics of RC slab in this study is considered through a three-dimensional multi-directional smeared crack model in which cracks and reinforcing bars are idealized as being distributed or smeared over the whole element. Therefore, reinforcing bars may be reflected by the reinforcement ratios. The reinforcement ratios of the slab is 0.1% to depict the weakest case of the concrete slab (equivalent to 41.7 kg/m³, 37.6 kg/m³, 33.9 kg/m³, 28.2 kg/m³, and 22.6 kg/m³ of thickness 250mm, 200mm, 180mm, 150mm, and 120mm, respectively) and 1.0% to illustrate the strong concrete slab (equivalent to 417 kg/m³, 376 kg/m³, 339 kg/m³, 282 kg/m³, and 226 kg/m³ of thickness 250mm, 200mm, 180mm, 150mm, and 120mm, respectively). The plane dimension of soil is

20000mm x 3000mm x 2000mm as length, width and depth, respectively. The relative density (RD) of soil is 50% (loose supporting foundation) and 75% (dense one) [6].

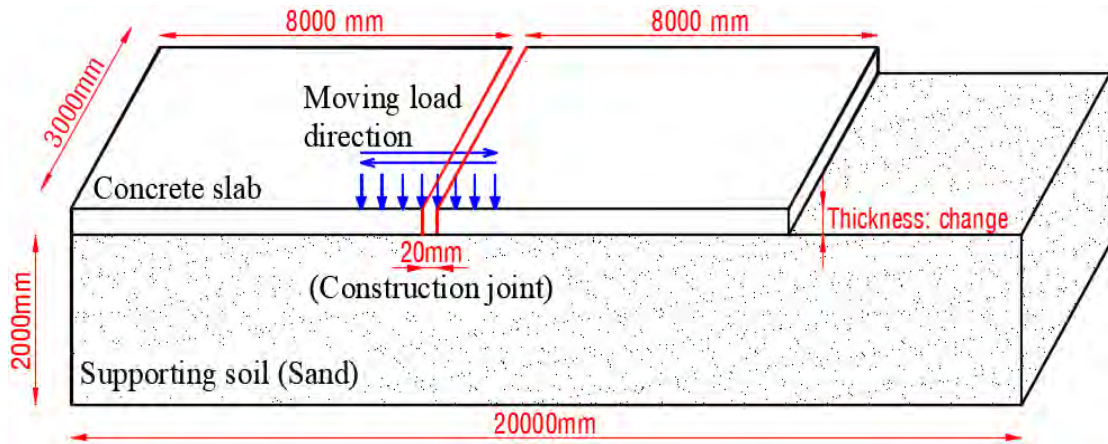


Fig. 6-4 Simulation model for investigation of construction-joint effects to fatigue life

The cyclic moving load 156 kN is applied between two concrete pavement slabs. Due to the fact that this coupled code program has been applied the binary increasing magnification with each passage along the slab axis [7], 60 time-steps are conducted in one single pass and around 2,000 time-steps for the entire path of simulation. The multi-frontal direct linear sparse matrix solution in FEM is also applied. The drying shrinkage has been automatically reproduced owing to the development of the thermo-hydro action in order that it can equilibrate with ambient relative humidity 60% and temperature 20°C [8].

To fully investigate the impacts of construction joints on the fatigue life of the model, continuously reinforced concrete has been also simulated. The properties of the concrete slab and soil are similar to the jointed concrete slab.

6.3 Computation for the Fatigue Life of Jointed and Continuously Reinforced Concrete with Reinforcement Ratio 1.0%

Figure 6-5 illustrates the comparison of the fatigue life between the continuous and jointed concrete pavement in the event of reinforcement ratio 1.0% (equivalent to 471 kg/m³, 376 kg/m³, 339 kg/m³, 282 kg/m³ and 226 kg/m³ of thickness 250mm, 200mm, 180mm, 150mm, and 120mm, respectively), and relative density of soil 50% and 75%, respectively [6].

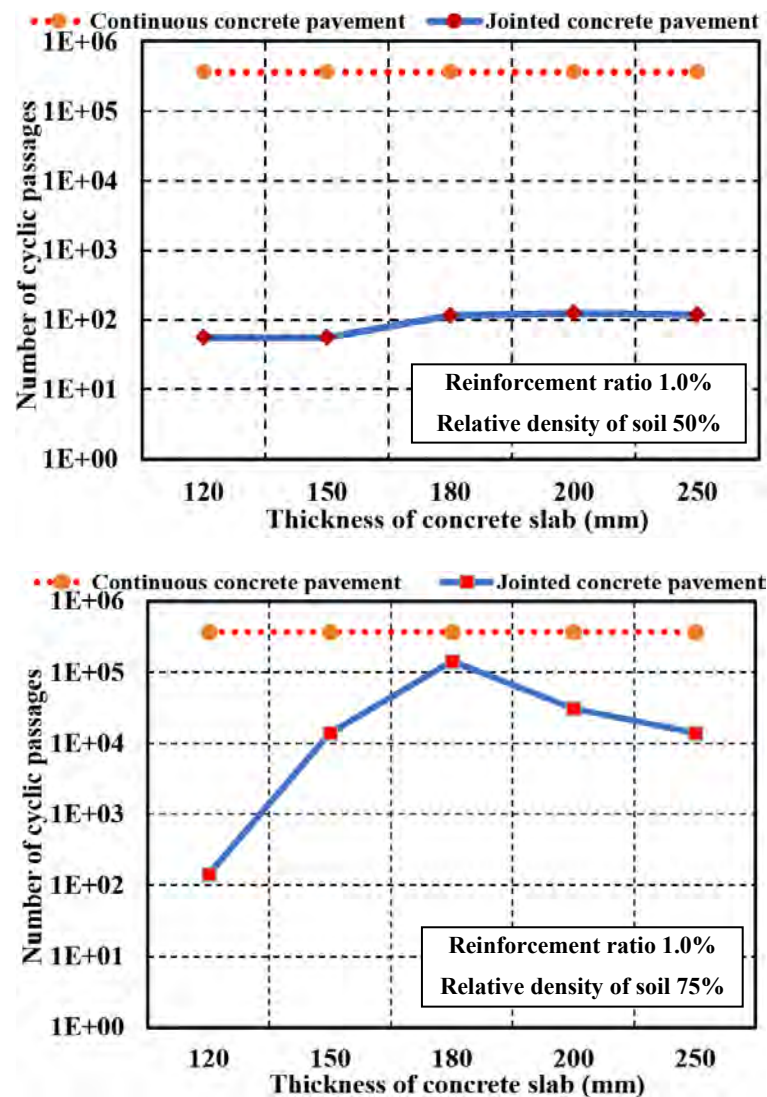
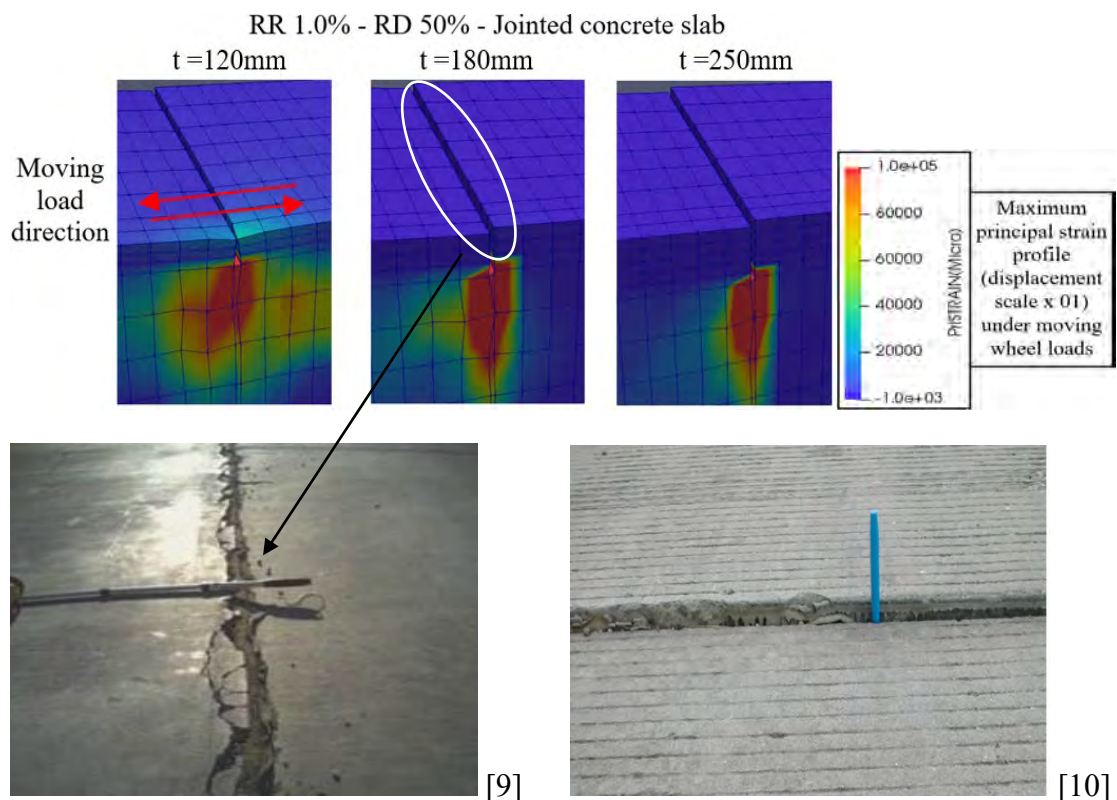


Fig. 6-5 The comparison of fatigue life between continuous and jointed concrete pavement (RR 1.0%).

As can be seen in Fig. 6-5, the fatigue life of the jointed concrete pavement is dramatically reduced compared to the continuous one. It is pointed out that the fatigue life of the continuous concrete pavement is similar to all cases irrespective of the thickness or the status of soil foundations (RD 50% or 75%). On the contrary, in the case of RD 50% of jointed concrete pavement, there is less different of the fatigue life from thickness 120mm to 250 mm. Meanwhile, there exists a distinction of the fatigue life of the jointed concrete pavement if relative density of soil is 75%. The underneath soil is a key determinant to support the life-cycle of the concrete pavement.

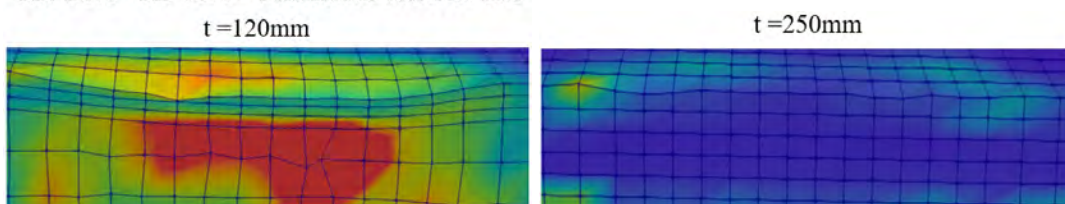
One critical and interesting thing is the fact that under the dense supporting foundation (RD 75%) and the strong concrete slab (reinforcement ratio 1.0%), the longest fatigue life of jointed concrete of pavement is the one of thickness 180mm. It

can be explained by the observation of the failure mode as shown in Fig. 6-6. In the event of thickness 180mm of jointed concrete pavement, the shear band of soil becomes more dispersed and the drastic damage of concrete occurred at two edges of the concrete slab concurrently. Meanwhile, the other cases showed the severely localized damage of soil and the deterioration of concrete only took place at one slab. It is clearly necessary to design the rational thickness for jointed concrete slab under the dense supporting soil. Large thickness (250mm) or thin one (120mm) is not the optimized method in design. This is a discussing point of chapter 5. The failure mode of the jointed concrete slab in the case of RR 1.0% and RD 50% focuses on the transverse joint faulting (the difference in elevation between adjacent slabs across a joint). Faulting is caused by the erosion beneath the leave slab and the buildup on the approach slabs of base fines by the action of pumping under the traffic moving. The pumping is thought to be the basic mechanism that leads to faulting [12].



The difference in elevation between two slabs (the loose soil foundation RD 50%)

RR 1.0% - RD 50% - Continuous concrete slab



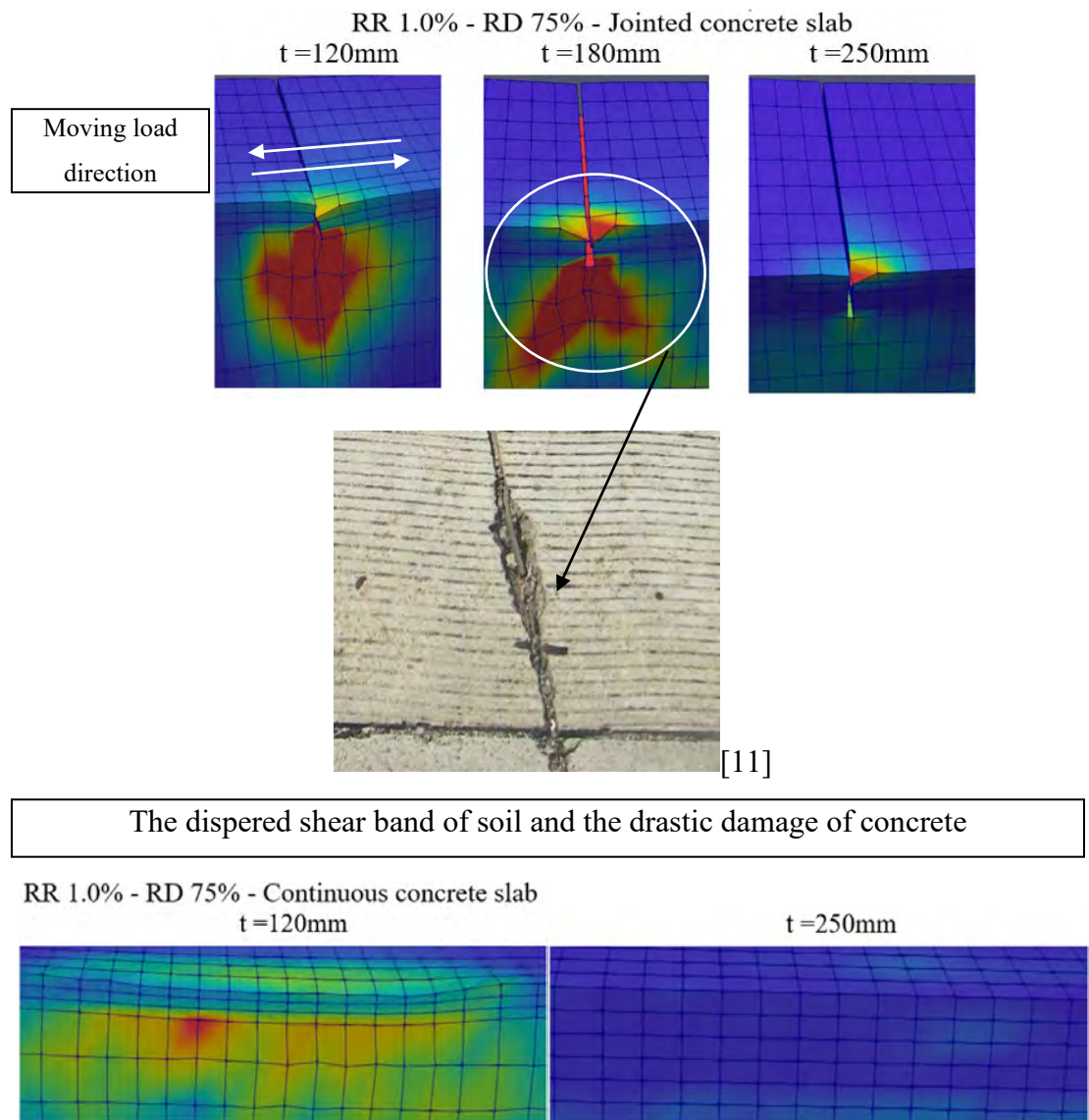


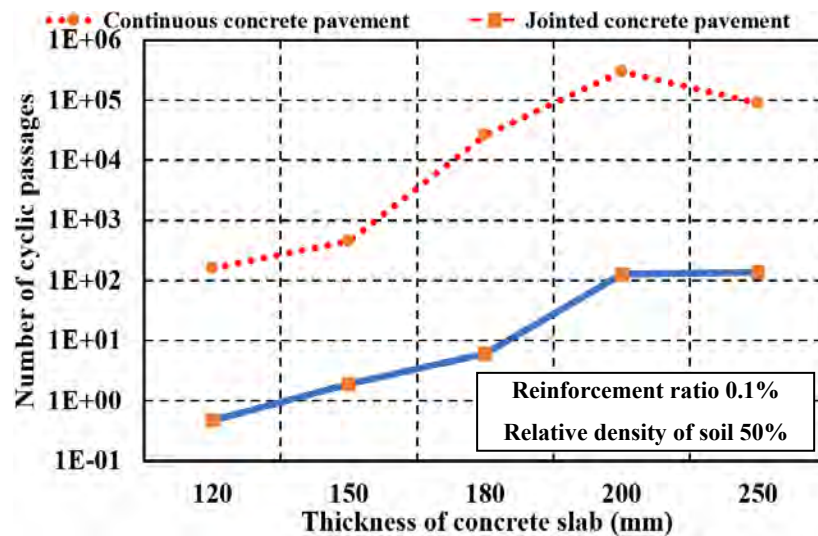
Fig. 6-6 The comparison of failure mode between continuous and jointed concrete pavement (RR 1.0%).

The effect of loose soil (RD 50%) demonstrates that the fatigue life of the jointed concrete pavement may not be supported by the thickness or reinforcement ratio of the concrete slab. The shear failure of soil plays an important role to reduce the fatigue life as clearly seen in the differences of elevation in between two concrete slabs under the moving load. There is no damage of concrete slabs, even in the case of the thin slab (120mm).

By investigating the typical failure modes of some cases as shown in Fig. 6-6, the most critical position of concrete slabs can be defined as the edges between the transverse joints where the shear failure of soil as well as the deterioration of concrete slabs are localized.

6.4 Computation for the Fatigue Life of Jointed and Continuously Reinforced Concrete with Reinforcement Ratio 0.1%

To check the effects of reinforcement ratio, a light one 0.1% (equivalent to 47.1 kg/m³, 37.6 kg/m³, 33.9 kg/m³, 28.2 kg/m³ and 22.6 kg/m³ of thickness 250mm, 200mm, 180mm, 150mm, and 120mm, respectively) was applied to compare with 1.0%. As shown in Fig. 6-7, in the case of RD 50% of soil, there is less different in the fatigue life of jointed concrete pavement (RR 0.1% compared to 1.0%), especially in the thick slabs (200mm or 250mm). There is clear diversity in the fatigue life if supporting soil for jointed concrete slab is the dense one (75%), because reinforcement ratio shows its influence on the dense soil of the concrete pavement by the significant decrease of fatigue life in the event of RR 0.1% compared to RR 1.0%. The mechanism for the reduction of fatigue life in the jointed concrete pavement compared to the continuously reinforced concrete in Fig. 6-7 is therefore explained by the severe localized damage of the slab and soil near the edges of the construction joints. Meanwhile, the damage of the slab and soil in the continuously reinforced concrete pavement is more distributed along the moving load direction. The damage is thus less critical and the fatigue failure is prolonged compared to the jointed concrete pavement.



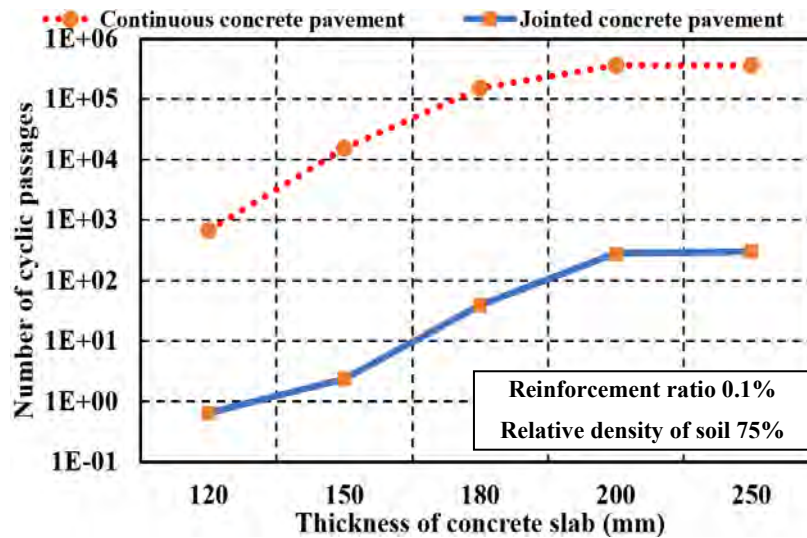
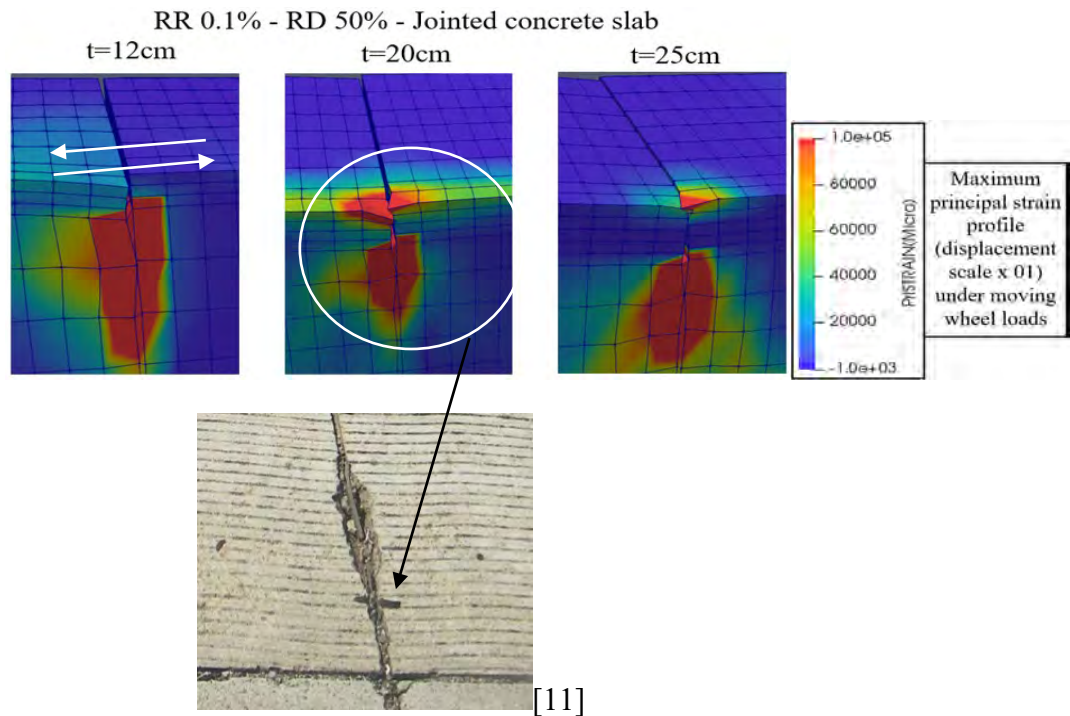


Fig. 6-7 The comparison of fatigue life between continuous and jointed concrete pavement (RR 0.1%).

In view of the design, under the moving load, the fatigue life of jointed concrete cannot be supported if the loose soil is applied irrespective of RR 1.0% or 0.1%, or even the thickness of the concrete slab 200mm or 250mm. This is the fact that the damage of the concrete slab and soil is localized nearby the edges of slabs between construction joints as shown in the failure mode. The lower reinforcement ratio 0.1% shows more severe damage than 1.0%.

On the contrary, soil foundations play a key role to increase in the fatigue life of the continuous concrete pavement. If the concrete slab is thin as 120mm, 150mm or 180mm, the assistance of soil to increase the service time is inconsiderable. But, in case the thick slabs (200mm or 250mm) and the dense soil are applied, there is almost the same fatigue life of continuous concrete pavement RR 0.1% compared to RR 1.0%. The actual working condition of the concrete pavement under the loose or dense soil with different reinforcement ratios or thickness of concrete slabs should be coupled in the concrete pavement design and maintenance works.

Figure 6-8 depicts the comparison of the failure mode between the continuous and jointed concrete pavement in the event of reinforcement ratio 0.1%.



The dispersed shear band of soil and the drastic damage of concrete

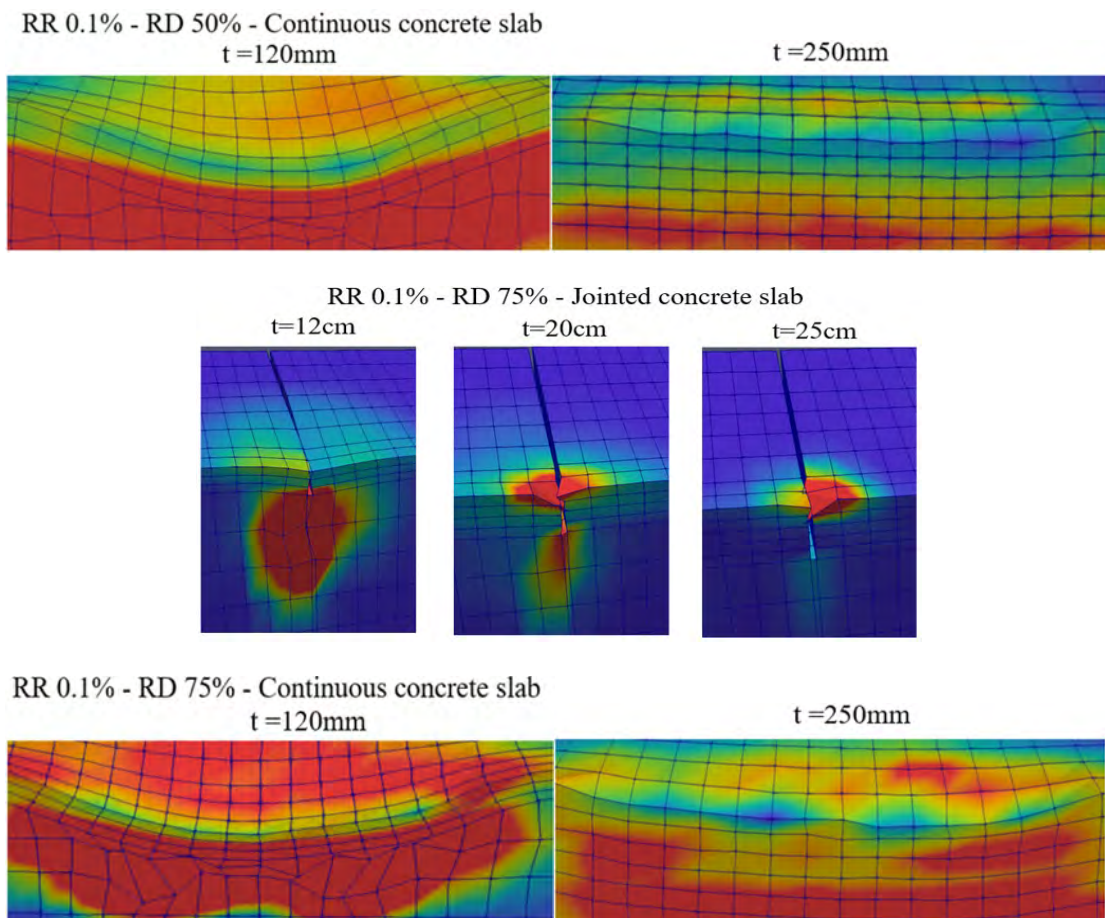


Fig. 6-8 The comparison of failure mode between continuous and jointed concrete pavement (RR 0.1%).

It can be clearly seen that the failure modes of reinforcement ratio 0.1% for jointed concrete pavement are fairly close in all cases irrespective of soil conditions. This is also the coupling of the localized damage of soil and the concrete slab at the joint construction. The failure mode of continuous concrete shows the clear impacts of thickness by the critical displacement of the concrete slab (thickness 120mm) compared to the thick one (thickness 250mm) as shown in Fig. 6-8.

6.5 Conclusions for Chapter 6

The effects of the construction joint in the transverse direction are computationally investigated by utilizing the three-dimensional high-cycle fatigue for coupling of soil and concrete slabs. The numerical analysis shows the drastic decrease in the fatigue life of jointed concrete pavement compared to the continuous one, and the following conclusions are obtained.

1. The existence of construction joints may cause the dramatic reduction of fatigue life due to the localized damage of soil and concrete slabs at the edges.
2. The reinforcement ratio is computationally estimated to have a major effect to the fatigue life in both cases of jointed and continuous concrete pavement.
3. Soil foundations may be a sufficient tool to support the fatigue life of jointed concrete pavements if dense soil and the rational thickness of the concrete slab are examined concurrently. The failure of dowel bars to support the load transfer between the construction joints has been computationally investigated. It shows the primacy of continuously reinforced concrete compared to jointed one in the life-cycle assessment.

References in Chapter 6:

- [1] Website, “<https://www.in.gov/indot/div/aviation/pavement-inspection/pci-review/distresses-pcc/joint-sealant-damage.html>.” .
- [2] H. Bing Sii, “Three-dimensional finite element analysis of concrete pavement on weak foundation,” Griffith University, 2014.
- [3] T. Nishizawa, “Study of mechanical behavior of dowel bar in transverse joints of concrete pavements,” *Proc. JSCE*, vol. 683/V–52, 2001.
- [4] FHWA, “Tolerance of dowel bar placement,” *Dep. Transp. Fed. Highw. Adm. Off. Res. Dev. Washingt. D.C.*, 1983.
- [5] Website, “<https://www.pavementinteractive.org/reference-desk/maintenance-and-rehabilitation/maintenance/joint-repair/>.” .
- [6] H. Q. H. Nguyen, K. Maekawa, and S. Komatsu, “Numerical simulation of construction-joint effects for fatigue-life assessment of concrete pavement subjected to traveling wheel-type load,” *Proc. Japan Concr. Inst.*, vol. 41, pp. 1397–1402, 2019.
- [7] K. Maekawa, E. Gebreyouhannes, T. Mishima, and X. An, “Three-dimensional fatigue simulation of RC slabs under traveling wheel-type loads,” *J. Adv. Concr. Technol.*, vol. 4, no. 3, pp. 445–457, 2006.
- [8] H. Q. H. Nguyen, K. Maekawa, and S. Komatsu, “Three-dimensional high-cycle fatigue simulation of soil-concrete pavement slab interaction under moving loads,” *Proc. 8th Int. Conf. Asian Concr. Fed.*, pp. 1207–1216, 2018.
- [9] Website, “<https://theconstructor.org/transportation/types-failures-in-rigid-pavements-causes-repair/16105/>.” .
- [10] Website, “Manual Notice 2018-2-
http://onlinemanuals.txdot.gov/txdotmanuals/pdm/manual_notice.htm.” .
- [11] Ayers, M., Cackler, T., Fick, G., Harrington, D., Schwartz, D., Smith, K., Snyder, M.B., and Dam, T.V. “Guide for concrete pavement distress assessments and solutions: identification, causes, prevention, and repair,” *Iwota State University, National Concrete Pavement Technology Center*, 2018.
- [12] R. B. Mallick and T. E. Korchi, “ Pavement Engineering - Principles and

Practice,” *Taylor and Francis*, 2nd Edition, 2013.

CHAPTER 7

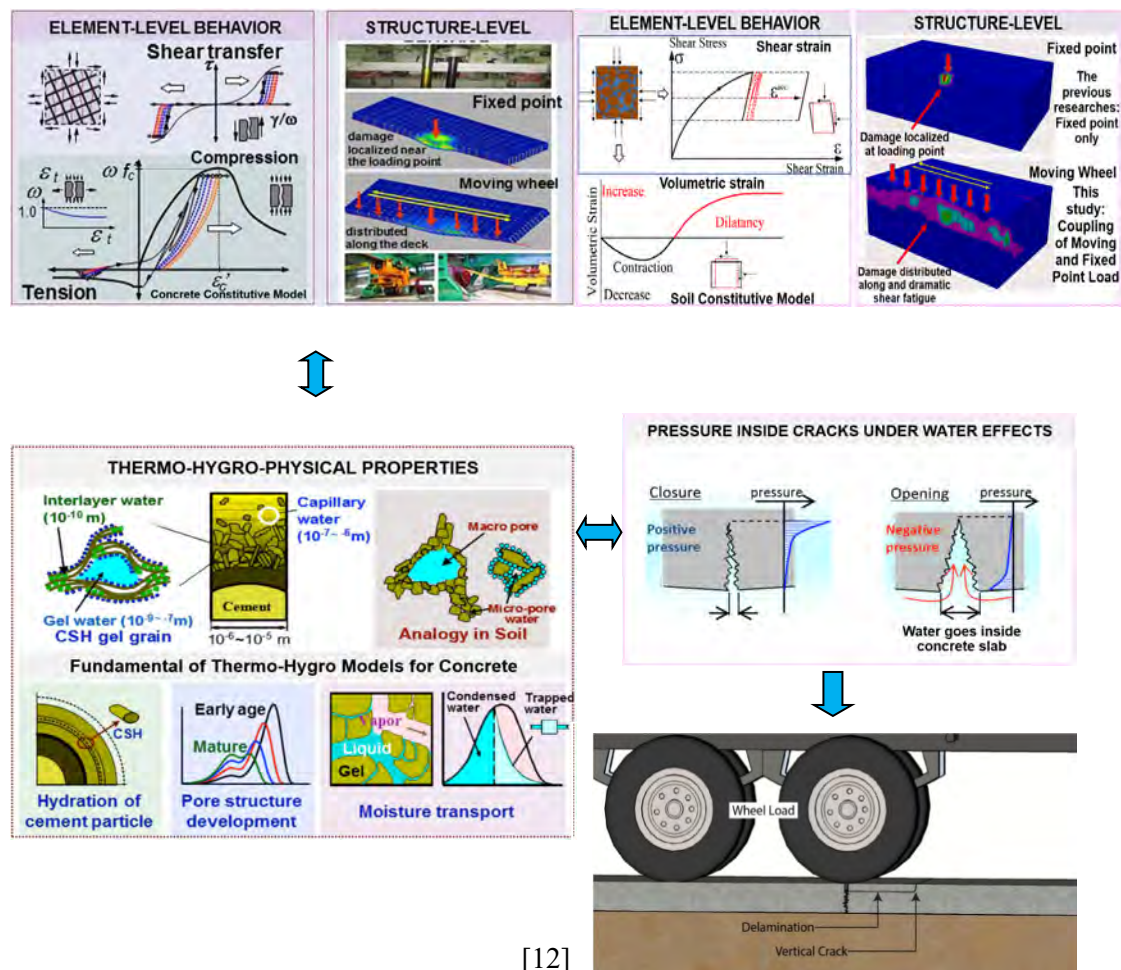
WATER COUPLED CRACKS ON LIFE-CYCLE ASSESSMENT OF CONCRETE PAVEMENTS UNDER MOVING LOADS

7.1 Introduction

The ambient environment has huge impacts to the fatigue life of the concrete pavement. If structures are maintained in the freezing temperature, the concrete performance is degraded compared to the dry case [1], [2]. The consideration of water effects in the life-cycle assessment of RC slab decks showed the sharp decrease compared to the fully dry RC slabs [3]. In engineering practices, water on the top or bottom surface of concrete slabs can come from the rainwater or the underground. It can easily ingress and be stagnant in the cracks. Maekawa and Fujiyama [4], [5], Maekawa et al. [6], and Nguyen et al. [7] depicted the intimate relations between the deformation and stagnant water inside concrete cracks and these behaviors have been coupled in crack-water interaction modeling by using the theory of Biot [8], [9] as the multi-phase model of the liquid-solid composite. The stagnant water inside concrete can migrate under the deformation of the solid-concrete skeleton and cause the increase of the pore pressure. Figure 7-1 shows the effects of water kinematics from nanoscale to meter developed in multi-scale chemo-physical integrated models to simulate the nonlinear mechanics of concrete slabs under moving loads (compression, tension, and shear transfer), and coupled with the stagnant water in crack gaps [7], [10].

The mechanism for the damage of concrete slabs with water effects can be observed by examining the water pressure inside concrete. Under moving loads, the cracks can open and close, hence the water pressure may be negative or positive. When the cracks close, the development of high pressure inside cracks occurs. It can cause the large internal force around the crack tips and leads to further crack propagation [5], [11]. Matsui [3] showed that at the beginning of erosion, cracks in the concrete slab are hard to be observed by naked eyes and they are obviously difficult to be detected. But, these may continuously propagate and affect to the concrete cover [6].

The condensed moisture in the concrete cracks is an exigent study in concrete pavements to evaluate how the fatigue life is reduced as well as the prediction for the remaining service of concrete slabs when cracks appear. It has never been studied in the concrete pavement before. In this chapter, three-dimensional high-cycle fatigue analysis under the moving load to investigate the effects of stagnant water inside the cracks of the concrete slab is proposed. By incorporating the constitutive models of the concrete slab, the soil foundation coupled with the multi-scale modeling for pore water inside cracks, the fatigue life of concrete pavements may be accurately predicted. It shows the dramatic shortage of the fatigue life in case of water effects compared to the fully dry slab.



[12]

Stagnant water can ingress from the vertical crack

Fig. 7-1 Multi-scale simulation scheme of water-crack interaction in pavement.

Under the traffic loading, the vertical crack can appear from the top surface of the slab as shown in Fig. 7-1. As a result, the delamination of the slab occurs in the horizontal plane near the top surface of the slab. Stagnant water from the top surface

of the slab can easily ingress through vertical cracks. When cracks close, the high water pressure inside crack gaps can dramatically increase. This result is similar to the horizontal cracking appearing near the top surface of RC slab decks under the moving load.

7.2 Fundamentals for the Water-Crack Interaction in Concrete Pavements

To computationally simulate the behaviors of the concrete pavement with/without the interaction of the stagnant water and cracks, the coded program has proposed and coupled these issues in multi-scale, multi-chemo-physical analysis of concrete slabs and soil foundations. The meso-scale model of stagnant water inside concrete cracks has been coupled by Maekawa and Fujiyama [4]. This coupled code has been developed based on a couple of experiments to verify in each scale as the high-cycle fatigue for concrete slab decks [13], the shear band of the soil foundation [14] and the movement of the stagnant water in concrete cracks [4].

The equations for saturated concrete in the study of coupling the stagnant water with cracked concrete has been proposed by Maekawa and Fujiyama [4], [5], and Maekawa et al. [6] based on the theory of Biot [8], [9] for soil skeleton and pore water. Concrete is also assumed as two-phase composite, including solid skeleton and pore water. The total density of saturated concrete is calculated as,

$$\rho = (1 - n)\rho_c - n\rho_f \quad (1)$$

Where $(1 - n)\rho_c$ is concrete skeleton and $n\rho_f$ is pore water inside cracked concrete. ρ_c is the density of concrete skeleton, and ρ_f is the density of pore water. n is the pore volume ratio.

The total stress of uncracked concrete σ_{ij} is a sum of the skeleton stress and the isotropic pore water pressure as,

$$\sigma_{ij} = \sigma'_{ij} + \delta_{ij}p \quad (2)$$

Where p is pore pressure and σ'_{ij} is the effective stress tensors on the solid skeleton.

It is noted that the pore water inside uncracked concrete in equation (2) is assumed as an isotropic manner. Hence this formula is applied to the stagnant water inside capillary pores.

After cracking, the pore water pressure becomes anisotropy in the concrete pore (capillary and crack gaps) [5]. It is convinced that there is a large amount of stagnant water which is located in a thin layer surrounded by a couple of crack planes, and the interaction with cracked concrete is anisotropic [5]. The pore water pressure inside crack gaps is therefore perpendicular to a pair of parallel crack planes as,

$$\sigma_{ij} = \sigma'_{ij} + \delta_{ij} l_i p \quad (3)$$

Where l_i is the unit directional vector normal to a crack plane. It is thought that in practical engineering, the crack width is about 0.1mm to 1.0mm. Thus, if the mesh size of the finite element should be larger than the maximum size of the coarse aggregate (around 15mm to 30mm), the convergence of equation (3) shows the minimum error for calculation (1.0-3.0% only). This assumption may be therefore acceptable for the precision of the computational analysis [5].

Figure 7-2 shows the sensitivity of the permeability of concrete at pre and post cracking. It can be seen that cracks are the source of anisotropy of moisture migration. Uncracked concrete demonstrates the similar permeability of each direction (it is around 10^{-9} cm/s). On the contrary, cracked concrete shows the significant magnification of permeability at cracked directions (it is about 10^{-3} cm/s or more). The sensitivity of crack mouth opening has conducted in the experiment by Wang et al. (1977) [5].

The mean permeability of cracked concrete along the i axis is assumed as,

$$K_i = K' \left\{ 1 + \left(\frac{\varepsilon_{jj} + \varepsilon_{kk}}{a} \right)^4 \right\} \quad (4)$$

K' is the intrinsic water permeability of uncracked concrete. $\varepsilon_{jj} + \varepsilon_{kk}$ is the mean transverse in plane strain. The constant a is used for the purpose of being consistent with the experimental results from Wang et al. [5].

As previously stated, skeleton and pore water in cracks are two components of saturated concrete, and it is necessary to verify the dynamic equilibrium equations of these components. For saturated skeleton, the equations are formulated in the view of dragging forces rooted in the permeability (K) of pore water in each direction i through the concrete pore and crack gaps as [4], [5],

$$\sigma_{ij,j} + \rho g_i = \rho u_{i,tt} + \rho_f w_{i,tt} \quad (5)$$

Where ρg_i is the gravity force, $u_{i,tt}$ is the acceleration of skeleton, and $w_{i,tt}$ is the acceleration of water.

The dynamic equilibrium equation for fluid materials in skeleton is shown as,

$$\rho_i + \rho_f g_i = 1/K w_{i,tt} + \rho_f (u_{i,tt} + w_{i,tt} / n) \quad (6)$$

Where $1/K w_{i,tt}$ is the viscosity, and $\rho_f (u_{i,tt} + w_{i,tt} / n)$ is the force and equal to the mass x acceleration. The value of n is a constant before loading and considered as capillary pore porosity of concrete mixture.

The details of the framework for the couple of concrete skeletons and stagnant water are illustrated in Fig. 7-2.

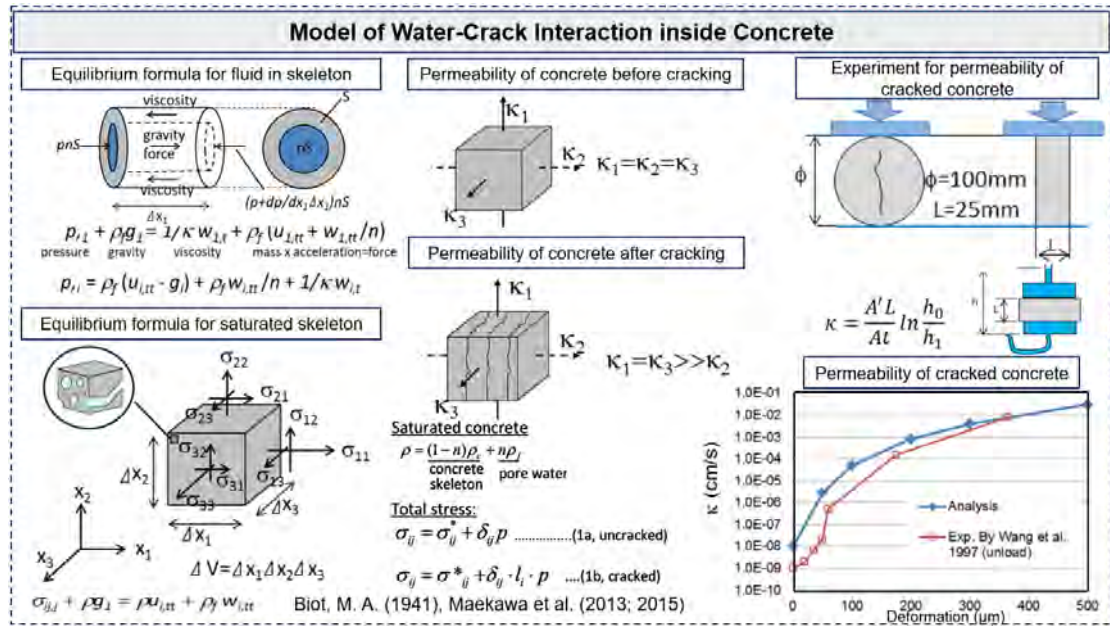


Fig. 7-2 Modeling of stagnant water inside cracked concrete.

Under the traffic moving, cracks may close and open. As a result, the pore pressure develops. When cracks close, the water pressure rises. When cracks open, water pressure becomes negative and can cause the phase change as vaporization. The damage of concrete is therefore accelerated. In the event of RC slab decks, moving loads were reported as a cause to affect the severe deterioration at the surface layer of concrete slabs [4]–[6]. In the case of concrete pavement, it has not been yet investigated the effects of stagnant water in the concrete slabs. The code based on the constitutive models for high-cycle fatigue of concrete slabs and soil foundations to be coupled with the multi-phase model for the liquid soil composites has been verified and validated in this study. It can currently be applied in the research of the water-crack interaction in the concrete pavement. The detail for the coded program of the concrete slab, the soil foundation and pore water in cracked concrete is summarized in Fig. 7-3.

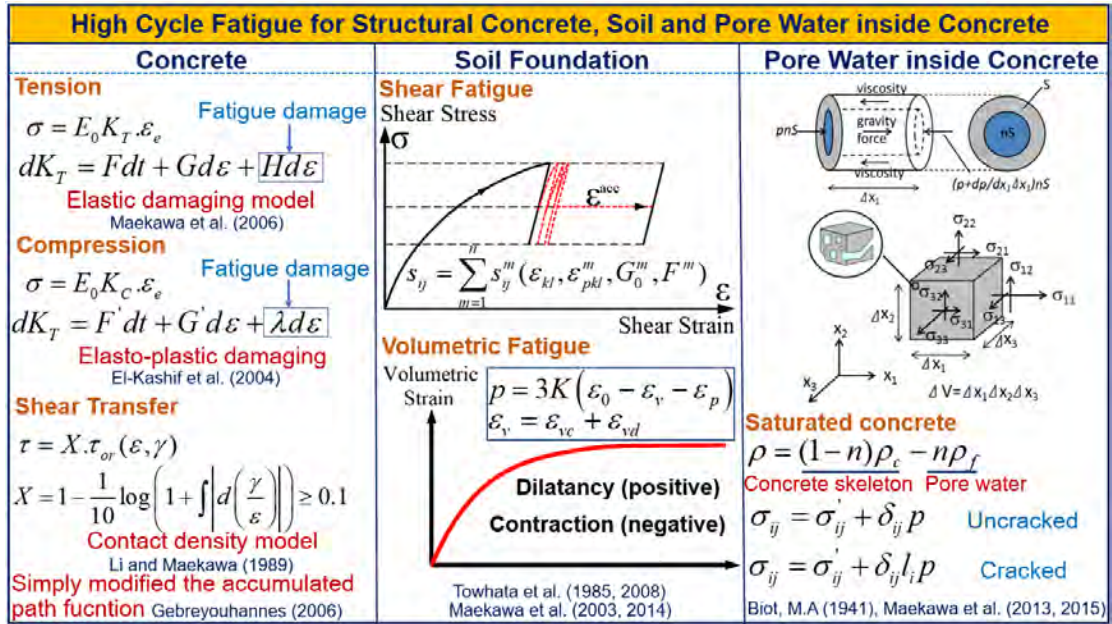


Fig. 7-3 Summary of the coupled code for concrete, soil and pore water inside cracks.

7.3 Nonlinear FEM Analysis for the Water-Crack Interaction

The full-scale three-dimensional FE simulation to the end of fatigue life on the concrete pavement is presented as shown in Fig. 7-4. The half-domain of the concrete pavement with X-coordinate (moving load direction) is applied as the symmetric axis. The constitutive laws for nonlinear modeling of reinforced/plain concrete interacted with the soil foundation and water are described in the previous section. The

dimension of the soil foundation is 3000mmx8000mm in plane and 2000mm in depth, and the concrete slab is 3000mmx4000mm in plane and 250mm (25cm) thickness. The moving load of 156 kN is produced by applying the linearly nodal force in each load step at the symmetric axis (X-direction). Therefore, the total nodal force is always kept constant during the passage of moving loads. The concrete slab consists of five layers, each one is 50mm (5cm) in depth.

Four main variables are considered in the simulation, i.e. the position of stagnant water effects in concrete slabs, the reinforcement ratio of concrete slab, the compaction of soil foundation (relative density), and the effects of concrete strength. The effects of water saturation conditions consist of the top layer slab 5cm, the top layer slab 10cm, the whole depth slab (five layers of 25cm of slab) and the fully dry slab. There are seventh reinforcement ratios (RR) in concrete slab investigated including 0.1%, 0.3%, 0.4%, 0.5%, 0.6%, 0.8%, and 1.0%, respectively. There are eighth water-to-cement ratios examined in the concrete slab as 30%, 35%, 40%, 45%, 50%, 55%, 60% and 65%. The fully dry layers are demonstrated by overlapping of reinforced/plain concrete and pore water elements, whilst the dry layers are represented only by the concrete elements. The soil foundation is assumed as sand with relative density (RD) 50% and 75% to illustrate the loose and dense compaction, respectively.

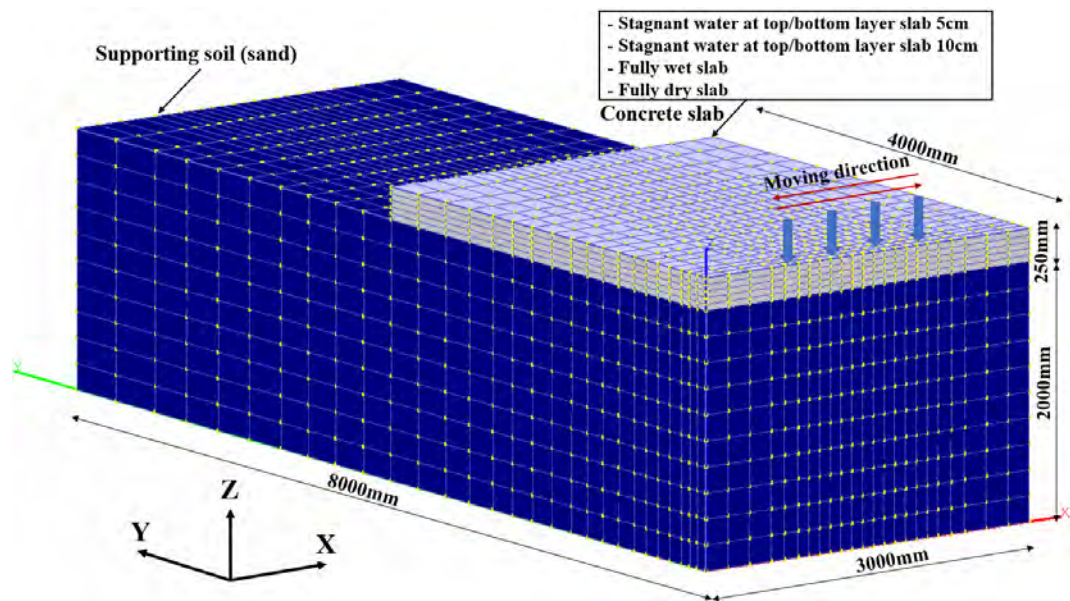


Fig. 7-4 Simulation model for water coupled cracks in concrete pavement.

The magnified direct path integral was applied in simulation by utilizing binary increasing magnification with each passage along the slab axis [15]. There are around 60 time-steps implemented in one single pass and about 2,000 time steps for the entire path of simulation. The multi-frontal direct linear sparse matrix solution in FEM solution was also applied to accumulate the time calculation. The drying shrinkage has been automatically reproduced as the thermo-hygro action develops so that it may equilibrate with ambient relative humidity 60% and temperature 20°C.

7.3.1 Effects of the Stagnant Water Position in the Concrete Slab

Figure 7-5 depicts four critical positions for the effects of water inside cracks of the concrete slab (RR 1.0%). FEM analysis is investigated in the stagnant water at the top layer 5cm, top layer 10cm and/or bottom layer 5cm, bottom layer 10cm as well as the fully saturated slab. The stagnant water from the rainwater or the underground is therefore fully examined, and the reduction of the fatigue life on the concrete pavement may be predicted. It is reported from the previous study [19], the runoff coefficient of rainwater on concrete roads is around 0.67 which is lower than that of asphalt (0.89). The degradation state of the pavement might be affecting these variable results as water can infiltrate through joints and cracks [19]. Therefore, the rainwater can go through cracks and may be stagnant due to the low runoff coefficient, especially in case of the bad situation of the slab surface.

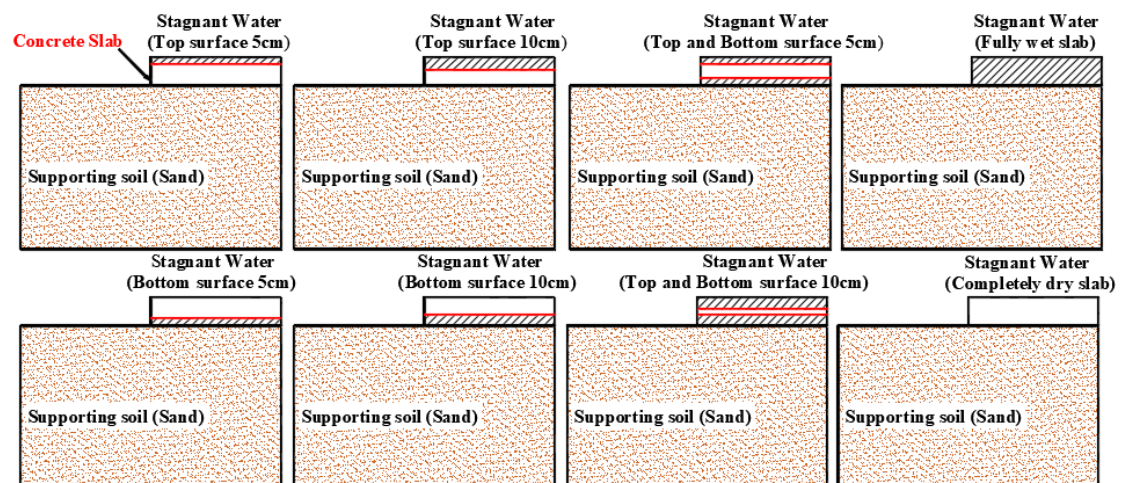


Fig. 7-5 The stagnant water position in the slab of FEM analysis.

Figure 7-6 shows the decrease of the fatigue life of the concrete pavement slab under the effects of stagnant stagnant water at the top layer of 5cm and 10cm. It can

be explained by the serious deterioration of the concrete pavement slab by checking the failure mode at the final stage of the model. In case of the dry slab, the damage of the concrete slab is not severe and vice versa for the case of stagnant water. If the concrete pavement is affected by the top layer 5cm of stagnant water, the severe damage will also develop around this position. The same trend can be seen in the top layer of 10cm affected by stagnant water.

Under the water impacts in both cases, the displacement of the concrete pavement sharply rises nearly equal to the final cycle of the dry slab at the very early stage. The top layer of 10cm shows the sudden increase in the displacement at nearly final stage compared to the top layer of 5cm. As discussed in the preceding section, cracks can close or open and the water pressure will be repeatedly negative or positive. The high-water pore pressure appears and causes the increase in internal stresses in micro-pores of concrete. The damage of concrete pavement chiefly attributes to the decay of the top layer on which bending compression develops and the erosion in the surface layer of the concrete slab may be occurred. The rising pore water pressure leads to the disintegration of the concrete composite system. This figure demonstrates that if the stagnant water stays on the surface of concrete pavement, it can be a key factor to reduce the fatigue life of the concrete pavement.

One important point is the faster evolved displacement in case of the water impact at the top layer of 5cm compared to the case of 10cm layer. It shows that the effect of water is great near the slab's surface (at the top layer 5cm) than the further position (at the top layer 10cm). Under the moving load, the water pressure highly rises over a large number of passages, and it results in increasing principal strains accompanying the erosion [4], [5]. As the concrete principal strain is an indirect measure of cracked concrete damages, this value has been checked in terms of the stagnant stagnant water on the upper layer. The dramatic increase in the principal strain of the top layer of 5cm causes the early damage compared to the case of 10cm. Consequently, the displacement of the concrete pavement evolves suddenly as shown in Fig. 7-6.

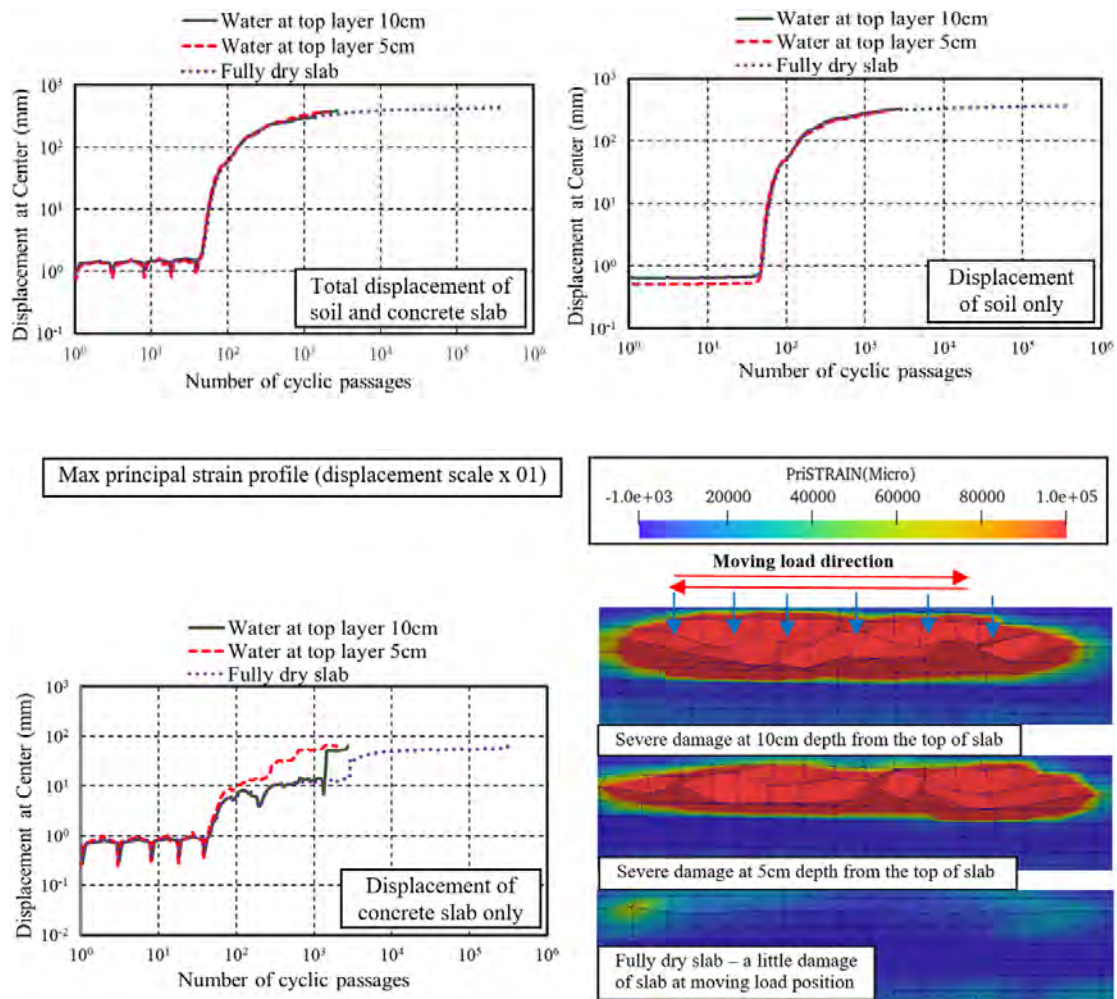


Fig. 7-6 Fatigue life and failure mode with water at top layer of 5 and 10 cm.

Similar to the top layer of slabs, the stagnant water was computationally placed around the bottom layer as shown in Fig. 7-7. It can be seen that the stagnant water in the bottom layer of the slab will not affect the fatigue life computationally. We can say that damage of the concrete pavement chiefly attributes to the deterioration of the top layer surfaces in bending compression. When the stagnant water exists inside the top 10cm of the slab, water suction inside cracks in open mode occurs. As a result, stagnant water goes through the bending tension zone when flexural cracks open. The water pressure is therefore decreased (negative pressure) compared to the case of water at top 5cm zone where bending compression primally develops. As previously stated in Fig. 7-1, delamination in concrete pavements may be thought as the mechanism for the development of a horizontal crack within the slab that results in separation of the surface layer to the depth from the remaining concrete. This damage can occur anywhere in the concrete slab. Under the traffic moving, the vertical cracks can appear from the top surface of the slab and the delamination of the slab occurs in

the horizontal plane near the top surface of the slab. It is consistent with the previously conducted experiment showing the horizontal cracks appearing nearby the top layer of concrete bridge decks as shown in Fig. 7-8.

In Fig. 7-7, the stagnant water at the bottom layer is assumed from the underneath soil and interacted with the concrete pavement as above. The coupling between soil and the concrete slab has been implemented through the node connection. The stagnant water can freely move in this intersection. The soil may get more mixed in comparison with its initial status. That is the reason why the displacement of soil in both cases of 5cm and 10cm bottom layer water effect is larger than the dry slab.

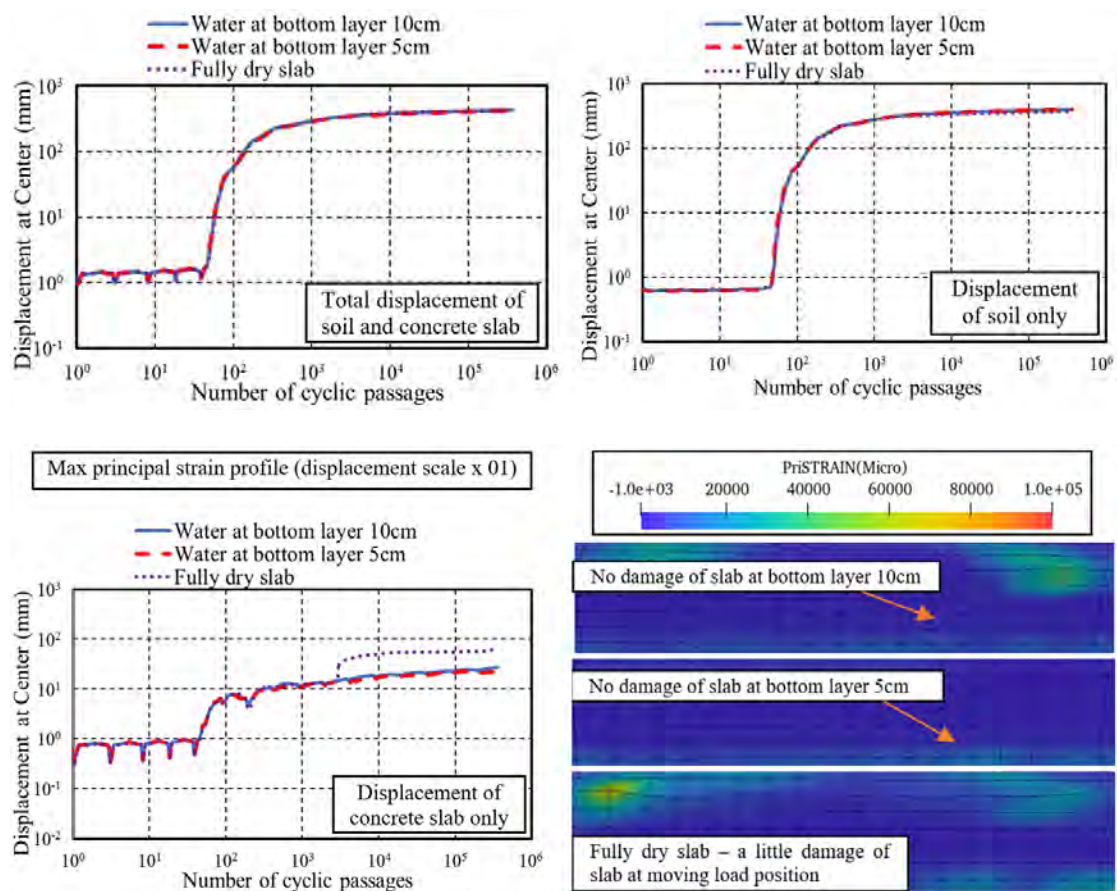


Fig. 7-7 Fatigue life and failure mode subjected to water at the bottom layer.

Due to the wider support by the foundation, the displacement and the damage of the concrete pavement slab are decreased compared to the case of dry slab. In the previous studies of RC decks, it is pointed out [4], [6] that the existence of water can affect the rate-dependency of structural performance and the effects of negative pore pressures in cracks under high-speed wheel movement are obvious at the wet-upper part deck, and the bottom layer of bridge deck will not be affected by stagnant water.

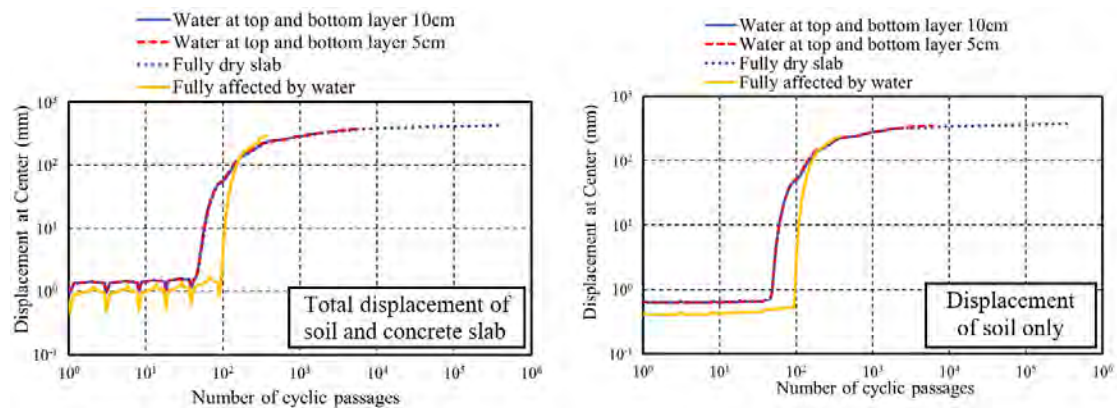
It is similar to the simulation results of the concrete pavement under the water impacts at the bottom layer 5cm or 10cm.



Fig. 7-8 Horizontal cracking at top surface of concrete bridge deck under moving loads [16].

To discuss the overall impacts of stagnant water to inside cracks of concrete, the combined cases were conducted to the top and bottom layer at 5cm and 10cm as well as the whole layer of the slab as shown in Fig. 7-9.

As mentioned previously, the fatigue life of the concrete pavement is strongly governed by the stagnant water staying at the top layer. In the case of coupling stagnant water at the top and the bottom layer concurrently, the severe damage is just localized at the top layer of the slab, and its total fatigue life is not much different compared to the top layer water effects only. In case where the whole slab is affected by stagnant water, the damage is mostly severe. Consequently, and the displacement of the concrete pavement is quickly increased.



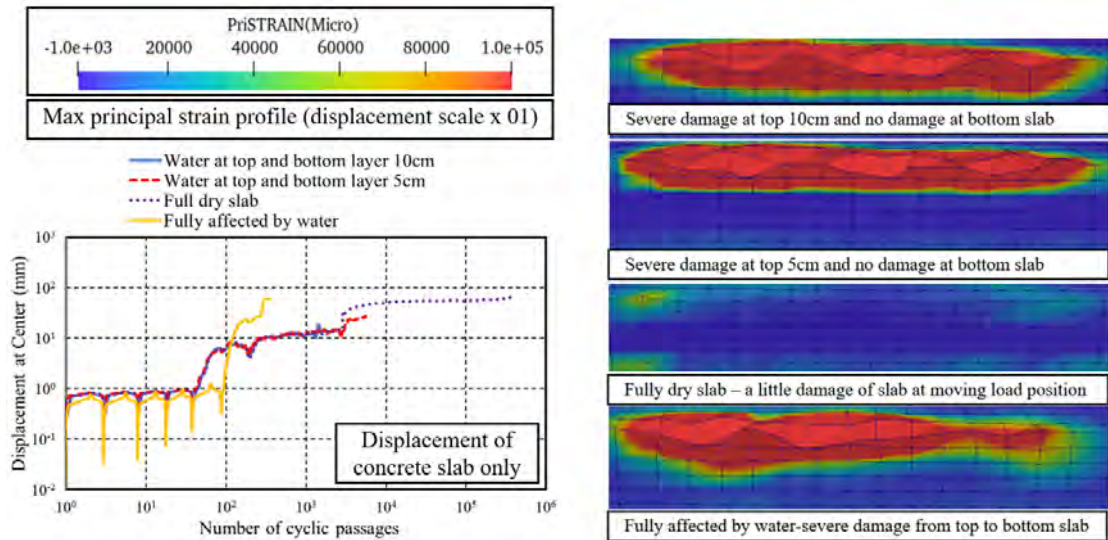


Fig. 7-9 Fatigue life and failure mode under water effect at each layer.

7.3.2 Effects of Reinforcement Ratios

The seventh specific cases of reinforcement ratios are shown from Fig. 7-10 to Fig. 7-16, respectively. In these figures, the fatigue life and failure mode of the concrete pavement with the loose soil foundation (RD 50%) are observed under the stagnant water effects and the dry condition of concrete slabs. As the preceding section, the nonlinear mechanics of RC slab in this study is considered through a three-dimensional multi-directional smeared crack model which reinforcing bars may be reflected by the reinforcement ratios. The arrangement of transverse and longitudinal reinforcements can be covered anywhere due to the fact that stagnant water is investigated in the depth of 5cm, 10cm, and whole slab.

Firstly, the lightest reinforcement ratio ($RR=0.1\%$) is applied as illustrated in Fig. 7-10. It is observed that the fatigue life is dramatically shortened when the water exists in the concrete slab. Under the water impacts, the displacement of the concrete pavement significantly rises almost equal to the final cycle of the dry slab at the very early stage. The concrete slab is severely damaged at the final stage of the model. In case of the dry slab, the deterioration of the concrete slab is not serious and vice versa for the case of stagnant water. If the concrete slab is affected by the top layer 5cm of stagnant water, the severe damage will also develop around this position. The same trend can be seen in the top layer of 10cm affected by stagnant water. In the event of being fully saturated, the damage of the concrete slab is focused on the top layer of

the slab only. The stagnant water at the bottom layer of the concrete slab will not affect the failure mode in computation. Once again, we can say that the damage of the concrete pavement chiefly attributes to the deterioration of the top layer surfaces in bending compression. It can be explained that the principal strain at the top layer of the concrete slab under water stagnant increases due to the rise of the water pressure over a large number of passages. The typical case for the principal strain and pore water pressure inside cracked concrete is illustrated in section 7.4. In the previous studies of RC decks, the existence of stagnant water can affect the rate-dependency of structural performance, and the effects of negative pore pressures in cracks under high-speed wheel movement are at the wet-upper part deck only [4], [5], [7]. The bottom layer of the bridge deck will not be affected by stagnant water. It is similar to the FEM analysis in this study. It is also consistent with the previous experiment which showed that the horizontal cracks just appeared nearby the top layer of concrete bridge decks as shown in Fig. 7-8. Under the moving and fully dry slab, the damage of the concrete slab at the final stage is not severe and only localized at the moving position and the top surface of the slab. the total fatigue life is therefore dramatically increased compared to the stagnant water slabs.

The existence of stagnant water at top layer 5cm shows the faster increase in displacement at nearly the final stage compared to the top layer 10cm (as can be seen from the displacement of the slab only in Fig 7-10, the displacement of stagnant water at top layer 5cm (the blue dot) is increased faster than the stagnant water at top layer 10cm (the red dot)). Consequently, the fatigue life is shorter than the case of 10cm layer. It shows that the effect of water is more critical near the slab's surface (at the top layer 5cm) than the further position (at the top layer 10cm). As a preceding section, under the moving load, the vertical cracks appear from the top surface of the concrete pavement slab and the delamination of the slab occurs in the horizontal plane near the top surface. Water can easily ingress and be stagnant in the vertical cracks. Cracks can open or close, and the water pressure will be repeatedly negative or positive. The high pore pressure appears and causes the increase in internal stresses in micro-pores of concrete. As a result, the concrete damage and erosion are also accompanied. The rising of pore water pressure leads to the disintegration of concrete composite system.

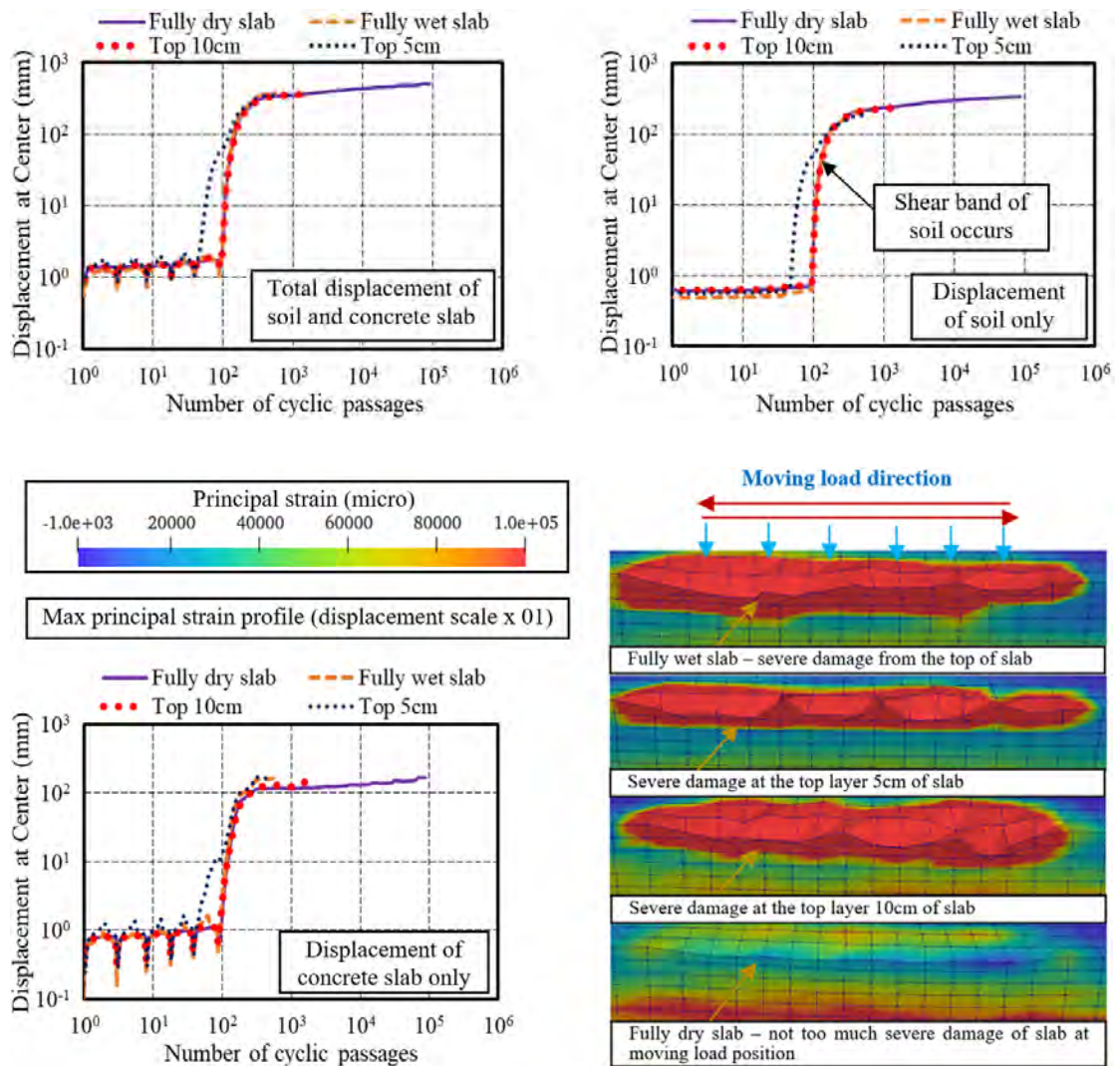


Fig. 7-10 Fatigue life and failure mode of concrete pavement under water effects with RR 0.1%.

The water pressure highly increases over the large number of passages, and it causes the rise of principal strains accompanying the erosion [4]. As we know, the principal strains of concrete is an indirect measure of cracked concrete damages. Therefore, the faster evolution of the displacement and the damage of the concrete slab in the case of stagnant water at top layer 5cm and fully wet slab can be explained based on this assumption (section 7.3.1).

The light reinforcement ratio (0.1%) can not make a contribution to the fatigue life of the concrete pavement if the stagnant water exists in the cracks. the proposal is to increase the reinforcement ratio (0.3%) to check how the fatigue life is different from the previous case. Figure 7-11 shows the fatigue life and failure mode of the concrete pavement under water effects with reinforcement ratio 0.3%.

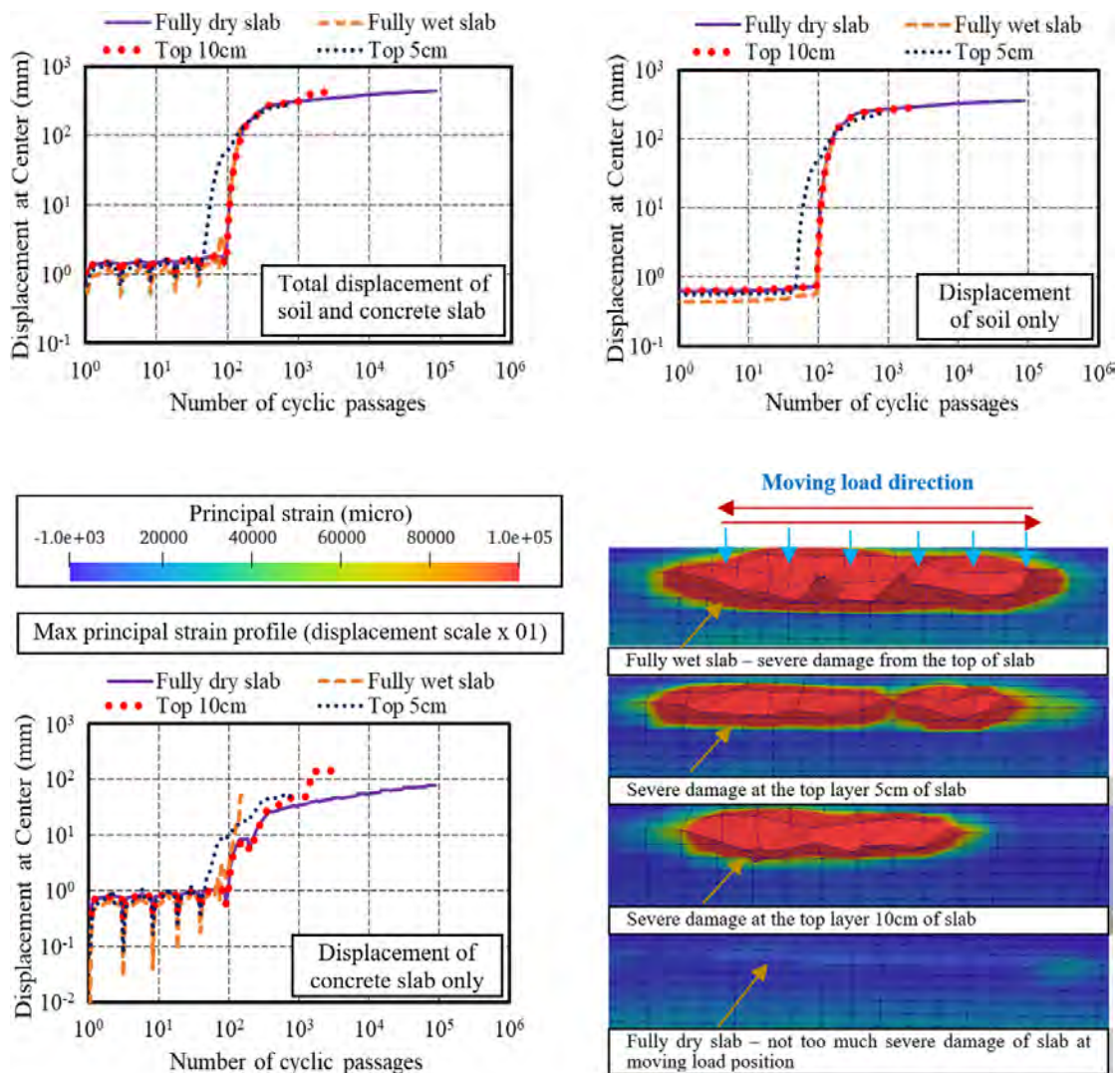


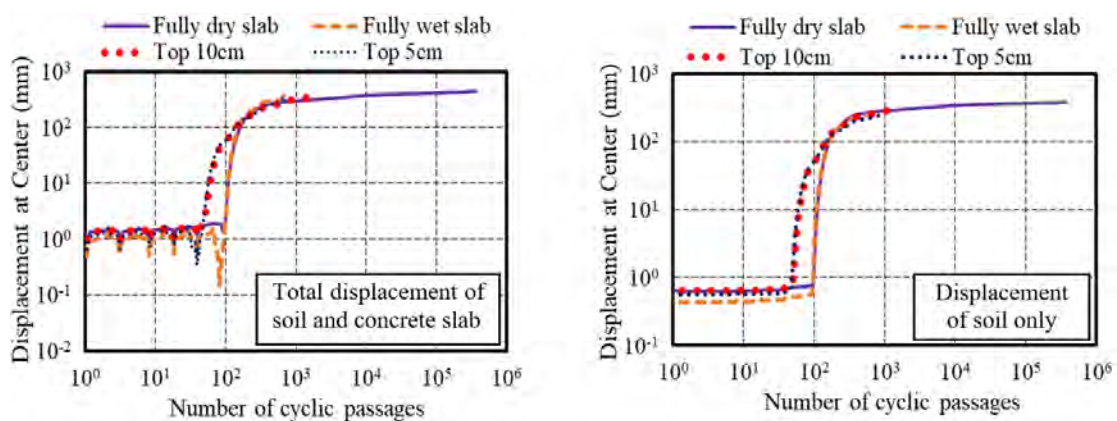
Fig. 7-11 Fatigue life and failure mode of concrete pavement under water effects with RR 0.3%.

There is a little increase in the fatigue life of the case of top layer 10cm compared slab 0.1%. Other stagnant water cases are nearly not different from the slab of RR 0.1%. The assumption for the critical positions of stagnant water in the concrete slab is strengthened in this simulation. The fully wet slab demonstrates the most severe damage and its deterioration is distributed under the moving load at the top surface only. It is similar to the slab of RR 0.1 %, there is no damage of the concrete slab observed in this computation at the bottom layer. The displacement of concrete pavement evolves suddenly in the event of the fully wet slab and stagnant water at the top layer 5cm. The dramatic increase in the principal strain can be applied to explain in these cases. Due to the higher reinforcement ratio (0.3%), the damage of the fully dry slab at the final stage is not severe compared to RR 0.1% as shown in Fig.

7-11. The displacement of the dry slab is also therefore smaller. Figure 7-11 shows the diminutive support from the increase of reinforcement ratio 0.3% in stagnant water at top layer 10cm only. We can say that the upgrade of reinforcement ratio from 0.1% to 0.3% is worthless under the stagnant water at cracked concrete.

The failure mode and fatigue life of the concrete pavement with RR 0.4% show in Fig. 7-12. It can be seen that owing to the higher reinforcement, the total fatigue life of the case of dry slab considerably increases. The life cycle of the concrete pavement under the effects of stagnant water at top layer 5cm and 10cm is less different from the case of RR 0.3%. However, we can see the increase of this value in the case of the fully wet slab.

It is similar to RR 0.1% and RR 0.3%, the damage of the concrete slab under the water effects becomes serious and is only distributed at the top surface of the slab under the moving load. It can be seen from the fully stagnant water in the slab, the displacement is rapidly increased at the nearly final stage but not suddenly as the slab of RR 0.3%. Comparing to the same cycle of the dry slab with RR 0.3%, the displacement of the slab of RR 0.4% shows the lower value. The deterioration of the concrete slab is therefore less critical. The effects of reinforcement ratio 0.4% in the concrete slab is shown in the case of the fully wet and dry slab only. The other critical positions of water impacts (top layer 5cm and 10cm) can not be supported if the reinforcement ratio is increased from 0.3% to 0.4%.



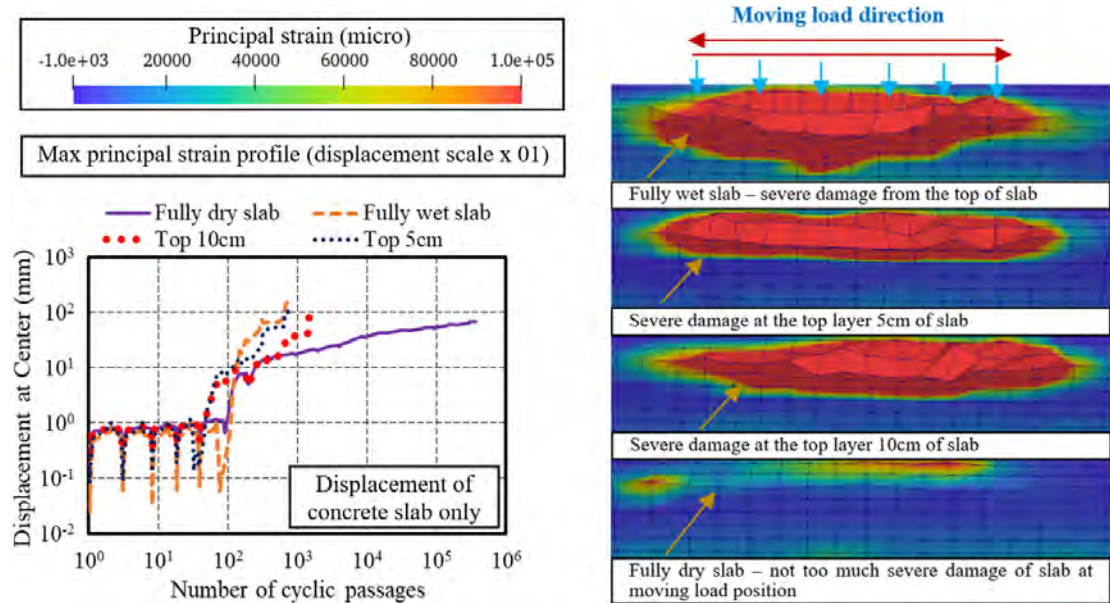
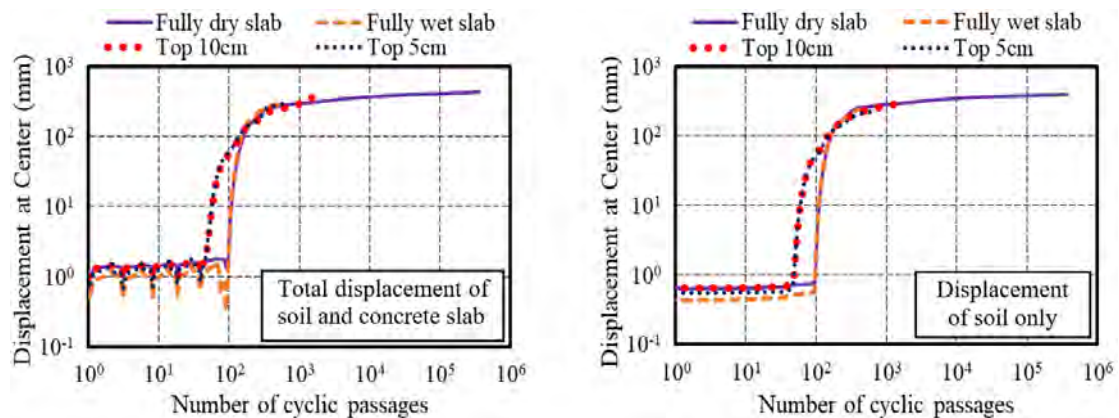


Fig. 7-12 Fatigue life and failure mode of concrete pavement under water effects with RR 0.4%.

The medium reinforcement ratio 0.5% and 0.6% are investigated as shown in Fig. 7-13 and Fig. 7-14. Under the stagnant water effects, the fatigue life of the concrete pavement is rather similar to the slab of RR 0.4%. The devastation of concrete slabs is distributed at the top layer slab (5cm or 10cm) depending on the positions of stagnant water as the other cases of reinforcement ratio.



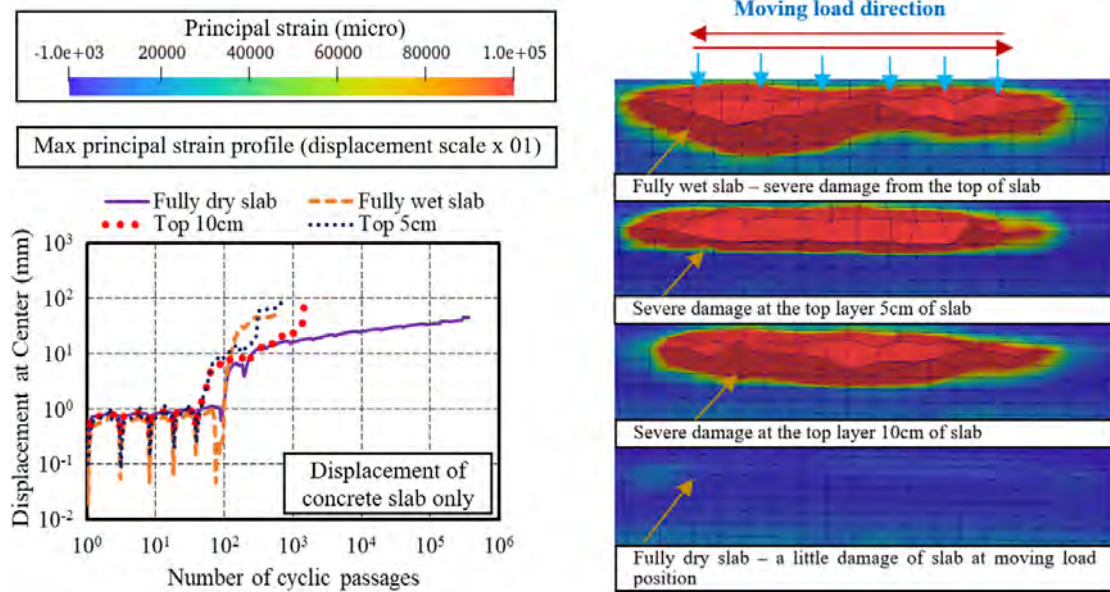


Fig. 7-13 Fatigue life and failure mode of concrete pavement under water effects with RR 0.5%.

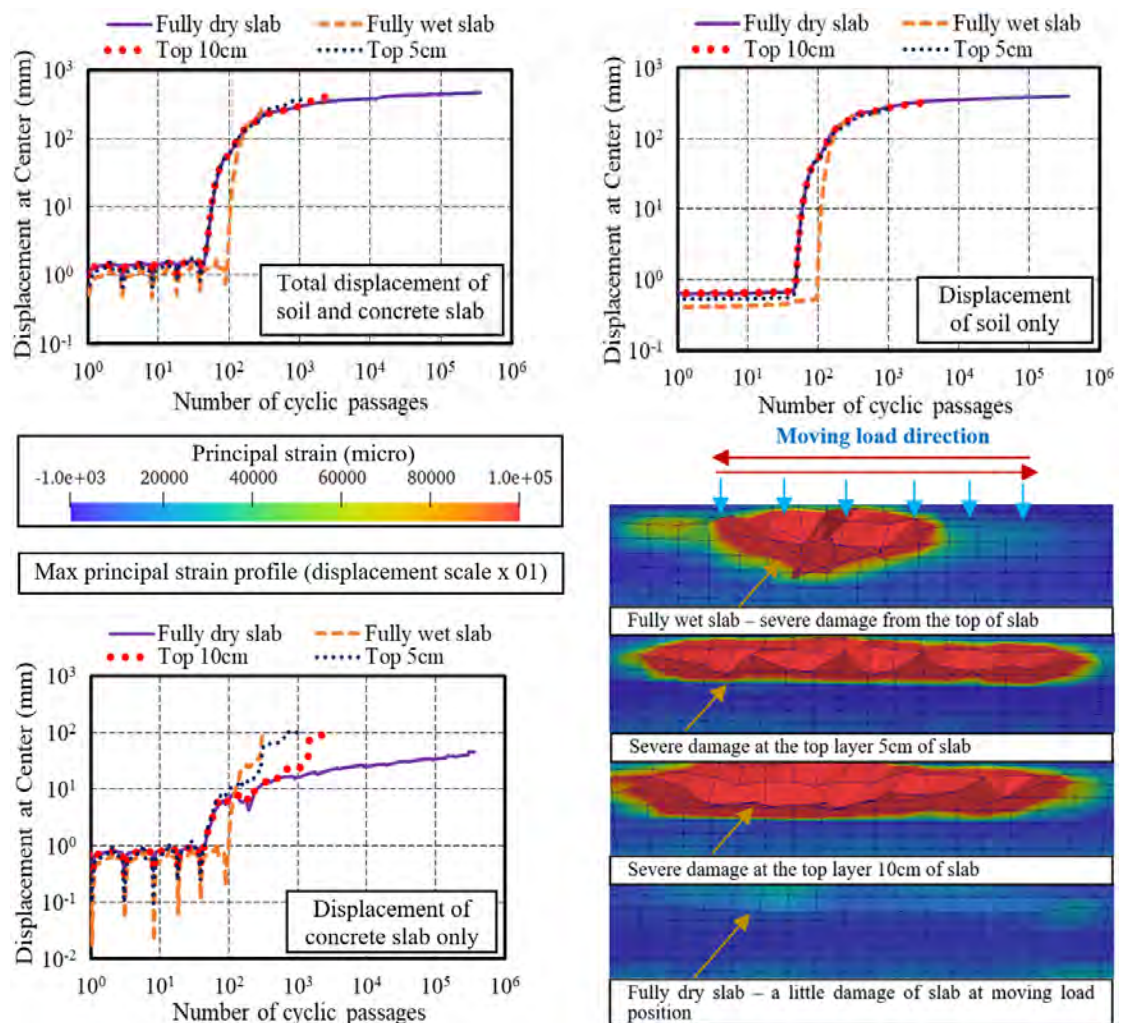
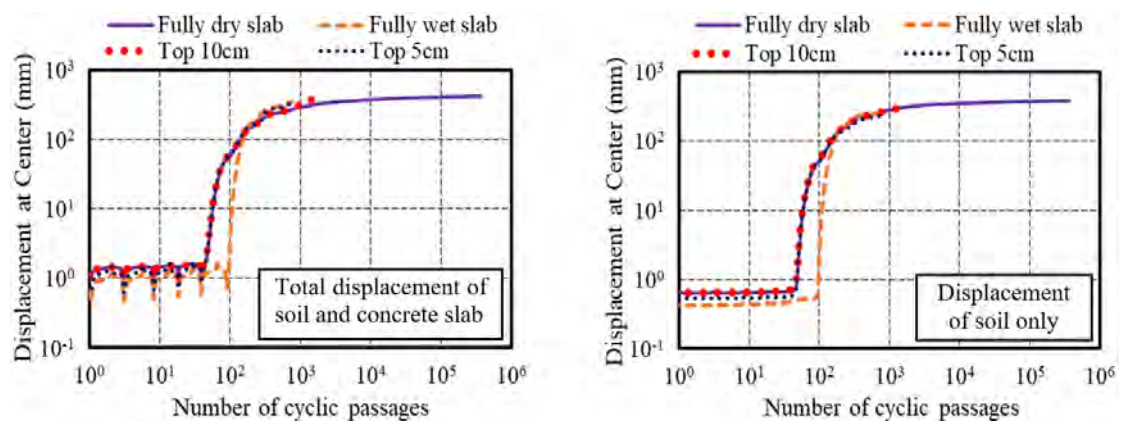


Fig. 7-14 Fatigue life and failure mode of concrete pavement under water effects with RR 0.6%.

In the event of fully wet slab, the damage of the concrete slab is also focused on the top surface only. There is no deterioration at the bottom side of the slab observed in this simulation. It can be said that the medium reinforcement ratio 0.5% and 0.6% can not support to the fatigue life of the concrete pavement subjected to the stagnant water inside cracked concrete.

The heavy reinforcement ratios 0.8% and 1.0% are also investigated as shown in Fig. 7-15 and Fig. 7-16, respectively. It can be said that the displacement of the concrete slab in the case of the stagnant water at the top layer 5cm and fully saturated slab rapidly increases compared to the stagnant water at the top layer 10cm. Irrespective of the heavy reinforcement ratio, water at the top layer 5cm and whole slab is shown as the critical cases. In the event of water effects at the top layer 10cm, the increase of the displacement has coincided with the fully dry slab at the first thousand cycles. However, the displacement suddenly rises at the final stage. The fatigue life is therefore dramatically reduced. The support of the heavy reinforcement clearly shows in the fully dry slab due to the very little damage of the concrete slab observed in the numerical simulation. Under the water effects, the failure fatigue is similar to the lower reinforcement ratio as discussed above. It can say that the heavy reinforcement ratio has also a minor influence on the fatigue life if water exists in the concrete slabs. It is due to that the pore pressure and principal strain in the cracked concrete are significantly increased at any scale of reinforcement ratios under stagnant water. The damage of the concrete slab is therefore accelerated simultaneously. It can be seen through Fig. 7-10 (reinforcement ratio = 0.1%) and Fig. 7-16 (reinforcement ratio = 1.0%), the maximum principal strain profiles show a similar failure mode at the final stage of fatigue life. The damage of the concrete slab is thus severe in both cases.



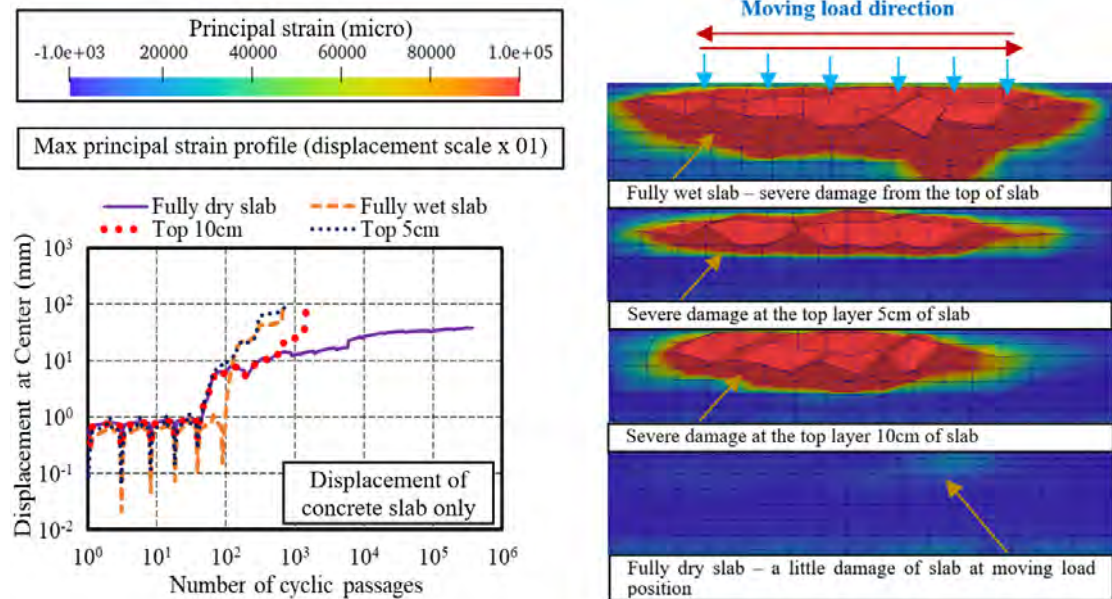


Fig. 7-15 Fatigue life and failure mode of concrete pavement under water effects with RR 0.8%.

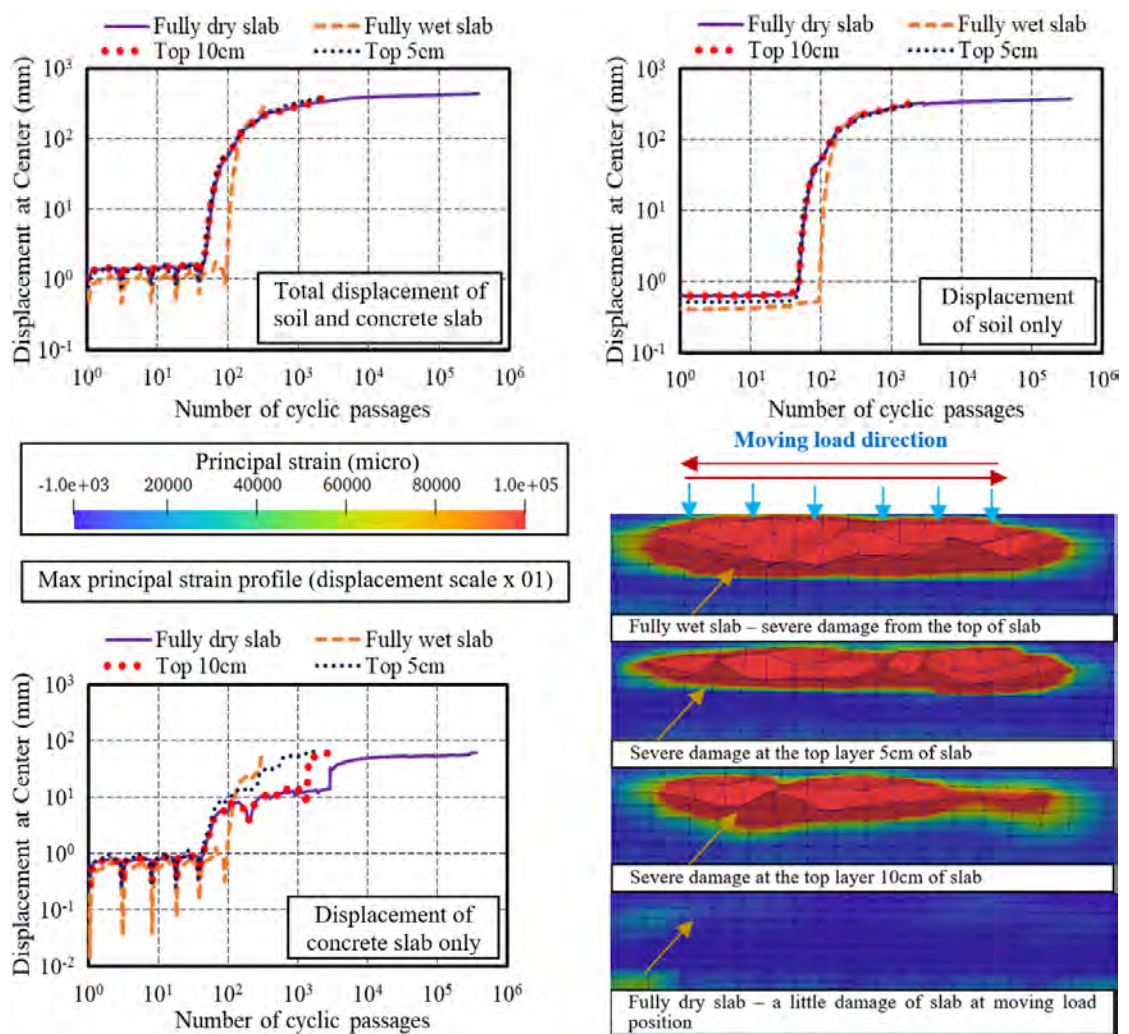


Fig. 7-16 Fatigue life and failure mode of concrete pavement under water effects with RR 1.0%.

7.3.3 Effects of Soil's Density

As mentioned previously, the fatigue life of the concrete pavement is strongly governed by the stagnant water at the top surface of the slab. In case the whole slab is affected by stagnant water, the damage is mostly severe. Consequently, the displacement of the concrete pavement is quickly increased. To investigate the sensitivity of reinforcement to the fatigue life, a mass of reinforcement ratio of concrete slabs is examined from 0.1% to 1.0% under water impacts. The total fatigue life of the concrete pavement is nearly similar at any scales of reinforcement. It can be seen that the effect of reinforcement ratio is inconsiderable and it can be negligible when the stagnant water exists in cracked concrete under moving loads.

The second variable is considered in the simulation of water effects, i.e. the support of soil's density. The lightest reinforcement ratio 0.1% and the heaviest one 1.0% are numerically simulated with the dense soil foundation of RD 75% as shown in Fig. 7-17 and Fig. 7-18, respectively. It can be seen that the dense foundation has a great contribution to increase the fatigue life in the case of top layer 10cm affected by water. As previously stated, the stagnant water at the top layer 5cm and the whole slab is defined as the critical positions for the concrete pavement. It is identical to the case of RD 75%. Irrespective of the dense soil foundation or reinforcement ratio, the fatigue life in these two cases is nearly coincidental to the RD 50%.

The total fatigue life of the concrete slab of RR 1.0% in stagnant water at the top layer 5cm and 10cm with soil's density 50% is nearly resembling. However, it can be seen a huge gap in the fatigue life of stagnant water at top layer 5cm and 10cm with supporting soil RD 75%. The displacements of the fully wet slab and water at the top layer 5cm slab are rapidly increased at the nearly final cycle, and it is virtually equal to the displacement of the concrete slab with water at the top layer 10cm at the very further cycle. The development of the displacement of the concrete slab with stagnant water at top layer 10cm is accompanied with the displacement of the dry slab. Under the light reinforcement ratio 0.1%, the damage of the wet-top layer 10cm slab is earlier than the slab of RR 1.0%. The pore pressure is also assumed to increase more suddenly and faster than the slab of RR 1.0%.

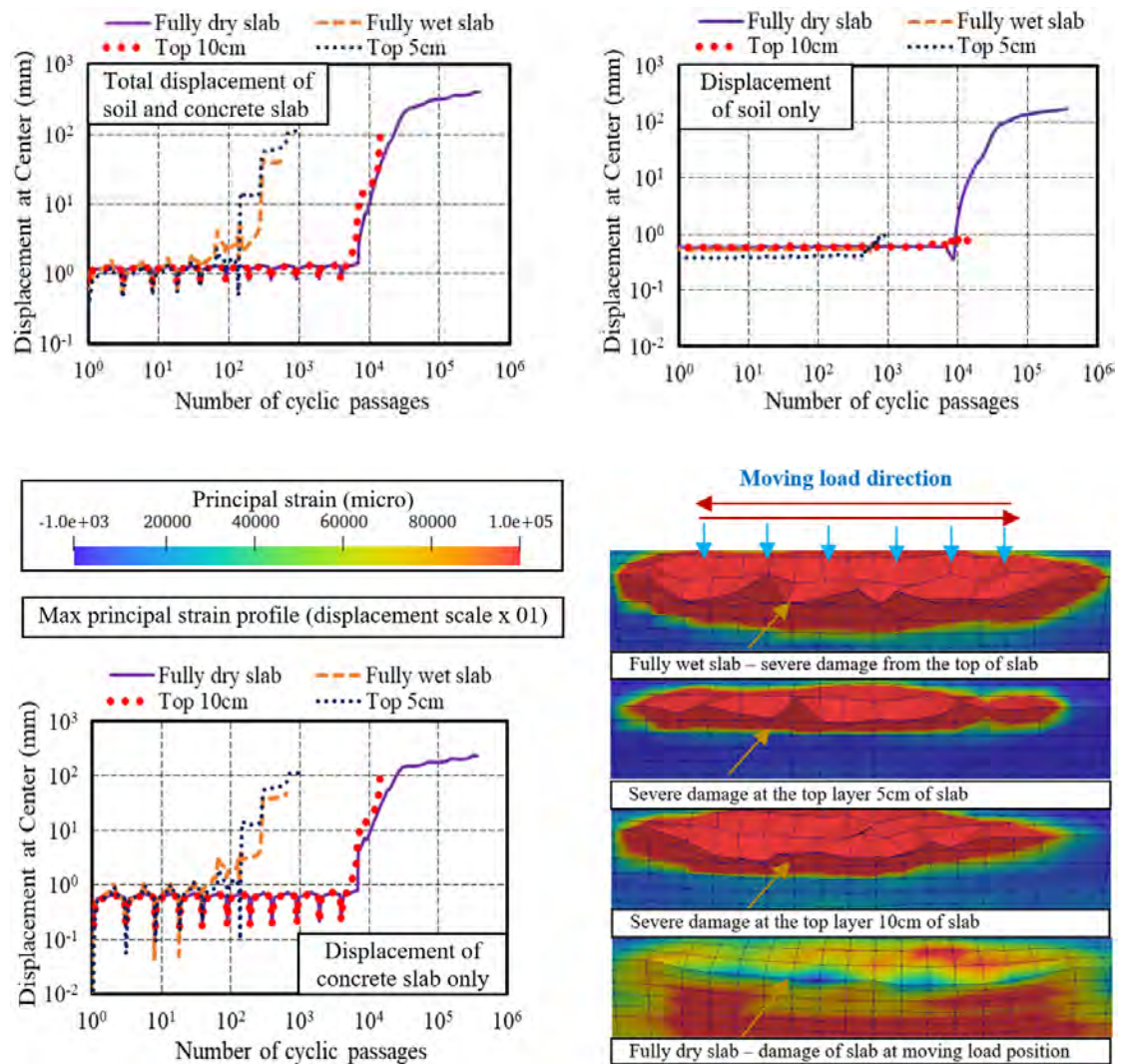
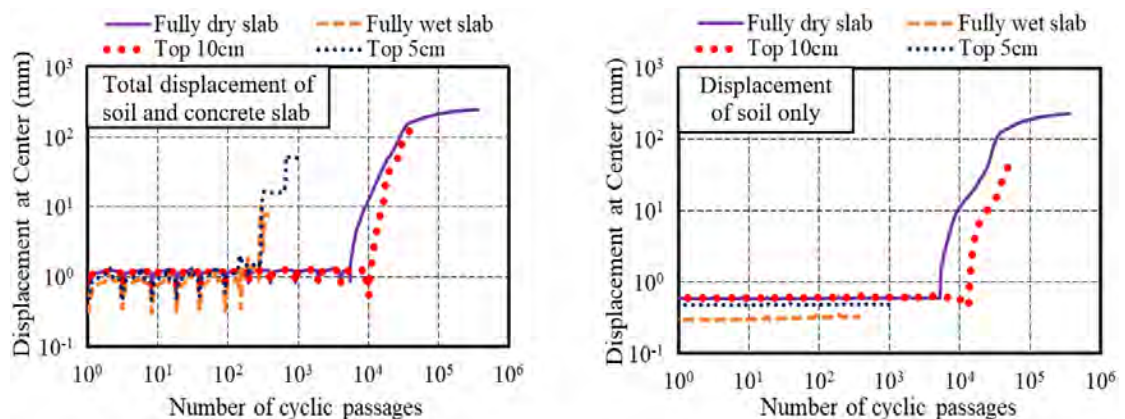


Fig. 7-17 Fatigue life and failure mode of concrete pavement under water effects with RR 0.1% and RD 75%.



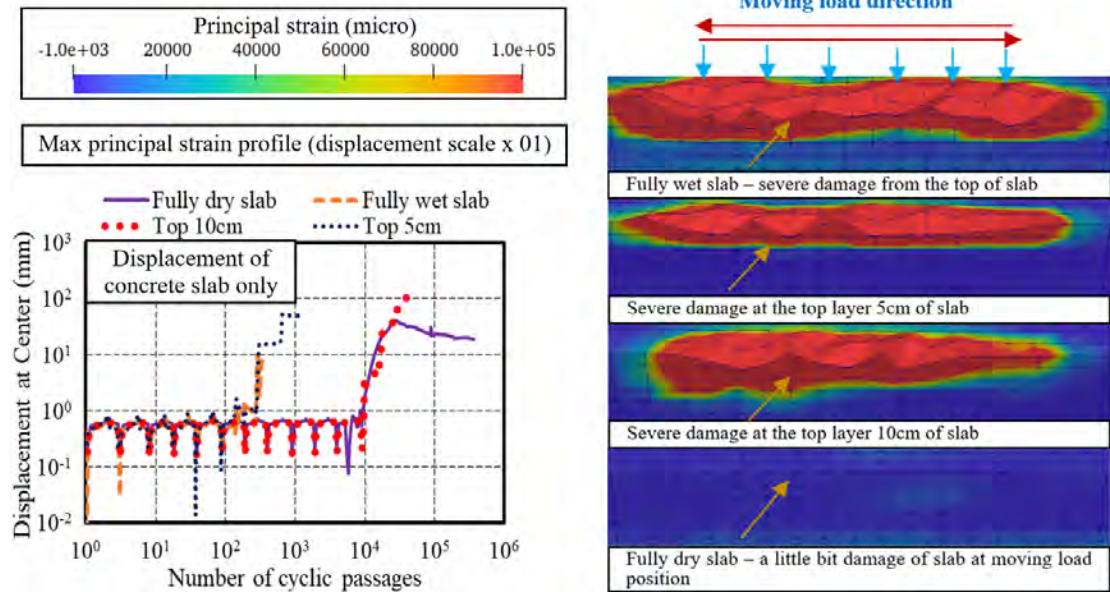


Fig. 7-18 Fatigue life and failure mode of concrete pavement under water effects with RR 1.0% and RD 75%.

Comparing to the case of the wet-top layer 10 cm slab with RD 50%, the more critical deterioration of the concrete slab in the case of RD 75% can be seen. However, the very longer fatigue occurs in RD 75%. It is explained due to the small shear failure of the soil foundation. The damage of the concrete slab depends on the position of water effects only. Meanwhile, soil's density 50% shows the coupling damage of the concrete slab and underneath soil. Therefore, the damage can be seen in both of the concrete slab and the soil foundation. It can be seen that the fatigue life of RR 1.0% under the water effects at the top layer 10cm of the slab is expanded in comparison with RR 0.1% of soil's relative density 75%.

The positions of the critical effects of water are obviously at the whole wet and the top layer 5cm slab under stagnant water. If the stagnant water exists at these positions, the support of reinforcement ratio or dense soil is imperceptible. There is less different from the failure mode of the concrete slab at the final cycle in the case of RD 50% and 75%. The serious deterioration of the concrete slab is focused on the top surface of the slab only (under the fully wet slab) and at the position of water effects (top layer 5cm or 10cm). There is no occurrence of the damage of the concrete slab at the bottom side of the slab even if the fully saturated slab is considered. It can say that the effects of water at the bottom surface is not critical and it may be negligible in the study of the concrete pavement.

As discussed in Fig. 5-6 and Fig. 5-7, the loose soil foundation is recommended to reduce the slab thickness in case of the dry slab compared to the PCA or ACI 325. In the event of the wet condition, the water drainage or waterproof should be considered to increase the service life of the concrete pavement under the loose foundation. Similar to the loose soil, the dense one has been also proposed the new balanced thickness of the slab in Fig. 5-6 and Fig. 5-7 (increase at least 20mm). In comparison of the fatigue life when water is stagnant, the dense soil shows better support in case of the stagnant water at the top layer of 10cm. Other cases (water at top layer 5cm or fully wet slab) depict a similar decrease of fatigue life compared to the loose soil. Once again, the water drainage or waterproof should be carefully maintained. Depending on the construction conditions of local regions and the requirements/standard for the limit state of the concrete pavement as discussed in section 4.3 (after over the limit state of FEM analysis, the road can be used or not depending on the requirements under unusual operation), the soil density of the pavement foundation can be determined based on real conditions.

7.3.4 Effects of Strength of Concrete

This section shows the effects of water-to-cement ratio in the pavement to investigate how the strength of concrete can support the fatigue life when the stagnant water is remaining in the slab.

The eighth specific cases of the effects of the concrete strength for the fatigue life of pavement in case of stagnant water in the concrete slabs are illustrated from Fig. 7-19 to Fig. 7-26, respectively. There are three types of concrete investigated in this study as the high strength (W/C 30%, 35%, 40%, 45%) [17], the normal one (W/C 50%, 55%, 60%) [17], and the weak one (W/C 65%).

Let us start from the highest strength concrete as depicted in Fig. 7-19. It can be seen that the fatigue life of the concrete pavement is strongly supported when the low water-to-cement ratio is used. As discussed above, when the water exists in the concrete slabs, the high pore pressure appears and causes the increase in internal stresses in micro-pores of concrete. The damage of concrete is therefore accelerated dramatically. It is observed in the previous works [18] that an increase in the gel pore volume fraction occurs gradually, and the ratio of finer porosity to coarser porosity

increases for the low water-to-cement ratio. It means that when the low water-to-cement ratio is applied, the large number of the finer micro-pores can exist in concrete structures compared to the high water-to-cement ratio.

In the study of the modeling of pore water inside cracks, the motion of pore water in concrete structures can be determined by the relative displacement from the concrete solid matrix and related to the displacement of the concrete skeleton and the pore water. The governing accumulation of the concrete damage is thus demonstrated in terms of the dragging forces rooted in the permeability of pore water through the concrete micropore and the crack gap [5]. When there are lots of the coarser pore size in concrete structures, this dragging accumulation is obviously increased. As a result, the deterioration of concrete structures has risen simultaneously.

The damage of concrete structures under the effect of stagnant water may be accelerated by the internal stress caused by high pore pressure. The total stress of the concrete-liquid system can be assumed as the summation of the skeleton stress and the isotropic pore water pressure as shown in equation (2). This assumption can be applied to the stagnant water inside capillary pores of concrete before cracking. In case of cracked concrete, the pore water pressure will act as anisotropy in the concrete pore (capillary and crack gaps). It can say that the acceleration of internal stresses of cracked concrete is increased proportionally to the number of capillary pores in concrete structures. The rise of the accelerated internal stress in the low water-to-cement ratio is therefore less critical compared to the high ones.

The study of the effects of water in the cracks of concrete is investigated based on thermo-hydro-physical properties (nanometer to micrometer), element level (millimeter) and structural level (meter). This is expected to discuss the kinetics of both visible and invisible cracks in concrete due to their relation in cracking propagation. At the beginning of erosion, cracks in concrete slabs are hard to be observed by naked eyes. But these ones may continuously propagate and affect to the concrete cover. However, the visible cracks are mainly examined in this study.

Figure 7-19 shows the fatigue life and failure mode of the concrete pavement with W/C 30%. It can be seen that the fatigue life of the concrete slab is little decreased when the stagnant water exists at the top layer 5cm, 10cm or the fully wet slab

compared to the dry slab. It is pointed out that the displacement of the concrete slab in the case of the fully wet slab is suddenly increased at the nearly final stage. The damage of the slab is therefore more critical than other cases. As previously stated, under water effects, the fatigue life of the concrete pavement is dramatically reduced due to the acceleration of the internal stress caused by the high pore water pressure. Even the high strength concrete is applied, this assumption rationally remains. However, there is less different in both fatigue life and failure mode with/without water effects as shown in Fig. 7-19. Due to the soft soil foundation used in this FEM analysis, the fatigue failure is strongly governed by the shear band of soil. We can say that water-to-cement ratio may significantly support the fatigue life of the pavement when the stagnant water exists in cracked concrete.

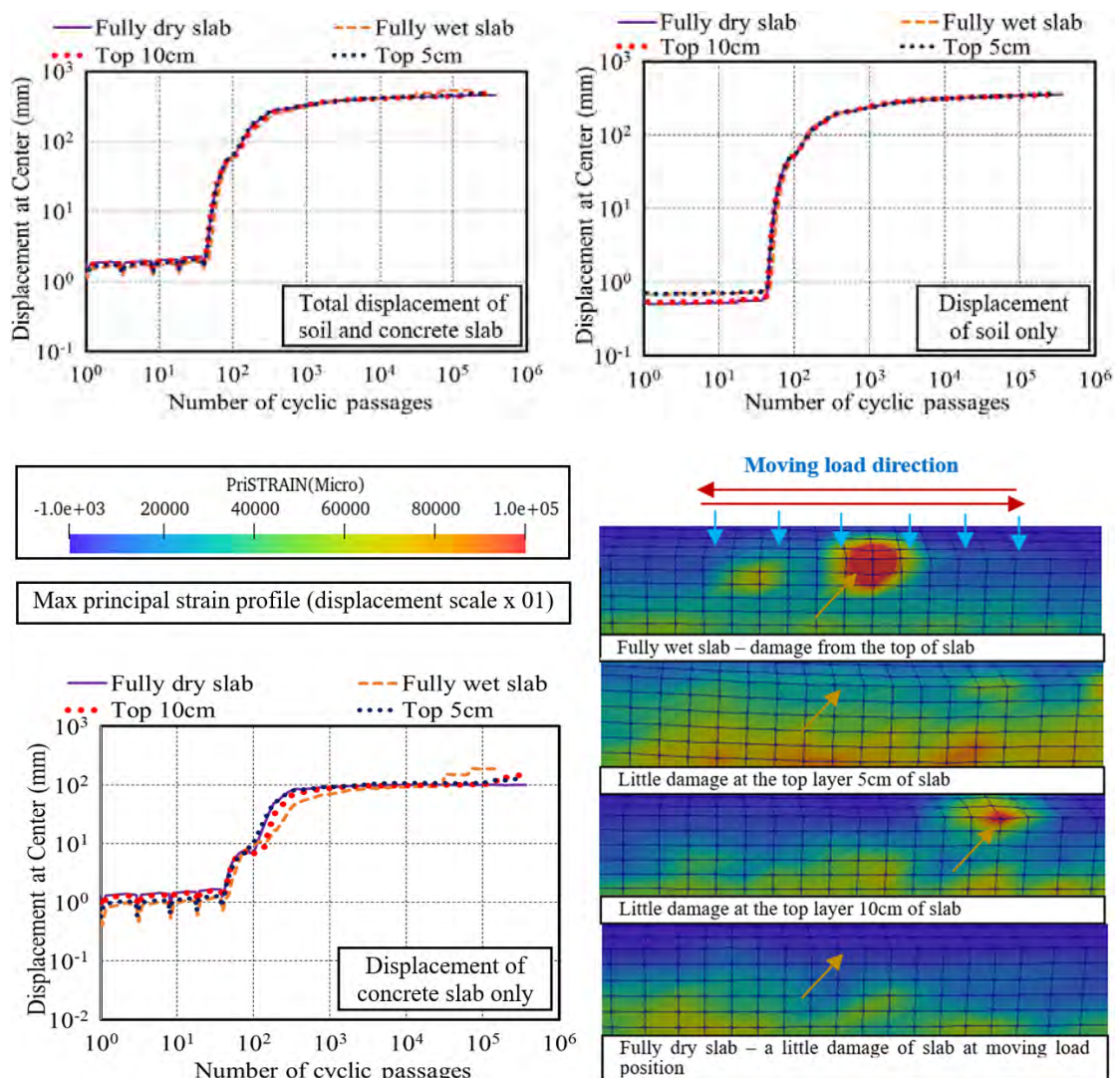


Fig. 7-19 Fatigue life and failure mode of concrete pavement under water effects with W/C 30%.

It is similar to the case of W/C 30%, the fatigue life of the concrete pavement with W/C 35% as shown in Fig. 7-20 is sharply supported irrespective of stagnant water in cracks and this value is shortened than the case of WC 30%. It is due to the gradual increase of the capillary pore in concrete structures as discussed above. The damage of the concrete slab is therefore more critical. However, the displacement of the slab is still less severe than the soil foundation. The fatigue failure is thought to be concentrated on the failure of soil.

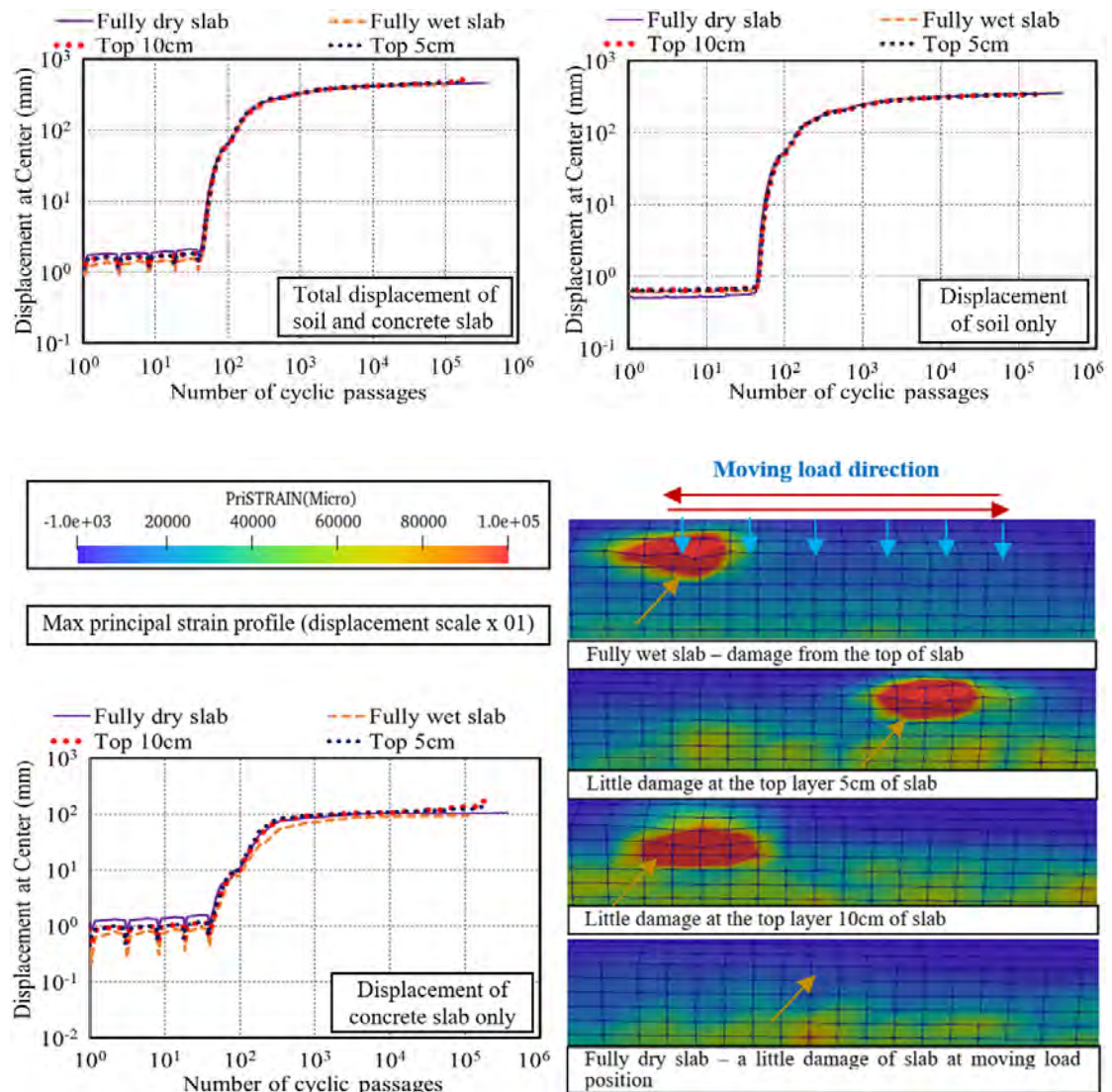


Fig. 7-20 Fatigue life and failure mode of concrete pavement under water effects with W/C 35%.

Figure 7-21 demonstrates the fatigue life and failure mode of the concrete pavement with W/C 40%. It can be seen that the fatigue failure in the slab is more critical than the case of W/C 35%. The fatigue life is therefore reduced. The fatigue

failure in the case of W/C 40% may be strongly governed by the shear band of soil due to the severe displacement of soil as shown in Fig. 7-21. In the comparison of W/C 30%, 35%, 40%, the damage of the concrete slab under the water effects is gradually increased. The fatigue life is thus decreased proportionally to the increase of water-to-cement ratio. The most critical case focuses on the deterioration of the fully wet slab, top layer 5cm, top layer 10cm, respectively. This trend is similar to other cases as discussed in the previous chapter. The deterioration is distributed along with the moving load and focused on the top surface of the slab. There is no damage at the bottom slab even if the fully wet slab is applied.

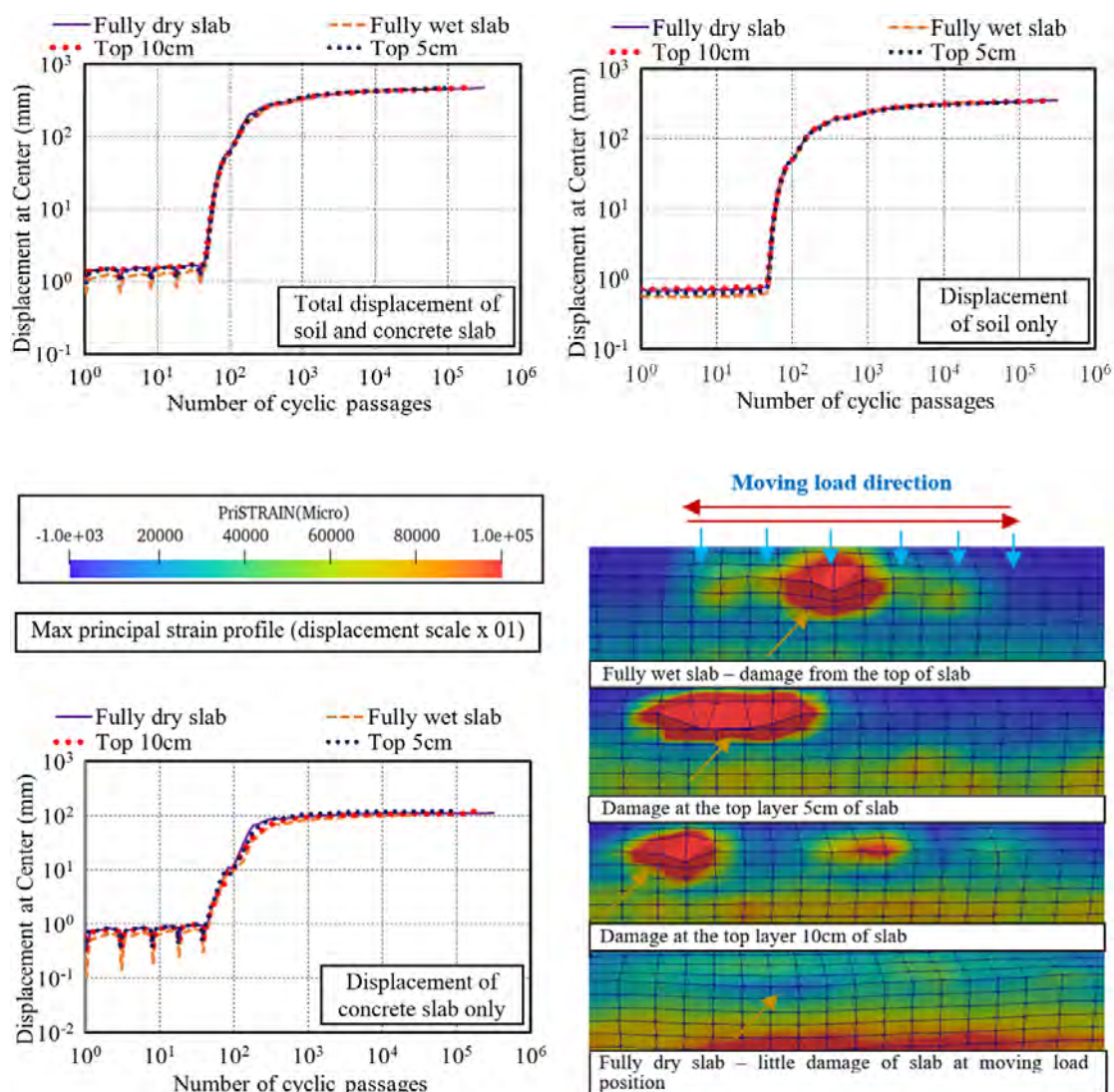


Fig. 7-21 Fatigue life and failure mode of concrete pavement under water effects with W/C 40%.

Figure 7-22 depicts the fatigue life and failure mode of the pavement with W/C 45%. The fatigue life is dramatically decreased compared to the three cases above. The damage of the concrete slab becomes more severe and is distributed along the moving load direction. It can be seen that the displacement of the concrete slab is suddenly increased at the final stage. The reduction of the fatigue life under water effects can be explained as the increase of the internal stress caused by the high pore water pressure. Comparing to the lower water-to-cement ratio, the capillary pore in the case of W/C 45% is excessive, the dragging force for the damage of the slab is therefore faster than other cases as discussed above. The fully wet slab is still the most critical case when water exists in the slab. The behavior of top layer 5cm or 10cm shows the same trend to previous works.

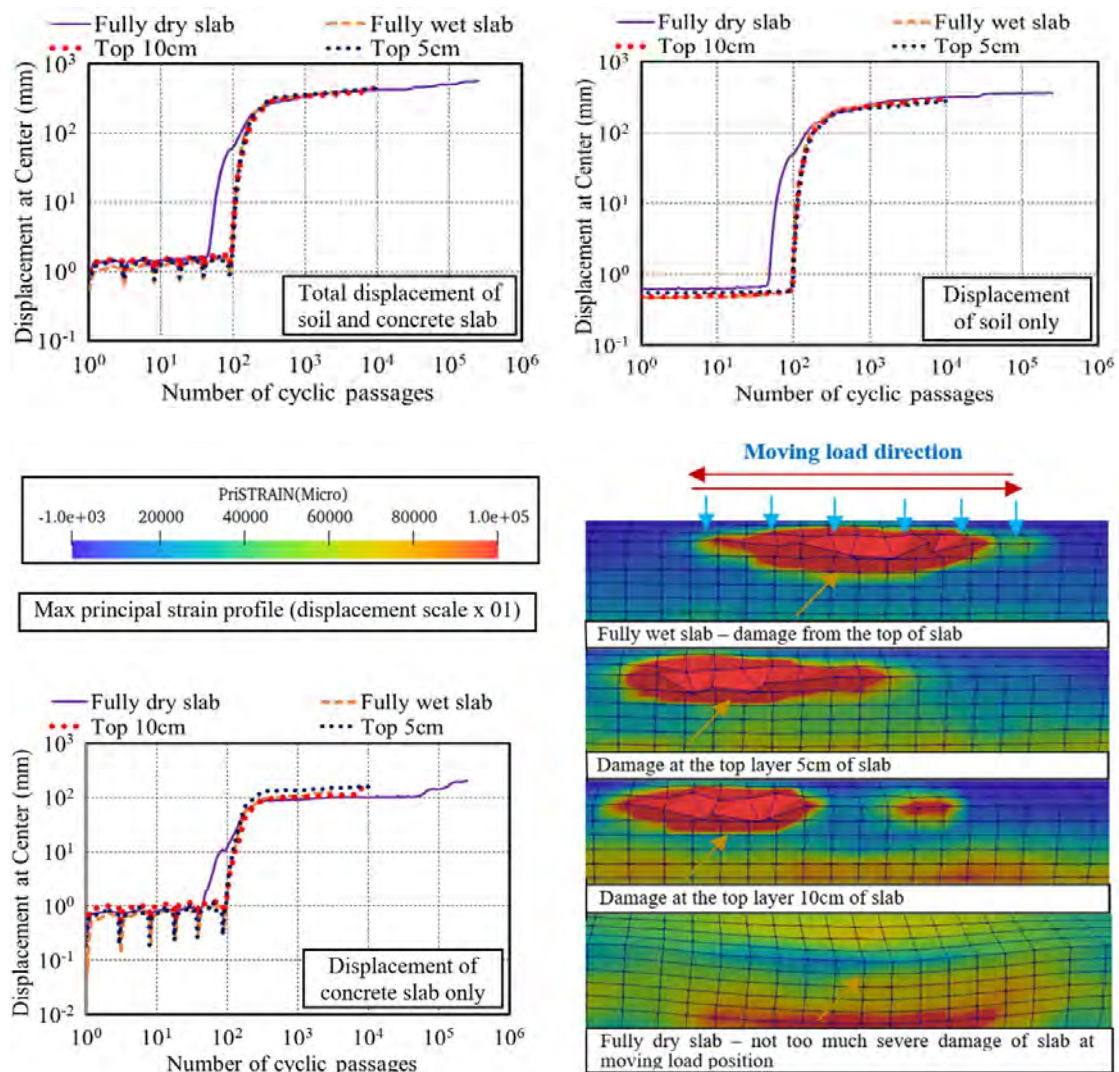


Fig. 7-22 Fatigue life and failure mode of concrete pavement under water effects with W/C 45%.

Figures 7-23, 7-24, and 7-25 demonstrate the fatigue life and failure mode of the concrete pavement with W/C 50%, 55%, and 60% as the normal one in practice, respectively. It can be seen that the fatigue life is significantly reduced, especially in the case of W/C 55% and 60%. The damage of the concrete slab is more severe than the case of high strength concrete. The normal concrete shows the insufficiency to support the fatigue life of the concrete pavement under water effects.

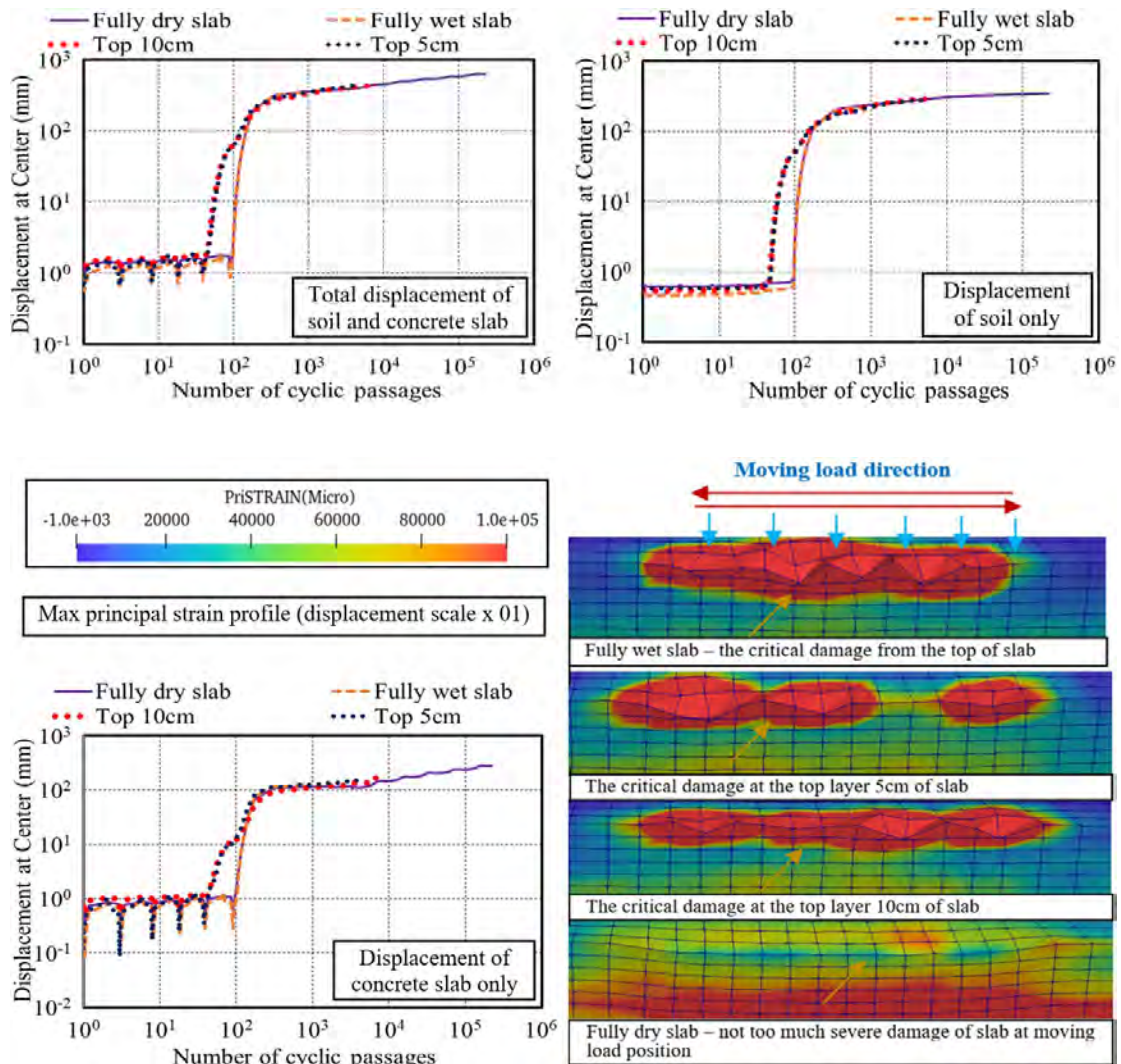


Fig. 7-23 Fatigue life and failure mode of concrete pavement under water effects with W/C 50%.

As can be seen in Fig 7-23, owing to the weaker concrete used in FEM analysis, the displacement of the concrete slab in the dry slab is sharply increased compared to the case of W/C 45%. The damage of the slab is therefore more critical. The displacement of the slab under the water effects is nearly similar to the case of

W/C 45%. However, this value can be obtained at the earlier stage and the damage is thus more severe and distributed along the moving load direction.

In case of W/C 55%, the damage becomes more critical with or without water effects. The fatigue life of the concrete pavement in the event of top layer 5cm affected by water or the fully saturated slab is less different. The displacements of the concrete slab in these two cases are approximately equal to the displacement of the dry slab at the very early cycle. When the stagnant water exists at the top layer 10cm of the slab, the fatigue life is prolonged. The displacement of the concrete slab is therefore less than other cases. The assumption for the severe position of stagnant water in the concrete slab may be thus applied in normal concrete as discussed above.

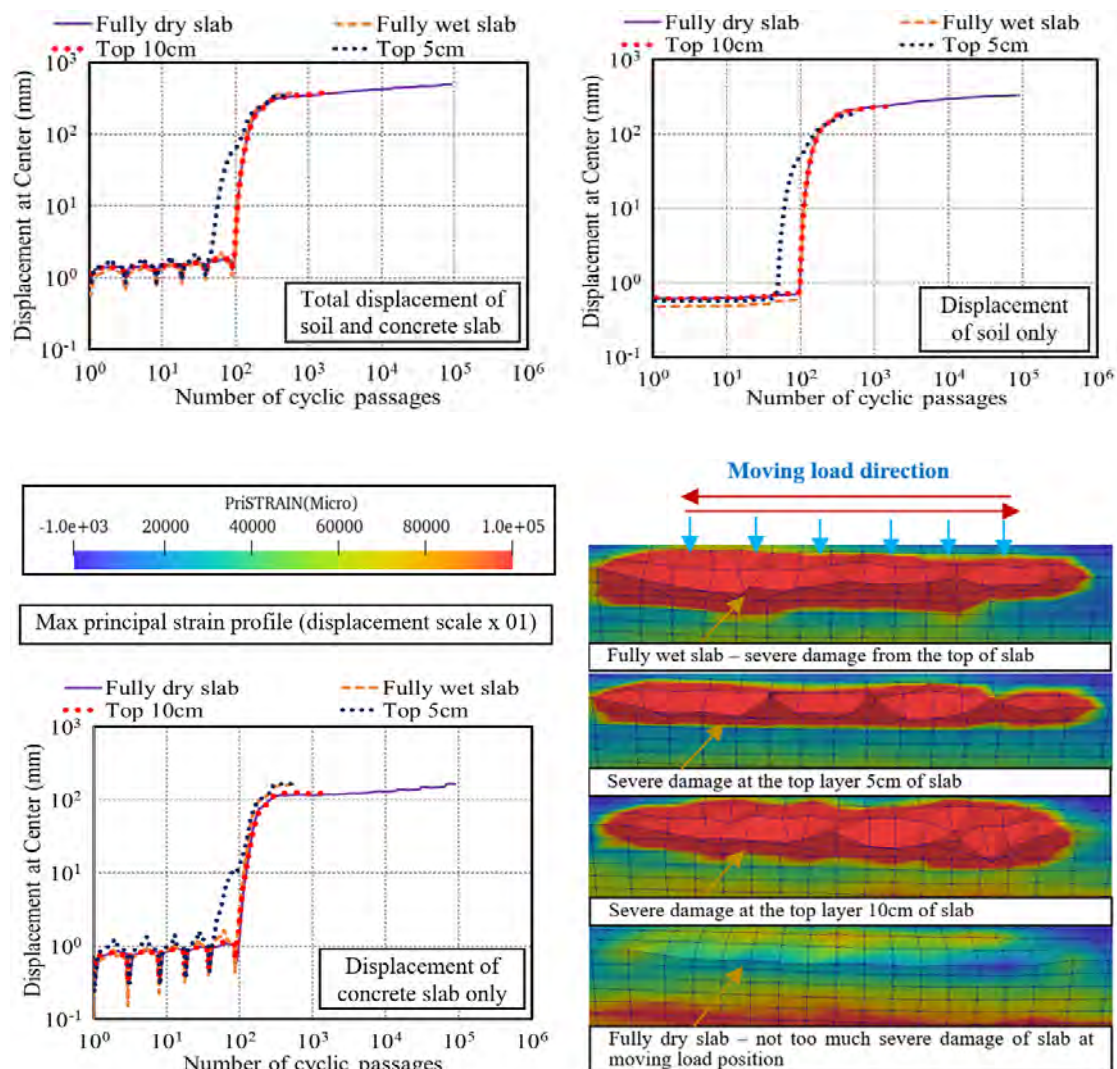


Fig. 7-24 Fatigue life and failure mode of concrete pavement under water effects with W/C 55%.

In consideration of W/C 60%, we can easily see the significant reduction of fatigue life compared to W/C 55%. It is less different in the fatigue life and failure mode in three cases of water effects. The damage of the concrete slab in the dry case is also more critical. Comparing to the displacement of soil, the displacement of the concrete slab depicts the higher development, especially in the case of the stagnant water at the top layer 5cm or the fully wet slab. It can say that the fatigue failure of the concrete pavement with W/C 60% under the water effects is strongly governed by the damage of the concrete slab irrespective of the soft foundation applied in FEM analysis. This assumption may be again explained by a large number of capillary pores in concrete structures when the high W/C ratio is used. The slab's damage is therefore accelerated.

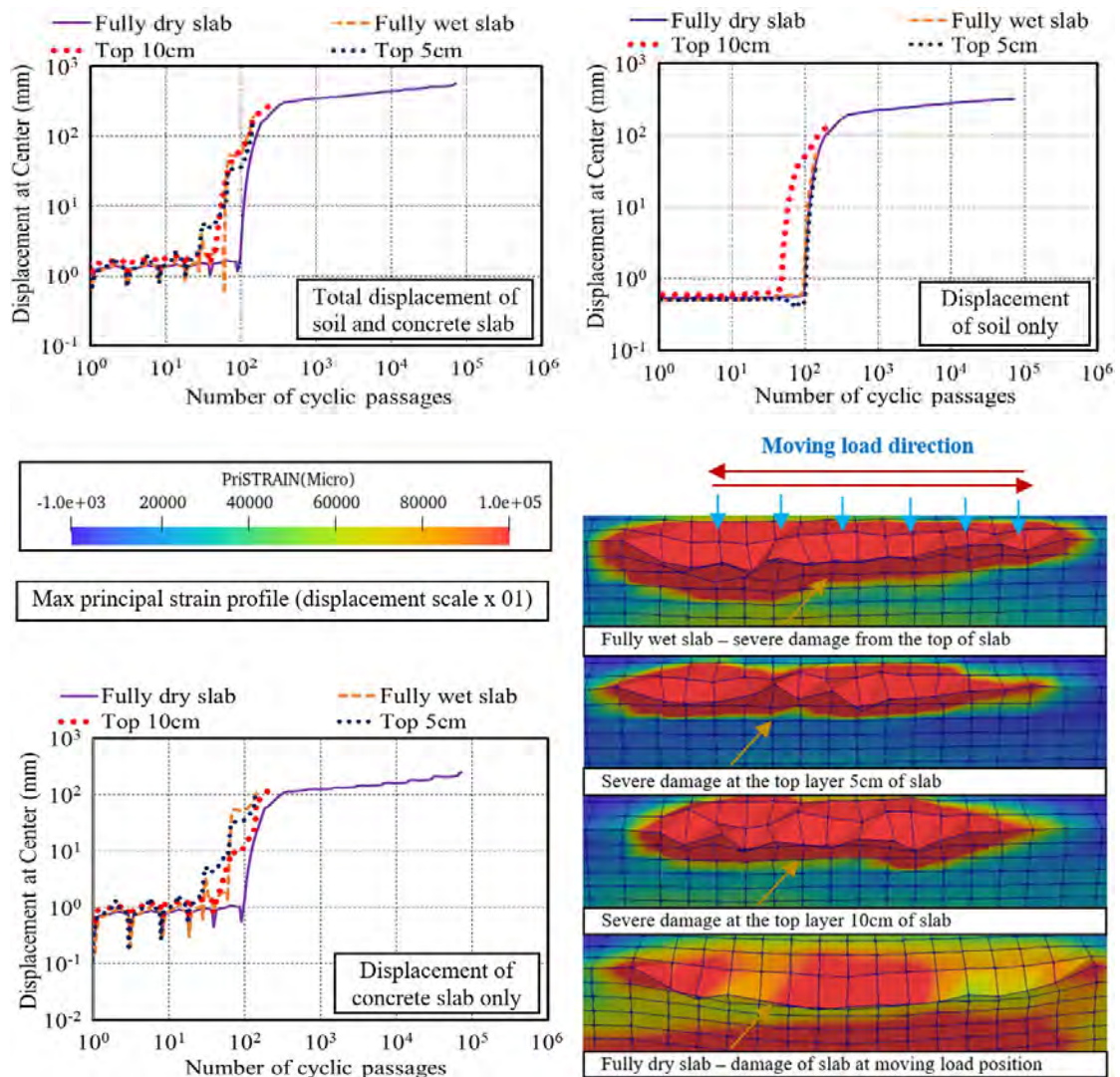


Fig. 7-25 Fatigue life and failure mode of concrete pavement under water effects with W/C 60%.

It is similar to the case of W/C 60%, when the very weak concrete is applied (W/C 65%) as shown in Fig. 7-26, the damage of the concrete slab is severe. The fatigue life is dramatically decreased. The stagnant water at top layer 10cm shows less impact compared to other cases. However, there is not too much different in these cases. The displacement of the concrete slab is clearly higher than the soil's one. The fatigue failure is thus governed by the damage of the slab. The fatigue life of the dry slab is also decreased. We can say that when the very weak concrete is applied, the fatigue damage is absolutely governed by the deterioration of the slab in all cases. In case of existing stagnant water in the concrete slab, this damage becomes more critical. The severe damage of the slab occurs after a hundred of cycles when the moving load is applied.

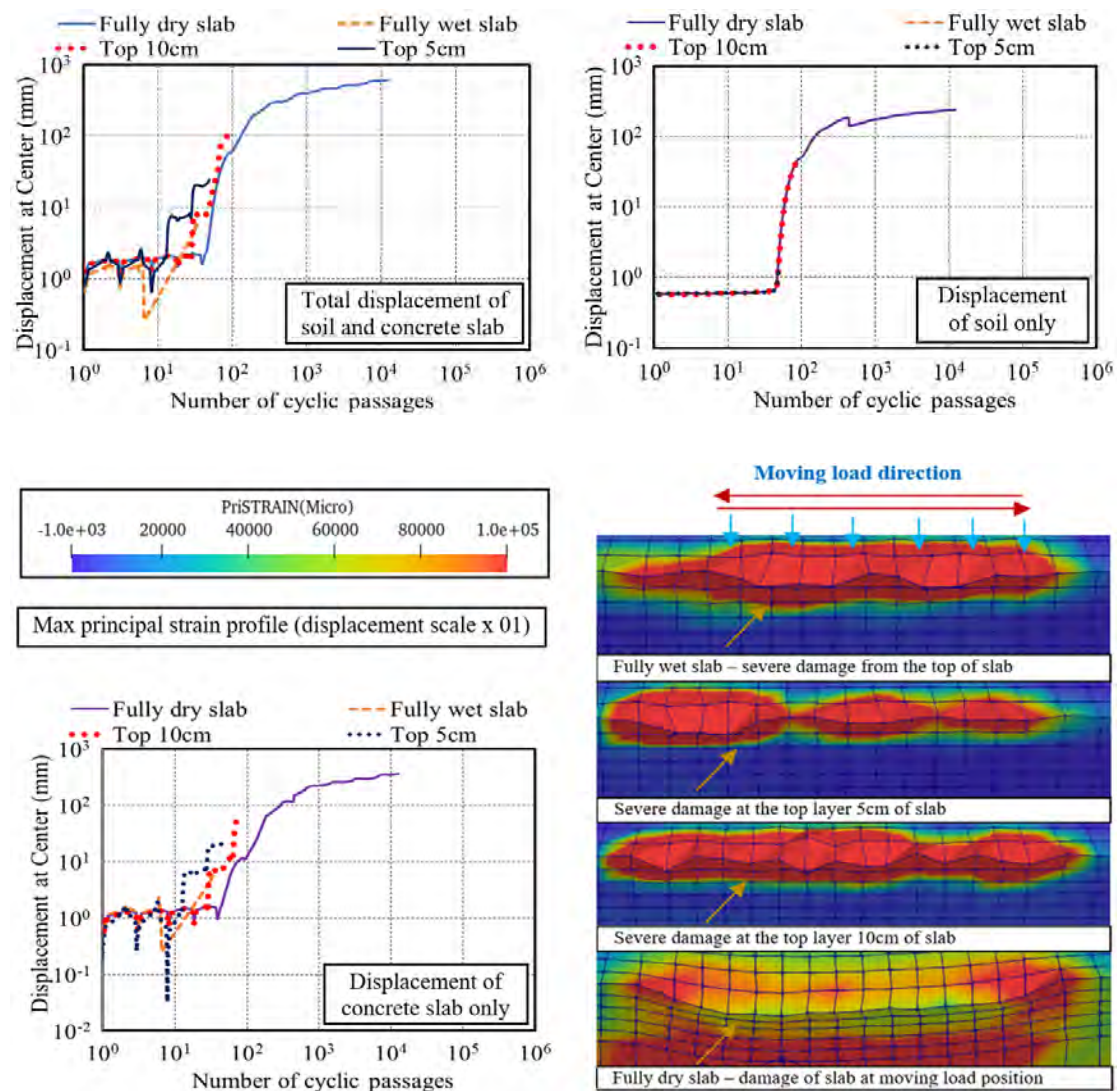


Fig. 7-26 Fatigue life and failure mode of concrete pavement under water effects with W/C 65%.

Figure 7-27 summarizes the effects of stagnant water to the fatigue life of concrete pavements which have been considered in the diverse water-to-cement ratios. It can be clearly seen that there are less influence of stagnant water to the fatigue life of concrete pavement under the high strength of concrete, especially in the case of W/C 30% or 35%. When the normal concrete is used as W/C 50%, 55%, 60%, the reduction of the fatigue life is clearly observed. The most critical case is weak concrete (W/C 65%). The reduction of the fatigue life under water effects is faster than two or three times compared to the decrease of the dry slab at the same water-to-cement ratio of the normal or weak concrete. We can say that when stagnant water exists in the concrete slab, it can become a key factor to accelerate the damage at the top surface of the slab. It is recommended to utilize the high strength concrete in pavement construction to minimize the effects of water when cracks occur under the moving load.

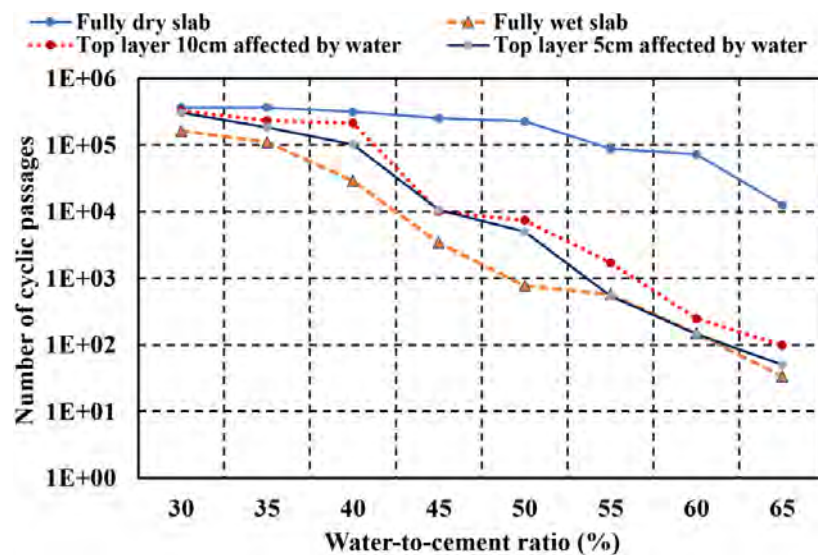


Fig. 7-27 Summary for the fatigue life of pavement under water effects.

7.4 Pore Pressure and Principal Strain of Crack inside Concrete Slab

To evaluate the effects of stagnant water, the pore water pressure and concrete principal strain at the top layer of 5cm, 10cm and fully saturated slab are investigated as shown in Fig. 7-28. It can be seen that when the concrete slab is fully wet, the pore water pressure suddenly increases faster than other cases of stagnant water impacts. As a result, the principal strain also rises at the earliest stage. The high water pore pressure causes the fast development of internal stresses in the concrete slab which accelerates the disintegration of structural concrete concurrently [4,5]. In case of the

stagnant water at the top layer of 5cm, the pore water pressure increases faster than the case of the wet top layer of 10cm. The principal strain and the concrete damage proceed at the earlier stage than the case of the wet top layer of 10cm. Water kinetics in cracked concrete is thought to be the main reason for the reduced fatigue life under water.

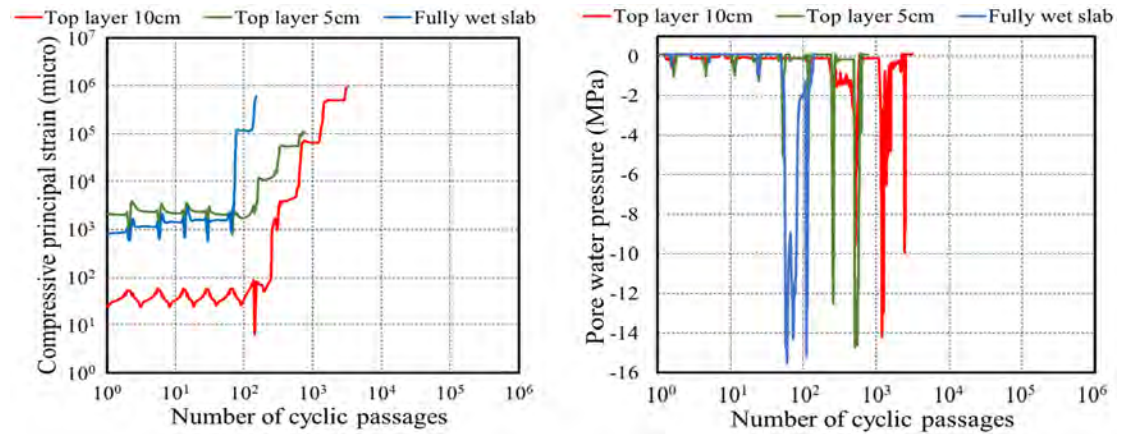


Fig. 7-28 Pore water pressure and principal strain of concrete slab at the top surface with RD 50% and RR 0.3%.

7.5 Computed Fatigue Life for the Fully Dry and Saturated Wet Slab

To investigate the effects of water on the fatigue life of concrete pavement, one representative case of the concrete slab with $pt=0.1\%$ and soil's density $RD=75\%$ is focused. Figure 7-29 offers the computed S-N diagram for the concrete pavement under the wheel-moving passages of fully dry and saturated concrete slabs. The computed fatigue life is dramatically reduced under submerged conditions as much as the case of RC decks on bridge girders [13]. In fact, the deterioration of concrete slabs under submerged conditions is faster than two or three orders compared to the dry conditions under lower magnitude of loads. But, for the greater amplitude, the decay of the fatigue life is comparatively less. It is due to the minor effect of the shear transfer [13]. The computationally derived S-N diagram matches the one of bridge slabs [3]. The open-closure of crack planes with sandwiched water may govern the disintegration of concrete rather than the accumulated damage of crack shear transfer.

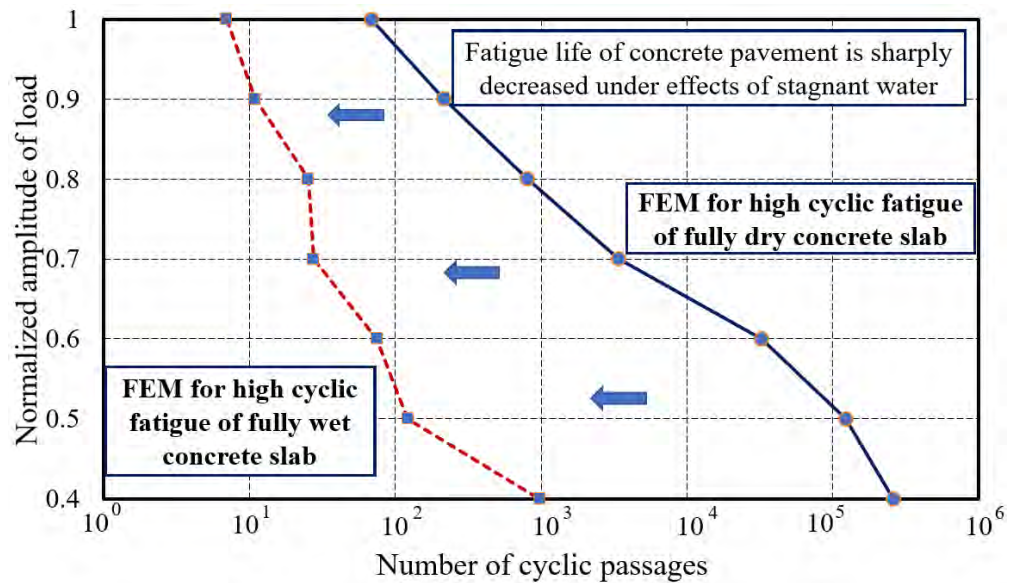


Fig. 7-29 Computed S-N diagram for concrete pavement with fully dry and wet slab under moving loads.

7.6 Conclusions for Chapter 7

The impact of stagnant water residing in cracked concrete are computationally estimated in views of the fatigue life of the concrete pavement on the nonlinear soil foundation. In reference to the experimental facts, nonlinear three-dimensional finite element analyses of plain and so-called reinforced concrete slabs were systematically conducted with nonlinear soil foundations, and the following conclusions are earned with different ambient states as;

1. The presence of the stagnant water in cracks of the concrete slab influenced the structural performance and caused the rapid decrease of the fatigue life.
2. The pore pressure aggravated by the crack kinetics evolves in micro-pores in concrete. Computationally, the history of the pore pressure and principal strain signifies that the damage of concrete slab is accelerated by the high pore pressure in crack gaps.
3. The existence of water can produce the high pore pressures in concrete and its effect may reach the concrete near the surface in bending compression. Hence, the damage caused by the pore pressures does not approach the bottom surface of the concrete slab irrespective of the fully saturated slab applied in numerical modeling.

4. Reinforcement ratio is computationally simulated to have an inconsiderable impact on the support for the fatigue life of concrete pavement if the stagnant water exists.
5. Compared to other cases, the pore water pressure gradually rises at the top surface slab of 10cm. Therefore, the dense foundation solely has a great effect on the increase of the fatigue life for concrete pavement if the stagnant water stays at this position.
6. The increase of the finer micropores and the reduction of the coarser ones can become a key factor to support the fatigue life of concrete pavement when stagnant water exists in the visible/invisible cracks of concrete. It is thus recommended to utilize the high strength concrete in the pavement construction.

The failure mode and fatigue life of the concrete pavement in this study demonstrate the worst case of water effects in the concrete slab coupled the soil foundation (water always exists in cracks of the concrete slab). The concrete pavement should be carefully waterproofed and maintained to prevent the effects of the stagnant water.

References in Chapter 7:

- [1] H. J. Gilkey, “The effect of varied curing conditions upon the compressive strength of mortar and concrete,” in *Proceedings of ACI*, 1926, pp. 395–436.
- [2] H. Matsushita, H. and Onoue, “Moisture content dependency of the strength of cement based materials from the viewpoint of surface energy,” *Annu. Rep. Cem. Technol.*, vol. 35, pp. 130–133, 2006.
- [3] S. Matsui, “Fatigue strength of RC-slabs of highway bridge by wheel running machine and influence of water on fatigue,” *Proc. JCI*, no. 9(2), pp. 627–632, 1987.
- [4] K. Maekawa and C. Fujiyama, “Crack water interaction and fatigue life assessment of RC bridge decks,” *Poromechanics V ASCE 2013*, pp. 2280–2289, 2013.
- [5] K. Maekawa and C. Fujiyama, “Rate-dependent model of structural concrete incorporating kinematics of ambient water subjected to high-cycle loads,” *Eng. Comput. (Swansea, Wales)*, vol. 30(6), pp. 825–841, 2013.
- [6] K. Maekawa, T. Ishida, N. Chijiwa, and C. Fujiyama, “Multiscale coupled-hygromechanistic approach to the life-cycle performance assessment of structural concrete,” *J. Mater. Civ. Eng.*, vol. 27, no. 2, pp. A4014003-1–9, 2015.
- [7] H. Q. H. Nguyen, K. Maekawa, and S. Komatsu, “Effects of water-coupled cracks on life-cycle assessment of concrete pavement under moving load,” *Proc. Airf. Highw. Pavements*, pp. 110–121, 2019.
- [8] M. A. Biot, “General theory of three-dimensional consolidation,” *J. Appl. Phys.*, pp. 155–164, 1941.
- [9] M. A. Biot, “Theory of elasticity and consolidation for a porous anisotropic solid,” *J. Appl. Phys.*, vol. 26(2), pp. 182–185, 1955.
- [10] K. Maekawa, T. Ishida, and T. Kishi, “Multi-scale Modeling of Concrete Performance: integrated material and structural mechanics,” *J. Adv. Concr.*

Technol., vol. 1, no. 2, pp. 91–126, 2003.

- [11] A. Shinmura and V. E. Saouma, “Fluid fracture interaction in pressurized reinforced concrete vessels,” *Mater. Struct. Constr.*, vol. 30, pp. 72–80, 1997.
- [12] Ayers, M., Cackler, T., Fick, G., Harrington, D., Schwartz, D., Smith, K., Snyder, M.B., and Dam, T.V., “Guide for concrete pavement distress assessments and solutions: identification, causes, prevention, and repair,” *Iwota State University, National Concrete Pavement Technology Center*, 2018.
- [13] K. Maekawa, E. Gebreyouhannes, T. Mishima, and X. An, “Three-dimensional fatigue simulation of RC slabs under traveling wheel-type loads,” *J. Adv. Concr. Technol.*, vol. 4, no. 3, pp. 445–457, 2006.
- [14] M. Soltani and K. Maekawa, “Numerical simulation of progressive shear localization and scale effect in cohesionless soil media,” *Int. J. Non. Linear. Mech.*, vol. 69, pp. 1–13, 2015.
- [15] K. Maekawa, K. Toongoenthong, E. Gebreyouhannes, and T. Kishi, “Direct path-integral scheme for fatigue simulation of reinforced concrete in shear,” *J. Adv. Concr. Technol.*, vol. 4, no. 1, pp. 159–177, 2006.
- [16] K. Maekawa, Y. Hiratsuka, T. Ishida, and Y. Tanaka, “Numerical modeling and data assimilation for life-cycle assessment of concrete bridge structures,” *Conf. Strateg. Sustain. Concr. Struct. Brazil*, no. December, 2015.
- [17] O. Büyüköztürk and D. Lau, “High performance concrete: fundamentals and application,” *Cambridge Dep. Civ. Environ. Eng. Massachusetts Inst. Technol.*
- [18] K. Maekawa, T. Ishida, and T. Kishi, *Multi-scale modeling of structural concrete*. London: Taylor and Francis, 2008.
- [19] S. Angrill, A. Petit-Boix, T. Morales-Pinzon, A. Josa, J. Rieradevall, and X. Gabarrell, “Urban rainwater runoff quantity and quality - A potential endogenous resource in cities?” *Journal of Environmental Management*, vol. 189, pp 14-21, 2017.

CHAPTER 8

CONCLUSIONS AND RECOMMENDATIONS

8.1 General Conclusions

The principles of concrete pavement design have been developed for a very long time based on Westergaards's theory and spring dense elastic foundation. The existing design codes for pavements have currently applied these principles and the concentrated truck axle load. In engineering practice, the nonlinear soil and concrete slab as well as the wheel-type load should be considered in pavement research. Therefore, two experimental programs were implemented with the nonlinear FEM analysis in this study. The high cycle fatigue for soil-concrete slab interaction has been verified and validated in the coupled code under the moving wheel load. The failure mechanism of concrete pavements under moving loads can be obtained in FEM analysis. It is promising that the new philosophy in the study of concrete pavements can be approached. The nonlinear FEM analysis may propose a convenient assessment method to revise the existing codes for pavement designs. Based upon the experimental and analytical results, the following conclusions are summarized.

8.2 Experimental and Analytical Study for High Cycle Fatigue of Concrete Pavements

Small-scale experiments of the soil foundation and concrete slab interaction subjected to moving loads are presented. Based on these experiments, a coupled code for the study of concrete pavement under moving loads has been verified by utilizing constitutive models for high-cycle fatigue of concrete structures and soil foundations. The coupled program shows the description of behaviors and failure modes of the concrete slab (tension, compression, and shear) and nonlinear mechanics of soil (shear and volumetric fatigue). The three-dimensional finite element analysis was applied in the small-scale mock-ups. The summary of the experimental results are obtained as follows:

1. The fatigue life of concrete pavements is strongly governed by both the slab thickness and the relative density of soil. The exaggerated slab can cause the reduction of fatigue life on the soft soil foundations. The thin slab laid on the dense soil foundation may be the main reason to dramatically reduce the service life owing to the critical flexural tension focused at the bottom side of slabs.
2. Due to nonlinearity of soil, the balanced thickness of the slab in the loose foundation is smaller than the medium dense one. The sharp reduction of the life cycle and the severe damage of the slab may occur if the slab thickness is not selected rationally.
3. Depending on the thickness and soil's density, the fatigue failure of the concrete pavement addresses the deterioration of the slab, the shear band of soil and/or both of them. The optimized failure mode is the integrated soil-slab composite.

The thinner thickness of the concrete slab on the non-compacted soil is computationally and experimentally observed. Conversely, the thicker one on the compacted soil is required when the nonlinear coupling of the concrete slab and soil is investigated. The fatigue damage of nonlinear modeling can occur in the soil, the concrete slab or both of them, opposite to the sole damage of the concrete slab under the concentrated truck axle load in the existing design code of pavement. The balanced thickness of the concrete slab in this study is therefore considered based on the density of the soil foundation subjected to the moving wheel-type load. This will be a key factor to revise the design code of pavement which has been modeled based on in-plane theory on elastic foundation without considering shear localization.

8.3 Failure Mechanism of Concrete Pavements – Diverse Soil's Density Coupled Moving and Fixed-Point Pulsating Loads

The comparison of the fixed-point pulsating and moving load in the couple with the diverse soil foundation is computationally estimated in the views of the fatigue life of the concrete pavement. The three-dimensional finite element analysis indicates the dramatic reduction of fatigue under the moving loads, and the following conclusions have been obtained.

1. The failure mode of concrete pavements under the fixed-point and moving load is greatly different. One is the localized damage of the concrete slab and soil. Other is the distributed deterioration of the slab and the severe shear band of soil. The fatigue life of the moving load case is therefore significantly reduced.
2. Three-dimensional high-cycle fatigue simulation of soil-concrete slab interaction shows three types of failure mode depending on the soil's density and load amplitudes as the damage of the soil foundation (the non-compacted one), the coupling damage of the concrete slab and soil (the compacted one), and the damage of the slab only (the very compacted one), respectively.

The study of the concrete slab coupled the soil foundation has been investigated. The traveling-wheel type loads and nonlinear mechanics of soil coupled with the concrete slab should be considered to predict the fatigue life of the concrete pavement.

8.4 Nonlinear FEM Analysis for the Approach to Predict the Balanced Thickness of Concrete Pavements

The nonlinear FEM analysis for the new approach to predict and assess the idealized thickness of the concrete pavement slab under moving loads has been implemented with a mass of soil's density. Then, we earn the followings.

1. The required pavement thickness on the loose soil foundation is found to be thinner than the medium/dense one. This is opposite to the on-going design concept based upon the linearity of soil foundation. A key factor can be presented in discussing the rationale of design principle of concrete pavement. In other words, the thickness of the pavement on the medium compacted soil shall be increased than the current design requirement.
2. The design principle for the concrete pavement should be based on the nonlinear mechanics of soil and concrete slab interaction under the moving wheel-type loads. This couple can be dealt with using the constitutive models for the concrete slab and the soil foundation in FEM analysis.
3. Depending on the soil's density, the failure mode can be occurred in the concrete slab, the soil foundation or both of them (the couple damage of the slab and soil). The balanced thickness of the slab is therefore different.
4. The current design code shows the damage at the concrete slab only due to the linear, elastic and homogeneous foundation. It is thus matched to the fatigue

failure of FEM analysis in the very compacted soil. Other soil's density depicts as a predominant factor in the pavement design.

5. The balanced thickness of the concrete pavement slab is computationally confirmed to be a primary factor to the total fatigue life. The supernumerary slab's thickness is not demonstrated as the best selection since the greater burden is reproduced in the part of the foundation as shown in case of the loose/medium soil foundation. Meanwhile, the thicker slab is required in the event of the dense soil thanks to its support when coupling with the concrete slab. The fatigue damage is therefore combined the deterioration of the slab the shear band of soil.

The numerical code has been used in the coupling of finite element analysis for the concrete pavement under moving loads. The foreseen optimized thickness of slabs in association with the soil compaction is the target for validation of the computational scheme proposed in this study. The balanced thickness of the slab has been proposed based on the nonlinear principle. It is an important issue to make a contribution to revising the current design code for the concrete pavement. The balanced thickness of the concrete slab on the nonlinear soil in this study is proposed based on the results of small-scale mock-ups and the full-scale FEM analysis. This study can be fundamental for future discussion when the analytical results are compared to real-size experiments. This is a strategic point to revise the existing design codes of concrete pavements.

8.5 Effects of Construction Joints in Life Cycle Assessment of Concrete Pavements

The effects of the construction joint in the transverse direction are computationally investigated by utilizing the three-dimensional high-cycle fatigue for coupling of soil and concrete slabs. The numerical analysis shows the drastic decrease in the fatigue life of jointed concrete pavement compared to the continuous one, and the following conclusions are obtained.

1. The existence of construction joints may cause the dramatic reduction of fatigue life due to the localized damage of soil and concrete slabs at the edges.
2. Reinforcement ratio is computationally estimated to have a major effect to the fatigue life in both cases of jointed and continuous concrete pavement.
3. Soil foundations may be a sufficient tool to support the fatigue life of jointed

concrete pavements if dense soil and the rational thickness of the concrete slab are examined concurrently. The failure of dowel bars to support the load transfer between the construction joints has been computationally investigated. It shows the primacy of continuously reinforced concrete compared to jointed one in the life-cycle assessment.

8.6 Water Coupled Cracks on Life-Cycle Assessment of Concrete Pavements

The impact of stagnant water residing in cracked concrete are computationally estimated in views of the fatigue life of the concrete pavement on the nonlinear soil foundation. In reference to the experimental facts, nonlinear three-dimensional finite element analyses of plain and so-called reinforced concrete slabs were systematically conducted with nonlinear soil foundations, and the following conclusions are earned with different ambient states as;

1. The presence of the stagnant water in cracks of the concrete slab influenced the structural performance and caused the rapid decrease of the fatigue life.
2. The pore pressure aggravated by the crack kinetics evolves in micro-pores in concrete. Computationally, the history of the pore pressure and principal strain signifies that the damage of concrete slab is accelerated by the high pore pressure in crack gaps.
3. The existence of water can produce the high pore pressures in concrete and its effect may reach the concrete near the surface in bending compression. Hence, the damage caused by the pore pressures does not approach the bottom surface of the concrete slab irrespective of the fully saturated slab applied in numerical modeling.
4. Reinforcement ratio is computationally simulated to have an inconsiderable impact on the support for the fatigue life of concrete pavement if the stagnant water exists.
5. Compared to other cases, the pore water pressure gradually rises at the top surface slab of 10cm. Therefore, the dense foundation solely has a great effect on the increase of the fatigue life for concrete pavement if the stagnant water stays at this position.

6. The increase of the finer micropores and the reduction of the coarser ones can become a key factor to support the fatigue life of concrete pavement when stagnant water exists in the visible/invisible cracks of concrete. It is thus recommended to utilize the high strength concrete in the pavement construction.

The failure mode and fatigue life of the concrete pavement in this study demonstrate the worst case of water effects in the concrete slab coupled the soil foundation (water always exists in cracks of the concrete slab). The concrete pavement should be carefully waterproofed and maintained to prevent the effects of the stagnant water.

8.7 Recommendations for the Further Study

1. The nonlinear experimental and analytical results in this study are conducted under 28-day strength of concrete pavements. It is due to based on the recommendations of the existing design codes for pavements. However, the time to open the traffic operation can be reduced if the effects of early-age damage are considered. The current design codes can be more revised in terms of the effects of early opening for traffic vehicles after construction.
2. The effects of the iced water can cause the severe damage in cracked concrete under the moving load. The nonlinear FEM analysis should be more investigated in the freezing and thawing cycle (FTC) of stagnant water in cold areas.
3. The fatigue life in case of the damage of dowel bars at the transverse construction joints has been computationally simulated compared to the continuously reinforced concrete pavement. The normal support for the load transfer of the dowel bars (no failure) under the moving load should be more considered to investigate fatigue life of the jointed concrete pavement.